THE UNIVERSITY
of EDINBURGH

Translational Control of mRNAs in the Brain in Health and Disease

Investigations into protein synthesis in the brain and related neuropsychiatric disorders.

THE UNIVERSITY
of EDINBURGH

Konstanze Simbriger

Centre for Discovery Brain Sciences
University of Edinburgh

This dissertation is submitted for the degree of
Doctor of Philosophy

June 2019

Dedication

I would like to dedicate this thesis to my loving parents and my cats, who taught me that curiosity is an attitude towards life.

Declaration

I hereby declare that except where specific reference is made to the work of others, the contents of this dissertation are original and have not been submitted in whole or in part for consideration for any other degree or qualification in this, or any other university. This dissertation is my own work and contains nothing which is the outcome of work done in collaboration with others, except as specified in the text and Acknowledgements.

Konstanze Simbriger
Monday 14th October, 2019

List of publications

Parts of this thesis have been published or submitted for publication in peer-reviewed journals:

Inês Silva Amorim*, Sonal Kedia*, Stella Kouloulia*, Konstanze Simbriger*, Ilse Gantois, Seyed Mehdi Jafarnejad, Yupeng Li, Agniete Kampaite, Tine Pooters, Nicola Romanò, and Christos G. Gkogkas **Loss of eIF4E phosphorylation engenders depression-like behaviors via selective mRNA translation**, *Journal of Neuroscience*, 24 January 2018, 2673-17; DOI: 10.1523/JNEUROSCI.2673-17.2018, *These authors contributed equally

Konstanze Simbriger, Inês S. Amorim, Gilliard Lach, Kleanthi Chalkiadaki, Stella Kouloulia, Seyed Mehdi Jafarnejad*, Arkady Khoutorsky* and Christos G. Gkogkas* **Uncovering salient memory genes in contextual fear conditioning using ribosome profiling**, *in preparation*, *co-senior authors

Konstanze Simbriger, Inês S. Amorim, Kleanthi Chalkiadaki, Gilliard Lach, Seyed Mehdi Jafarnejad, Arkady Khoutorsky and Christos G. Gkogkas **Monitoring translation in synaptic fractions using a ribosome profiling strategy**, *Journal of Neuroscience Methods*, accepted 5 October 2019

Acknowledgements

First of all, I would like to thank Dr. Christos Gkogkas, for his continued support and supervision during the past four and a half years. I like to think that we both grew with the challenges that we faced during this time. Thank you for sharing your scientific expertise and giving me the opportunity to be part of many national and international collaborations, but also work on my own (crazy?) ideas. Remember to apply for that grant from McDonald Beef ;-)!

I would also like to thank Dr. Paul Skehel and Dr. Mandy Jackson, for co-supervising and chairing my PhD committee. You made the annual meetings feel like chatting about science over a good cuppa tea. Thank you for giving advice and supporting me fully, when times were difficult, but also for always having a smile and some kind words ready when we passed each other in the hallway.

I would further like to thank Dr. Athina Tzinia, who collaborated with us on the MMP-9 project and kindly shared their mouse line with us. Thank you to you and your group for your continued support and all the help with collecting tissue.

Thank you to the Sonenberg Lab at McGill, in particular Ilse and Mehdi, for collaboration on several projects.

Thank you to Gottfried Simbriger for providing me with a powerful server for some calculations when needed most and for tirelessly supplying litre after litre of home-brewed green tea (a.k.a. fuel).

I would not have made it through these years without the support both in the lab and outside of some of the past and present members of the Gkogkas lab, who have become dear friends as well. Stella, you were there from the beginning and we shared so many hours in the lab and the office, it would have

been lonely without you and certainly less productive. Inês, you joined me on the ribosome profiling side of life and always had an open ear for discussing anything and answering questions, no matter what they were. Thank you also for carrying out some experiments, supporting me with analyses, and reading my thesis carefully. Agnietė, you are a great friend and you are the only one in the lab I managed to convince to come to the dark side, i.e. join Tango society, but of course your support in the lab is invaluable too, as it helps us focus on experiments. Gilli you are the go-to person for animal and behaviour matters, thank you for contributing to my experiments as well! Alex, you only joined the lab at towards the end of my time there, but we shared lots of laughs and discussions (and coffee). Rita, Izzy, and Sonal, you left a while ago, but I still remember all our times together fondly. I wish you all the best for your current adventures and that you succeed. I will miss all the cake and sweets we shared in the office, although it will probably be beneficial for my blood sugar.

Thank you to the students I had the pleasure of supervising and working with, Katerina, Lewis, and Sally.

Jini, I am sure you know about everything I am grateful for, but I would like to give a short summary here anyway. You are probably the best housemate I ever had and an awesome friend, you cook delicious food for me, you have an open ear for any rant I need to have, and generally share all of my moments in life whether they are the good ones or the bad ones. I don't know where I would be without our friendship. And of course, all the dancing.

Martín, if there was a flatmate ranking, you would be a close second to Jini, but more importantly, you are a great friend. You and Aleks are always there with some kind words and two sets of open ears and hearts.

There are several more people I would like to thank for being my friends and supporting me through the journey that was my PhD: Jet, Iva, Teresa, Erica and Paris, Karolis and Susana, Julia, Jana, Anna, Sarah, and the lovely people always waiting with a warm embrace in Edinburgh Tango and New Scotland.

I would like to thank Vera, who gave me a home away from home in the beginning and at the end of my time in Edinburgh. Thank you for all the good times we spent blabbing and watching Strictly. You offered up your home and your friendship and made me feel like family.

Last but not least, I would like to thank my family, my parents Maria and Gottfried, my sister Valerie, and of course the cats. You have been nothing short of the best and most supportive people in my life and I would not be where I am today without you. Thank you, I love you lots.

Abstract

Neuropsychiatric disorders, e.g. autism spectrum disorders and depression, present an increasing burden on society. Diagnoses are on the rise and despite a constantly increasing body of research, causes and mechanisms of disease generation remain elusive. To date, treatment is either difficult or unavailable.

mRNA translation is an essential process for normal cell function. It is tightly regulated on both a global and local scale in cells. Local translation is particularly important for highly compartmentalised cells, such as neurons. mRNA translation is essential to the most basic processes in the brain, which include memory formation. Furthermore, dysregulation of translation, due to mutations in components of the translational machinery, has been shown to be both contributing and causal to some of the key phenotypes observed in neuropsychiatric disorders, e.g. autism spectrum disorders (ASD) or depression.

For the work presented in my thesis, we employed a novel method based on deep sequencing, known as ribosome profiling, to quantitatively measure changes in mRNA ribosome occupancy, which can be used to predict changes in translation of individual transcripts at an omic scale. We applied ribosome profiling to a novel neuropsychiatric model resembling fragile X syndrome (FXS) phenotypes, TgMMP9. FXS is a genetic syndrome, in which patients show severe neurological and physiological symptoms and the currently most common known cause of ASDs. TgMMP9 is a mouse line overexpressing human matrix metalloproteinase 9 (MMP-9), conditionally in the brain. MMP-9 is a key molecule in the extracellular matrix of the brain and has been associated with memory, ASDs (FXS in particular), Alzheimer's disease, and memory formation in the brain. We characterised translational regulation in TgMMP9 animals, using methods to study both global changes in translation and activation levels of known upstream regulators of translation. Furthermore, we carried out ribosome profiling of a well established mouse model of FXS, the *Fmr1* knock-out.

Likewise, we used ribosome profiling to study changes in translation in a novel mouse model of depression, eIF4ESer209Ala, entailing a mutation in an important molecular regulator of cap-dependent translation (eukaryotic initiation factor 4E, eIF4E), leaving the protein unphosphorylatable. Phosphorylation of eIF4E has previously been shown to be key in regulating transcript-specific translation. We also identified molecular pathways in these animals that impinge on translation and the dysregulation of which may in part be causative for the behavioural phenotypes we observe.

Additionally, we identified genes important in early fear memory formation by carrying out ribosome profiling on hippocampal tissue from fear conditioned animals. To dissect the effect of the electrical shock and the actual memory formation, we profiled changes in mRNA expression and translation in two controls (naïve and shock only). We identified genes and confirmed their expression using quantitative real-time PCR, that change expression specifically in fearful memory formation.

Finally, we adapted the ribosome profiling method for use in synaptoneurosomes, allowing us to study localised translation at synaptic terminals. In a brief experiment, we show that it is feasible to profile ribosome occupancy of mRNAs in biochemically isolated synaptic terminals, using two different protocols. This provides a powerful technique to study local translation at the synaptic compartment in both health and disease.

Altogether, the work contained in this thesis, highlights the importance of mRNA translation regulation to the development of diverse neuropsychiatric disorders. We show regulation of specific subsets of mRNAs in these disorders both at a global and more local scale, as well as changes in the activation of pathways upstream of translation.

Lay summary

Psychiatric disorders, such as autism and depression occur frequently in our population and have great socio-economic impacts. Affected individuals may require long-term medical treatment and/or care, which puts a considerable burden on relatives and patients themselves, as well as the healthcare system. Although some pharmacological intervention is available, it is not efficient in all patients, partially due to a lack of understanding of how these disorders work at a molecular level. To make matters worse, most psychiatric disorders present themselves as a “spectrum”, which refers to the immense heterogeneity among them and that almost no two patients will show the exact same symptoms, let alone causes. Therefore, gaining a better understanding at the molecular level and identifying common druggable cellular mechanisms is of extreme importance to improve treatment of neuropsychiatric disorders.

Brain cells are highly specialised cells that need to be able to respond timely to minimal signals at connections with other cells and synthesise or break down protein. Therefore, they are more sensitive to changes in the way proteins are synthesised and broken down. A very basic process in cells, the translation of genes from mRNA (which serves as a template) into proteins, has been shown to be altered in neuropsychiatric disorders. Thus, by studying mRNA translation and how this process is changed from the baseline in e.g. disease or memory forming experiences, we can gain a better understanding of the basic process and how it contributes to the generation of neuropsychiatric disorders.

Since several neuropsychiatric disorders show a link to altered protein synthesis, working towards this thesis, we investigated the activation status of diverse proteins in the cell that are known to regulate the translation of mRNA into protein. Furthermore, we explored how the mRNA translation in neurons is altered in models of autism and depression (genetically modified mice, carrying mutations that predispose them to the development of neuropsychiatric traits

related to autism and depression). We used a novel method to investigate how translation of each individual mRNA into protein by cellular machinery is changed in these disorder models compared to healthy control animals, in the brain. These experiments resulted in lists of genes that show different abundances between our disorder models and healthy controls, that we analysed for common features in terms of function, cellular and tissue location, and involvement in cellular pathways or diseases. This provided us with important information with regard to which regulatory elements within cells may be involved in the generation of the disorder and therefore may be targeted for novel drug development.

Intact protein synthesis is also key to the formation of novel memories, so we proceeded to investigate which mRNAs need to be translated in a classical Pavlovian conditioning paradigm. In classical conditioning, two stimuli are paired in the experience of the animal to form a memory that will later elicit a reaction to one of the stimuli, without the presence of the second stimulus. In fear conditioning, an association between an originally neutral, but novel; context and an electrical shock (aversive/fearful stimulus) is formed. When placed in the same context later, the animal will exhibit fearful behaviour because it remembers receiving a painful, although harmless electrical shock. How translation of specific mRNAs affects memory formation is highly relevant to our understanding of its basic mechanism and still poorly defined.

Taken together, the work presented in this thesis, shows novel (groups of) genes which are involved in the generation of neuropsychiatric disorders and whose translation is specifically regulated by changing the availability of proteins that have previously been associated with psychiatric disorders. This is important because it will further our understanding of said disorders and hopefully help us in improving treatment options.

Table of contents

List of figures

List of tables

List of abbreviations

4E-BP2	eukaryotic translation initiation factor 4E binding protein 2
4EKi	4E knock-in mice
ADH DRE	alcohol dehydrogenase 3' UTR downregulation control element
Akt	protein kinase B
AMP kinase	5' adenosine monophosphate-activated protein kinase
ANOVA	analysis of variance
APP	amyloid precursor protein
ASD	autism spectrum disorder
ATP	adenosine triphosphate
BDNF	brain-derived neurotrophic factor
BP	biological process
BSA	bovine serum albumin
CC	cellular component
cDNA	complementary DNA
CFC	contextual fear conditioning
CPE	cytoplasmic polyadenylation element
CS	conditioned stimulus
CYFIP1	cytoplasmic FMRP interacting protein 1
DAVID	Database for Annotation, Visualisation, and Integrated Discovery
DTT	dithiothreitol
DEG	differentially expressed gene
DIV	day *in vitro*
DMRT1 RE	DMRT1 regulatory element
DTG	differentially translated gene
ECM	extracellular matrix
EDTA	ethylenediaminetetraacetic acid
eIF2	eukaryotic translation initiation factor 2
eIF3	eukaryotic translation initiation factor 3
eIF4A	eukaryotic translation initiation factor 4A
eIF4B	eukaryotic translation initiation factor 4B

eIF4E	eukaryotic translation initiation factor 4E
eIF4F	eukaryotic translation initiation factor 4F
eIF4G	eukaryotic translation initiation factor 4G
EPM	elevated plus maze
ERK	extracellular signal-related kinase
EU	European Union
FAK	focal adhesion kinase
FASS	fluorescence activated synaptosome sorting
FC	fold change
FDR	false discovery rate
FMR1	fragile X mental retardation 1
Fmr1KO	Fmr1 knock-out mouse
FMRP	fragile X mental retardation protein
FST	forced swim test
FXS	fragile X syndrome
GAIT	gamma interferon inhibitor of translation
GC	guanine-cytosine
GO	gene ontology
GRE	GU-rich destabilization element
HEK293	human embryonic kidney 293 cells
HEPES	4-(2-hydroxyethyl)-1-piperazineethanesulfonic acid
HPA axis	hypothalamic pituitary adrenal axis
IEG	immediate early gene
IFNγ	interferon gamma
IL	interleukine
IPA	ingenuity pathway analysis
IRES	internal ribosome entry site
IκBα	inhibitor of kappa B alpha
KEGG	Kyoto encyclopedia of genes and genomes
KO	knock-out
LPS	lipopolysaccharide
LTD	long-term depression
LTP	long-term potentiation
MAP	molecule activity prediction
MAPK	mitogen-activated protein kinase
MBP	myelin basic protein
MDD	major depression disorder
MEK	MAPK/ERK Kinase
MF	molecular function
mGluR	metabotropic glutamate receptor

MMP-9	matrixmetalloproteinase 9
Mnk	MAPK-interacting serine/threonine-protein kinase
mTOR	mechanistic target of rapamycin
mTORC	mechanistic target of rapamycin complex
MWM	Morris water maze
NF-κB	nuclear factor kappa-light-chain-enhancer of activated B cells
NFKBIA	nuclear factor kappa-light-chain-enhancer of activated B cells mRNA
NP-40	Nonidet P-40
NSF	novelty suppressed feeding
OF	open field
OL	object location
ORF	open reading frame
PABP	poly(A)-binding protein
PAGE	polyacrylamide gelelectrophoreses
PAS	polyadenylation signal
PCR	polymerase chain reaction
PDGF-B	platelet-derived growth factor B-chain
PG4	G-quadruplex structure
PI3K	phosphoinositide 3-kinase
PRB	puromycin release buffer
PTEN	phosphatase and tensin homolog
qRT- PCR	quantitative real-time polymerase chain reaction
RCF	relative centrifugal field
RF	reading frame
RGD	arginylglycylaspartic acid
RIPA	radioimmunoprecipitation assay
RNA-Seq	RNA sequencing, next generation sequencing
RPF	ribosome protected fragments/ribosome profiling
RPKM	reads per kilobase per million
RPS6	ribosomal protein S6
RT	room temperature
S209A	serine 209 alanine mutation
S6K	ribosomal protein S6 kinase
SDS	sodium dodecyl sulfate
SP	synaptoneurosomes
SSRI	selective serotonin re-uptake inhibitor
SUnSET	surface sensing of translation
SXL BS	SXL binding site
TBE	tris-borate-EDTA
TBS-T	tris-buffered saline Tween-20

TE	translational efficiency
TGF-β	transforming growth factor beta
TgMMP9	transgenic mouse line overexpressing hMMP-9 in the brain
TNFα	tumor necrosis factor alpha
TOP	terminal oligopyrimidine
TRAP	translating ribosome affinity purification
TrkB	tropomyosin receptor kinase B
TSC	tuberous sclerosis complex
TST	tail suspension test
UNR BS	UNR binding site
uORF	upstream open reading frame
US	unconditioned stimulus
UTR	untranslated region
VEGF	vascular endothelial growth factor
WHO	world health organisation
WT	wildtype

Chapter 1

General introduction

1.1 Neuropsychiatric disorders and their socioeconomic impact

Neuropsychiatric disorders is an umbrella term for a group of mental disorders, grouped into several disorders, but generally characterised by a combination of abnormal perceptions, emotions, thoughts, behaviours, and relationships with other individuals. They include, but are not limited to, major depression disorder (MDD), bipolar affective disorder, schizophrenia, dementia, intellectual disabilities, and autism spectrum disorders (ASDs). The burden of neuropsychiatric disorders keeps growing (Table 1.1), affecting variables such as premature death, ability to work, and mental heath of caretakers. Treatments are available, but often have a major impact on patients' quality of life, in spite of treating the disorder or are ineffective. Therefore, it is pivotal to gain a better understanding of these disorders, in order to provide support for people affected by them (Global Burden of Disease Collaborative Network, 2018; World Health Organization, 2017b).

MDD is the most common form of mental disorders, with 163 million (estimates of undiagnosed depression reach 350 million) affected by it (Table 1.1). More females show signs of depression than males, according to World Health Organisation (WHO) estimates, and MDDs are one of the top 10 causes of disability. Depression comes in many shapes and forms, hence it is described as a spectrum of disorders, rather than a single disorder. MDDs are defined

Table 1.1 Prevalence of generalised mental disorders, MDD, and ASD at global, UK, and Scottish scales. Retrieved from Global Burden of Disease Collaborative Network (2018)

Region	Parameter	Mental disorders	MDD	ASD
Global	Number of people affected	970,812,351	163,044,068	31,179,664
Global	Prevalence	13.17%	2.21%	0.42%
United Kingdom	Number of people affected	9,352,703	1,809,421	394,580
United Kingdom	Prevalence	14.87%	2.88%	0.63%
Scotland	Number of people affected	772,606	152,620	30,107
Scotland	Prevalence	14.70%	2.90%	0.57%

by low self-worth, sadness, tiredness, loss of interest or pleasure in everyday activities, poor concentration, and disturbed sleep or appetite. A person can experience a single depressive episode during their life, have recurrent episodes, or even chronic symptoms. Being in a depressed state severely affects a person's ability to cope with normal daily life and in severe cases can lead to suicide. Thus, the impact on the healthcare system and the economy is considerable. Effective therapies include psychotherapy/talking therapy and antidepressants, depending on the severity of symptoms (Global Burden of Disease Collaborative Network, 2018; World Health Organization, 2017b). Due to the high variability in symptoms that patients present with and individual in differences physiology, however, antidepressants are not effective in all patients. This highlights the need to better understand antidepressant action, as well as the molecular background of depression and how different forms of the disorder converge to result in similar symptoms. Answering these questions may support the development of more specialised and effective treatments.

ASDs are a heterogeneous group of neurodevelopmental disorders that usually have a childhood onset, but persist into adulthood. Patients with ASDs display impairments in three key domains: social behaviour, communication, and repetitive/stereotypic behaviours (American Psychiatric Association, 2000). The prevalence of ASDs globally is about 0.42% (Table 1.1), with a higher incidence in males than in females, and has increased drastically over the past decades (Baxter et al., 2014; Global Burden of Disease Collaborative Network, 2018). Currently, treatment options are scarce and, depending on the severity of the disorder in the individual patient, individuals with ASD may never be able to live a self-sufficient life and require long-term specialised care. Therefore, the need to better understand the aetiology of ASDs and find novel treatment and management options is of great importance.

1.2 Regulation of mRNA translation

mRNA translation is pivotal for the survival and normal function of cells. Therefore, it is a tightly regulated process, both globally and locally. Most eukaryotic mRNAs contain a cap-structure at the 5'-UTR (m^7G-cap) (Jung et al., 2014), which can bind to the cap-binding protein eIF4E (eukaryotic initiation factor 4E) to subsequently recruit the translation initiation complex. Cap-dependent translation is a form of translation regulated by eIF4E. It is the main form of mRNA translation and requires the formation of the eIF4F complex, containing eIF4E (cap-binding protein), eIF4G (modular scaffolding protein interacting with eIF3 to recruit the 40S ribosomal subunit), and eIF4A (ATP-dependent helicase that unwinds secondary structures in the 5'-UTR), to initiate translation (Gkogkas et al., 2010). eIF4E is mainly regulated through phosphorylation of its repressors 4E-BPs (eIF4E binding proteins; 4E-BP2 is the predominant isoform in brain), and through direct phosphorylation by Mnk kinases (Figure 1.1) (Gkogkas et al., 2010; Hay and Sonenberg, 2004).

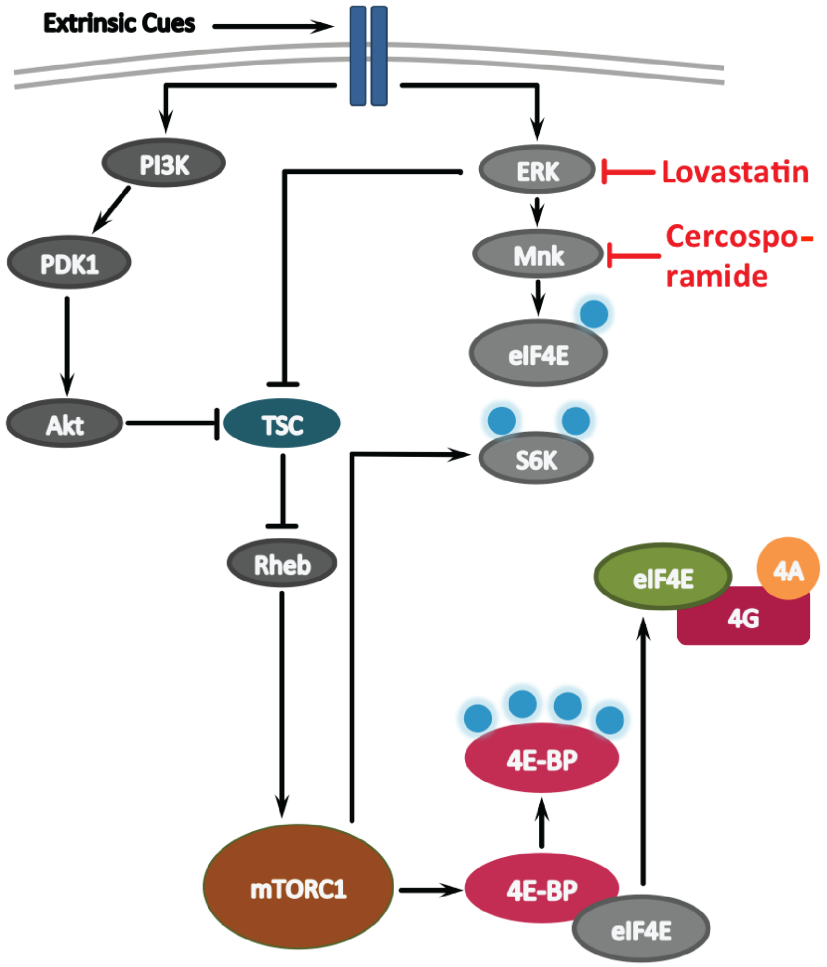

Figure 1.1 Schematic of how cap-dependent translation is regulated. Extracellular signals activate second messenger cascades intracellularly. Two major signalling pathways are involved: The Ras/ERK/Mnk pathway phosphorylates the cap-binding protein eIF4E directly and thereby activates translation, whereas activation of the PI3K/Akt/mTOR pathways leads to hyperphosphorylation of 4E-BPs, leading to their dissociation from eIF4E, thus stimulating assembly of the initiation complex (Hay and Sonenberg, 2004). mTORC1 furthermore phosphorylates S6 kinases (S6K1/2), which in turn phosphorylate ribosomal protein S6 and stimulate activity of eIF4B, a factor of the eIF4F complex that facilitates ribosome recruitment.

1.2.1 The mTOR and Mnk/eIF4E signalling axes

mTOR (mechanistic target of rapamycin) is a kinase that is a major component of two molecular complexes. mTORC1 (mechanistic target of rapamycin complex 1) and 2 are molecularly distinct and carry out different functions in the cell, relating to energy homeostasis and cell growth (including protein synthesis and lipid & nucleotide biosynthesis). These complexes function as integrators of external stimuli that are relayed into the cell to adapt to the current physiological needs (Laplante and Sabatini, 2012; Saxton and Sabatini, 2017). Extrinsic cues activate the PI3K/Akt pathway, which in turn regulates the activity of tuberous sclerosis complex 1 and 2 (TSC1/2), an inhibitor of mTORC1 activity (Figure 1.1 and 1.3). When mTORC1 is activated, it stimulates the translation of mRNAs through two main avenues, phosphorylation of ribosomal protein S6 kinases, which phosphorylate ribosomal protein S6, and phosphorylation of 4E-BPs, which leads to release of eIF4E and allows cap complex formation (Figure 1.1 and 1.3). Mutations in several of the proteins involved in theses signalling cascades have been implicated in the development of neuropsychiatric disorders (including ASD, schizophrenia and depression), e.g. TSC1/2; PTEN, another inhibitor of mTOR activity; and 4E-BPs (Figure 1.2 and 1.3) (Amorim et al., 2018b; Costa-Mattioli and Monteggia, 2013). Memory formation is mTORC1-dependent and inhibited by rapamycin, which has been extensively used to show varying aspects of memory depend on proper mTORC1 function. Furthermore, downstream effectors of mTOR are commonly phosphorylated after memory-forming experiences (Roesler, 2017).

A second major pathway that regulates mRNA translation in response to extracellular stimuli is the Ras/Raf/MEK/ERK pathway. Extracellular signals are integrated through Ras activation, which elicits a phosphorylation cascade, activating first Raf, followed by MEK, ERK, and the Mnk kinases. The mRNA cap-binding protein eIF4E is phosphorylated by the Mnk kinases on serine residue 209 to stimulate translation (Figure 1.1 and 1.3). Dysregulated translation downstream of eIF4E has been associated with depression, ASD, and schizophrenia (Amorim et al., 2018a,b; Gkogkas et al., 2013; Santini et al., 2013).

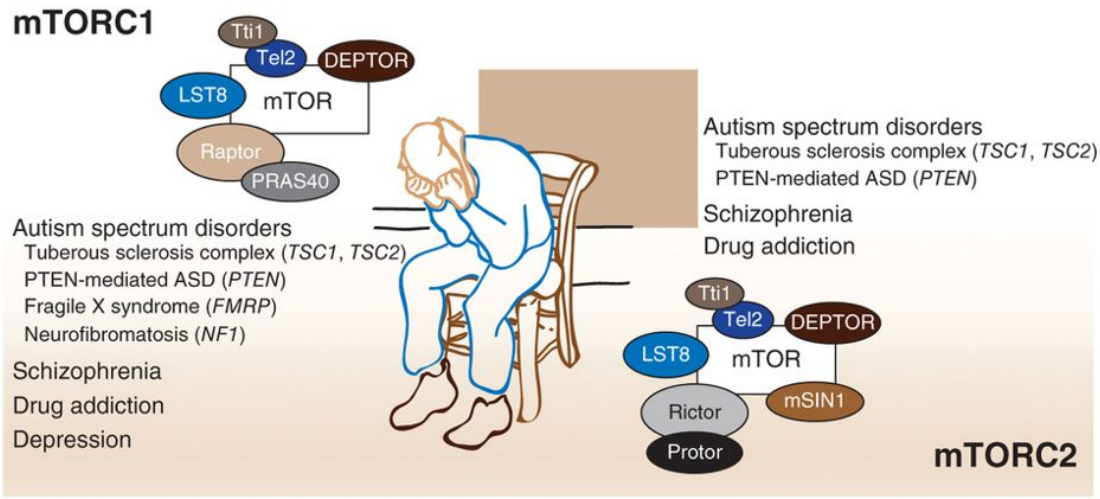

Figure 1.2 mTOR and neuropsychiatric disorders. The protein mTOR is part of two distinct molecular protein complexes, both of which, including upstream regulators and downstream effectors, have been implicated in several neurodevelopmental and neuropsychiatric disorders. **Left** the components of mTORC1 and a list of neuropsychiatric disorders that have been connected with its dysregulation. **Right** the components of mTORC2 and a list of neuropsychiatric disorders that have been connected with its dysregulation. Figure taken from Costa-Mattioli and Monteggia (2013)

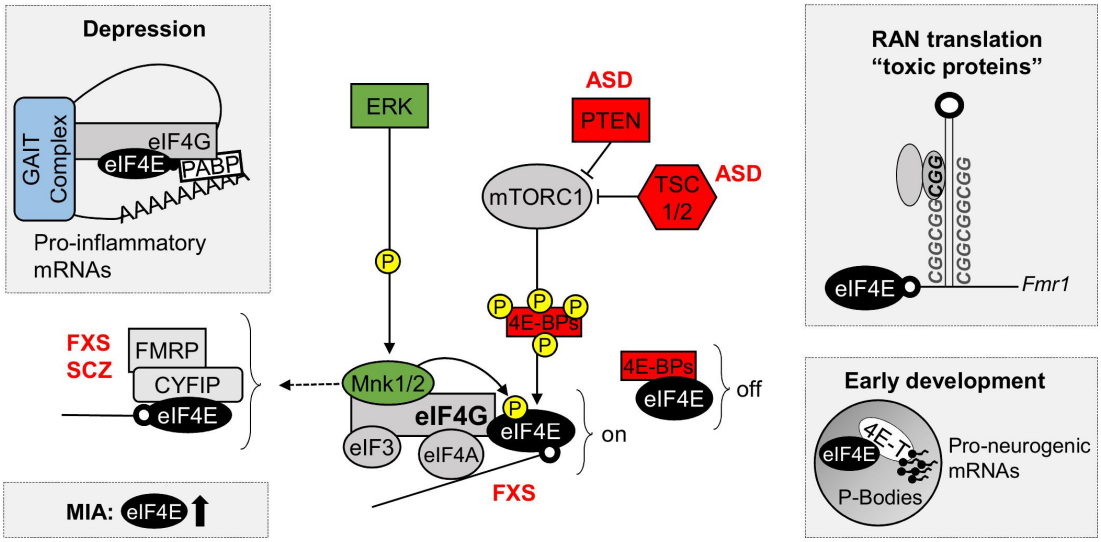

Figure 1.3 eIF4E in neurodevelopmental and neuropsychiatric disorders. Diagram of eIF4E function and how it is regulated by the ERK/Mnk and mTOR signalling axes. The insets highlight the roles that eIF4E has been shown to play in the generation of several neurodevelopmental and neuropsychiatric disorders. Top left: Impaired phosphorylation of eIF4E relieves repression of inflammatory mRNA translation through the GAIT complex and promotes depressive and anxiety behaviours. Bottom left: after maternal immune activation (MIA), eIF4E and mTOR are dysregulated in gene expression profiles. MIA is a known risk factor for ASD. Top right: eIF4E is required for RAN translation, a process that synthesises toxic polypeptides from polynucleotide repeat expansion containing transcripts, such as Fmr1. Bottom right: eIF4E and 4E-T interact in P-bodies to sequester and repress translation of pro-neurogenic mRNAs during early development. 4E-BPs, eIF4E-binding proteins; 4E-T, eIF4E transporter; ASD, Autism Spectrum Disorders; CYFIP1, cytoplasmic FMRP interacting protein; eIF3, eukaryotic initiation factor 3; eIF4A, eukaryotic translation initiation factor 4A; eIF4E, eukaryotic translation initiation factor 4E; eIF4G, eukaryotic translation initiation factor 4G; ERK, extracellular signal–regulated kinase, also known as mitogen-activated protein kinase (MAPK); FMRP, Fragile X mental retardation protein; FXS, Fragile X Syndrome; GAIT complex, interferon (IFN)-γ-activated inhibitor of translation complex; MNK 1/2, mitogen-activated protein (MAP) kinase-interacting serine/threonine-protein kinases 1/2; MIA, maternal immune activation; mTORC1, mechanistic target of rapamycin complex 1; off, repression of translation; on, active translation; P, phosphorylation site; PABPs, poly-A binding proteins; PTEN, phosphatase and tensin homolog; RAN, repeat-associated non-AUG; SCZ, Schizophrenia; TSC1/2, Tuberous sclerosis proteins 1/2. Figure taken from Amorim et al. (2018b)

1.2.2 The importance of mRNA translation in the brain

mRNA translation is particularly important in neurons, as their various compartments, such as synapses and dendritic spines, require differential levels of regulation to adequately process information (Gkogkas et al., 2010; Jung et al., 2014). Synthesis of new proteins and translational control are essential for several forms of synaptic plasticity and for the remodelling of connections between neurons (Gkogkas et al., 2010; Kandel, 2001; Richter and Klann, 2009). Aberrant regulation of translation in the brain has been associated with neuropsychiatric, neurodegenerative, and neurodevelopmental diseases (Jung et al., 2014).

The requirement of *de novo* protein synthesis (mRNA translation) for memory formation was hypothesised as early as 1948 (Monné, 2006). However, only after the discovery of protein synthesis inhibitors in the late 1950s (Yarmolinsky and Haba, 1959), protein synthesis dependency for novel memory formation was first demonstrated in mice performing a simple Y-maze avoidance memory task after injection with the translation inhibitor puromycin in 1963 (Flexner et al., 1965). In the following two decades, researchers made every effort to show in different species and various memory-dependent behavioural tasks that protein synthesis is required for several forms of memory and synaptic plasticity (Davis and Squire, 1984). These experiments further evidenced that the storage of long-term memories is dependent on a critical period of *de novo* protein synthesis shortly after the relevant experience (Davis and Squire, 1984; Sutton and Schuman, 2006). Later, when genetic approaches became more feasible, mutations in key protein synthesis regulators were shown to severely affect memory performance as well, further supporting the role of mRNA translation in memory formation (Banko et al., 2006; Costa-Mattioli et al., 2005; Kelleher et al., 2004). Moreover, injecting protein synthesis inhibitors during different stages of training and memory formation narrowed the critical windows of protein synthesis dependency during memory formation to a two-phase pattern, more precisely during training and ~3-4 h after training (Bourtchouladze et al., 1998; Grecksch and Matthies, 1980; Quevedo et al., 1999). Most of the attention was focussed on the requirement of protein synthesis for memory formation for a long time, but more recently, scientists have tried to dissect the regulatory mechanisms behind it (Buffington et al., 2014; Costa-Mattioli et al., 2009; Kelleher et al., 2004; Santini et al., 2014). Learning new behaviours results in specific

neuronal activity, which in turn activates cell-surface receptors upstream of intracellular signalling pathways. Activation of these pathways then regulate gene expression and *de novo* protein synthesis through various mechanisms (Alberini, 2009; Kandel et al., 2014; McGaugh, 2000). Translation, which is one of the most important steps during *de novo* protein synthesis, is comprised of three main phases, initiation, elongation, and termination and disruption of any of these can result in aberrant protein synthesis rates and memory formation. It follows that several translation initiation and elongation factors are of key importance for synaptic plasticity and during memory consolidation, as has been shown through pharmacogenetic inhibition of said factors (Buffington et al., 2014; Costa-Mattioli et al., 2009; Gal-Ben-Ari et al., 2012; Kelleher et al., 2004; Santini et al., 2014). Furthermore, gene specific mechanisms have been described, that may regulate translation rates of specific transcripts, such as UTR elements. An example are cytoplasmic polyadenylation elements (CPE), which are usually located at the end of the distal UTR. CPEs can be bound by CPE binding protein (CPEB), which suppresses the translation of the transcript. Upon phosphorylation, CPEB releases the bound mRNA and translation is de-repressed (Kelleher et al., 2004; Macdonald, 2001; Mayford et al., 1996). Lastly, non-coding mRNAs, in particular microRNAs, have also been implicated as regulatory mechanisms in synaptic plasticity and memory formation through recent work (Bicker et al., 2014; Gao et al., 2010; Griggs et al., 2013; Konopka et al., 2010; Saab and Mansuy, 2014; Thomas et al., 2014).

Due to their high specialisation and compartmentalisation, neurons require tight spatiotemporal control of protein synthesis to maintain their basic functions and respond efficiently to activity and other external stimuli. The dendrites and presynaptic regions are situated at a considerable distance from the cell soma (Figure 1.4). Therefore, specific mechanisms are required to ensure proteins are at the location where they are needed. To cope with this challenge, neurons have developed mechanisms that transport mRNAs to the different compartments and initiate protein synthesis in a local and timely manner (Holt and Schuman, 2013; Rangaraju et al., 2017). Dysregulated local translation plays a key role in several neuropsychiatric and neurodegenerative disorders (Liu-Yesucevitz et al., 2011).

Protein synthesis was believed to be localised solely to the cell body in neurons (with the exception of mitochondrial translation), until Bodian (1965) demonstrated the presence of ribosomal particles in the proximal dendrites of

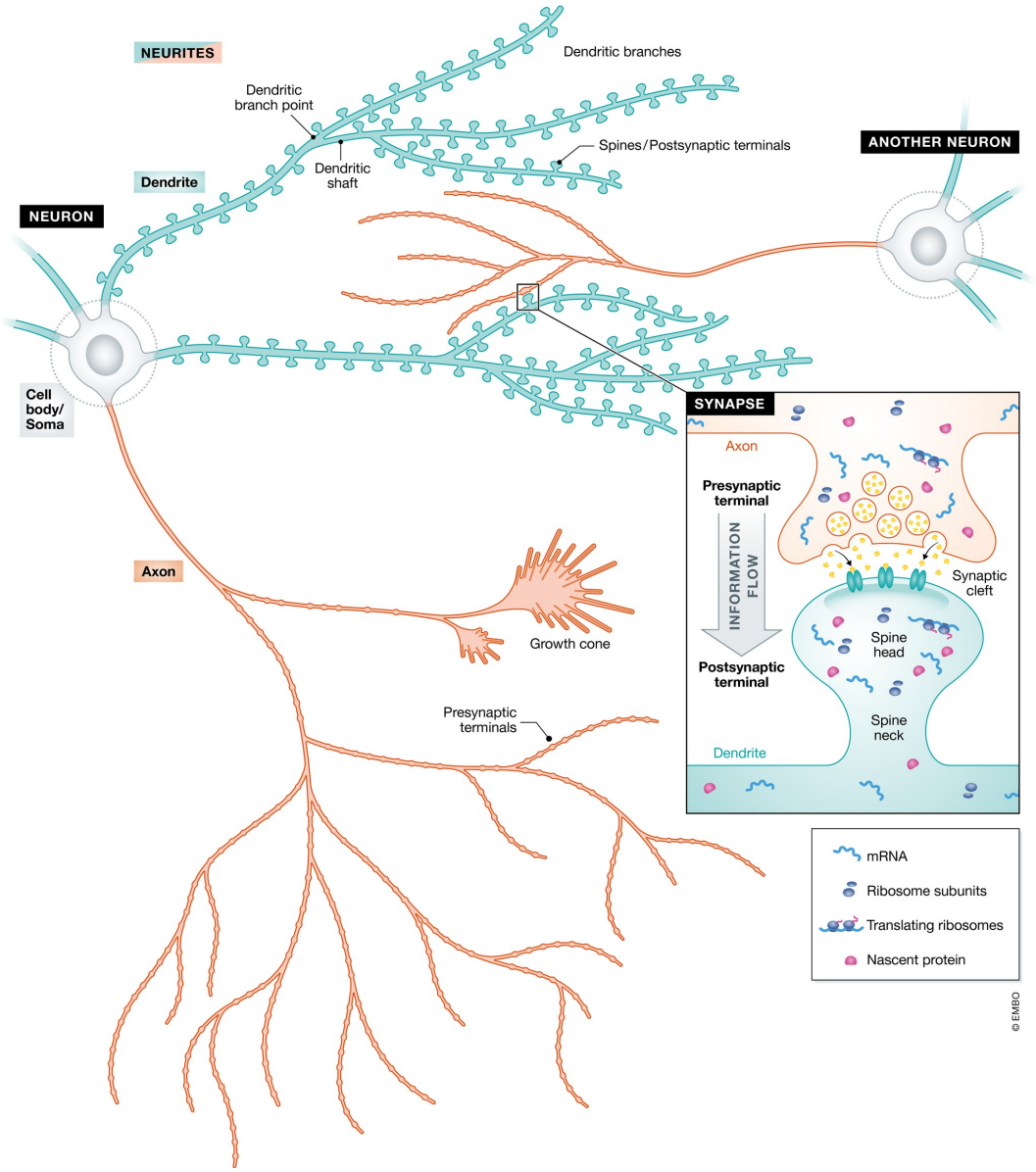

Figure 1.4 Cell compartments of neurons that require differential regulation of translation. Diagram of neuronal cells, highlighting different structural compartments of the cell that may require localised translation. Showing the cell body (gray) and neurites - composed of dendrites (blue) and axons (red). In the inset is a more detailed view of a synapse, formed by a presynaptic (red) and a postsynaptic (blue) terminal. All of these compartments may require newly synthesised protein independently from each other or co-dependently. Figure from Rangaraju et al. (2017).

monkey spinal chord motor neurons. The first evidence of translation at the synapse, however, was not found until Steward and Levy (1982) used electron microscopy to show that polyribosomes localised to the distal dendrites of dentate granule cell neurons. Following up on these experiments, localising components of the translational machinery to the synapse, incorporation of radioactively labelled amino acids in biochemically isolated synapses (Rao and Steward, 1991; Torre and Steward, 1992; Weiler and Greenough, 1991) and in live slice preparations (Feig and Lipton, 1993) was shown, providing the first evidence of active translation independent of the cell soma. Furthermore, measuring response times to stimuli in these experiments showed that time frames were too short (within minutes) to support a hypothesis in which proteins are synthesised in the cell bodies and transported to the synapse. The first functional association of dendritic protein synthesis and neuronal activity was discovered in 1996, demonstrating that dendritic translation is required for the strengthening of synaptic transmission after stimulation with brain derived neurotrophic factor (BDNF) (Kang and Schuman, 1996). Later work evidenced that while the translation in dendrites is critical to normal neuronal function, somatic translation may even be dispensable (Sutton and Schuman, 2006).

Synaptic plasticity is a term used to describe both long term potentiation (LTP, a strengthening of individual synaptic connections) and long term depression (LTD, a weakining of individual synaptic connections) and generally believed to be the basis of memory formation. It is comprised of two phases, an early phase (1-3 h) that is independent of *de novo* protein synthesis and a late phase that is more persistent and dependent on *de novo* protein synthesis (Frey et al., 1988; Stanton and Sarvey, 1984). Isolated hippocampal dendritic fields have been shown to be able to support late LTP formation, suggesting that somatic translation can be neglected for this process (Cracco et al., 2005; Huang and Kandel, 2005; Vickers et al., 2005). Furthermore, the focal application of protein synthesis inhibitors on dendrites resulted in inhibition of late LTP, while application of the inhibitor to the soma did not result in any significant changes in synaptic plasticity (Bradshaw et al., 2003).

Most of the work on localised translation at the synapse has been focussed on the post-synapse/dendrite, due to it being the "response element" of the synapse and the sheer technical challenge of studying translation at the pre-synapse. However, recent work has produced significant evidence for pre-synaptic translation using expansion microscopy to visualise both synap-

tic compartments and contained translational machinery. PolyA mRNAs and ribosomes were shown to be localised to both the pre- and post-synapse and biochemical isolation of excitatory pre-synaptic terminals and following RNA extraction and next generation sequencing demonstrated presence of synaptically relevant transcripts that are likely to be translated locally (Hafner et al., 2019).

Studying localised translation in a tissue context still proves challenging, since neurons and their different compartments are fully intermingled. Moreover, most of the published work has used mRNA abundance as a measurement of gene expression, which does not necessarily correlate with final protein expression levels (Hafner et al., 2019; Rangaraju et al., 2017; Tushev et al., 2018).

1.2.3 Ribosome profiling as a method to study translation in the brain

Ribosome profiling was established as a technique to study translation fairly recently (Ingolia et al., 2012, 2009), but has been used extensively since. The rationale behind it is that translating ribosomes can be isolated from cells with their associated mRNA (polysomes). The extracted polysomes are then digested using RNase I, in a classical footprinting assay, where mRNA that is inaccessible to the nuclease because of a bound ribosome remains intact. These ribosomal footprints, which are generally between 28 and 32 nucleotides in length, can then be purified and used for sequencing library generation. To gain a general insight into the transcriptional state of the cells or tissue under investigation, total mRNA from the same sample (undigested) is prepared into libraries, after random fragmentation into similarly sized pieces to the footprints, and sequenced along with the footprinting libraries. After aligning the sequencing results to the genome, counts and reads per kilobase of transcript per million mapped reads (RPKM) values can be extracted/calculated from the data. These quantitative values can then be used to assess firstly, which genes are present as mRNAs, and secondly, by dividing RPKM values of the footprints by the RPKM values of the total mRNA, the translational efficiency (TE, a value to represent ribosome occupancy of each gene normalised to its abundance) can be calculated (Figure 1.5). mRNA expression levels can be statistically compared between conditions using standard RNA-Seq frameworks, such as

DESeq2 (Love et al., 2014), or z-scores (Quackenbush, 2002) and TE with z-scores or especially developed tools such as Xtail (Xiao et al., 2016). All of these tools provide means to compare two sets of replicates, baseline/wildtype versus treatment/genetic model, calculate p-values, and filter for statistically significantly changed genes.

Ribosome profiling is a very powerful tool to study translation in an omics approach and it creates rich datasets, that can be analysed in various ways. It is particularly valuable for neuroscience research, because translation is a tightly regulated process in neurons and several diseases and disorders affecting the nervous system have been linked to dysregulated translation (Amorim et al., 2018b; Costa-Mattioli and Monteggia, 2013).

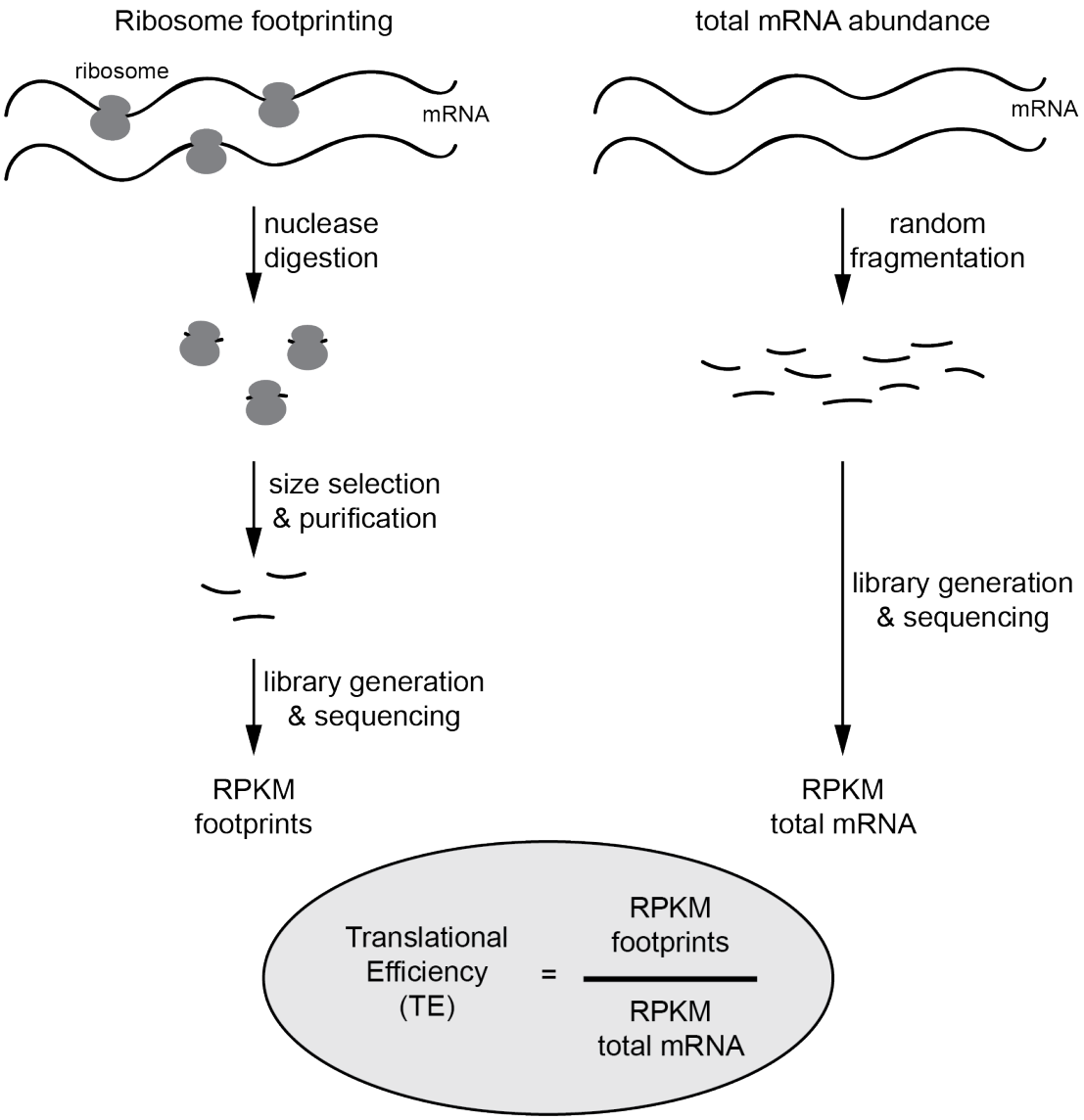

Figure 1.5 Schematic of the ribosome profiling method. Polysomes are extracted from cells or tissue and two aliquots are prepared from the lysate. One aliquot is digested with RNase I, leaving only fragments protected from digestion by the ribosomes ("ribosomal footprints" or ribosome protected fragments) intact. These fragments are purified and size selected before cDNA library generation for next generation sequencing. The other aliquot is processed for RNA Seq by random fragmentation and library generation (total RNA sample), and provides an overview over the transcriptional state of the cells/tissue. After bioinformatic processing of the sequencing results, normalised count values for sequencing reads aligning to each gene (RPKM, reads per kilobase of transcript per million mapped reads) are obtained. RPKM values for the total RNA sample can be used to assess transcriptional changes, whereas by dividing RPKM values of the ribosome foot prints by RPKM values of total RNA for each gene yield translational efficiency (TE) values, which resemble the translational state of genes.

1.2.4 Aims

With this thesis, I aimed to answer several questions, to gain a better general understanding of how translation, both globally and of specific mRNAs, contributes to the aetiology of neuropsychiatric disorders, such as ASD and MDD. Furthermore, we developed a strategy to study translation locally in biochemically extracted synaptic compartments.

Specifically the aims were:

Aim 1 To dissect the molecular contribution of MMP-9 to the exaggerated translation phenotypes observed in FXS.

Aim 2 To elucidate the role of cap-dependent translation in MDD, with a focus on the Mnk/eIF4E signalling axis.

Aim 3 To describe the transcriptional and translational landscape of contextual fear memories in the dorsal hippocampus and examine the used footshock for its contribution to the elicited gene expression.

Aim 4 To establish ribosome profiling as a method to study local translation at the synapse.

Chapter 2

General materials and methods

2.1 Transgenic mouse lines

All procedures were performed in accordance with United Kingdom Home Office (Scientific Procedures Act 1986) and the Canadian Council on Animal Care regulations and were approved by the University of Edinburgh and McGill University, respectively. Animals were kept under standard husbandry conditions and food and water were provided *ad libitum*. Pups were kept with their dams until weaning at postnatal day 21. After weaning, mice were group housed (maximum of 4 per cage) by sex. Cages were maintained in ventilated racks in temperature (20℃ - 21℃) and humidity (55%) controlled rooms, on a 12 h circadian cycle (7:00 AM to 7:00 PM light period). For all behavioural testing, mice were handled/habituated for 3 to 4 consecutive days before experimental testing.

All mouse lines were on a C57BL/6J background. Wildtype (WT) mice were obtained from a C57BL/6J colony at the animal facility at the Centre for Discovery Brain Sciences. Mice were genotyped in-house using conventional PCR on genomic DNA extracted from ear clips.

2.2 Ribosome profiling

Tissue was homogenised in an appropriate volume of lysis buffer, in a glass dounce homogenizer on ice, containing the following:

Table 2.1 TruSeq Polysome Lysis Buffer 1 ml

Reagent	Volume [µl]
5X TruSeq Mammalian Polysome Buffer (Illumina)	200
DNase I (1U/µl)	10
Cycloheximide (50 mg/ml)	2
RNAse-free water	788

DTT (1 mM final concentration), Triton X-100 (1% final concentration), and NP-40 (0.1% final concentration) were added to the homogenate and mixed well to support cell lysis. After incubation on ice for 10 min, with periodic inversions, lysates were centrifuged for 10 min at 20,000 RCF at 4℃. A_{260} was measured (on a NanoDrop™ 2000) for the supernatant.

For ribosome footprinting aliquots, 5 units of TruSeq Ribo Profile Nuclease (Illumina) were added per A_{260}/ml. Samples were then footprinted for 45 min at 4℃ with constant agitation. Nuclease digestions were quenched by adding 1.5 U SUPERase•In per µl digested lysate (ThermoFisher).

Ribosome protected fragments (RPFs) were purified using Illustra MicroSpin S-400 columns. Columns were equilibrated by letting 300 µl of 1X Mammalian Polysome Buffer drip through the column under gravity. To ensure all buffer had left the columns, they were centrifuged for 4 min at 600 RCF at room temperature (RT). 100 µl of the nuclease-digested sample were applied immediately and the columns centrifuged for 2 min at 600 RCF at RT, collecting the flow-through. SDS was added to both the nuclease-digested sample and an equivalent volume of undigested lysate to a final concentration of 1% and the RNA extracted using the RNA Clean & Concentrator™-25 Kit (Zymo Research).

All samples were quantified using a Nanodrop and balanced for the rRNA depletion reaction using the Ribo-Zero Gold Kit (Illumina). rRNA depletion was followed by a purification using the RNA Clean & Concentrator™-5 Kit (Zymo Research).

At this point, RPFs of 28-32 nt were size selected on a 15% TBE-Urea Polyacrylamide gel (ThermoFisher) and purified. Total RNA samples were randomly heat-fragmented and both samples were end-repaired using a Polynucleotide-kinase (Illumina, Promega), following the manufacturer's instructions. cDNA libraries for sequencing were generated with either the TruSeq® Riboprofiling Kit (Mammalian) (Illumina) or NEXTflex® Small RNA Sequencing Kit v3 for Illumina Platforms (Bioo Scientific).

2.2.1 TruSeq® Riboprofiling Kit (Mammalian) (Illumina)

Following the end-repair and purification with the RNA Clean & Concentrator™-5 Kit (Zymo Research), a 3' Adapter was ligated to the all samples. Excess adapter was digested with the TruSeq Ribo Profile Adapter Removal Enzyme.

The samples were then reverse transcribed into cDNA and purified using a RNA Clean & Concentrator™-5 Kit (Zymo Research). To minimise adapter contamination, samples were separated on a 10% TBE-Urea Polyacrylamide gel (ThermoFisher) and cDNA fragments cut and purified from the gel.

The cDNA was then circularised using TruSeq Ribo Profile CircLigase. cDNA libraries were amplified using rolling circle amplification, according to the manufacturers instructions, for 9 cycles. During the PCR reaction, the libraries were indexed with Illumina indexing primers to allow for multiplexing on the sequencing flow cell. Indexing primers used are summarised in Table 2.2

Table 2.2 Illumina Indexing Barcodes (i7)

Index Number	Barcode Sequence
04	TGACCA
05	ACAGTG
06	GCCAAT
07	CAGATC
09	GATCAG
10	TAGCTT
11	GGCTAC
12	CTTGTA

Following the PCR reactions, cDNA libraries were purified using the Agencourt AMPure XP Kit (Beckman Coulter). The completed libraries were analysed for size, quantity, and purity on an Agilent Bioanalyzer, using the High Sensitivity DNA kit. If needed, contaminations were removed by running the libraries on a 8% native TBE Polyacrylamide gel (Novex, ThermoFisher) and fragments of the desired size were cut and purified from the gel.

2.2.2 NEXTflex™ Small RNA Sequencing Kit v3 for Illumina Platforms (Bioo Scientific)

Because the Illumina Ribo Profile kit became obsolete, we changed over to the NEXTflex™ kit for library generation from fragmented RNA. After the end-repair, samples were quantified using the Agilent Small RNA Kit. Input was balanced between samples to ensure similar output. The manufacturer's protocol was followed, using the lowest input option, due to total sample quantities below 1 ng.

In brief, an adenylated 3' adapter was ligated, followed by an adenylated 5' adapter ligation. The RNA fragments were then reverse transcribed into cDNA and amplified using PCR (18 cycles). During the PCR, individual samples were barcoded for multiplex sequencing using the barcoding primers compatible with Illumina sequencing, included in the kit.

Indexing primers used are summarised in Table 2.3. The PCR products were size selected on an 8% native TBE-PAGE gel (Novex, ThermoFisher) and purified from the gel according to the manufacturer's instructions. The cDNA libraries were then analysed for size, quantity and quality using the Agilent High Sensitivity DNA kit.

Samples were balanced and pooled for sequencing with Edinburgh Genomics on NovaSeq S1/2 flow cells yielding 50 bp paired-end reads.

2.2.3 Next generation sequencing

Libraries of sufficient quality and quantity (according to the sequencing facility's requirements) were pooled and submitted for sequencing with Edinburgh

Table 2.3 NEXTflex™ Indexing Primers

NEXTflex™	Index Sequence	Reverse Complement
PCR Primer 1	CGTGAT	ATCACG
PCR Primer 2	ACATCG	CGATGT
PCR Primer 3	GCCTAA	TTAGGC
PCR Primer 4	TGGTCA	TGACCA
PCR Primer 5	CACTGT	ACAGTG
PCR Primer 6	ATTGGC	GCCAAT
PCR Primer 7	GATCTG	CAGATC
PCR Primer 8	TCAAGT	ACTTGA
PCR Primer 9	CTGATC	GATCAG
PCR Primer 10	AAGCTA	TAGCTT
PCR Primer 11	GTAGCC	GGCTAC
PCR Primer 12	TACAAG	CTTGTA
PCR Primer 13	TTGACT	AGTCAA
PCR Primer 14	GGAACT	AGTTCC
PCR Primer 15	TGACAT	ATGTCA
PCR Primer 16	GGACGG	CCGTCC
PCR Primer 17	CTCTAC	GTAGAG
PCR Primer 18	GCGGAC	GTCCGC
PCR Primer 19	TTTCAC	GTGAAA
PCR Primer 20	GGCCAC	GTGGCC
PCR Primer 21	CGAAAC	GTTTCG
PCR Primer 22	CGTACG	CGTACG
PCR Primer 23	CCACTC	GAGTGG
PCR Primer 24	GCTACC	GGTAGC
PCR Primer 25	ATCAGT	ACTGAT
PCR Primer 26	GCTCAT	ATGAGC
PCR Primer 27	AGGAAT	ATTCCT
PCR Primer 28	CTTTTG	CAAAAG

Genomics on either a HiSeq2500 v4 50 bp single-end reader, or more recently on NovaSeq S1 flow cells yielding 50 bp paired-end reads.

2.2.4 Bioinformatics analysis

Bioinformatic/statistical consulting was provided by omics2view.consulting GbR, Kiel (Germany). All bioinformatic analysis was performed by omics2view, using a customised pipeline, adapted for ribosome profiling results. omics2view was blinded to the genotype and no randomisation was carried out in these experiments. Pilot experiments in the Gkogkas lab showed that 2 replicates per library, given the sequencing depth by Edinburgh Genomics, were sufficient for this type of analysis.

In summary, the FASTX Toolkit v0.0.14 (Gordon and Hannon, 2010) was used to trim adapter sequences from raw reads of both RPF and total RNA samples and RPF reads below 18 bp removed from the data. Next, undesired sequences (ribosomal RNAs and tRNAs) were removed from the datasets using Bowtie v1.1.2 (Langmead et al., 2009).

The Filtered RPF and total reads were then aligned to an indexed reference genome (built from GRCm38 primary genome assembly and the corresponding gene structure information, retrieved from GENCODE), using STAR v2.5.2b (Dobin et al., 2013). Only uniquely mapped reads were considered for the output. Data, including counts was summarised in a table including several columns:

- Ensembl gene ID
- Gene symbol
- Gene type
- Chromosome
- Gene length
- Non-coding (a binary value indicating whether or not the gene is coding or non-coding)
- Pseudogene (binary value, compare to non-coding)

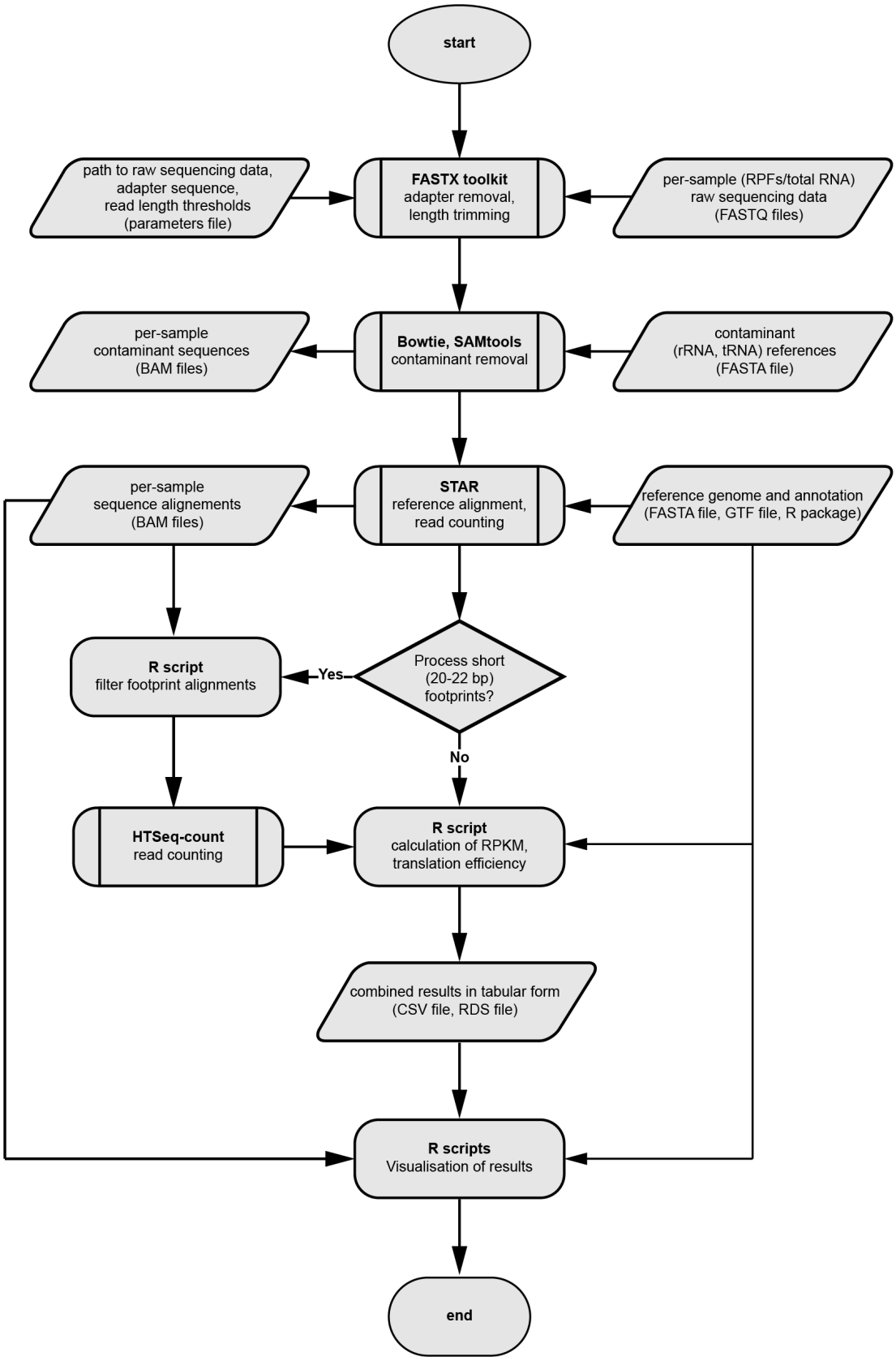

Figure 2.1 Schematic depiction of the bioinformatics pipeline workflow.

- Entrez gene ID
- Official gene ID (gene description)

Further, the table contained reads per kilobase of transcript per million mapped reads (RPKM) and translational efficiency (TE) values for each gene/condition and replicate that were calculated as follows:

$$RPKM_i = \frac{n_i}{\frac{l_i}{10^3} \cdot \frac{\sum_{i=1}^{k} n_i}{10^6}}$$

where n_i is the number of reads mapped to a gene i of length l_i. $\sum_{i=1}^{k} n_i$ is the sum of read counts for the given sample over all k genes in the reference genome. Results were rounded to 4 decimal places.

For each gene i in a given sample, the translational efficiency (TE_i) was calculated as:

$$TE_i = \frac{\frac{RPF_i}{\sum_{i=1}^{k} n_i \ RPF_i}}{\frac{total \ mRNA_i}{\sum_{i=1}^{k} n_i total \ mRNA_i}}$$

RPF_i and $total\ mRNA_i$ is the respective number of reads mapped to gene i for the ribosome protected fragments and total mRNA. $\sum_{i=1}^{k} n_i \ RPF_i$ and $\sum_{i=1}^{k} n_i \ total \ mRNA_i$ are the sums of the read counts, respectively, over all k genes in the reference genome. Again, results were rounded to four decimal places.

Both of these values were added to the summarised results table.

Further, the pipeline produced graphical outputs summarising the data.

Reproducibility Plots are pairwise plots between biological replicates, showing the reproducibility between replicates. The squared Pearson product-moment correlation coefficient r^2 is calculated as a coefficient of determination. These plots are generated from log_2-transformed RPKM and TE values.

Per-sample size distribution Plots show the length (in nucleotides) of 100,000 randomly sub-sampled RPF and total mRNA, respectively, for each sample in the same plot, for comparison.

Cumulative footprint 5' end positions relative to all start and stop codons plots are generated by mapping 5' end positions to positions in a window of $\pm$30 nt around the starting nucleotide of any start and stop codon, respectively. These mapped positions are then transformed into offset positions (relative to the start codon of the respective gene). These offset positions are combined for all genes and RPF positions are displayed as peaks, while total mRNA positions are visualised as a line in the background.

Cumulative reading frame usage plots show the relative abundance of respective reading frames within a sample. The reading frames are calculated as follows:

$$ops\ mod\ 3$$

ops stands for the offset 5' end position of a read, relative to the start codon (as determined for the cumulative footprint 5' end positions relative to all start and stop codons plots). $mod\ 3$ is the modulo, also called the remainder, after Euclidean division by 3. 5' end positions are added up for each reading frame and converted to relative abundances.

Histogram of translational efficiencies The translational efficiencies across all replicates are averaged for each protein coding gene. 0 values are excluded and all remaining values are log_2-transformed and plotted as superimposed histograms.

Violin plots of translational efficiencies the same values as for the histogram plots are plotted in violin plots.

Changes in TE and transcription were analysed for pairwise comparisons, based on experimental design, using microarray normalisation methods, as reviewed by Quackenbush (2002). For each treatment, an average across replicates was calculated for TE/RPKM values, using the geometric mean on a per-gene basis. Two statistics were then derived from these averages, for each gene:

Ratio which is calculated by dividing the value for the *alternative treatment/knock-out/transgenic* by the value for the *base-level treatment/WT*.

Intensity which is calculated by multiplying the afore-mentioned values

Data was ordered by increasing $log_{10}(Intensity)$. Along this ordered set of values, mean $log_{10}(Intensity)$, as well as mean and standard deviation of $log_2(Ratio)$ were calculated within a sliding window of 100 genes at steps of 50 genes. Each gene was assigned to the window with a mean $log_{10}(Intensity)$ closest to the gene's $log_{10}(Intensity)$.

A z-score was calculated for each gene i using the respective window's $log_2(Ratio)$ mean and standard deviation as follows:

$$z_i = \frac{log_2(Ratio_i) - \mu^{window}_{log_2(Ratio)}}{\sigma^{window}_{log_2(Ratio)}}$$

p-values were derived for each gene i from the z-score by treating it as a quantile of the standard normal distribution:

$$p_i = 2 \times (1 - \Phi(|z_i|))$$

The sliding window was used to adequately represent the inherent structure of the data. Similar to microarray data, TE ratios and – particularly – transcription ratios are more variable at low intensities. With z-scores simply calculated from the overall mean and standard deviation of the data, one might misidentify extreme $log_2(Ratio)$ values as significant at low intensities. At higher intensities, on the other hand, genes with significant $log_2(Ratio)$ values might not be identified. The intensity-dependent z-score is calculated with a subset of data from genes with similar intensity. This takes local data structure into account, allowing a more accurate determination of differential TE and transcription.

For TE values, we further used the R package Xtail v1.1.5 (Xiao et al., 2016), a tool that has been specifically developed for analysing ribosome profiling data.

For both the z-score-based p-values and the p-values derived with Xtail, false-discovery-rates (FDR) were calculated *sensu* Benjamini and Hochberg (1995), according to three (adjustable) parameters:

- Low TE/RPKM ratio threshold (generally pre-set to 0.666)

- High TE/RPKM ratio threshold (generally pre-set to 1.5)
- Minimum across all samples (generally pre-set to 40)

2.2.5 UTR analysis

Analysis of untranslated regions (UTR) of differentially translated genes (DTG) was performed using a custom-scripted pipeline implemented in R. The pipeline analyses a list of genes provided as ensembl gene IDs in a .txt file and consists of several modules:

Reference Preparation the pipeline downloads the latest reference data and compiles a UTR database from them

Input check the gene IDs provided as an input are matched against the UTR database and filtered according to user commands (3'/5', all/longest UTR sequences)

Basic statistics this module extracts information such as UTR sequence length and GC content for each sequence

Clustering an optional module that aligns UTR sequences using MAFFT v7.407 (Katoh and Standley, 2013). Pairwise dissimilarities are calculated from the multiple sequence alignment and used to construct a dendrogram with the complete-linkage hierarchical clustering method. The optimal number of clusters is determined according to the *C-Index* (Hubert and Levin, 1976)

Gibbs free energy mfold v3.6 (Zuker, 2003) is used to calculate Gibbs free energy for each sequence and results are represented as values and in image form

Motifs all sequences are scanned for known motifs using a stand-alone version of Utrscan (Pesole and Liuni, 1999)

Output the results of individual modules are combined in a tab-separated file for the user to interpret

2.2.6 Gene ontology analysis

Gene ontology (GO) analysis was performed on DEGs and DTGs using the Database for Annotation, Visualization and Integrated Discovery (DAVID) version 6.8 (Huang et al., 2009a,b). GO annotations were gathered for the following categories:

Molecular function (MF) tests for molecular function GO terms enriched in the analysed data.

Biological process (BP) tests for biological process GO terms enriched in the analysed data.

Cellular component (CC) tests for cellular component GO terms enriched in the analysed data.

KEGG pathways maps the dataset to Pathways in the KEGG (Kyoto Encyclopedia of Genes and Genomes) database and tests for any enrichment.

BIOCARTA pathways maps the dataset to Pathways in the BioCarta database and tests for any enrichment.

Only GO terms with associated p-values <0.05 were considered.

2.2.7 Ingenuity Pathway Analysis (IPA)

DEG and DTG datasets were uploaded on IPA (IPA; QIAGEN Inc.) and submitted to Core Analysis. Analysis settings were set to include direct and indirect relationships, and experimentally observed nervous system data. In more detail, the gene sets were analysed for enrichment, based on p-value, in the following categories:

Canonical Pathways determines most significantly affected, established signalling and metabolic pathways. Can predict activation/inhibition of pathways and identify overlapping pathways in the dataset.

Upstream Regulators predicts which molecules (including microRNA and transcription factors) may be causing the observed changes in the data being analysed.

Diseases and Functions predicts changes downstream of the observed expression changes, in the tissue or cells studied.

Mechanistic networks (incl. molecule activity prediction) generates plausible signalling cascades, based on the data, that may describe the potential mechanism leading to gene expression changes in the data. Molecule activity prediction (MAP) can be used to overlay the generated networks, predicting activity of the nodes, based on expression changes observed in the data.

Sub-cellular localisation genes get assigned to one category (cytoplasm, extracellular space, nucleus, plasma membrane, other). This information can be used to determine whether there was an enrichment/depletion in any of the locations.

Type categorises genes based on their function in the cell (including cytokine, enzyme, G-protein coupled receptor, growth factor, ion channel, kinase, ligand-dependent nuclear receptor, peptidase, phosphatase, transcription regulator, translation regulator, transmembrane receptor, transporter, other)

2.3 Western blotting

Samples for Western blotting were homogenised in an appropriate volume of RIPA buffer (50 mM Tris pH 8.0, 150 mM NaCl, 1% NP-40, 0.5% sodium deoxycholate, 0.1% SDS), containing protease and phosphatase inhibitors (Roche). Homogenates were incubated on ice for 15 min with occasional vortexing and were cleared by centrifugation at 16,000 RCF at 4℃ for 20 min. The supernatant was used for Western blotting, after each sample was quantified using the DC Protein Assay (Bio-Rad).

20-50 µg of protein per lane were prepared in SDS Sample Buffer (50 mM Tris pH 6.8, 100 mM DTT, 2% SDS, 10% Glycerol, 0.1% bromophenol blue), heat-denatured at 98℃ for 5 min and resolved on 10-16% home-made polyacrylamide gels (Bio-Rad gel-pouring system). The resolved proteins were transferred to 0.2 µm nitrocellulose membranes (Bio-Rad), blocked with 5% BSA in TBS-T (10 mM Tris pH 7.6, 150 mM NaCl, 0.1% Tween-20) for 1 h

Table 2.4 Primary antibodies

Target	Species	Supplier	Cat No	WB
4E-BP1	rabbit	New England Biolabs	9644	1:1000
4E-BP1 phospho Thr37/46	rabbit	Cell Signalling	2855	1:1000
4E-BP2	rabbit	New England Biolabs	2845	1:1000
Akt	rabbit	Cell Signalling	9272	1:1000
Akt phospho Ser473	rabbit	Cell Signalling	9271	1:1000
Akt phospho Thr308	rabbit	Cell Signalling	9275	1:1000
eIF4E	mouse	BD Biosciences	610270	1:1000
eIF4E phospho Ser209	rabbit	abcam	ab76256	1:1000
FAK	rabbit	Millipore	06-543	1:1000
FAK phospho Tyr397	rabbit	Thermo Scientific	44-624G	1:1000
GAPDH	rabbit	Cell Signalling	2118S	1:5000
HDAC3 7G6C5	mouse	GeneTex	GTX83173	1:1000
HSC-70	mouse	Santa Cruz	sc-7298	1:1000
MAPK (ERK1/2, p44/42)	rabbit	Cell Signalling	4695	1:1000
MAPK (ERK1/2, p44/42) phospho Thr202/Tyr204	rabbit	Cell Signalling	9101	1:1000
Myelin Basic Protein	mouse	abcam	ab62631	1:1000
PSD95	rabbit	Cell Signalling	3450	1:1000
Puromycin	mouse	Millipore	MABE343	1:1000
Ribosomal Protein L10a	rabbit	abcam	ab174318	1:1000
Ribosomal Protein L11	rabbit	Cell Signalling	18163	1:1000
Ribosomal Protein L13	rabbit	Cell Signalling	2765	1:500
Ribosomal Protein S6	mouse	Santa Cruz	sc-74459	1:1000
Ribosomal Protein S6 phospho Ser235/236	rabbit	Cell Signalling	2211S	1:1000
Ribosomal Protein S6 phospho Ser240/244	rabbit	Cell Signalling	2215S	1:1000
Ribosomal Protein S6 phospho Ser240/244 XP	rabbit	Cell Signalling	5364	1:1000
Ribosomal Protein S15	rabbit	abcam	ab157193	1:1000
SV2A	mouse	DSHB University of Iowa	AB_2315387	1:1000
Synaptophysin 1	rabbit	Synaptic Systems	101 002	1:1000

Table 2.5 Secondary antibodies

Description	Species	Supplier	Cat No	WB
IRDye® 680RD Donkey anti-Mouse IgG (H + L)	Donkey	LiCOR Biosciences	926-68072	1:5000
IRDye® 680RD Donkey anti-Rabbit IgG (H + L)	Donkey	LiCOR Biosciences	926-68073	1:5000
IRDye® 800CW Donkey anti-Mouse IgG (H + L)	Donkey	LiCOR Biosciences	926-32212	1:5000
IRDye® 800CW Donkey anti-Rabbit IgG (H + L)	Donkey	LiCOR Biosciences	926-32213	1:5000

at RT, incubated with primary antibodies (summarised in Table 2.4) at 4℃ overnight, and with secondary antibodies (summarised in Table 2.5) at RT for 1 h. Membranes were washed extensively in TBS-T between the incubations. The membranes were imaged using an Odyssey Imaging System (Li-COR Biosciences) at a resolution of 169 µm and quantified using the Image Studio™ Software Version 5.x (Li-COR Biosciences). The intensity of each protein band was measured in triplicate and averaged to minimize measuring variability.

2.4 Statistical analysis

Quantitative data were collected and organised in Microsoft Excel®. Data was visualised and statistical analysis was carried out using GraphPad Prism® 6 software. Details of statistical tests used are outlined in the results sections or within the associated figure legends. Statistical significance was set to 0.05 *a priori*.

Chapter 3

The role of overexpression of MMP-9 in fragile X syndrome

3.1 Introduction

3.1.1 Autism and Fragile X Syndrome

Autism spectrum disorders (ASDs) are a heterogeneous group of neurodevelopmental disorders, in which patients exhibit impairments in three core domains: communication, social behaviour, and repetitive/stereotypic behaviours (American Psychiatric Association, 2000). The global burden of ASDs has increased drastically over the last few decades, with a prevalence of 1 in 132 people on the spectrum (Baxter et al., 2014). ASDs exhibit a strong genetic component and several single-gene neurodevelopmental disorders are frequently co-diagnosed with ASD. For instance, tuberous sclerosis complex (TSC) accounts for 1-4% of ASD patients (Kelleher III and Bear, 2008), whereas fragile X syndrome (FXS), currently the most prevalent known inherited cause of autism, accounts for approximately 5% of the ASD population (Budimirovic and Kaufmann, 2011).

Patients with FXS clinically present with a variety of symptoms, including intellectual disability, hyper-excitability, anxiety, repetitive behaviours and morphological abnormalities (Zoghbi and Bear, 2012). In addition, 50-60% of patients are co-diagnosed with ASDs (Budimirovic and Kaufmann, 2011).

FXS results from expanded CGG repeats in the FMR1 gene, leading to hypermethylation (silencing) of the locus and, subsequently, loss of fragile X mental retardation protein (FMRP) expression (Budimirovic and Kaufmann, 2011). FMRP is an mRNA binding protein that plays an important role in regulating synaptic translation (Darnell et al., 2011) and has been linked to aberrant translation of subpopulations of mRNAs (Gkogkas et al., 2013; Jung et al., 2014; Santini et al., 2013). Both Fmr1 knock-out (Fmr1KO) mice and patients exhibit abnormal dendritic spine morphology (Comery et al., 1997; Janusz et al., 2013; Rudelli et al., 1985), suggesting that synaptic connections might not be established correctly. Synaptic plasticity is altered in Fmr1KO mice, further supporting this hypothesis (Gkogkas et al., 2014; Huber et al., 2001; Osterweil et al., 2013).

According to the mGluR theory of FXS, loss of FMRP leads to an upregulation in translation of mRNAs through two major signalling axes: PI3K/Akt/mTOR (mechanistic target of rapamycin) (Sharma et al., 2010) and Ras/ERK (extracellular signal-regulated kinase)/Mnk (mitogen-activated protein kinase interacting kinases) (Osterweil et al., 2010). Upregulation of these pathways results in exaggerated global translation, altered synaptic plasticity (e.g. enhanced mGluR-dependent late long-term depression), and ASD-like behaviours in mice (Gkogkas et al., 2014; Osterweil et al., 2013).

3.1.2 FXS and MMP-9

Expression of matrix metalloproteinase 9 (MMP-9) is regulated through cap-dependent translation (Furic et al., 2010; Gkogkas et al., 2014) and its mRNA is translationally regulated by FMRP (Janusz et al., 2013). MMP-9 levels are elevated in tissues from Fmr1KO mice, and post-mortem tissue and plasma from FXS patients (Dziembowska et al., 2013; Gkogkas et al., 2014; Sidhu et al., 2014). Abdallah et al. (2012) *et al* reported elevated levels of MMP-9 in amniotic fluid from mothers of ASD patients. In addition, a mouse model overexpressing MMP-9 in the brain recapitulates some of the key phenotypes of FXS, such as abnormal dendritic spine morphology, repetitive/stereotypic behaviours, and social deficits (Gkogkas et al., 2014).

MMP-9 is a well-studied effector in neuroinflammation that has also been implicated in the regulation of synaptic plasticity and dendritic spine remodelling

(Nagy et al., 2006; Szepesi et al., 2013; Wiera et al., 2013). Correction of high levels of MMP-9 using inhibitors of the Ras/ERK/Mnk pathway (e.g. Lovastatin, Cercosporamide), inhibitors of MMP-9 (e.g. minocycline) or genetic deletion of upstream activators (Figure 3.1) has been shown to ameliorate several of the FXS phenotypes in Fmr1KO mice (Bilousova et al., 2008; Gkogkas et al., 2014; Janusz et al., 2013; Lovelace et al., 2016; Sidhu et al., 2014). Furthermore, treatment of Fmr1KO mice with metformin, a commonly used drug for diabetes that suppresses translation through inhibition of AMP-activated kinase upstream of both mTORC1 and ERK pathways, rescued several of the key FXS phenotypes, including elevated levels of MMP-9 (Gantois et al., 2017). Minocycline has also proven effective in treating FXS patients (Dziembowska et al., 2013).

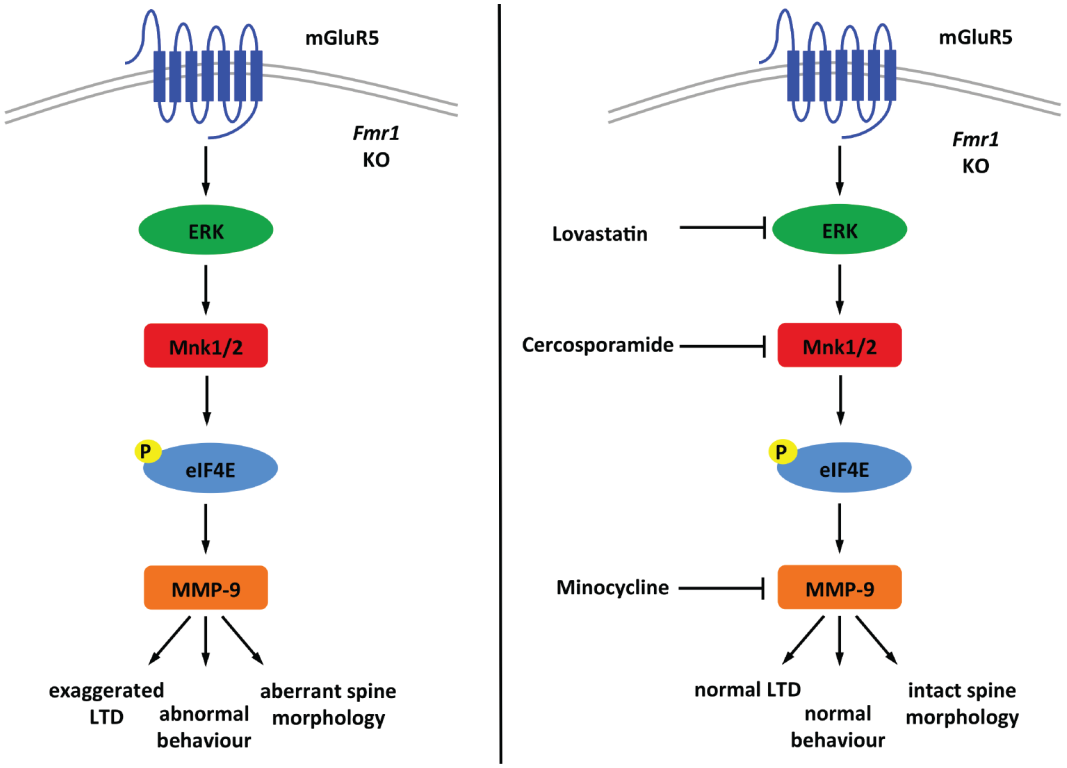

Figure 3.1 Regulation of Mmp-9 translation through mGluR5 and the Ras/ERK/Mnk pathway. In response to mGluR activation eIF4E is phosphorylated by Mnk1/2 and upregulates cap-dependent translation of Mmp-9. Right panel shows currently available and tested inhibitors of the pathway and at which stage they inhibit signalling.

MMP-9 cleaves several substrates within the extracellular matrix (ECM) that have the ability to influence intracellular signalling (Huntley, 2012). For instance, MMP-9 has been shown to cleave β1-integrins, cell surface receptors

that interact with the ECM and activate the PI3K/Akt/mTOR pathway (Sidhu et al., 2014; Yong, 2005), an important regulator of cell growth and translation in particular (Hay and Sonenberg, 2004). MMP-9 and other matrix metalloproteinases appear to play an important role in ASDs by proteolysing molecules such as neuroligins (Peixoto et al., 2012), cadherins, integrins and growth factors (Figure 3.2), some of which have previously been implicated in autism (Abdallah and Michel, 2013).

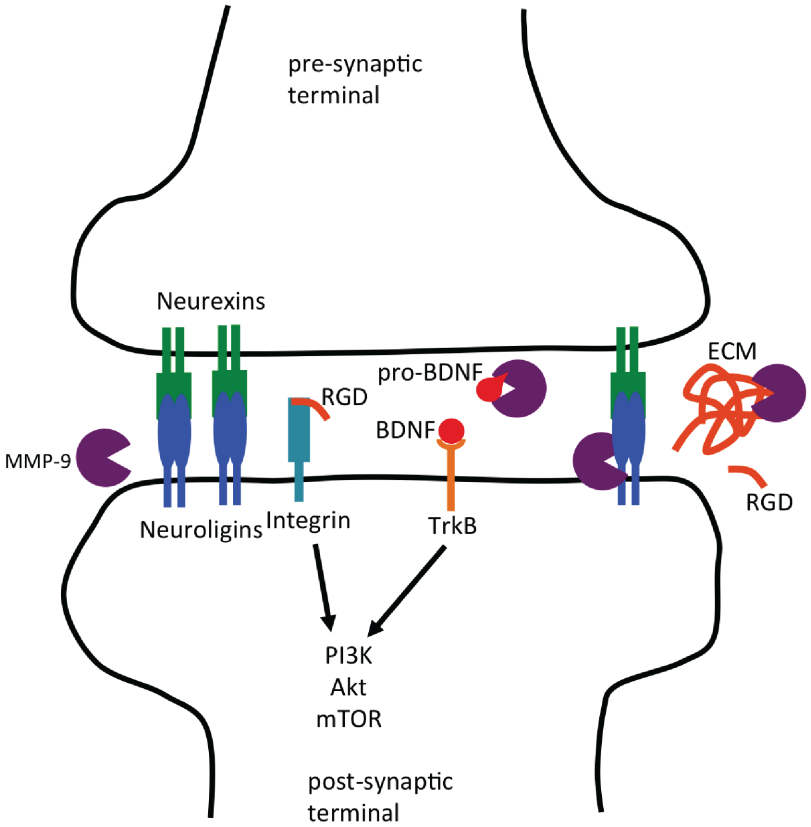

Figure 3.2 Cleavage substrates of MMP-9 at the synapse Previously established substrates of MMP-9 and how they may influence cell signalling. MMP-9 has been shown to cleave neuroligins in an activity-dependent fashion, altering synaptic transmission. Furthermore, MMP-9 has been shown to cleave growth factors such as pro-BDNF into its active form (BDNF), activating TrkB and downstream mTORC1 signalling. MMP-9 cleaves various components of the ECM, resulting in short RGD (arginylglycylaspartic acid) peptides, which can activate integrin signalling, which is upstream of the PI3K/Akt/mTORC1 cascade.

3.1.3 Aims

With the experiments presented in this chapter, we aimed to elucidate the role of upregulated MMP-9 in FXS. It has been extensively shown that upregulation of MMP-9 plays a significant role in the aetiology of FXS and several studies lowering MMP-9 levels either pharmacologically or genetically have been shown to treat key phenotypes of FXS in rodent models and patients. We hypothesised that MMP-9 contributes to FXS phenotypes through regulating a secondary wave of upregulated translation. Specifically, we wanted to understand the effects of upregulating MMP-9 in the brain outwith the context of FXS on several levels of translation regulation: global translation, regulation of signalling pathways impinging on translation, and transcript-specific changes in translation. Lastly, we also aimed to compare these results to a commonly used model of FXS, a *Fmr1* knock-out mouse.

3.2 Materials and methods

3.2.1 TgMMP9 mice

TgMMP9 mice overexpress full-length human proMMP-9 under the PDGF-B (platelet-derived growth factor B-chain) promoter, which provides brain-specific expression of MMP-9 (Fragkouli et al., 2012). A genetic construct containing the PDGF-B promoter and the MMP-9 cDNA, was injected into fertilised mouse oocytes, where it randomly inserted into the genome, to generate transgenic founders (Figure 3.3). All animal experiments were carried out in agreement with the ethical recommendation of the European Communities Council Directive of 22 September 2010 (2010/63/EU). Tissue was obtained from transgenic mice and wildtype controls directly from Dr. Tzinia's lab at the National Center for Scientific Research Demokritos.

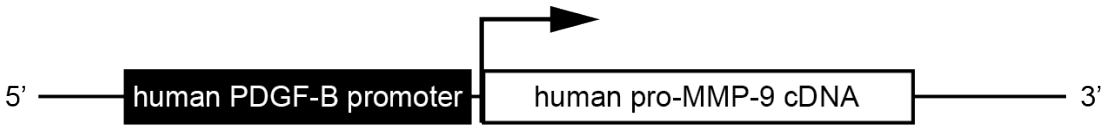

Figure 3.3 TgMMP9 genetic design. Schematic depicting the cloned cDNA construct that was injected into fertilised mouse oocytes to generate transgenic founder mice. The cloning procedure was described in Fragkouli et al. (2012), the construct contains full length human pro-MMP-9 cDNA under the control of the human PDGF-B promoter.

3.2.2 Fmr1KO mice

All procedures were in accordance with United Kingdom Home Office and were approved by the University of Edinburgh. Animals were kept under standard husbandry conditions, with *ad libitum* access to food and water, unless otherwise specified. The animal facility was operated on a 12 h light/dark cycle.

$Fmr1^{Y/-}$ mice were obtained from Jackson Laboratories (003025) and were originally generated trough a targeted mutation at Dr Ben Oostra's laboratory at Erasmus University in the Netherlands (The Dutch-Belgian Fragile X Consortium, 1994) (Figure 3.4).

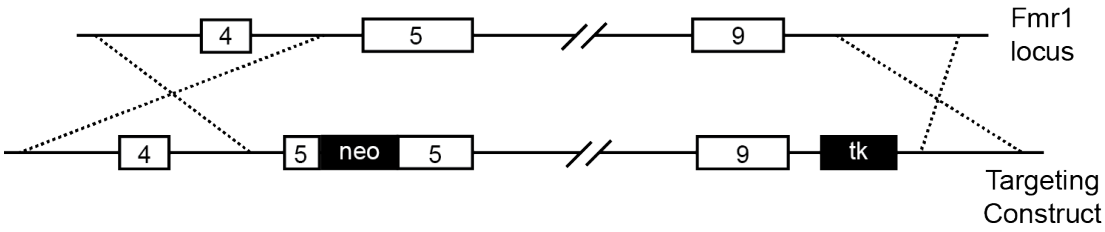

Figure 3.4 Fmr1KO genetic design. A scheme showing how the *Fmr1* targeted mutation was designed. Exon 5 of the gene was disrupted by inserting a neomycin resistance cassette (*neo*). Further, thymidine kinase (*tk*) was inserted 3' of the genomic sequence as a negative selection marker gene. Adapted from The Dutch-Belgian Fragile X Consortium (1994).

3.2.3 Puromycin release assay

The Puromycin release assay was carried out in the Gkogkas lab by Dr. Inês S. Amorim.

This method was adapted from Eacker et al. (2017), which uses a variation of the SUnSET method (Schmidt et al., 2009) and was previously described in Biever et al. (2015). Frozen forebrain tissue was homogenised in 1 ml puromycin release buffer (10 mM HEPES pH 7.4, 5 mM $MgCl_2$, 150 mM KCl, 200 µM emetine, 0.5 mM DTT, EDTA-free protease inhibitors, 200 µM ATP, 100 µM GTP), using a motorised pestle. The homogenate was incubated on ice for 15 min, with occasional vortexing. The lysate was cleared by centrifugation at 12,000 RCF for 10 min at 4℃ and the supernatant transferred to a fresh tube. The protein concentration was determined by A_{280} absorbance measurements on a NanoDrop™ 2000 (ThermoFisher, ND-2000) and all samples adjusted to 5 mg/ml protein concentration with puromycin release buffer (PRB).

Puromycin (Merck, P7255-100MG) was added to 100 µl sample aliquots to a final concentration of 1.25 mM. The samples were incubated for 10, 30, or 60 min at 37℃. Once the incubation was finished, reactions were stopped by adding EDTA at a final concentration of 25 mM. To prepare samples for Western blotting, 50 µl of the Puromycin incorporation reactions were diluted with 20 µl ddH_2O and mixed with 30 µl of 4X SDS-PAGE Loading Buffer (200 mM Tris-HCl pH 6.8, 400 mM DTT, 8% (w/v) SDS, 40% (v/v) Glycerol, 0.4% Bromophenol Blue).

3.2.4 Other methods

Ribosome profiling (including GO analysis and UTR analysis) and Western blotting methods are outlined in Chapter 2 "General materials and methods".

3.3 Results

3.3.1 Global protein synthesis is unaffected in animals conditionally overexpressing human MMP-9 in the brain

Since loss of FMRP has been shown to result in global upregulation of translation (Gkogkas et al., 2014; Osterweil et al., 2013; Sharma et al., 2010), we wanted to see whether a transgenic mouse model overexpressing human pro-MMP-9 under the control of a brain specific promoter (from here on referred to as TgMMP9), would result in a similar molecular phenotype. TgMMP9 animals have previously been shown to mimic the social deficits, repetitive/stereotypic behaviours, and abnormal dendritic spine morphology observed in models of FXS. To test our hypothesis, we used an *in vitro* Puromycin incorporation assay, which functions in a pulse-chase fashion and labels all proteins newly synthesised during the duration of the experiment.

We tested whole forebrain lysates from TgMMP9 animals and wildtype (WT) littermates at three different timepoints (10, 30, and 60 min) of Puromycin incorporation. Although we found a trend towards decreased Puromycin incorporation at the 60 min timepoint in the TgMMP9 animals (Figure 3.5 E, F), we did not observe any statistically significant differences in protein synthesis rates between TgMMP9 and WT animals at any of the timepoints (Figure 3.5).

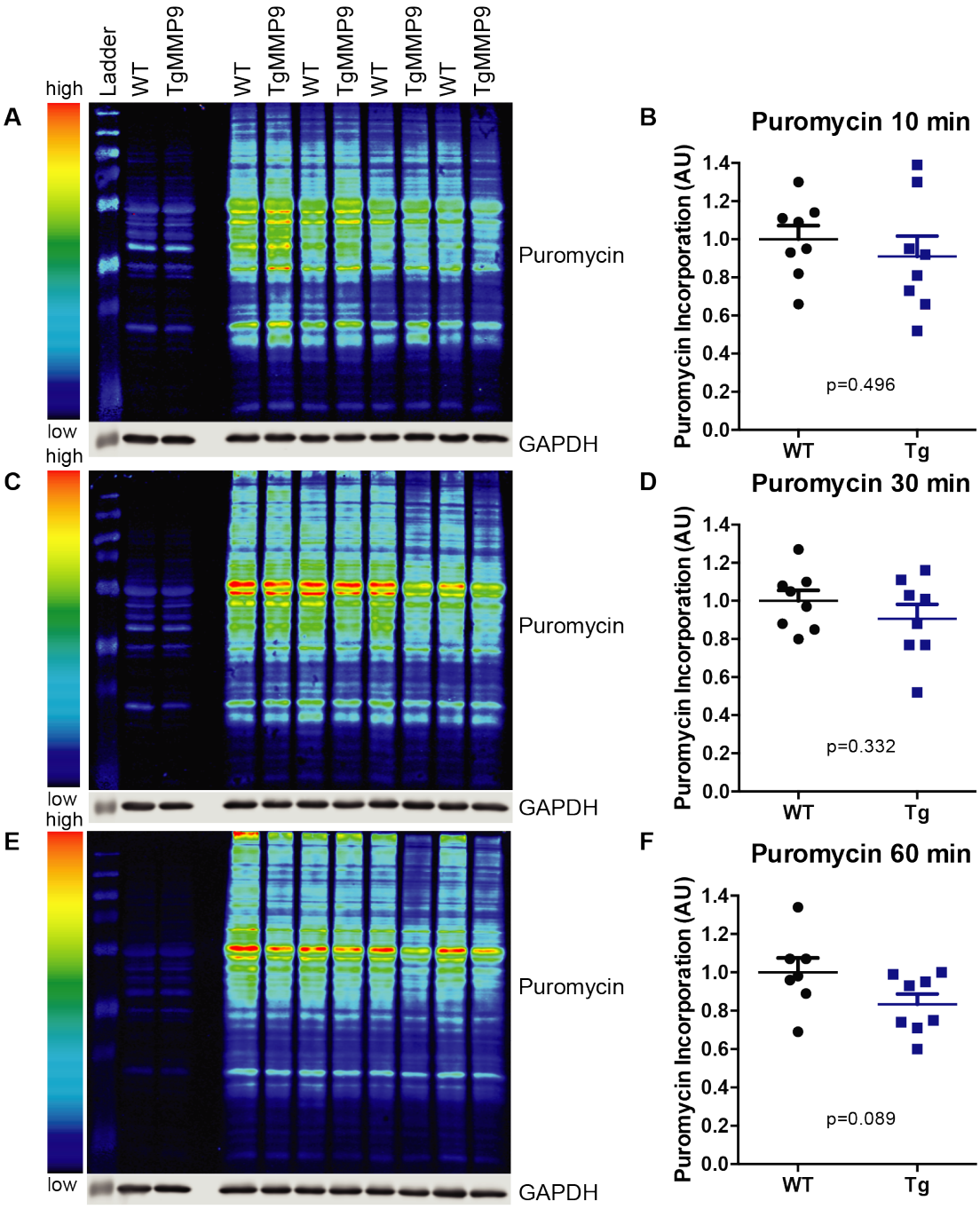

Figure 3.5 Global translation activity levels are unchanged in TgMMP9 brains. **A, C, E** Representative images of Western blots for samples run through Puromycin release assay (10, 30, 60 min). The blots were probed with an anti-Puromycin antibody and anti-GAPDH, as a loading control. **B, D, F** Quantification of Western blots for Puromycin, values were normalised to the loading control (n = 8 for each genotype) and are represented relative to WT average. Shown are mean and standard error of the mean (SEM), including individual data points. Student's t-test was used to evaluate changes. **A, B** Experimental timepoint 10 min. **C, D** Experimental timepoint 30 min. **E, F** Experimental timepoint 60 min.

3.3.2 Signalling pathways upstream of translation are unchanged in animals conditionally overexpressing human MMP-9 in the brain

To evaluate the role of MMP-9 upregulation in the brain, specifically, in regulation of translation, we probed for phosphorylation of major hubs in the PI3K/Akt/mTOR and Ras/ERK/Mnk pathways using Western blotting. We did not observe any significant changes in phosphorylation of PI3K/Akt/mTOR components AKT (Ser473, p = 0.7435) (Figure 3.6 C, F), ribosomal protein S6 (Ser235/236 p = 0.6832)(Figure 3.6 A, D), and 4E-BP1/2 (Thr34/46, p = 0.8048 and 0.2652, for isoforms 1 and 2, respectively) (Figure 3.6 A, D). Equivalently, we were not able to detect any differences in phosphorylation of components of the Ras/ERK/Mnk pathway, namely ERK (p = 0.2385) and eIF4E (p = 0.8194) (Figure 3.6 B, E).

Further, we probed for phosphorylated and total focal adhesion kinase (FAK) which had previously been shown to be upregulated in response to treatment with recombinant MMP-9 in hippocampal cultures (Sidhu et al., 2014). We did not observe any changes in phosphorylation of FAK in TgMMP9 animals (p = 0.6680) (Figure 3.6 C, F).

Taken together, we did not detect any significant changes in signalling pathways upstream of translation in forebrain tissue overexpressing MMP-9, compared to WT controls.

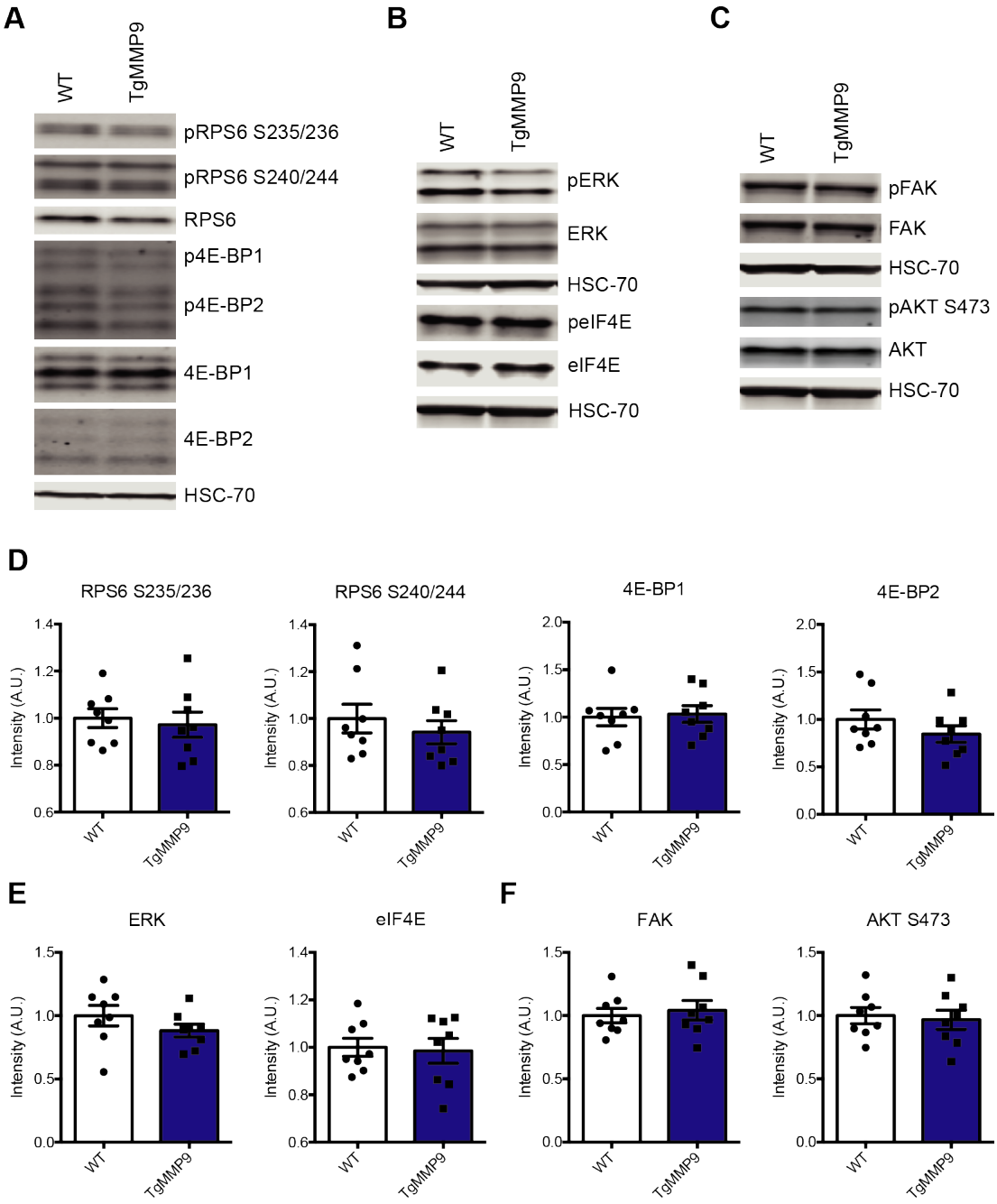

Figure 3.6 Phosphorylation levels of signalling pathways upstream of translation are unchanged in TgMMP9 brains. A-C Representative images of Western blots probed with phospho and total antibodies against the indicated signalling molecules, to assess activation levels. HSC-70 was used as a loading control. **A** Blots against key components of the mTOR pathway, ribosomal protein S6 (RPS6, two distinct phospho sites) and 4E-BP1/2. **B** Blots against key components of the ERK/Mnk pathway, extracellular signal-regulated kinase (ERK) and eukaryotic initiation factor 4E. **C** Blots against Protein kinase B (AKT, upstream signal of mTORC1) and focal adhesion kinase (FAK, important regulator of cell migration). **D-F** Quantification of the Western blots, n = 8 for each genotype. Values shown are phospho signal intensity normalised to total protein expression and relative to WT average. Shown are mean and standard error of the mean (SEM), including individual data points. No significant differences between WT and TgMMP9 were found in a Student's t-test.

3.3.3 Conditional overexpression of human MMP-9 in the brain does not significantly alter mRNA expression or translation

Faced with the apparent diversion of the global translation and signalling pathways phenotypes between TgMMP9 and Fmr1KO animals, we set out to explore translation in the TgMMP9 animals in a less biased and more global fashion. To study changes in translation of individual mRNAs in detail, we prepared ribosome profiling libraries from TgMMP9 whole forebrain samples. Ribosome profiling is an unbiased method that employs nuclease footprinting of translating ribosomes followed by next generation sequencing to quantitatively assess the translation status (i.e. ribosome occupancy) of each transcript present in the sample. The sequencing libraries we prepared showed great reproducibility between replicates for both footprint and total mRNA transcript abundance (Figure 3.7 A, $r^2 > 0.95$ for all replicate comparisons). Furthermore, as expected for ribosome profiling libraries, the ribosomal footprints showed a high read abundance between 28 and 30 nt, whereas total RNA, which was randomly fragmented to yield similar sized fragments, showed a more random size distribution and slightly larger fragments (Figure 3.7 B).

Reads from footprint samples aligned preferentially with the first open reading frame of their respective transcripts, while total mRNA reads aligned equally with all three reading frames (Figure 3.7 C). As demonstrated in Figure 3.7 D, footprint samples show a clear three nucleotide periodicity, when compared to total RNA reads, which align randomly along transcripts. Moreover, we observed a peak in footprint abundance around both the start and stop codons of messages, indicating that captured footprints originated indeed from translating ribosomes (Figure 3.7 D).

The overexpression of MMP-9 does not appear to have strong effects on the transcription and translation of specific mRNAs, which is in accordance with our Puromycin incorporation data. In the TgMMP9 animals, we observed 8 transcriptionally significantly upregulated mRNAs and 10 downregulated transcripts (Figure 3.8 A, Table A.1). We saw slightly more significant changes in translation with 22 translationally upregulated transcripts and 22 downregulated transcripts (Figure 3.8 B, Table A.2).

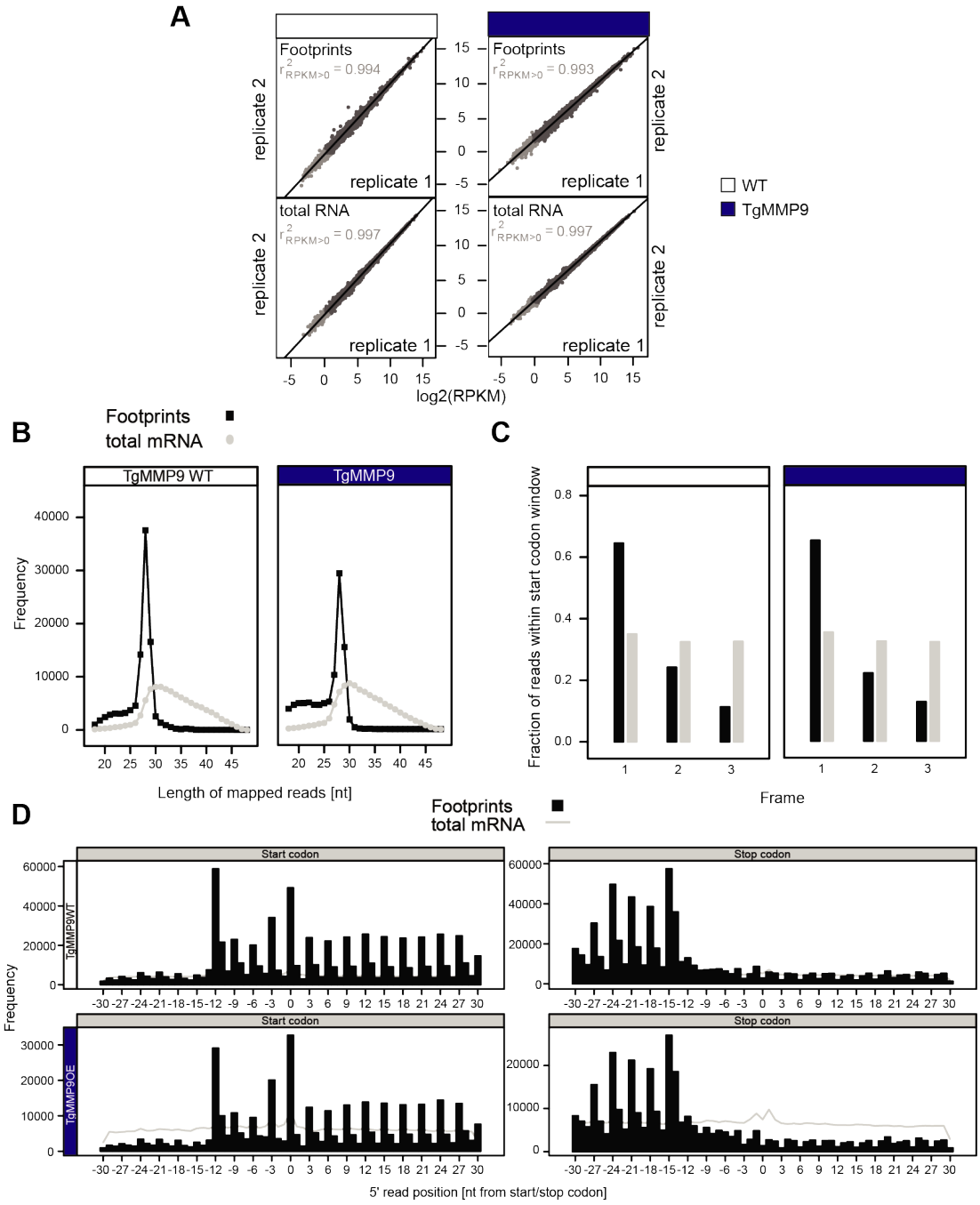

Figure 3.7 Ribosome profiling data for TgMMP9 is of high quality and reproducibility. A Replicates were plotted against each other and show a very high correlation between each other, confirming the reproducibility of our data. **B** Sequenced cDNA library fragments show the expected length distributions, a sharp peak between 28 and 30 nt for the footprints and a flat, random distribution for total RNA samples. **C** The majority of the footprints align with the first open reading frame of a transcript, whereas the randomly fragmented total RNA aligns equally to all reading frames. **D** Ribosomal footprints cluster around Start and Stop codons and show a 3 nt periodicity. Plots of representative samples, visualising how reads align relative to start and stop codons of their respective mRNA. Overall, footprints show peaks around start and stop codons, as well as a 3 nt periodicity, while total mRNA aligns randomly along the message.

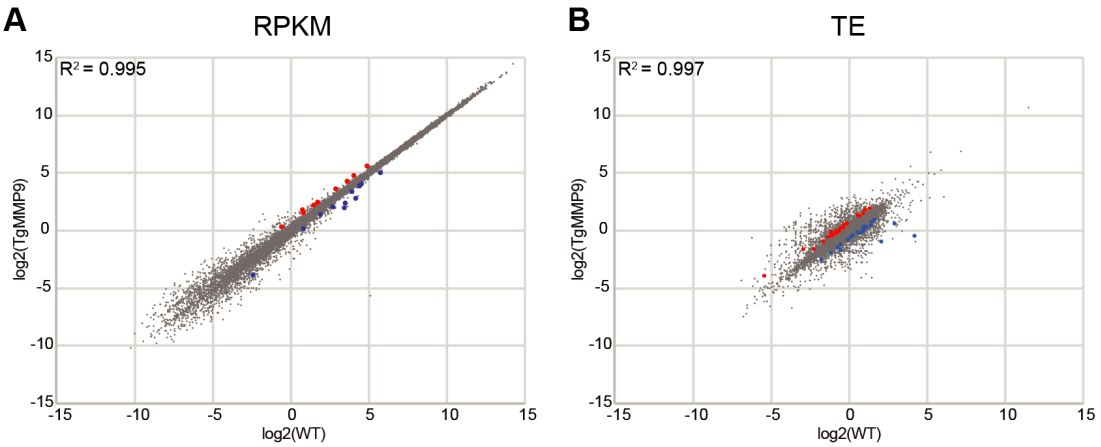

Figure 3.8 Read counts and TE of TgMMP9 show little differences compared to WT. Scatter plots (WT vs TgMMP9) of the $\log_2$ mean read count and mean TE values for each set of sequencing replicates (n = 3). Blue indicates significantly downregulated genes, red significantly upregulated genes in the dataset. **A** Mean read count of WT vs TgMMP9. R^2 = 0.99518785 **B** Mean TE of WT vs TgMMP9. R^2 = 0.996749746

3.3.3.1 Gene ontology analysis of TgMMP9 DEGs and DTGs

To determine any functional relationships within the DEGs and DTGs, we performed DAVID (Database for Annotation, Visualization and Integrated Discovery, v6.8) analysis (Huang et al., 2009a,b) and IPA (Qiagen). We identified significantly enriched GO terms in the biological process, cellular component, and molecular function categories in the DEG list using DAVID. Notable categories include glycinergic synaptic transmission, extracellular matrix organisation, and proteinaceous extracellular matrix (Figure 3.9 A). In the DTGs identified for TgMMP9 brains, only few terms were significantly enriched (Figure 3.9 B).

Similarly, we identified some interesting enriched Ingenuity Canonical Pathways and Diseases/Function Annotations, as well as networks in our data with the help of IPA, using a neuronal tissue specific analysis. In the DEGs, IPA identified Calcium signalling, FAK signalling, VEGF signalling, eIF2 signalling, and Integrin signalling. Moreover, molecules relating to familial Alzheimer disease, Alzheimer disease, and function of the blood-brain barrier were enriched in the data (Figure 3.10 A). We further identified a network (Figure 3.11 A), that includes interesting nervous system regulators (APP, neuropeptide Y, sodium- and chloride-dependent glycine transporter). Few terms were identified for the TgMMP9 DTGs but included synaptic long term depression and several nervous system development annotations, (Figure 3.10 B). Network analysis identified a

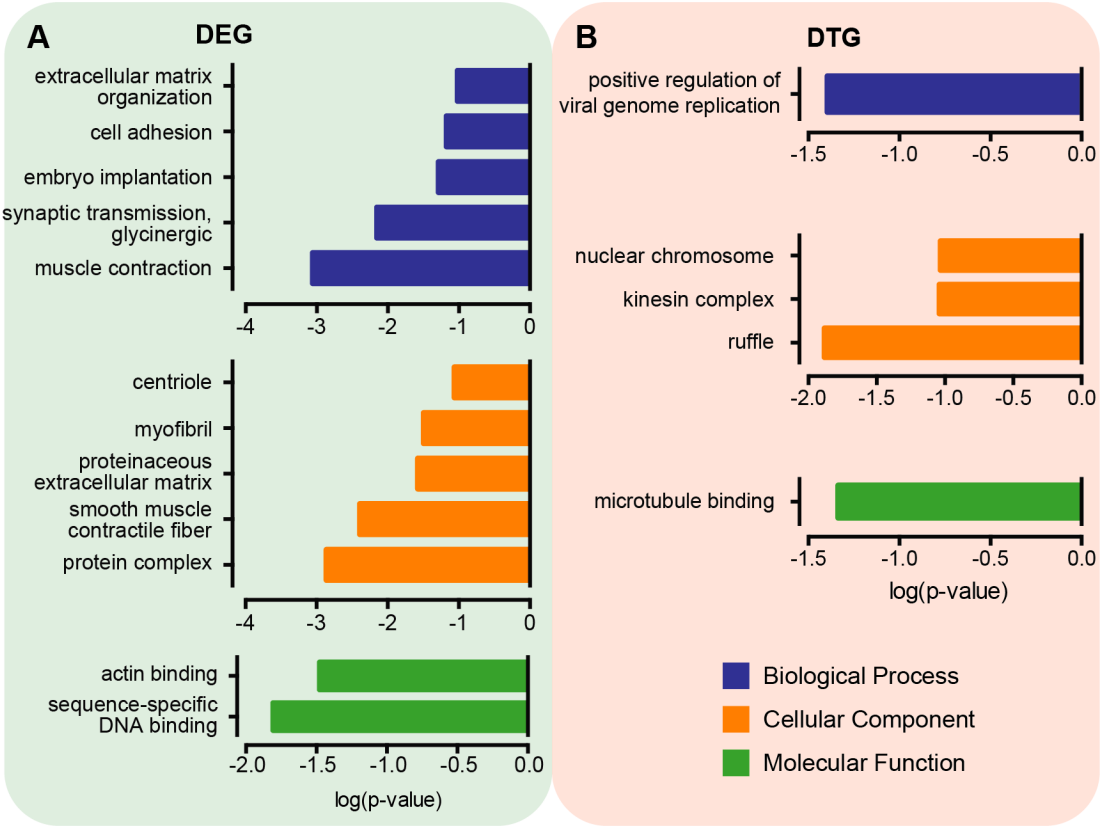

Figure 3.9 Significantly enriched GO categories in TgMMP9 DEGs and DTGs. Plots summarising the identified categories for DEGs and DTGs and associated p-values, retrieved from DAVID. **A** Functional categories identified in TgMMP9 DEGs. **B** Functional categories identified in TgMMP9 DTGs.

regulatory network including Fus (RNA binding protein), APP, and Presenilin-1 (Figure 3.11 B).

Taken together, GO analysis identified some interesting terms and annotations that may be relevant to the aetiology of the FXS. However, regulation of mRNA translation through overexpression of MMP-9 does not appear to explain the phenotypes observed in Fmr1KO animals. On the other hand, our data supports the previously studied involvement of MMP-9 in Alzheimer's disease (Fragkouli et al., 2012).

Figure 3.10 Significantly enriched Ingenuity Canonical Pathway and Diseases and Function annotations in TgMMP9 DEGs and DTGs. Plots summarising the identified categories for DEGs and DTGs and associated p-values, retrieved from IPA. **A** Functional categories identified in TgMMP9 DEGs. **B** Functional categories identified in TgMMP9 DTGs.

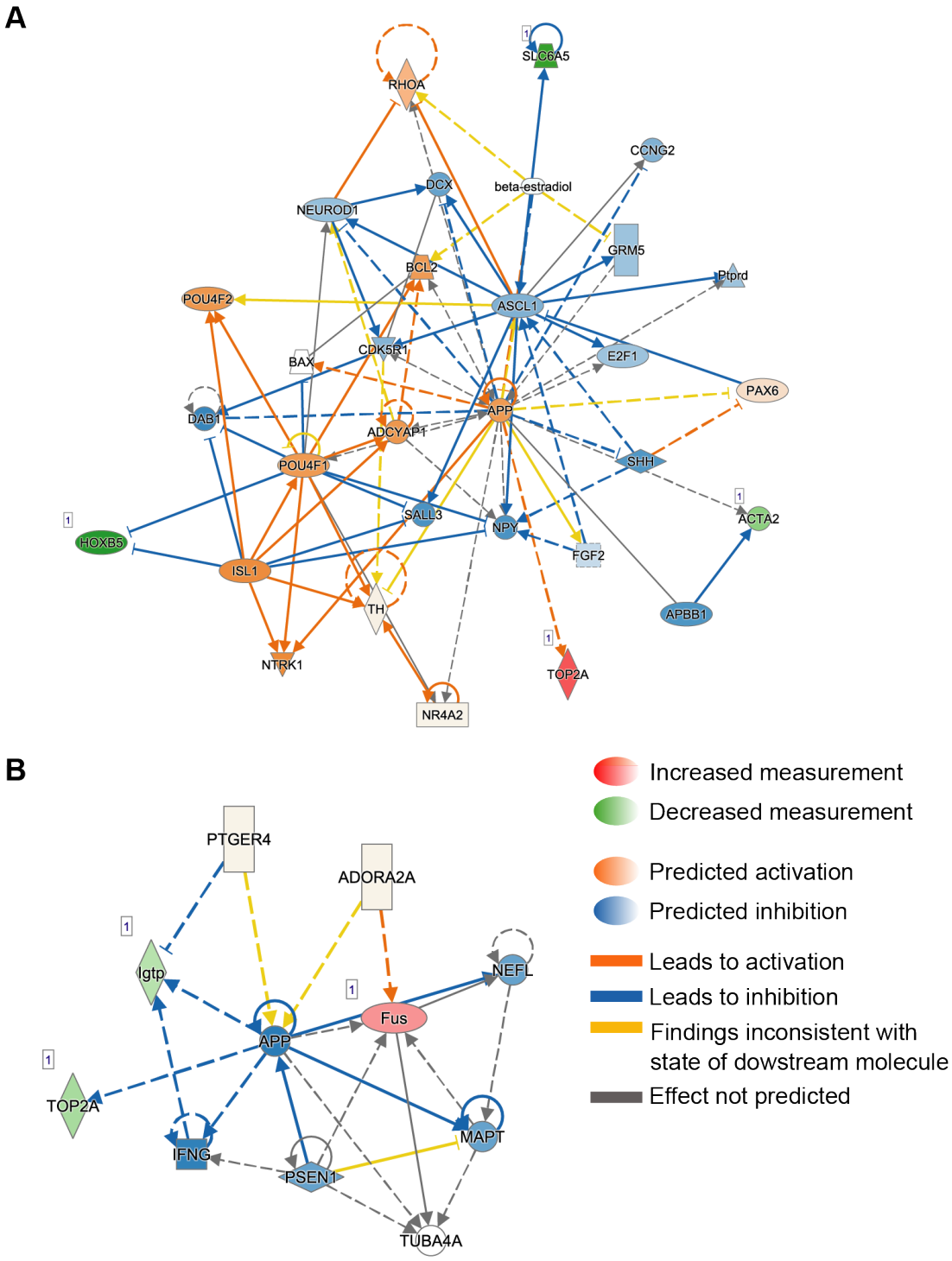

Figure 3.11 Significant networks including molecule activity prediction in TgMMP9 DEGs and DTGs. Networks identified in the DEG/DTG lists from the TgMMP9 data using IPA, including a molecule activity prediction (MAP) **A** Network identified in TgMMP9 DEGs. **B** Network identified in TgMMP9 DTGs.

3.3.3.2 UTR analysis of TgMMP9 DTGs

Untranslated regions (UTR) of transcripts can have a considerable effect on their stability and/or translation. Therefore, we carried out UTR analysis of the DTGs in our data, looking for common, known motifs and examining basic UTR statistics, namely guanine-cytosine (GC) content, length, and Gibbs free (folding) energy. We did not detect significant occurrence of any motifs in neither the 5' UTR nor the 3' UTR, comparing the up- and downregulated gene groups. However, there was a trend towards an increased number of upstream open reading frames (uORF) in the 5' UTRs downregulated genes (Figure 3.12 A, B). 3' UTRs of upregulated genes were significantly longer than 3' UTRs of downregulated genes. We did not find significant changes between any other UTR parameters (Figure 3.12 C, D).

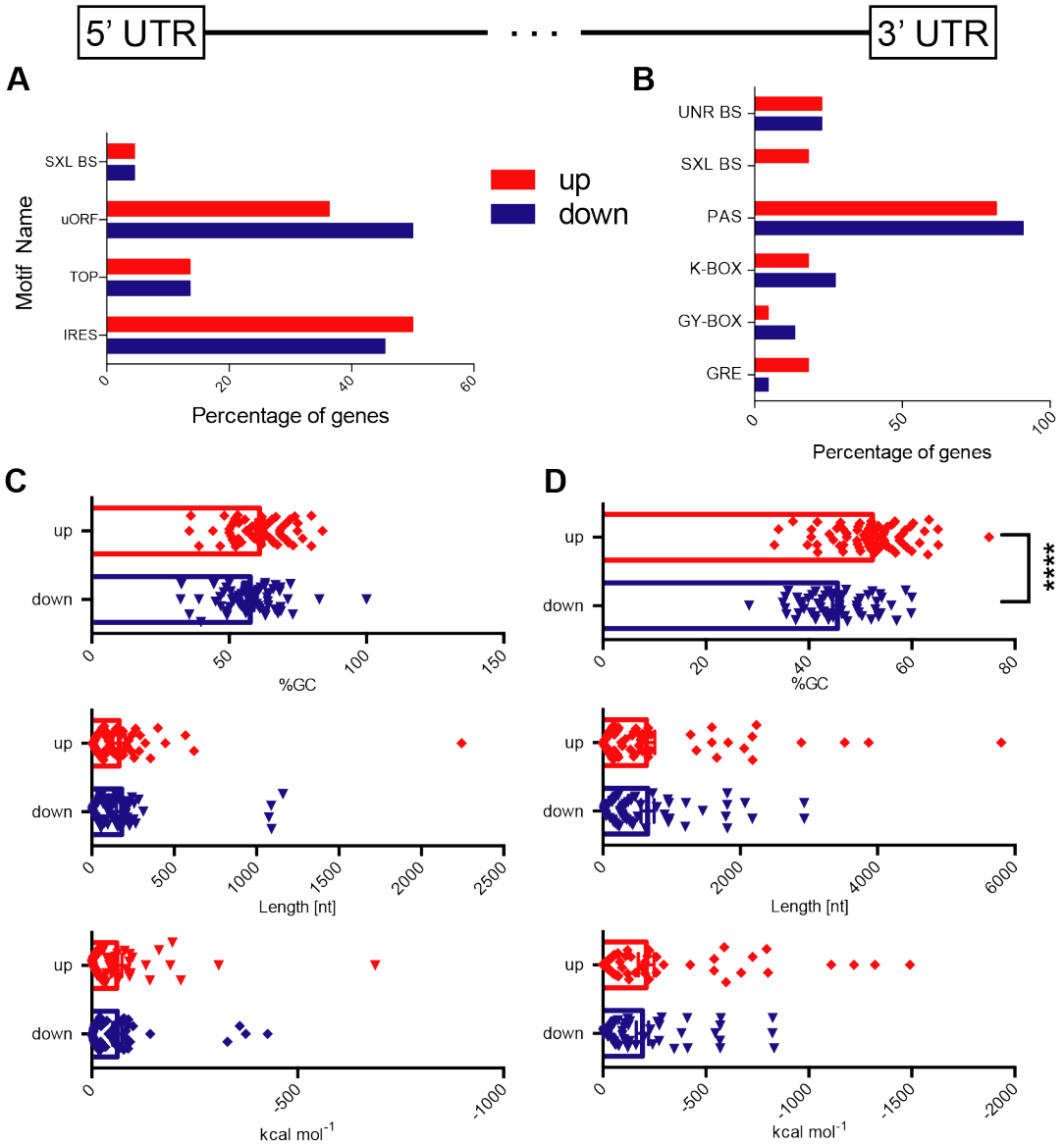

Figure 3.12 UTR motif and basic statistics analysis of TgMMP9 DTGs. **A** Motifs identified in the 5' UTR of up- and downregulated DTGs. The bars represent the percentage of genes (UTRs) containing one or more of the indicated motifs. **B** RNA motifs identified in the 3' UTR of up- and downregulated DTGs. The bars represent the percentage of genes (UTRs) containing one or more of the indicated motifs. **B-C** Bar graphs for the indicated values, represented as mean $\pm$ standard error of the mean, including the individual data points. Shown are percentage of GC nucleotides in the UTR, length of UTR, and Gibbs free (folding) energy of UTR sequence. **C** GC content, length and Gibbs free energy calculated for 5' UTRs of the DTGs. **D** GC content, length and Gibbs free energy calculated for 3' UTRs of the DTGs. *** $p \leq 0.0001$ Student's t-test.

3.3.4 Ribosome profiling of Fmr1KO brain tissue reveals minor changes in transcription and TE

To gain a better understanding of the translational profile of Fmr1KO brains and how it compares to the data collected on TgMMP9 animals, we proceeded to generate ribosome profiling libraries from adult Fmr1KO forebrains and WT controls. Fmr1KO libraries were of comparable quality to TgMMP9 libraries (Figure 3.13 A-D) and did not show gross changes in global translation (Figure 3.15). In Fmr1KO animals, 25 mRNAs were transcriptionally downregulated and only 3 transcripts upregulated, in our dataset (Figure 3.14 A, Table A.3). TE was also lightly affected by the mutation with 16 upregulated genes and 19 downregulated genes (Figure 3.14 B, Table A.3).

Same as for the TgMMP9 data, we carried out GO analysis using DAVID and IPA. Relevant GO terms enriched in the DAVID analysis of Fmr1KO animals were regulation of neuronal synaptic plasticity, extracellular region, extracellular space, and calcium ion (Figure 3.16 A). For the DTGs, we identified significantly enriched functional terms in the biological process, cellular component, molecular function, and Biocarta Pathway categories in DAVID. Some of the key categories enriched in the DTGs include positive regulation of MAP kinase activity, cytosolic small ribosomal subunit, intracellular ribonucleoprotein complex, and p38 MAPK Signalling Pathway (Figure 3.16 B).

In the IPA analysis for Fmr1KO DEGs, the categories include HIPPO Signalling, PI3K Signalling in B Lymphocytes, Calcium Signalling, Hyperpolarisation of neurons, Plasticity of neuronal synapse, and several transcriptional regulators, as well as cytoplasmic FMRP interacting protein 1 (CYFIP1) and amyloid precursor protein (APP) as upstream regulators of the genes in our data set (Figure 3.17 A). Interestingly enough, IPA also identified a network in the data (Figure 3.18 A) that relates to behaviour and nervous system development and function terms and predicts changes in activity in several genes related to disease and essential to normal function of the brain (APP, huntingtin, glutamate receptor 1 precursor).

For the DTGs in the Fmr1KO data, IPA found canonical pathways related to translation, namely STAT3 Pathway, p38 MAPK signalling, HIPPO Signalling, TGF-β Signalling, mTOR signalling, and eIF2 signalling. Furthermore, APP and apolipoprotein E were in the list of upstream regulators (Figure 3.17 B). A

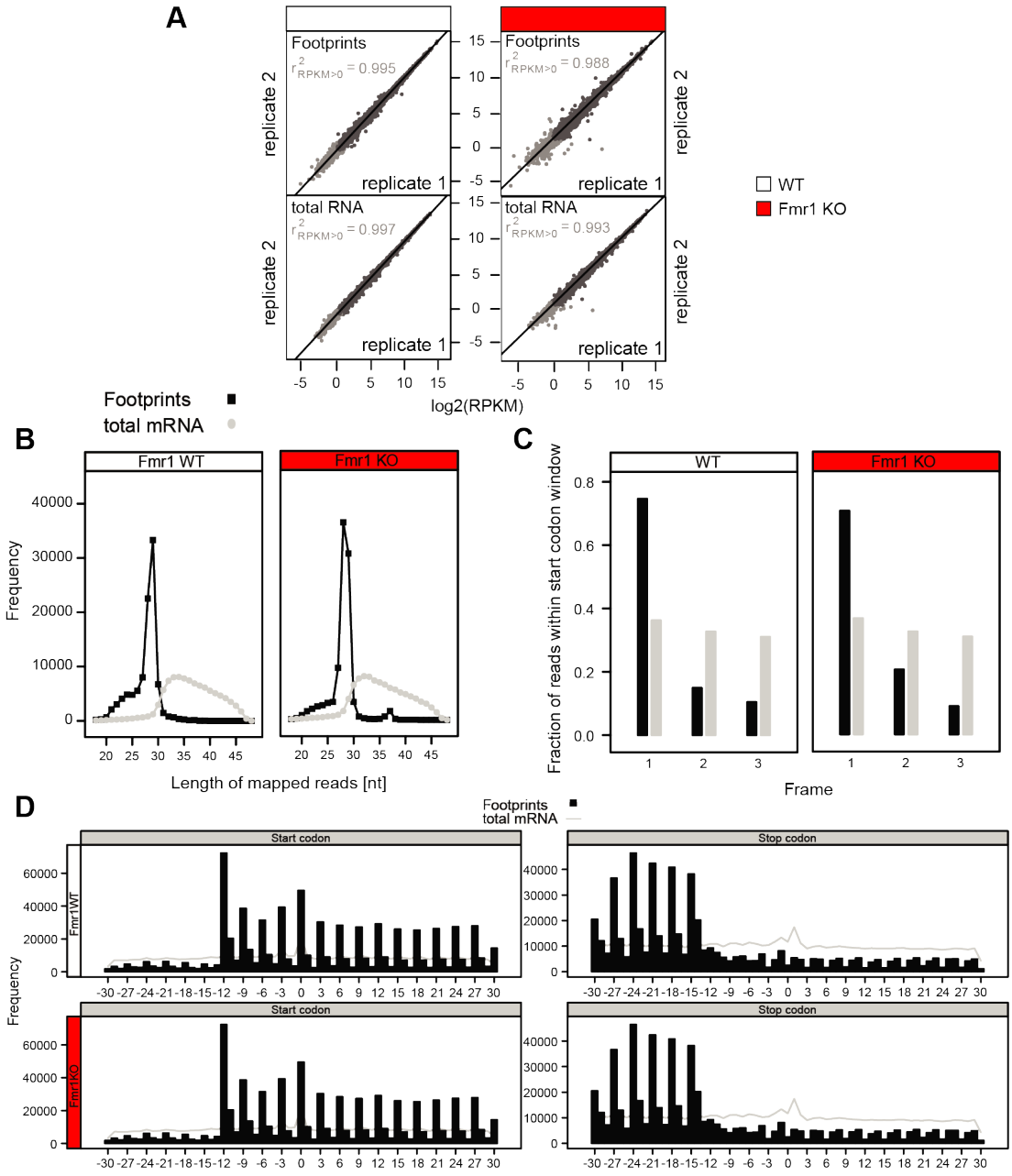

Figure 3.13 Ribosome profiling data for Fmr1KO is of high quality and reproducibility. A Replicates were plotted against each other and show a very high correlation between each other, confirming the reproducibility of our data. **B** Sequenced cDNA library fragments show the expected length distributions, a sharp peak between 28 and 30 nt for the footprints and a flat, random distribution for total RNA samples. **C** The majority of the footprints align with the first open reading frame of a transcript, whereas the randomly fragmented total RNA aligns equally to all reading frames. **D** Ribosomal footprints cluster around Start and Stop codons and show a 3 nt periodicity. Plots of representative samples, visualising how reads align relative to start and stop codons of their respective mRNA. Overall, footprints show peaks around start and stop codons, as well as a 3 nt periodicity, while total mRNA aligns randomly along the message.

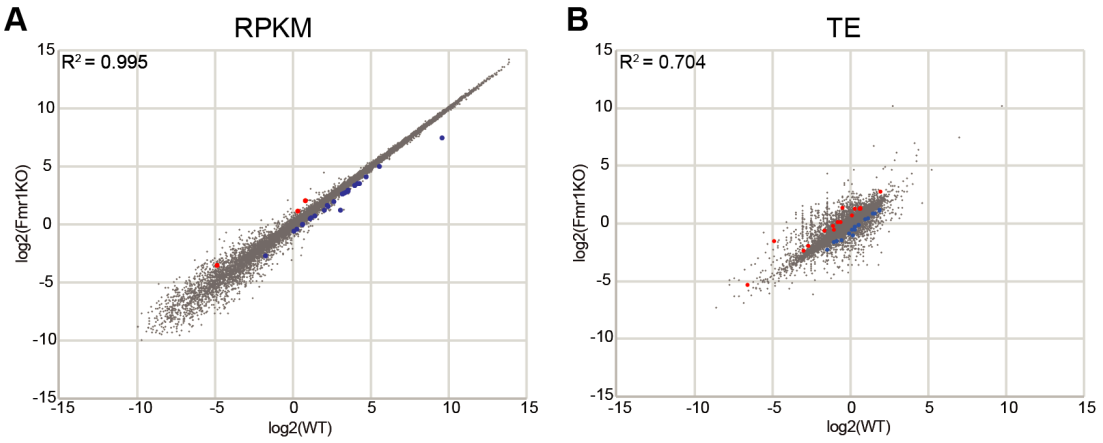

Figure 3.14 Read counts and TE of Fmr1KO show little differences compared to WT. Scatter plots (WT vs Fmr1KO) of the $\log_2$ mean read count and mean TE values for each set of sequencing replicates (n = 3). Blue indicates significantly downregulated genes, red significantly upregulated genes in the dataset. **A** Mean read count of WT vs Fmr1KO. R^2 = 0.99548689 **B** Mean TE of WT vs Fmr1KO. R^2 = 0.704016563

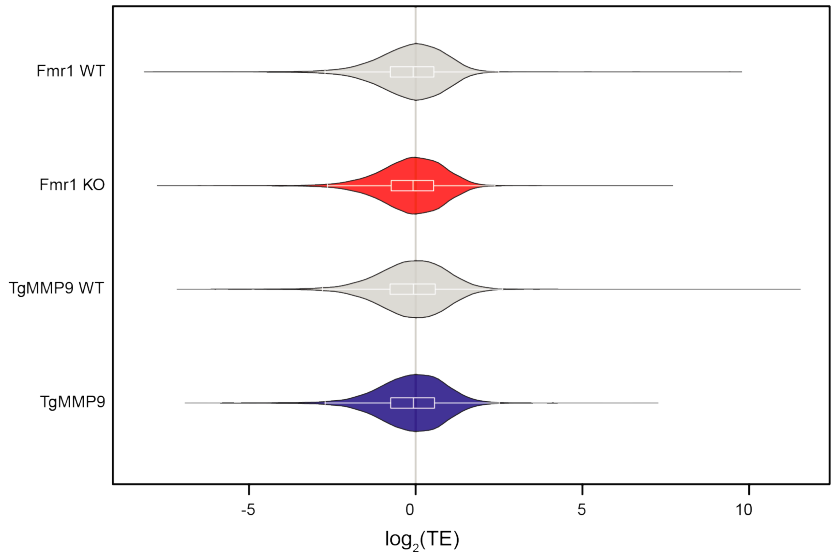

Figure 3.15 Ribosome profiling reveals no global changes in TE between WT, TgMMP9, and Fmr1KO. Violin plots of the translational efficiency by genotype, showing that there are no significant changes in global translation.

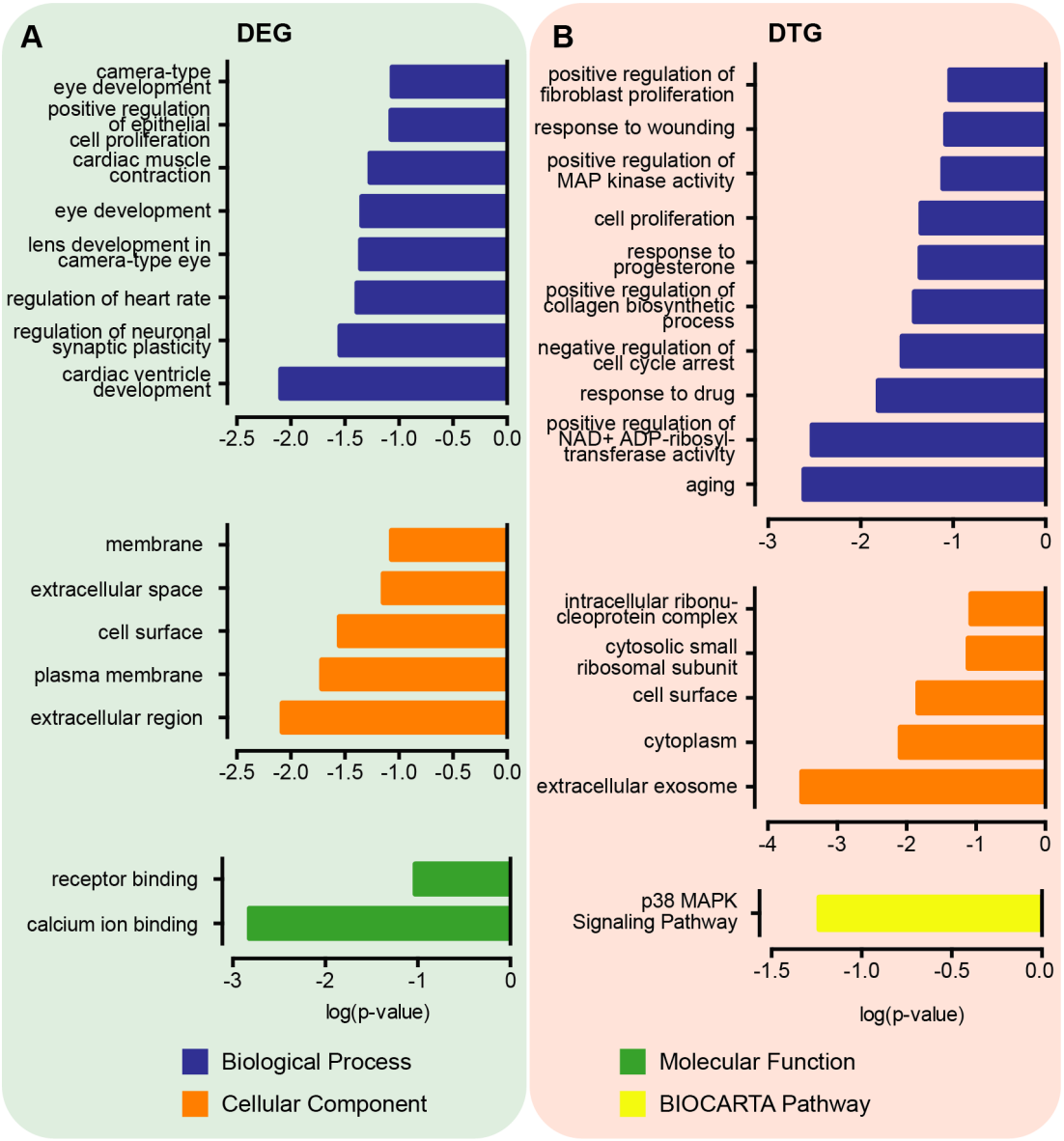

Figure 3.16 Significantly enriched GO categories in Fmr1KO DEGs and DTGs. Plots summarising the identified categories for DEGs and DTGs and associated p-values, retrieved from DAVID. **A** Functional categories identified in Fmr1KO DEGs. **B** Functional categories identified in Fmr1KO DTGs.

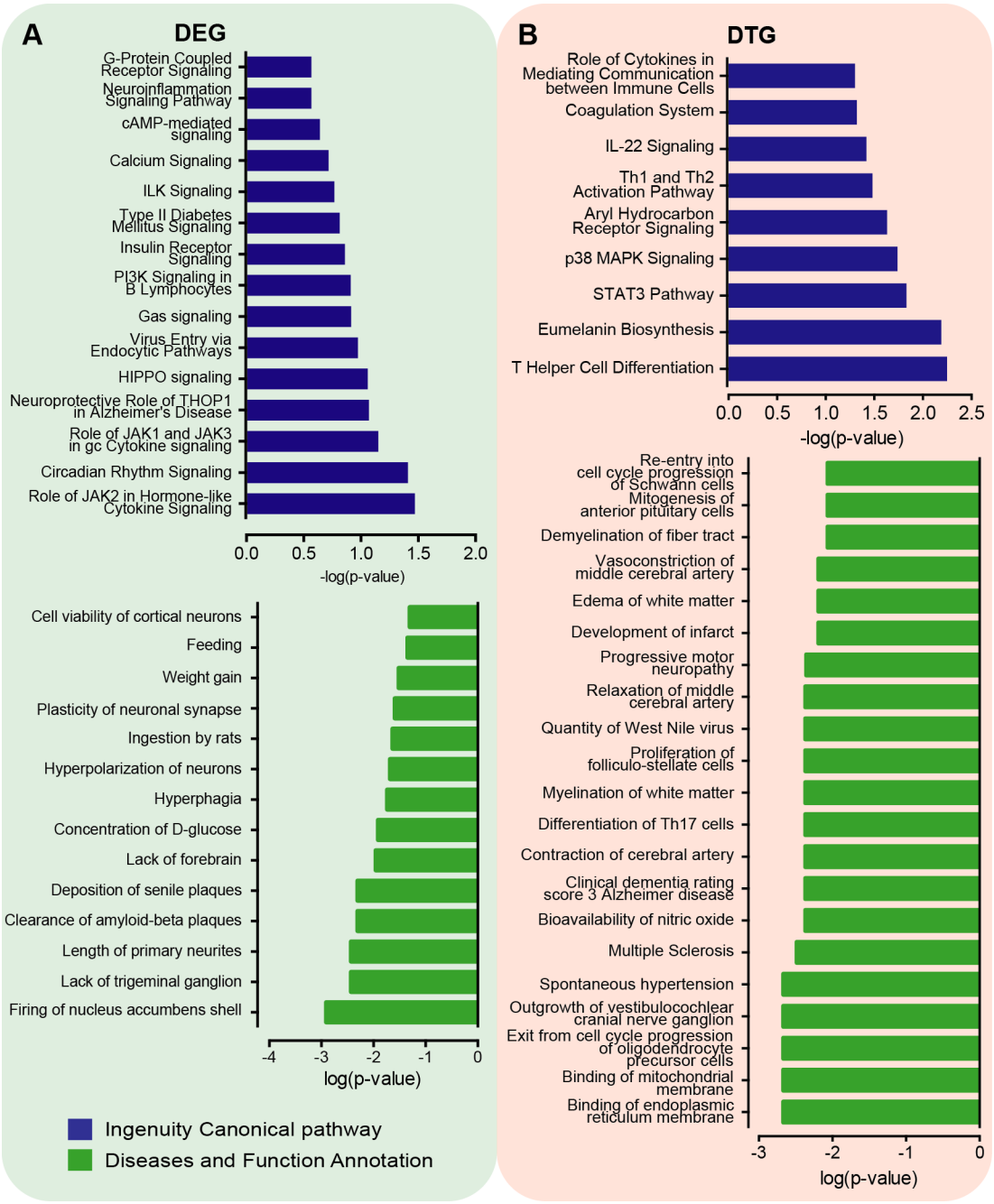

Figure 3.17 Significantly enriched Ingenuity Canonical Pathway and Diseases and Function annotation in Fmr1KO DEGs and DTGs. Plots summarising the identified categories for DEGs and DTGs and associated p-values, retrieved from IPA. **A** Functional categories identified in Fmr1KO DEGs. **B** Functional categories identified in Fmr1KO DTGs.

functional network centring around APP and TGF-β was also identified in the data and shows some interesting predicted changes (Figure 3.18 B).

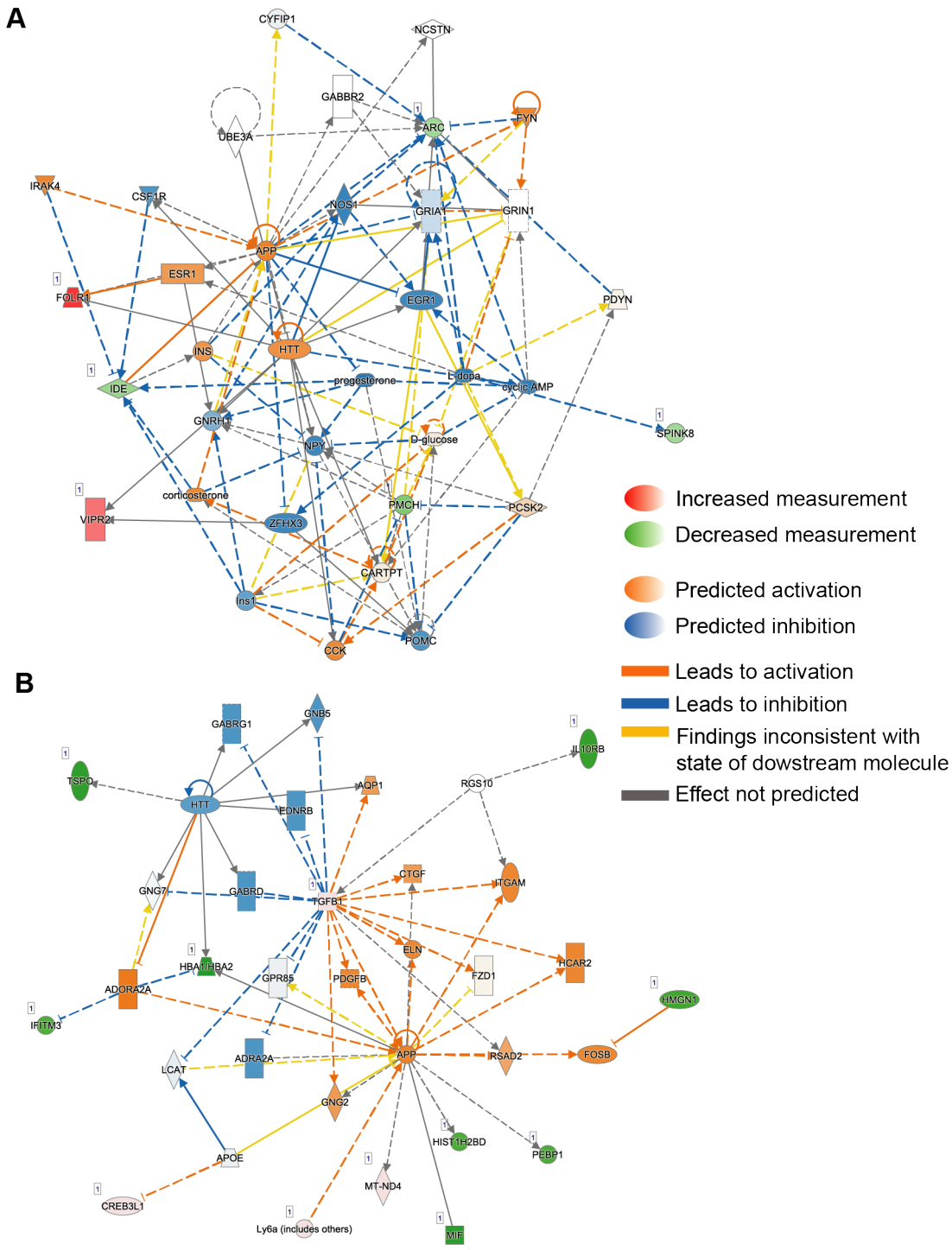

Figure 3.18 Significant networks including molecule activity prediction in Fmr1KO DEGs and DTGs. Networks identified in the DEG/DTG lists from the Fmr1KO data using IPA, including a molecule activity prediction (MAP) **A** Network identified in Fmr1KO DEGs. **B** Network identified in Fmr1KO DTGs.

Lastly, we also carried out UTR analysis for the Fmr1KO DTGs. Interestingly enough, three 5' UTR motifs, uORF, terminal oligopyrimidine (TOP) tracts, and internal ribosome entry sites, all of which have previously been associated with mTOR dependent regulation of translation, showed a trend towards enrichment in the upregulated genes (Figure 3.19 A, B). Furthermore, 3' UTRs of upregulated genes were longer and predicted to show more stable secondary structures compared to downregulated genes (Figure 3.19 C, D).

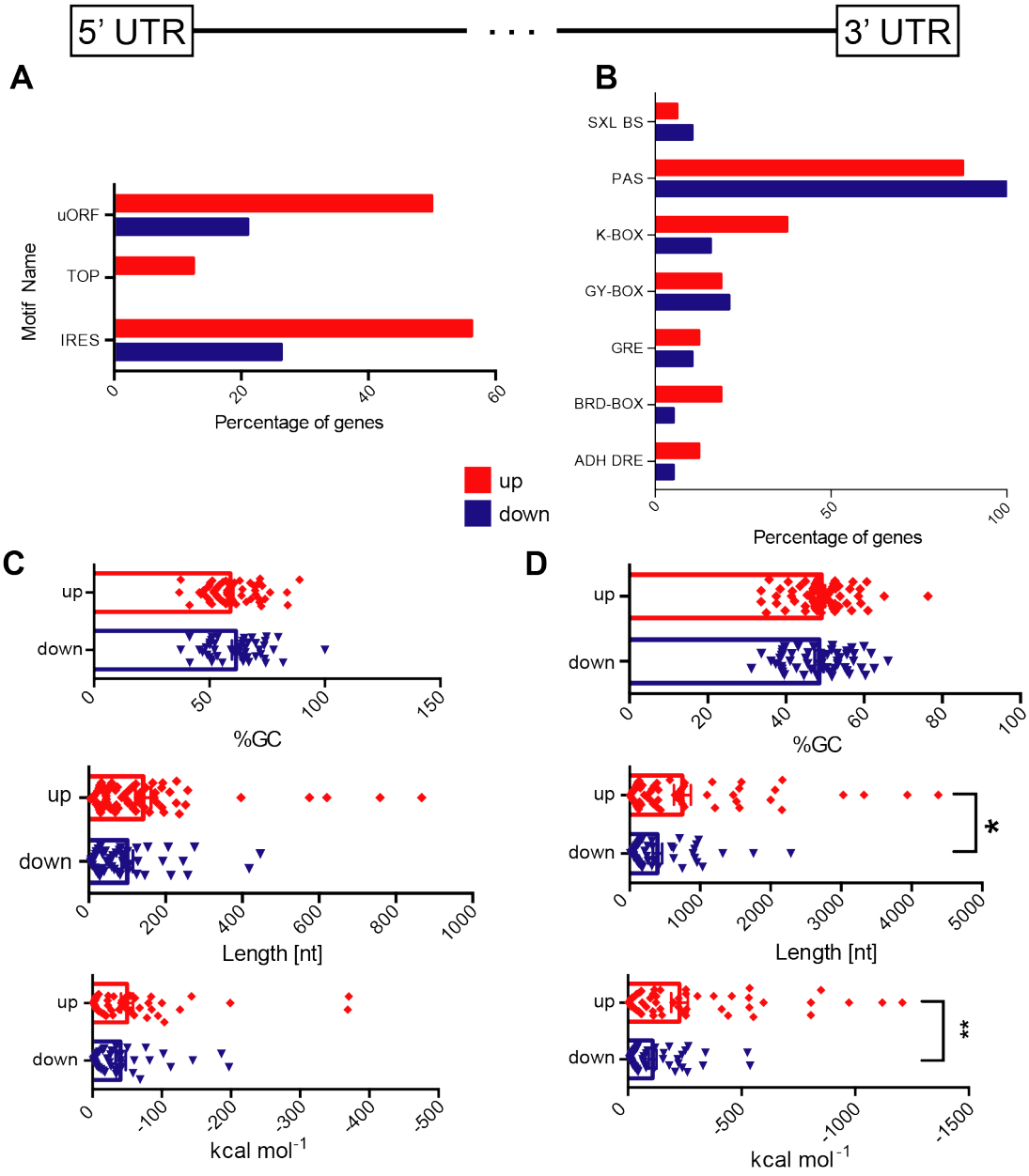

Figure 3.19 UTR motif and basic statistics analysis of Fmr1KO DTGs. **A** Motifs identified in the 5' UTR of up- and downregulated DTGs. The bars represent the percentage of genes (UTRs) containing one or more of the indicated motifs. **B** RNA motifs identified in the 3' UTR of up- and downregulated DTGs. The bars represent the percentage of genes (UTRs) containing one or more of the indicated motifs. **C-D** Bar graphs for the indicated values, represented as mean $\pm$ standard error of the mean, including the individual data points. Shown are percentage of GC nucleotides in the UTR, length of UTR, and Gibbs free (folding) energy of UTR sequence. **C** GC content, length and Gibbs free energy calculated for 5' UTRs of the DTGs. **C** GC content, length and Gibbs free energy calculated for 5' UTRs of the DTGs. **D** GC content, length and Gibbs free energy calculated for 3' UTRs of the DTGs. * $p \leq 0.05$, ** $p \leq 0.01$ Student's t-test.

3.3.5 No significant overlap in the translational and transcriptional landscapes of brain tissue overexpressing MMP9 and Fmr1 knockout brain tissue

Of the DEGs and DTGs in Fmr1KO brains and in TgMMP9 brains, very few genes were shared. Only one DEG overlapped in our data, Foxe3, a transcription factor important to eye development. No genes overlapped in the DTG datasets. In the DAVID analysis, none of the terms that were significantly enriched in the data overlapped between the two genotypes. When carrying out a comparison analysis between the two data sets with IPA, in the transcription datasets ILK signalling and calcium signalling were enriched in both, although less significantly enriched in Fmr1KO (Table 3.1). The TE data overlapped on "abnormal morphology of stereocilia bundles" (part of the inner ear) (Table 3.4). Notably, none of these common terms were statistically significant ($p < 0.05$). No other significant terms overlapped in the DEGs (Table 3.1, 3.2) or DTGs (Table 3.3, 3.4).

Table 3.1 DEG Canonical Pathways comparison between Fmr1KO and TgMMP9. Pathway name and associated $-log_2(p - value)$ are reported. All Pathways listed by IPA are included.

Canonical Pathway	Fmr1KO	TgMMP9
Hepatic Fibrosis/Hepatic Stellate Cell Activation	not detected	3.535347
ILK Signaling	0.767938	2.108334
Calcium Signaling	0.716509	1.999368
Cellular Effects of Sildenafil (Viagra)	not detected	2.482812
Agranulocyte Adhesion and Diapedesis	not detected	2.35298
Embryonic Stem Cell Differentiation into Cardiac Lineages	not detected	2.346318
Epithelial Adherens Junction Signaling	not detected	2.323488
Tight Junction Signaling	not detected	2.190149
Actin Cytoskeleton Signaling	not detected	1.947722
Fatty Acid α-oxidation	not detected	1.870978
Coagulation System	not detected	1.686765
Mechanisms of Viral Exit from Host Cells	not detected	1.506558
Role of JAK2 in Hormone-like Cytokine Signaling	1.469443	not detected
Cell Cycle: G2/M DNA Damage Checkpoint Regulation	not detected	1.449454
Cell Cycle Control of Chromosomal Replication	not detected	1.449454
Circadian Rhythm Signaling	1.412445	not detected
Eicosanoid Signaling	not detected	1.35432
Crosstalk between Dendritic Cells and Natural Killer Cells	not detected	1.345897
Caveolar-mediated Endocytosis Signaling	not detected	1.321606

Thus, we conclude that the overexpression of MMP-9 in FXS does not play a significant role in the dysregulation of translation observed in the disorder, but probably through a yet to be discovered mechanism.

Table 3.2 DEG Diseases and Biological Functions comparison between Fmr1KO and TgMMP9. Term name and associated $-log_2(p-value)$ are reported. All Diseases and Biological Functions listed by IPA are included.

Diseases and Bio Functions	Fmr1KO	TgMMP9
Cadasil	not detected	3.044575
Firing of nucleus accumbens shell	2.909877	not detected
Cerebrovascular dysfunction	not detected	2.909448
Uptake of chloride	not detected	2.743724
Familial Alzheimer disease	not detected	2.567811
Lack of trigeminal ganglion	2.433255	not detected
Length of primary neurites	2.433255	not detected
Clearance of amyloid-beta plaques	2.308565	not detected
Deposition of senile plaques	2.308565	not detected
Cerebral amyloid angiopathy	not detected	2.046179
Abnormal morphology of somatic nervous system	not detected	1.967354
Lack of forebrain	1.957629	not detected
Concentration of D-glucose	1.912121	not detected
Alzheimer disease	not detected	1.8066
Hyperphagia	1.737275	not detected
Hyperpolarization of neurons	1.683416	not detected
Function of blood-brain barrier	not detected	1.668459
Ingestion by rats	1.635609	not detected
Plasticity of neuronal synapse	1.592641	not detected
Ischemic injury of brain	not detected	1.544943
Weight gain	1.517915	not detected
Feeding	1.350636	not detected
Cell viability of cortical neurons	1.307046	not detected

Table 3.3 DTG Canonical Pathways comparison between Fmr1KO and TgMMP9. Pathway name and associated $-log_2(p-value)$ are reported. All Pathways listed by IPA are included.

Canonical Pathway	Fmr1KO	TgMMP9
T Helper Cell Differentiation	2.24876	not detected
Eumelanin Biosynthesis	2.194765	not detected
STAT3 Pathway	1.834282	not detected
p38 MAPK Signaling	1.744908	not detected
Aryl Hydrocarbon Receptor Signaling	1.627874	not detected
Fatty Acid α-oxidation	not detected	1.613582
Th1 and Th2 Activation Pathway	1.477928	not detected
IL-22 Signaling	1.423281	not detected
Coagulation System	1.319041	not detected
Role of Cytokines in Mediating Communication between Immune Cells	1.301001	not detected

Table 3.4 DTG Diseases and Biological Functions comparison between Fmr1KO and TgMMP9. Term name and associated $-log_2(p-value)$ are reported. All Diseases and Biological Functions listed by IPA are included.

Diseases and Bio Functions	Fmr1KO	TgMMP9
Abnormal morphology of stereocilia bundles	1.423281	1.535413
Abnormal morphology of lobule I	not detected	2.784938
Binding of endoplasmic reticulum membrane	2.670995	not detected
Outgrowth of vestibulocochlear cranial nerve ganglion	2.670995	not detected
Spontaneous hypertension	2.670995	not detected
Binding of mitochondrial membrane	2.670995	not detected
Exit from cell cycle progression of oligodendrocyte precursor cells	2.670995	not detected
Multiple Sclerosis	2.488532	not detected
Abnormal morphology of lobule III	not detected	2.484247
Abnormal morphology of lobule II	not detected	2.484247
Differentiation of Th17 cells	2.37041	not detected
Relaxation of middle cerebral artery	2.37041	not detected
Quantity of West Nile virus	2.37041	not detected
Clinical dementia rating score 3 Alzheimer disease	2.37041	not detected
Bioavailability of nitric oxide	2.37041	not detected
Proliferation of folliculo-stellate cells	2.37041	not detected
Myelination of white matter	2.37041	not detected
Contraction of cerebral artery	2.37041	not detected
Progressive motor neuropathy	2.357981	not detected
Abnormal morphology of cerebellum fissure	not detected	2.308494
Edema of white matter	2.194765	not detected
Vasoconstriction of middle cerebral artery	2.194765	not detected
Development of infarct	2.194765	not detected
Formation of cerebellar lobule	not detected	2.183894
Size of inferior colliculus	not detected	2.087322
Compound action potential of cochlear nerve	not detected	2.087322
Number of stereocilia	not detected	2.087322
Re-entry into cell cycle progression of Schwann cells	2.070271	not detected
Mitogenesis of anterior pituitary cells	2.070271	not detected
Demyelination of fiber tract	2.070271	not detected
Development of midbrain-hindbrain boundary	not detected	2.008479
Neuromuscular disease	1.982944	not detected
Function of brain	1.968389	not detected
Function of vestibular system	not detected	1.941871
Activation of sensory neurons	1.89507	not detected
Abnormal morphology of midbrain-hindbrain boundary	not detected	1.833403
Myelination of corpus callosum	1.771022	not detected
Abnormal auditory evoked potential	not detected	1.709478
Encephalitis	1.635136	not detected
Long term depression of Purkinje cells	1.596708	not detected
Apoptosis of cerebral cortex cells	1.59259	not detected
Abnormal morphology of tectum mesencephali	not detected	1.58589
Proliferation of neuroglia	1.565521	not detected
Inflammation of spinal cord	1.473546	not detected
Deposition of amyloid-beta plaques	1.473546	not detected
Fragmentation of DNA	1.447661	not detected
Quantity of outer hair cells	1.423281	not detected
Abnormal morphology of spiral ganglion	1.357664	not detected
Neuroinflammation	1.357664	not detected
Quantity of macrophages	1.319041	not detected
Abnormal morphology of granule neuron progenitor cells	not detected	1.303705

3.4 Discussion

In this chapter, we present an analysis of global translation and signalling pathways upstream of translation in murine forebrain overexpressing human MMP-9 (TgMMP9 animals). We further show ribosome profiling data comparing translation of specific transcripts in a mouse model of FXS (Fmr1KO), and TgMMP9 animals. TgMMP9 mice have previously been shown to resemble FXS phenotypes, specifically social deficits, repetitive and stereotypic behaviours, and abnormalities in dendritic spine morphology (Gkogkas et al., 2014). With this research we attempted to dissect the potential contribution of MMP-9 to dysregulated translation phenotypes in FXS.

Our observations of global translation in TgMMP9 forebrain tissue, using a Puromycin incorporation assay marking all newly synthesised proteins within the time frame of the experiment, do not resemble the global upregulation of protein production that has been shown in FXS before (Bear et al., 2004; Gkogkas et al., 2014). On the contrary, our data appears to show a trend towards decreased translation in TgMMP9 forebrain lysates, with increasing time of incorporation (Figure 3.5). This is interesting, since genetic or pharmacological restoration of MMP-9 levels to baseline in models of FXS has been shown to correct several of the key phenotypes, including exaggerated translation (Gkogkas et al., 2014; Sidhu et al., 2014).

When probing for phosphorylation of important components of the mTOR (RPS6 and 4E-BP1/2) and Mnk (ERK and eIF4E) signalling pathways in TgMMP9 forebrain lysates, we did not observe any significant changes in phosphorylation levels, compared to WT controls. We also did not detect any changes in phosphorylation of AKT, an upstream regulator of mTOR, or FAK, a molecule that had previously been shown to be hyperphosphorylated in DIV14 hippocampal neurons after treatment with recombinant MMP-9 (Sidhu et al., 2014). These results are fairly divergent from phenotypes commonly observed in models of FXS. A role for MMP-9 in FXS has been fairly well established (Abdallah and Michel, 2013; Gantois et al., 2017; Gkogkas et al., 2014; Sidhu et al., 2014). Nevertheless, we do not know about the molecular effects of solely upregulating MMP-9 expression *in vivo* in much detail. Previous research had strongly indicated that MMP-9 would contribute to the key FXS phenotypes through differentially regulating translation (Gantois et al., 2017; Gkogkas et al., 2014; Sidhu et al., 2014). Our data, however, does not support this hypothesis.

To illuminate whether overexpression of MMP-9 had an effect on translation and/or transcription of specific genes, we carried out ribosome profiling. Ribosome profiling in adult TgMMP9 whole brain identified few significant changes in both the internal transcription control (18 DEGs) and TE (44 DTGs). We performed GO analysis on these data sets, using DAVID and IPA. DAVID analysis for biological process, molecular function, and cellular component GO terms identified terms related to ECM and glycinergic synaptic transmission. ECM involvement may be an interesting avenue to further explore because it has previously been shown (Osterweil et al., 2010; Sharma et al., 2010; Wen et al., 2018), and it may present the missing link between MMP-9 and FXS.

IPA showed very interesting terms relating both to general function of the nervous system, as well as Alzheimer's disease. Fragkouli et al. (2012) have previously studied TgMMP9 animals with relation to Alzheimer's disease. In their study, TgMMP9 animals showed enhanced performance in the watermaze and novel object tasks, along with increased hippocampal late long-term potentiation. Overexpression of MMP-9 further resulted in increased soluble APPα secretion. TgMMP9 animals also exhibit a decreased preference for the social stimulus and social novelty in the three chamber task (Gkogkas et al., 2014). Furthermore, TgMMP9 animals present with increased dendritic spine density in the hippocampus (Fragkouli et al., 2012; Gkogkas et al., 2014).

UTR analysis of the TgMMP9 DTGs, consistent with the fairly small changes in translation and transcription, showed no gross differences in specific motifs between up- and downregulated genes. The length of 3' UTRs was significantly longer, on average, in upregulated than in downregulated genes, which may influence protein abundance (Mayr, 2017). Additionally, differential 3' UTR length has recently been associated with neuronal activity (Tushev et al., 2018).

Since our ribosome profiling data from TgMMP9 forebrain alone did not yield a clear answer as to whether MMP-9 was a regulator of transcript-specific translation in the context of FXS, we decided to prepare ribosome profiling libraries from adult Fmr1KO forebrain and compare the results with the TgMMP9 data. Fmr1KO ribosome profiling data was of high quality and reproducibility. Nevertheless, we identified only few significantly up- and downregulated genes. This is consistent with previous translational profiling of Fmr1KO animals (Thomson et al., 2017). Thomson et al. (2017) identified 121 differentially expressed genes, which may be due to their cell and region specific profiling approach

compared to our unbiased whole brain profiling, as well as the age groups used (P25-32 vs 6-8 weeks in our experiments).

GO analysis of the Fmr1KO DEGs and DTGs revealed ECM, synaptic transmission, and protein synthesis related terms, which agrees with recently published work that carried out ribosome profiling of P24 Fmr1KO mice (Sharma et al., 2019). Analysis of UTR motifs exposed a clear trend towards uORF, TOP, and IRES enrichment in the 5' UTR of upregulated genes, although not statistically significant. These motifs have been associated with regulation of cap-dependent translation (Hinnebusch et al., 2016; Sharma et al., 2019; Thoreen et al., 2012), which in turn is considered to be altered in FXS (Napoli et al., 2008). Comparing the TgMMP9 and Fmr1KO data sets showed minimal overlaps in DEGs and DTGs, as well as the GO analysis.

Taken together, our data highlight the differences between TgMMP9 mice and Fmr1KO mice. In spite of the similar behavioural phenotypes, we were unable to confirm similarities in the translation phenotypes of the two models. Global translation in TgMMP9 whole brain lysates was not significantly different from WT brain lysates, whereas Fmr1KO brain tissue has previously been shown to have increased Puromycin and ^{35}S incorporation (Bhattacharya et al., 2012; Dölen et al., 2007). Phosphorylation of important signalling molecules upstream of translation was unchanged in TgMMP9 brain lysates compared to WT controls. Several of these molecules have been shown to exhibit an altered phosphorylation pattern in Fmr1KO mice before (Sharma et al., 2010). Ribosome profiling identified only very few significantly regulated genes. However, they grouped under relevant terms in GO analysis.

Lastly, in spite of the established causal relationship between FXS and the upregulation of MMP-9, we only observed one overlap in the DEGs between our two models, namely Foxe3, which is downregulated in both Fmr1KO and TgMMP9. Foxe3 encodes for a transcription factor that is essential for correct lens development (Blixt et al., 2000; Brownell et al., 2000). Lack of Foxe3 leads to severe abnormalities during the formation of the eye, through reduced proliferation of the anterior lens epithelium and early differentiation of cells, resulting in smaller eyes that may never open in KO mice (Medina-Martinez et al., 2005). How it might be related to FXS and the upregulation of MMP-9 is currently unclear, however, it may be expressed in other tissues than the lens and play different roles at varying developmental timepoints.

A lot of work remains to be done to dissect the contribution of MMP-9 to the generation of psychiatric disorders. Possible targets to study are the ECM, as terms related to it were enriched in both mouse models. Another important factor to consider is the age of the animals that are being used, as some of the changes may be more prevalent at an earlier and more plastic period. Due to the use of whole forebrain, we may also have observed a diluted effect in specific regions and/or cell types. As indicated by behavioural phenotypes in TgMMP9 animals, described by Fragkouli et al. (2012); Gkogkas et al. (2014), the changes may be more pronounced in the hippocampus or regions of the cortex such as the entorhinal or perirhinal cortices, so investigating more defined brain regions may prove worthy.

3.5 Conclusions

In this study, we aimed to better define the contributions of MMP-9 to the phenotypes observed in FXS at a molecular level. Increased MMP-9 levels had previously been shown to substantially contribute to FXS pathophysiology. In our analysis of translation in mouse brains that overexpress human MMP-9, we found that TgMMP9 brain lysates do not resemble the increased global translation and upregulation of the mTOR pathway that has been observed in Fmr1KO animals. Furthermore, ribosome profiling of both Fmr1KO and TgMMP9 whole brain lysates showed only few genes that were differentially regulated overall and almost no overlaps between the results of the two genetic lines. Given the similarity of the mouse lines at a behavioural level, we conclude that what we may have been unable to detect bigger changes due to homeostatic effects in our genetic models or dilution of effects due to our use of whole brain as starting material rather than a smaller brain region or specific cell types. Moreover, pathways and structures other than translation regulation, e.g. ECM, may be responsible for the similarities observed between the two models.

Chapter 4

The role of Mnk/eIF4E translational control in depression-like behaviours

The work presented in this chapter has been reported in part in the following publication:

Inês Silva Amorim*, Sonal Kedia*, Stella Kouloulia*, Konstanze Simbriger*, Ilse Gantois, Seyed Mehdi Jafarnejad, Yupeng Li, Agniete Kampaite, Tine Pooters, Nicola Romanò, and Christos G. Gkogkas **Loss of eIF4E phosphorylation engenders depression-like behaviors via selective mRNA translation**, *Journal of Neuroscience*, 24 January 2018, 2673-17;
DOI: 10.1523/JNEUROSCI.2673-17.2018
*These authors contributed equally

4.1 Introduction

4.1.1 The socio-economic impact of major depression disorders

According to the World Health Organisation (WHO), the prevalence of major depressive disorders (MDD) is at 2.21% globally and continues to rise. In the UK alone, the prevalence in the population is 1.8 million (2.88%), in Scotland 153,000 (2.9%) (Global Burden of Disease Collaborative Network, 2018). MDD is a great contributor to disability, with as much as 50% of chronic sick leaves being accounted to MDD/anxiety in the EU. The associated cost to the health care system is a great challenge (Global Burden of Disease Collaborative Network, 2018; World Health Organization, 2017a). Current medications are limited and ineffective in about one third of patients, which further complicates treatment (Rush et al., 2006). This present situation highlights the need to better understand the pathophysiology of MDD and develop novel therapeutic targets.

4.1.2 The MAPK/ERK signalling axis and mRNA translation regulation in MDD

The MAPK/ERK (mitogen-activated protein kinases/extracellular signal-regulated kinases) signalling pathway (Figure 4.1) is highly conserved between species and responds to many different signals, both intra- and extracellularly (e.g. cytokines, mitogens, growth factors, hormones, neurotransmitters), adjusting gene expression to the cell's needs (Kelleher et al., 2004; Thomas and Huganir, 2004). Regulation of MAPK/ERK has been linked to long-term potentiation in excitatory signal transmission, learning and memory, and fear conditioning (Atkins et al., 1998; English and Sweatt, 1997; Kanterewicz et al., 2000; Kelleher et al., 2004; Schafe et al., 2000; Thomas and Huganir, 2004; Zhu et al., 2002). Moreover, the involvement of ERK1/2, mainly through reduced activation, in the pathophysiology of MDD is well accepted. In subjects suffering from MDD that committed suicide, the activity, protein, and mRNA levels of ERK1/2, an important hub of the MAPK/ERK pathway, were decreased in prefrontal and hippocampal areas, post-mortem (Dwivedi et al., 2001; García-

Fuster et al., 2014). Reduced activation (phosphorylation) of ERK1/2 promotes depression-like behaviours and blocks the antidepressant action of tricyclic compounds as well as selective serotonin reuptake inhibitors (SSRIs) and mood stabilisers (Chen and Manji, 2006; Duman et al., 2007; Gourley et al., 2008). Furthermore, in an animal model of depression and agressive behaviour, induced through dietary deprivation of n-3 polyunsaturated fatty acids, reduced p38 MAPK phosphorylation was reported (Rao et al., 2007). Additionally, depression-like behaviour elicited by chronic stress and immune mediators, presented with p38 MAPK hyperphosphorylation (Bruchas et al., 2011; Miller and Raison, 2016).

4.1.3 eIF4E phosphorylation in the brain

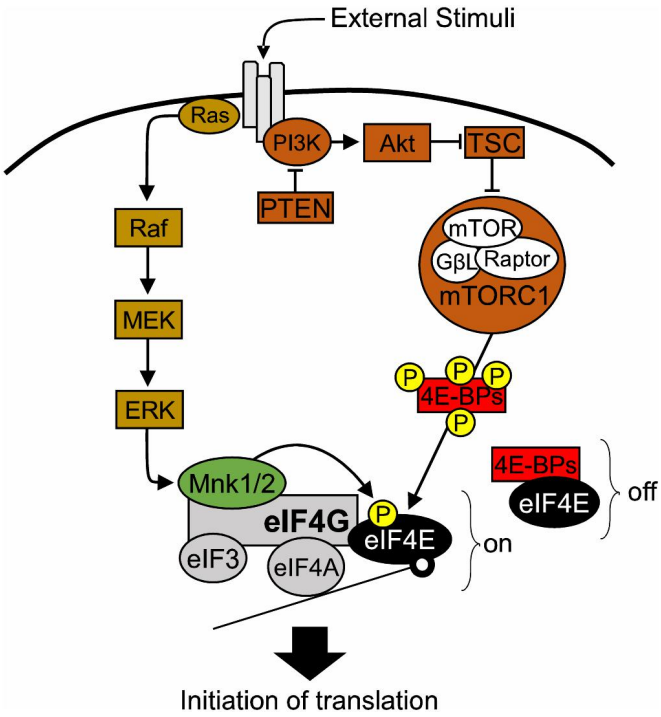

Figure 4.1 eIF4E phosphorylation in translational control. Diagram of the major signalling pathways upstream of eIF4E. External stimuli, e.g. Insulin, growth factors, activate the Ras/Raf/MEK/ERK Mnk1/2 pathway, which phosphorylates eIF4E on Ser209 to stimulate translation (left), or the PI3K/Akt/TSC/mTORC1 pathways, which in turn phosporylates 4E-BPs and thereby relieves 4E-BP's inhibitory sequestering of eIF4E. Figure taken from Amorim et al. (2018a)

ERK1/2 and p38 kinases phosphorylate MAPK-interacting serine/threonine protein kinase 1 and 2 (MNK1/2) (Joshi and Platanias, 2014; Waskiewicz et al., 1997), which in turn regulate translation through phosphorylating eukaryotic

initiation factor 4E (eIF4E) on serine residue 209 (Flynn and Proud, 1995; Joshi et al., 1995; Ueda et al., 2004). eIF4E binds to the 5' cap of mRNAs and forms the eIF4F complex together with eIF4G (scaffolding protein) and eIF4A (mRNA helicase), to recruit the preinitiation complex (PIC) and promote translation initiation (Figure 4.1) (Hinnebusch et al., 2016). Phosphorylation of eIF4E stimulates the translation of a specific subset of mRNAs ("eIF4E-sensitive"), rather than upregulating translation globally and some of these mRNAs have been shown to be key regulators in memory formation and regulation of circadian rhythms (Bramham et al., 2016; Cao et al., 2015; Furic et al., 2010). eIF4E phosphorylation has also been shown to play a role in depression-like behaviour (Aguilar-Valles et al., 2018; Amorim et al., 2018a) and ASD (Gkogkas et al., 2014). Since eIF4E promotes eIF4A helicase activity, it facilitates translation of mRNAs containing long and highly structured 5' untranslated regions (UTRs, e.g. proto-oncogenes and growth factors) (Feoktistova et al., 2013; Sonenberg and Hinnebusch, 2009).

Overall, the literature postulates an activating role for phospho-eIF4E in translation (Bramham et al., 2008; Lachance et al., 2002; Panja et al., 2014; Pyronnet et al., 1999), however, it was also suggested that it decreases cap-dependent translation (Knauf et al., 2001) or that phosphorylation is not required for translation initiation (McKendrick et al., 2001). Little is known about the subset of mRNAs that are regulated by phospho-eIF4E in the brain. In the hippocampus, phospho-eIF4E regulates the translation of *Mmp9* (Gantois et al., 2017; Gkogkas et al., 2014), whereas in the suprachiasmatic nucleus, it has been shown to regulate expression of *Per1/2* mRNAs (Cao et al., 2015). Several cancer studies identified phospho-eIF4E-sensitive mRNAs (Furic et al., 2010; Konicek et al., 2011; Robichaud et al., 2015). Interestingly, phospho-eIF4E controls Type I IFN production trough regulating translation of *NFKBIA* mRNA (coding for IκBα protein; nuclear factor of κ polypeptide gene enhancer in B-cells inhibitor, α), a key inhibitor of NFκB function. Antiviral responses and cytokine production are regulated through activation of the transcription factor NF-κB, which in turn is activated after IκBα downregulation through hypophosphorylated eIF4E (Herdy et al., 2012).

4.1.4 Behavioural effects of ablating eIF4E phosphorylation in a mouse

Phospho-eIF4E is widely expressed throughout the hippocampal formation (Figure 4.2), however, no effect on hippocampal learning and memory was detected in animals expressing a non-phosphorylatable form of eIF4E (termed *4EKi* from here on), specifically the Morris water maze and contextual fear conditioning (Table 4.1). Furthermore, late long-term potentiation was unchanged in hippocampal CA1 neurons of *4EKi* animals. Contrarily, *4EKi* mice performed poorly in behavioural tests for depression and anxiety, including a forced swim test (FST), a tail suspension test (TST), novelty suppressed feeding behaviour (NSF), open field test (OF), and the elevated plus maze (EPM, Table 4.1) (Amorim et al., 2018a). These observations support a role for phospho-eIF4E in depression and anxiety. Interestingly enough, Amorim et al. (2018a) also reported that chronic fluoxetine (an SSRI) treatment had no effect on depression-like behaviours (FST, TST) in *4EKi* mice. Fluoxetine treatment has previously been shown to induce phosphorylation of eIF4E (Dagestad et al., 2006) and alleviate depression-like phenotypes in mice (Dulawa and Hen, 2005).

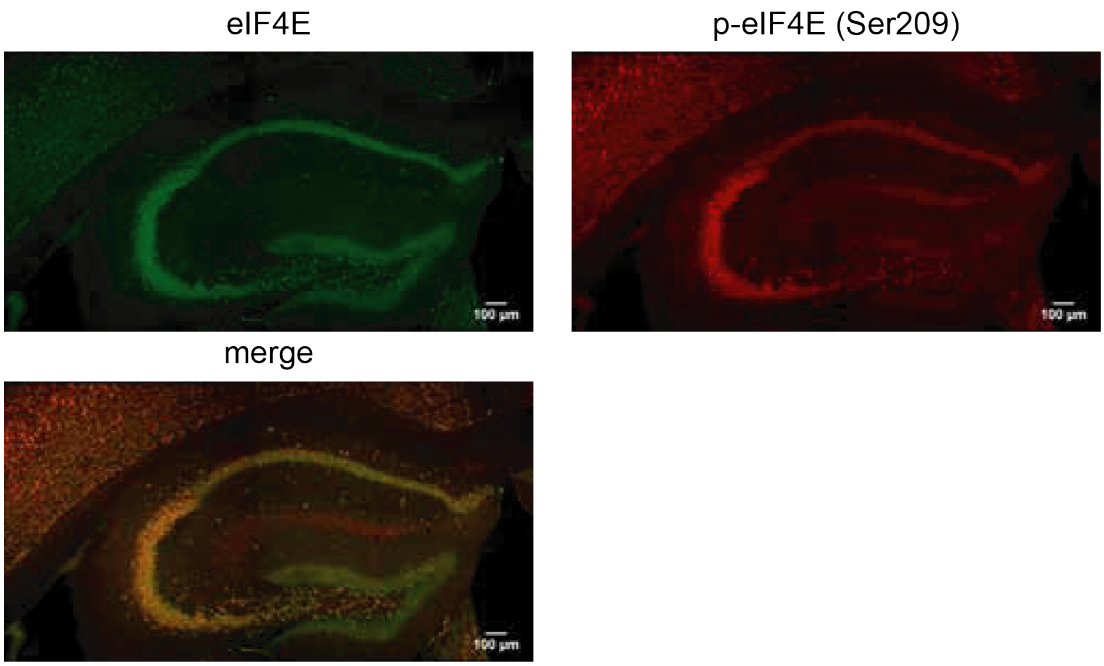

Figure 4.2 eIF4E phosphorylation in the dorsal hippocampus. Representative confocal images of immunofluorescent staining of WT dorsal hippocampi with antibodies against total and phospho-eIF4E (Ser209). Scale bar, 100 µm Figure from (Amorim et al., 2018a).

Table 4.1 Results summary of the behavioural data collected by Amorim et al. (2018a). Test and connected measures, as well as outcome (compared to WT) is reported. — no change compared to WT, ↑ elevated compared to WT, ↓ reduced compared to WT

Learning and memory	*4EKi*
Morris water maze (all measured parameters)	—
Contextual fear conditioning (freezing)	—
Depression- and anxiety-like behaviour	*4EKi*
Forced swim test (immobility time)	↑
Tail suspension test (immobility time)	↑
Novelty suppressed feeding (latency to feed)	↑
Open field test (time in center)	↓
Open field test (time spent close to walls)	↑
Elevated plus maze (time spent in open arms)	↓

Another recent publication examining the role of phospho-eIF4E in depression (Aguilar-Valles et al., 2018) found similar results in two different genetic mouse models of ablated eIF4E phosphorylation at Ser209, namely *4EKi* mice and Mnk1/2 double knock-out mice (*Mnk1/2*$^{-/-}$). Furthermore, they tested both males and females, revealing some gender differences (results summarised in Table 4.2). Both models exhibited increased immobility time in the FST (compared to WT littermates), in both sexes, although the difference was more pronounced in *Mnk1/2*$^{-/-}$ females than in males (Table 4.2). The authors were unable to accurately evaluate females in the TST, due to them climbing on their own tails, but males of both genetic models exhibited increased immobility. NSF latency was increased in *Mnk1/2*$^{-/-}$ and *4EKi* males and *4EKi* females, but not in *Mnk1/2*$^{-/-}$ females. On the other hand, *Mnk1/2*$^{-/-}$ females exhibited a latency to feed in the home cage after fasting, but not males of either line or *4EKi* females (Table 4.2). Males and females of both genetic lines spent significantly less time in the centre of the arena during an OF test. The total distance travelled during the OF test was unchanged in *4EKi* mice of both sexes, and decreased in *Mnk1/2*$^{-/-}$ animals of both sexes, suggesting decreased locomotion behaviour (Table 4.2).

Taken together, animals deficient in phosphorylation of eIF4E Ser209 (*4EKi* and *Mnk1/2*$^{-/-}$ mice) show depression-like and anxiety-related behaviours. Moreover, *4EKi* behaviours were resistant to chronic fluoxetine treatment.

Table 4.2 Results summary of the behavioural data collected by Aguilar-Valles et al. (2018). Test and connected measures, as well as outcome (compared to WT) is reported for each genetic model and gender. **—** no change compared to WT, ↑ elevated compared to WT, ↓ reduced compared to WT, **n.a**. test inconclusive

Test	*Mnk1/2*$^{-/-}$		*4EKi*	
	male	female	male	female
Forced swim test (immobility time)	↑	↑↑	↑	↑
Tail suspension test (immobility time)	↑	n.a.	↑	n.a.
Novelty suppressed feeding (latency to feed)	↑	—	↑	↑
Homecage feeding (latency to feed)	—	↓	—	—
Open field test (time in center)	↓	↓	↓	↓
Open field test (distance travelled)	↓	↓	↓	↓

4.1.5 Aims

In this chapter, we aimed to better understand how the phosphorylation of eIF4E at serine residue 209 regulates translation of specific mRNAs in the brain and how it affects depression-like behaviour in mice. Furthermore, we wanted to understand how absence of the phosphorylation signal on eIF4E changes the regulation of other pathways impinging on translation.

4.2 Materials and methods

4.2.1 *4EKi* mice

The eIF4E$^{S209A/S209A}$ mice (referred to as *4EKi* mice in the text) were obtained from the Sonenberg lab at McGill University, Montréal and were first described by Furic et al. (2010). The genetic construct to generate p-eIF4E-KI S209A contained the serine to alanine mutation in exon 8 and a Neo-TK selection cassette flanked by flippase recognition target sites within exon 7 (Figure 4.3).

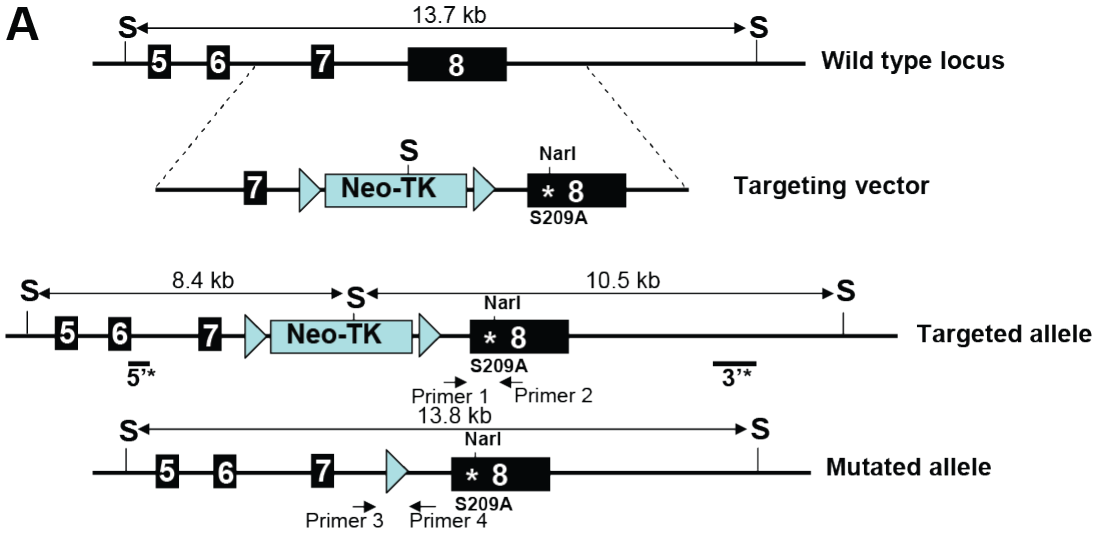

B

...AGCGGCTCCACCACT...
...S^{207}G^{208}S^{209}T^{210}T^{211}...
...AGCGGCGCCACCACT...
...S^{207}G^{208}A^{209}T^{210}T^{211}...

adapted from
Furic et al. 2010

Figure 4.3 *4EKi* design of the genetic targeting strategy. A The eIF4E gene was targeted with a vector encompassing exons 7 and 8, the serine to alanine mutation in exon 8, as well as a Neo-TK cassette after exon 7 as a selection marker. Primers 3 and 4 are used for genotyping. S, *Sac*I restriction site **B** The introduction of the Ser209Ala point mutation generated a new restriction site for *Nar*I (underlined) in exon 8, which was used to confirm the correct insertion.

4.2.2 Other methods

Ribosome profiling (including GO analysis and UTR analysis) and Western blotting methods are described in Chapter 2 "General materials and methods". DAVID analysis was carried out by Dr. Inês S. Amorim, results analysed and summarised by Konstanze Simbriger.

4.3 Results

4.3.1 Ribosome profiling of *4EKi* mouse whole brain

To gain a better insight into the role of phospho-eIF4E in the brain, we performed genome-wide analysis of translation using the novel method of ribosome profiling adapted from (Ingolia et al., 2012, 2009). We prepared sequencing libraries from forebrain tissue (olfactory bulb and cerebellum removed), from WT and *4EKi* animals (Figure 4.5 A). All sequenced libraries, both total mRNA and ribosomal footprints, were of high quality and reproducibility (Figure 4.4). This is demonstrated by the following: (1) the r^2 between the normalised read counts is > 0.99 for all comparisons (Figure 4.4 A); (2) the canonical distributions of footprint (28-32 nt) and total mRNA fragment (30-45 nt) sizes (Figure 4.4 B); (3) read distributions within the 3 main open reading frames (ORFs)(Figure 4.4 B).

We did not observe any significant changes in global transcription or translation in the brain of *4EKi* mice, compared to WT littermates ($R^2 = 0.9187$), which was in accordance with previous reports (Gkogkas et al., 2014). However, we did find that hypophosphorylation at Ser209 regulates the translational efficiency (TE) of a specific subset of mRNAs (Figure 4.5 B). The TE of 52 transcripts was significantly upregulated (displayed in red), while the TE of 651 mRNAs was significantly downregulated (displayed in blue) in the *4EKi* (Figure 4.5 B, Table B.1). Thus, phospho-eIF4E does not significantly regulate global translation, but preferentially regulates the translation of a subset of mRNAs in the brain.

To gain a better understanding of the groups of genes differentially translated in *4EKi* brain tissue, we carried out gene ontology (GO) analysis using the Database for Annotation, Visualization and Integrated Discovery (DAVID) v6.8 (Huang et al., 2009a,b). We identified several biological process and molecular function terms ($p < 0.05$; Figure 4.6 A) in the downregulated genes. Notable categories included response to stress, extracellular organisation and ECM, biological adhesion, and defence response. We further identified some key pathways (in the KEGG database) in our data, e.g. PI3K-Akt signalling pathway, ECM-receptor interaction, and focal adhesion, that were related to translation regulation and ECM (Figure 4.6 B). Some of the top genes that were identified to be translationally downregulated included genes encoding pituitary hormones (prolactin, growth hormon, and pro-opiomelanocortin-alpha) and extracellular

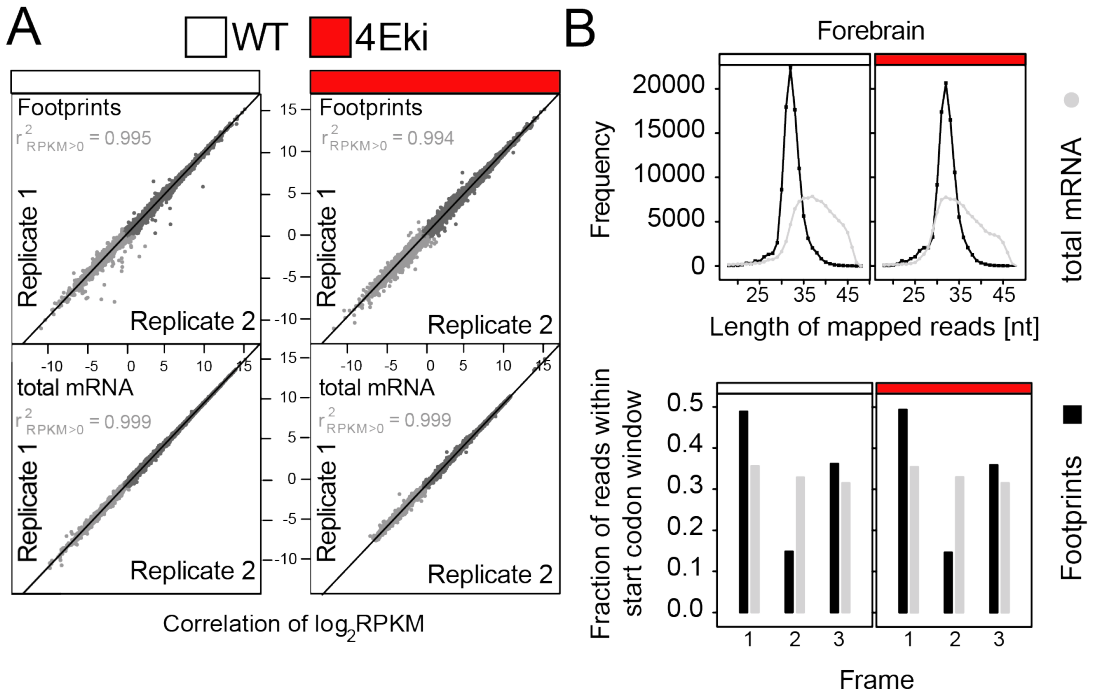

Figure 4.4 Ribosome profiling of *4EKi* forebrain is of high quality and reproducibility. A Scatter plots of the two replicates of each genotype, for footprints and total reads. The correlation coefficient r^2 for each set is noted on the graph. All replicates were highly reproducible, showing an $r^2 > 0.99$. **B** Length distributions of total mRNA (grey) and ribosomal footprint reads (black), for WT and *4EKi*. Footprints show a distinct peak between 28 and 34 nt length, whereas total mRNA samples are more broadly distributed due to the random fragmentation. Alignment of sequencing reads with the distinct codon windows (1-3). Footprints align preferentially with the first (coding) reading frame, while total mRNA reads align equally with all three frames (Amorim et al., 2018a).

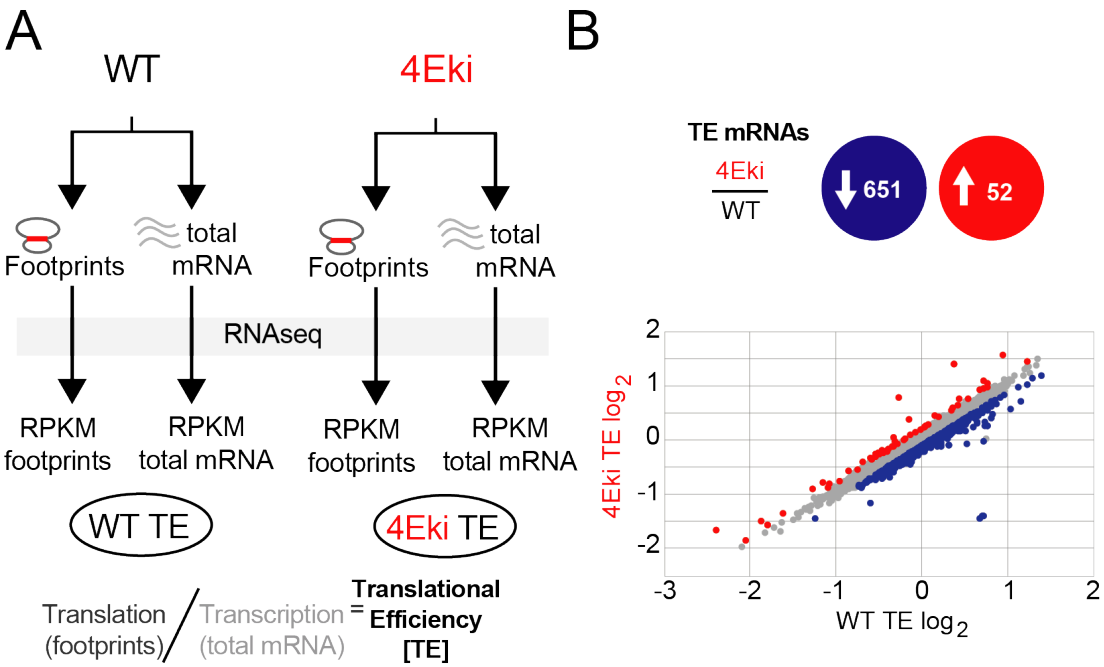

Figure 4.5 Ribosome profiling of *4EKi* forebrain reveals a great number of downregulated genes. **A** Cartoon of the ribosome profiling strategy as described in the method chapter. In brief, tissue was lysed and polysomes digested with an RNase (footprints), while part of the lysate was kept as an internal transcription control (total mRNA). All samples were prepared into cDNA sequencing libraries and sequenced on an Illumina system. To obtain translational efficiencies, normalised read counts (RPKM) for each gene for footprints were divided by total mRNA RPKMs. **B** Statistical comparison of WT and *4EKi* TE ($R^2 = 0.9187$) identified 651 downregulated genes (blue) and 52 upregulated genes (red). Scatter blot of the TE values for each gene of WT versus *4EKi* with the differentially translated genes marked in red and blue ($p < 0.05$ and $0.75 \geq TEratio \leq 1.5$). Gray represents unchanged mRNAs; $n = 2$ for footprints and mRNA (Amorim et al., 2018a).

matrix (ECM) genes (e.g. proteoglycan 2, aggrecan, tenascin C)(Figure 4.6 C). One of the identified genes was *Mmp9*, which had previously been shown to be regulated by phospho-eIF4E (Furic et al., 2010) and is a crucial player in the development of some of the key phenotypes in *Fmr1*$^{y/-}$ (Gantois et al., 2017; Gkogkas et al., 2014; Sidhu et al., 2014). Due to the smaller number of genes, the upregulated gene group showed less, but nevertheless significantly enriched GO categories and pathways. The most abundant category was cytosolic ribosome and the most significant pathway ribosome (Figure 4.6 D). Amongst the most significantly changed genes, we identified several ribosomal protein coding genes, but also genes related to the serotonin pathway (Figure 4.6 E). Taken together, this data points towards a role of phospho-eIF4E in regulating the ECM, pituitary hormones, the serotonin pathway, and ribosomal proteins.

Since untranslated regions (UTRs), flanking the coding sequence of transcripts at both ends, can harbour sequence motifs and basic features that can influence translation and stability of mRNAs, we continued to analyse the 5' and 3' UTRs of phospho-eIF4E-sensitive mRNAs, along with 325 mRNAs that were picked from the sequencing data, because they were unchanged (TE ratio of *4EKi*/WT of 1). Using a custom programmed pipeline that takes advantage of several available tools (mfold v3.6 and UTRscan) (Pesole and Liuni, 1999; Zuker, 2003), we analysed the UTR sequences for known UTR motifs, as well as length and guanine-cytosine (GC) content. Upstream open reading frames (uORFs), internal ribosomal entry sites (IRESs), and terminal oligopyrimidine tracts (TOP) were underrepresented in the downregulated DTGs, compared with the control and upregulated groups (Figure 4.7 A). Both up- and downregulated mRNAs contain significantly less cytoplasmic polyadenylation elements (CPEs) in their 3' UTRs, compared to control genes. 3' UTRs of downregulated genes further contain significantly less gamma interferon inhibitor of translation (GAIT) elements than control or upregulated genes (Figure 4.7 A). These data suggest that these identified regulatory elements that are significantly smaller in numbers in the downregulated group, may reveal yet to be described mechanisms of phospho-eIF4E regulation of translation in the brain. Lastly, we observed a significant increase in length of 5' UTRs of downregulated genes compared to control and upregulated genes, but not in GC content. We did not detect any changes in 3' UTR length or GC content (Figure 4.7 B). Taken together, these data indicate that the mechanism regulating translation downstream of phospho-eIF4E may be dependent on certain UTR elements (e.g. GAIT, TOP).

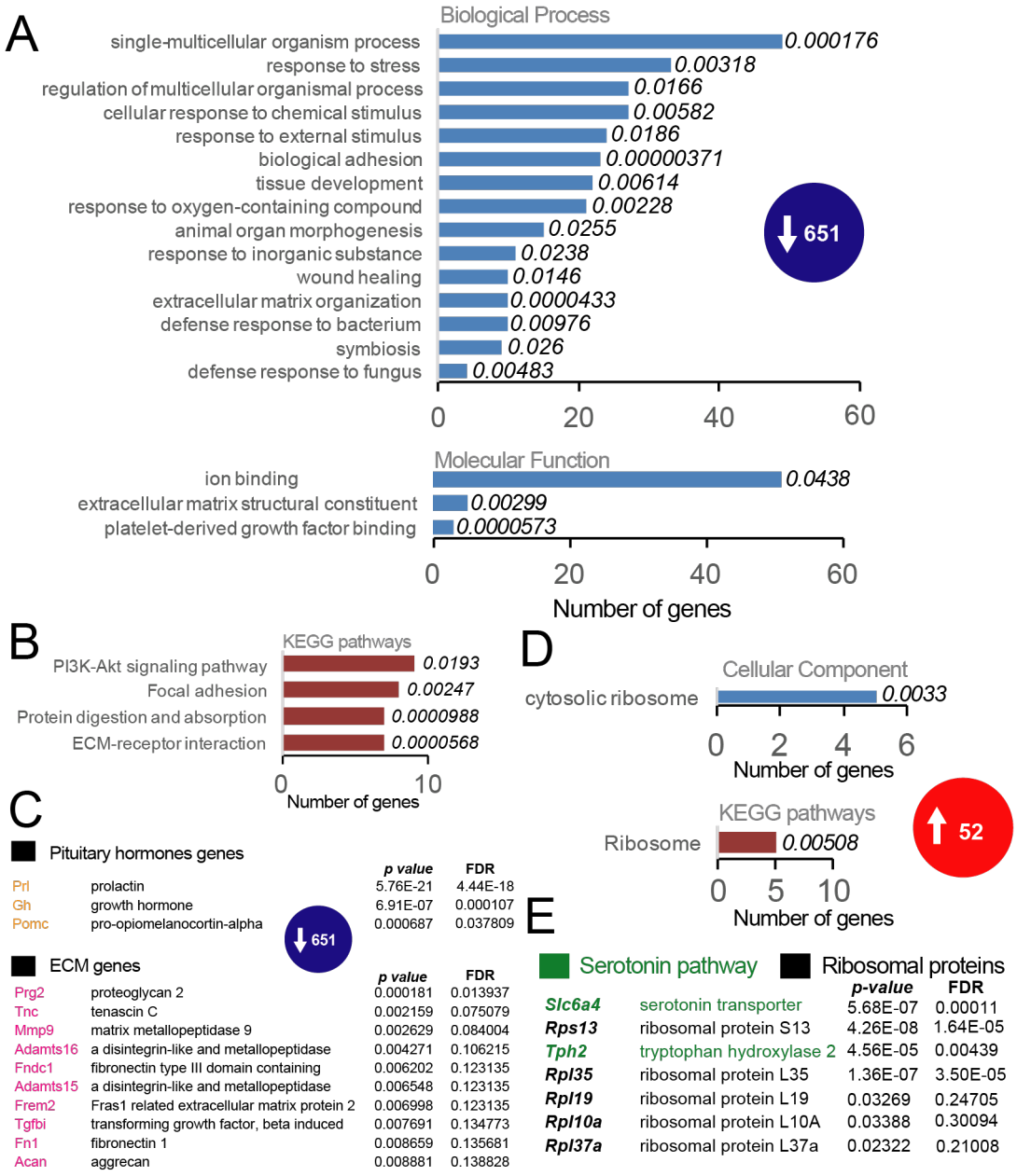

Figure 4.6 Gene ontology analysis of *4EKi* ribosome profiling data. Summary of GO terms identified in *4EKi* ribosome profiling data. **A** Gene ontology terms identified in downregulated genes, plots for biological process and molecular function categories with number of genes associated to them. The numbers displayed next to the bars are the p-values for the respective terms. **B** KEGG pathways identified for downregulated genes. **C** Main genes that were downregulated in *4EKi*, split into two categories, pituitary hormone genes and ECM genes, with the associated p-value and false discovery rate. **D** Gene ontology terms identified in upregulated genes, plots for cellular components and KEGG pathways. **E** Major genes that were upregulated in *4EKi*, split into two categories, serotonin pathway genes and ribosomal proteins, with the associated p-value and false discovery rate (Amorim et al., 2018a).

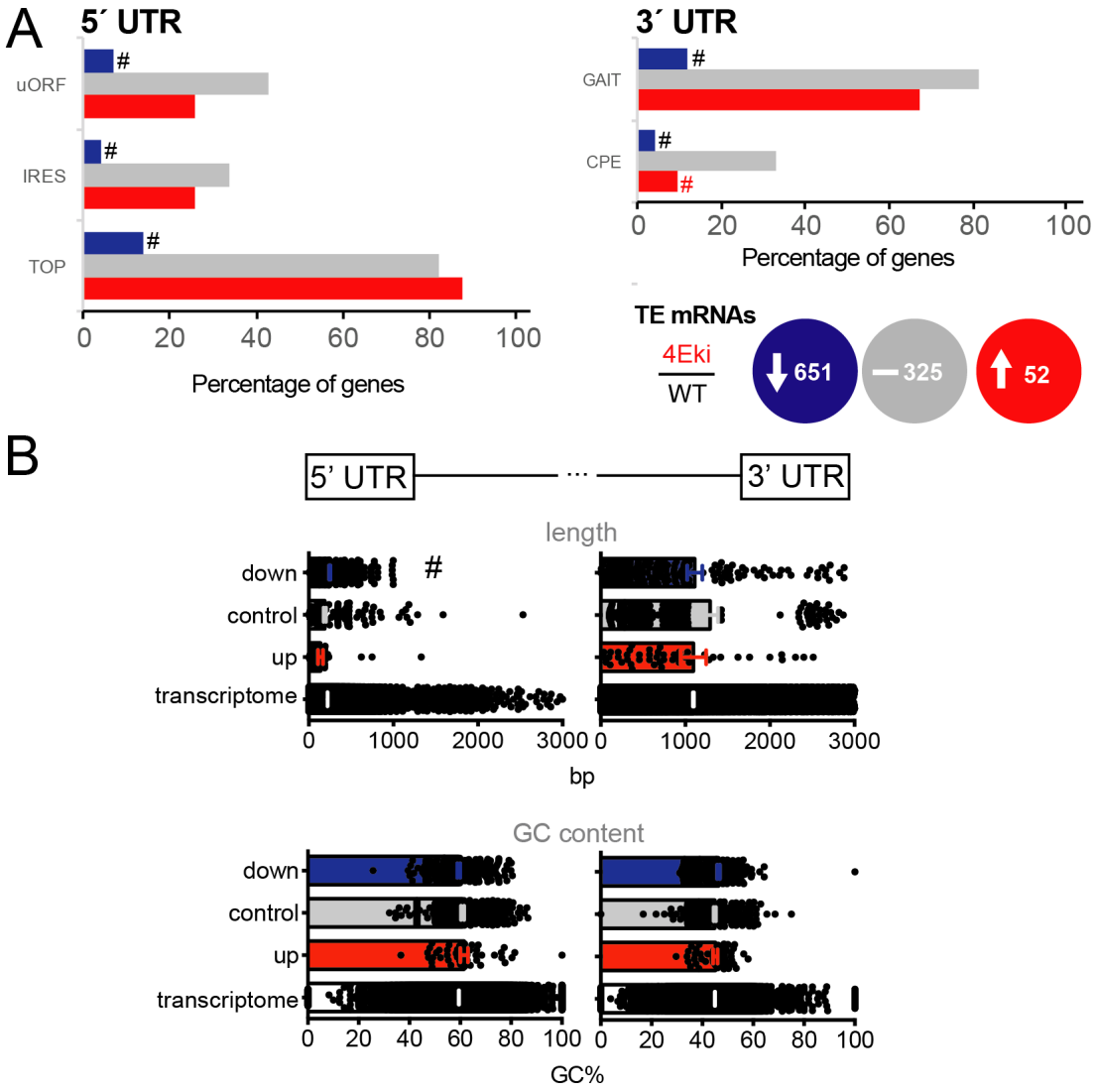

Figure 4.7 UTR analysis of *4EKi* ribosome profiling data. A Analysis for known 5' and 3' UTR motifs. Up- and downregulated genes were analysed along with control group of unchanged genes selected based on their TE from the ribosome profiling data. # Categories in downregulated or upregulated mRNAs, which are underrepresented compared with control mRNA. **B** Length and GC content of 5' and 3' UTRs of differentially translated genes, as well as the unchanged genes and the total transcriptome as controls. Values are represented as mean ± standard deviation, including the individual data points. # $p < 0.05$ difference from all other categories (one-way ANOVA with Tukey's post hoc); all other multiple comparisons between groups are not significant (Amorim et al., 2018a).

4.3.2 Regulation of signalling pathways impinging on translation in *4EKi* whole brain

Because the PI3K-Akt pathway was among the top categories in the KEGG pathway classification of downregulated mRNAs in *4EKi* forebrain, we examined signalling in *4EKi* mice, as compared to wild-type (Figure 4.8). Using Western blotting, we examined changes in phosphorylation of major hubs in the PI3K-Akt-mTOR and MAPK pathways. As expected, no changes were observed in ERK phosphorylation (Figure 4.8 A, D), upstream of eIF4E. However, we detected decreased phosphorylation of ribosomal protein S6 (both Ser240/244 and Ser235/236 phosphorylation sites)(Figure 4.8 B, E) and increased phosphorylation of 4E-BP2 Thr37/46 downstream of mTORC1 (Figure 4.8 A, D). Furthermore, we detected increased Akt Thr308 and Akt Ser473 phosphorylation (upstream of mTORC1), in *4EKi* forebrain lysates (Figure 4.8 C, F). Thus, ablation of the single phosphorylation site on eIF4E engenders selective translation of a subset of mRNAs possibly mediated by mRNA UTR elements (such as GAIT, Figure 4.7 A), and/or altered Akt/mTORC1 signalling.

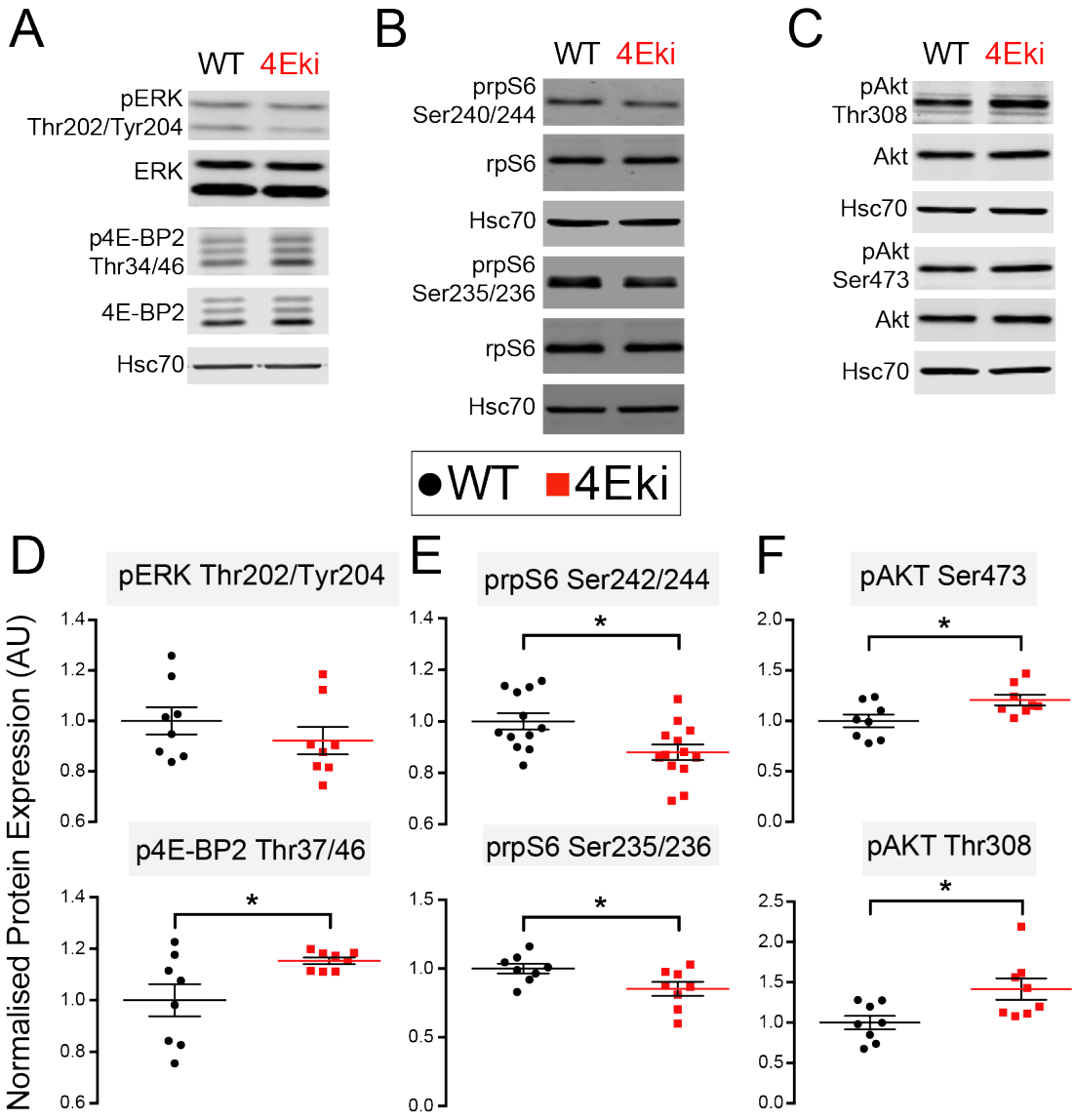

Figure 4.8 Increased mTOR signalling in *4EKi* mice. A-C Representative Western blots for phospho-proteins in the ERK and Akt/mTORC1 pathway in forebrain lysates from wild-type and *4EKi* mice. **D-F** Quantification of protein expression for proteins shown. Phospho-protein expression (arbitrary units) is shown, normalised to total protein. $n = 8$ for each genotype. Values are shown as mean and standard error with individual data points plotted in the same graph. Student's t-test; * $p < 0.05$

4.4 Discussion

In this chapter, we presented translational profiling data from brain tissue of a mouse model of ablated eIF4E phosphorylation that displays depression and anxiety related behaviour. In the ribosome profiling data, we saw no significant changes in global transcription or translation in *4EKi* brains, but significantly decreased translation of 651 genes and increased translation of 52 genes (Figure 4.5), in accordance with previous reports of eIF4E-sensitive mRNAs. Further analysis of the up- and downregulated groups revealed genes related to/involved in ECM and pituitary hormones in downregulated, and serotonin pathway and ribosomal proteins in upregulated genes (Figure 4.6). Analysis of the UTR sequences of DTGs highlighted several regulatory motifs that may be involved in their translational regulation, namely uORFs, IRES, and TOP motifs that were less abundant in 5' UTRs of downregulated genes and GAIT elements that were significantly reduced in number in the 3' UTRs of downregulated genes, as well as CPEs that were reduced in both up- and downregulated genes compared to control genes (Figure 4.7 A). Furthermore, we found that the average length of 5' UTRs of downregulated genes was significantly longer than 5' UTRs of control and upregulated genes, while GC contents of both 5' and 3' UTRs and length of 3' UTRs was unchanged (Figure 4.7 B). We probed for changes in phosphorylation of key signalling molecules impinging on translation in the brain and found that ERK1/2 (Thr202/Tyr204) phosphorylation was unchanged, while Akt (Thr308 and Ser473), an upstream regulator of mTOR, was mildly hyperphosphorylated and ribosomal protein S6 (Ser235/236 and Ser242/244), a downstream target of mTORC1 was slightly hypophosphorylated. Lastly, phosphorylation of mTORC1 target protein eIF4E binding protein 2 (4E-BP2, Thr37/46) was slightly increased compared to WT (Figure 4.8).

The selective translation of eIF4E-sensitive mRNAs has previously been reported in cancer models (Furic et al., 2010; Konicek et al., 2011; Robichaud et al., 2015), as well as in the brain (Cao et al., 2015; Gantois et al., 2017; Gkogkas et al., 2014) but all of these previous studies were limited to a small number of genes. Our ribosome profiling approach, however, allowed us to obtain translational efficiencies for all annotated genes in our samples and provided us with an unbiased view of the translational landscape in *4EKi* brain. We identified several significantly downregulated genes that code for pituitary

hormones and ECM constituents and upregulated genes that code for ribosomal proteins and serotonin pathway genes.

Interestingly, several ECM molecules have been linked to MDD (Dityatev, 2014; Pantazopoulos and Berretta, 2016) and antidepressant treatment efficacy (Alaiyed and Conant, 2019; Donegan and Lodge, 2017; Ohira et al., 2013). Given the link between antidepressant treatment and ERK/MAPK activation (Chen and Manji, 2006; Duman et al., 2007; Gourley et al., 2008) and the role that phospho-eIF4E appears to play in regulating the translation of ECM genes (Figure 4.6 A, C), as well as the role it plays in the control of cancer metastasis through the ECM (Furic et al., 2010; Robichaud et al., 2015), this is a highly interesting direction to take for further research. Furthermore, antidepressant efficacy has been linked to to perineuronal nets and matrix metalloproteinases (Alaiyed and Conant, 2019; Donegan and Lodge, 2017). The ECM as a functional component of the brain has been highly underestimated in the past and may prove a very interesting and promising line of investigation to pursue with respect to neuropsychiatric disorders and discovery of novel treatments.

The upregulation of serotonin uptake receptor (Slc6a4) and the enzyme tryptophan hydroxylase (Tph2) that we observed in our data (Figure 4.6 E) provides a strong link between phospho-eIF4E and depression/anxiety and has been further supported through decreased serotonin levels in the brain (Amorim et al., 2018a) and impaired serotonin transmission in the prefrontal cortex of *4EKi* mice (Aguilar-Valles et al., 2018). Furthermore, there is an interplay between the hypothalamic-pituitary-adrenal axis, serotonin, and dopamine (Hamon and Blier, 2013; Hoogendoorn et al., 2017), which may be further explained through the translational regulation exerted by phospho-eIF4E.

A link between phospho-eIF4E, eIF4E, and innate immunity has previously been reported (Colina et al., 2008; Herdy et al., 2012). As a UTR regulatory motif, GAIT elements serve as a "gatekeeper" of gene expression in response to inflammatory signals (Mukhopadhyay et al., 2008). It functions through interacting with both the GAIT element in the 3' UTR and the cap-bound eIF4F complex (Figure 4.9). Both clinical and preclinical data has been published in support of a strong link between mood disorders and inflammation and many pre-inflammatory mRNAs contain GAIT elements in their 3' UTRs, similar to our upregulated mRNAs. Some MDD patients show increased levels of cytokines, including TNFα and IL-6 (Dowlati et al., 2010; Goldsmith et al.,

2016). Furthermore, a well-understood risk factor of MDD and other mental disorders (Nanni et al., 2012), childhood trauma and abuse, can lead to elevated cytokine levels as well (Baumeister et al., 2016). In rodent models of depression, induced by chronic stress, these observations too have been replicated (Hodes et al., 2014; Kreisel et al., 2014). Moreover, sickness behaviours triggered by infections, which are reminiscent of the symptoms of depression, are treatable with classical antidepressants (Aguliar-Valles et al., 2014; O'Connor et al., 2009). Lastly, clinical trials have shown the efficacy of non-steroidal anti-inflammatory drugs in treating depression (Köhler et al., 2014), as well as successful treatment by blocking cytokine function using antibodies targeting TNFα (Kappelmann et al., 2018). On the other hand, antidepressants can also decrease inflammatory responses in MDD subjects (Więdłocha et al., 2018). Brain wide blocking of TNFα in *4EKi* mice resulted in diminished depressive-like behaviours and corrected serotonergic neurotransmission to WT levels (Aguilar-Valles et al., 2018).

Our group showed that in *4EKi* mice, a novel mouse model of depression, not only a bigger number of GAIT element containing mRNAs is present in the upregulated group than in the downregulated, but also that out of six major cytokines (IL-6, IL-10, IL-1B, IL-2, TNFα, IFNγ), two showed increased protein levels in the *4EKi* mice both at baseline and after immune challenge with lipopolysaccharide (LPS) (IL-2, TNFα), IFNγ was increased after LPS injection only, and all other cytokines showed no differences between WT and *4EKi* (Amorim et al., 2018a). Notably, IL-6, IL-10, and IL-1B are expressed by Th2-type T helper cells, while IL-2, TNFα, and IFNγ are expressed by Th1-type T helper cells (Romagnani, 2000). The role of the GAIT mechanism in the phenotypes observed in *4EKi* mice is further supported by reduced binding of rpL13a, a key component of the GAIT complex, to the eIF4F complex, as shown by cap-column (m^7GDP) pulldown from brain lysates (Amorim et al., 2018a). Since the GAIT complex suppresses the translation of GAIT sequence elements containing mRNAs and rpL13a binding is a key event in this process (Fox, 2015), the decreased cap binding of rpL13a may explain the increased expression of inflammatory genes in *4EKi* mice. Additionally, microglia showed significant activation in *4EKi* mice both at baseline and after LPS injection (Amorim et al., 2018a). Taken together, these data strongly support the role of eIF4E-dependent translation of specific mRNAs in the context of inflammation, serotonergic function (Figure 4.10), and depression and may open up new avenues for treatments when symptoms prove resistant to classic antidepres-

sants. To gain further understanding of the processes involved, cell type specific translational profiling such as TRAP (Heiman et al., 2008), of microglia or serotonergic cells, may prove valuable in the discovery of unknown mechanisms.

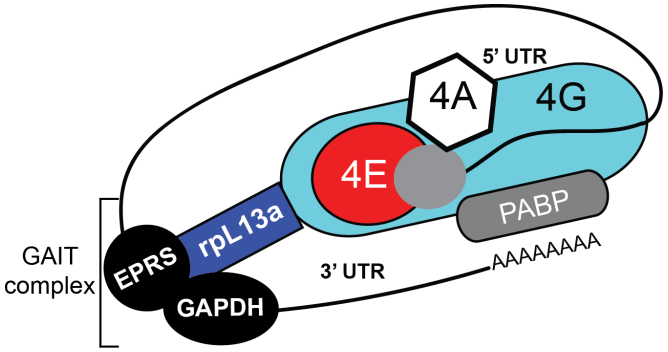

Figure 4.9 Diagram of the GAIT complex closed loop model. The GAIT complex, consisting of rpL13a, EPRS, and GAPDH, binds the 3' UTR GAIT element as well as the eIF4F complex through contact with the scaffolding protein eIF4G and consequently inhibits translation (Amorim et al., 2018a).

Apart from the inflammation-related GAIT elements, we also discovered an under-representation of uORFs, IRES, and TOP regulatory motifs in the 5' UTRs of downregulated genes, as well as an under-representation of CPEs in the 3' UTRs of both up- and downregulated genes. CPEs may exert a function through activity changes of poly(A)-binding protein, which initiate mRNA circularisation by bridging eIF4G, bound to the 5' complex, to the 3' poly(A) tail, that subsequently regulate translation of specific mRNAs (Smith et al., 2014). The eIF2α pathway may regulate translation of uORF-containing mRNAs in the brain (Costa-Mattioli et al., 2007), but also mTORC1 (Schepetilnikov et al., 2013). Considering the changes in phosphorylation of key Akt/mTOR pathway components, translation regulation of uORF-containing mRNAs through an mTORC1 dependent mechanism is more conceivable. Significant evidence supports mTORC1-sensitivity of TOP-containing mRNAs (e.g. ribosomal protein coding genes) (Avni et al., 1997; Thoreen et al., 2012), which is further backed by our data (Figure 4.6, 4.8). Long 5' UTRs require activity of the helicase eIF4A1 to allow the the eIF4G complex to scan for the start codon and initiate translation (Feoktistova et al., 2013). 5' UTRs of downregulated genes in the *4EKi* showed an increased length, compared to control and downregulated genes, which may point to a mechanism requiring phosphorylated eIF4E to bind and stimulate eIF4A1 activity. This is further supported by reduced cap-binding of eIF4A1 in *4EKi* brain lysates (Amorim et al., 2018a).

Finally, the signalling changes we observed in the Akt/mTORC pathway (Figure 4.8), may be a result of the downregulation of several mRNAs downstream of phospho-eIF4E (Figure 4.6 B) or could reflect homeostatic signalling changes, with other pathways trying to compensate for the ablation of the Ser209 site on eIF4E. These signalling changes could further be associated with the *4EKi* depression and inflammatory phenotype, as Akt activation (phospho-Thr308) can stimulate NFκB and TNFα, and mTORC1 by inhibiting phosphatase and tensin homologue on on chromosome ten (PTEN) (Carracedo and Pandolfi, 2008).

4.5 Conclusion

Altogether, we show that depression-like behaviour in *4EKi* animals, as reported by Amorim et al. (2018a), may stem from the differential regulation of a subset of phospho-eIF4E-sensitive mRNAs. We propose a mechanism (Figure 4.10), in which disinhibition of the GAIT complex translational repression downstream of phospho-eIF4E and reduced binding of the helicase eIF4A1 increases inflammation and depression-like behaviour through translationally downregulating pituitary hormones and ECM genes and upregulating serotonin pathway genes (Amorim et al., 2018a). Changes in the regulation of the Akt/mTORC1 signalling pathway may further contribute to these phenotypes and detailed experiments are needed to dissect the individual contributions of the discussed regulatory pathways.

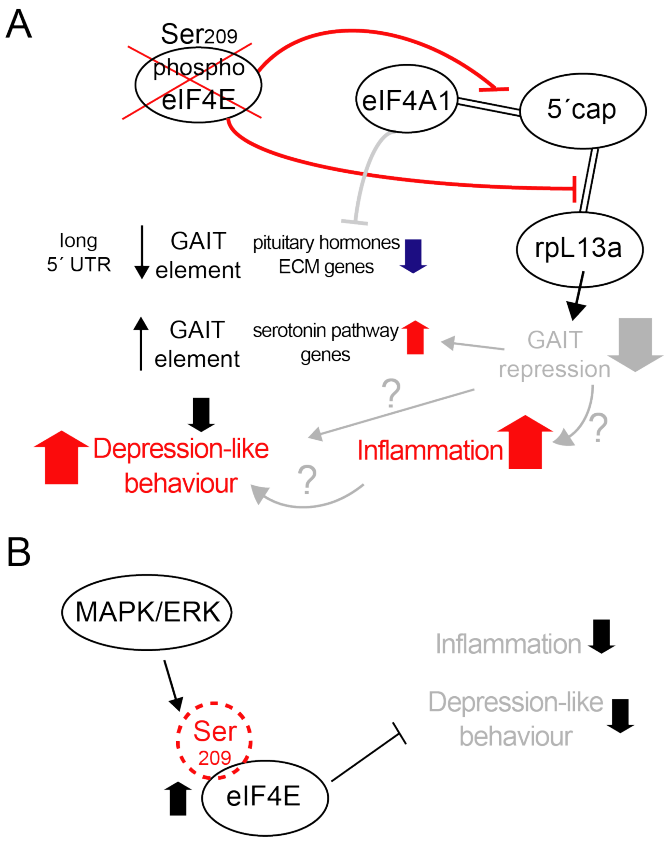

Figure 4.10 Ablation of eIF4E phosphorylation engenders depression-like behaviour through altered translational mechanisms. Cartoons of the proposed mechanism of phospho-eIF4E action in depression and inflammation in the brain. **A** Ablation of the key phosphorylation site on eIF4E through a point mutation (Ser209Ala) has no effects on global protein synthesis, but rather on the translational regulation of a subset of mRNAs harbouring GAIT elements. This differential regulation leads to a depression-like phenotype in *4EKi* animals, as well as increased expression of inflammatory cytokines. Disinhibition of GAIT translational repression, may be the cause of this increased expression in conjunction with the depression-like behaviours. Since altered cap-binding of both the helicase eIF4A1 and the GAIT complex protein rpL13a have been shown in *4EKi* mice, we propose that this could be the underlying mechanism behind translation regulation in this mouse model. **B** eIF4E phosphorylation stimulates anti-inflammatory and anti-depressant pathways in the brain (Amorim et al., 2018a).

Chapter 5

The translational Landscape of contextual Fear Memories

5.1 Introduction

5.1.1 Memory formation

Memory formation is a well-orchestrated mechanism of neurons and circuits of the brain to store relevant information for a short or long time. Storing information about past experiences allows the organism to retrieve it at a later time and alter future behaviour accordingly. This process and its correct functioning is key to the survival of the organism. At the cellular level, memories are stored through synaptic plasticity, a strengthening (long-term potentiation, LTP) or weakening (long-term depression, LTD) of specific neuronal connections. Synaptic plasticity is a complex process that has been shown to be reliant on several factors including transcription, translation, protein degradation pathways, and extracellular matrix components (Bourtchouladze et al., 1998; Costa-Mattioli et al., 2009; Dityatev et al., 2010; Mayford et al., 2012; Poo et al., 2016; Richter and Klann, 2009).

The hippocampus has been shown to be essential for both short and long-term memory formation, in particular spatial memory. It has been studied extensively at the behavioural, electrophysiological, and molecular levels, with regard to its role in memory formation. The dorsal hippocamus especially, has

been shown to be key in the formation of contextual fear memories (Pothuizen et al., 2004).

5.1.2 Pavlovian fear conditioning

Contextual fear conditioning (CFC) is a frequently used form of Pavlovian conditioning, in which animals are exposed to a novel environment/context, the fear conditioning apparatus (conditioned stimulus, CS), and receive a series of non-harmful electrical footshocks (unconditioned stimulus, US) via a metal grid at the bottom of the apparatus. Through the pairing of the originally neutral stimulus that is the novel context and a biologically relevant or aversive stimulus (i.e. pain), a memory is formed to represent the potential danger of the novel context. When returned to the apparatus 24 h later and up to several weeks, conditioned animals show quantifiable fearful behaviour, most commonly freezing, defined as the complete absence of somatic movements, except breathing (Curzon et al., 2009; Izquierdo et al., 2016). Since CFC is rapidly acquired, the outcome easy to measure, and the cortical and subcortical networks involved are fairly well described, the CFC paradigm is commonly used in studying memory. Furthermore, it is used in several adapted forms to study fear- and anxiety-related behaviours and the extinction of these, which is of high relevance for anxiety-related disorders (Chaaya et al., 2018).

5.1.3 Gene expression in memory formation

Storing information about potentially harmful environments is essential to an organism's survival and requires a well-coordinated spatio-temporal molecular response in the brain. Synaptic plasticity and memory formation, are dependent on gene expression, both at the level of transcription and translation (Bourtchouladze et al., 1998; Davis and Squire, 1984). Although there is plenty of evidence for the necessity of gene expression for memory formation, as well as some information about the dynamics of a defined set of immediate early genes (IEGs), only little is known about how the transcriptional and translational landscape changes at the gene level to encode a memory (Gallo et al., 2018; Peter et al., 2012). Despite the fact that the CFC paradigm is well established and often used in the field of learning and memory, as well as

anxiety-related research, a comprehensive view of gene expression, required to form these memories remains elusive. A few studies focussed on the expression of a small number of genes, in particular IEGs (Cho et al., 2017; Rosen et al., 1998; Tischmeyer and Grimm, 1999). Since the advent of quantitative genome-wide gene expression analysis tools (e.g. microarrays, RNA-Seq), a more generalised picture of gene expression during memory formation has been obtained (Barnes et al., 2012; Keeley et al., 2006; Poplawski et al., 2016; Rao-Ruiz et al., 2019), including translational profiling approaches (Cho et al., 2015; Eacker et al., 2017). In particular, changes in translation of genes remain understudied, simply because of the availability of suitable techniques. The recent establishment of ribosome profiling as a method to study genome wide regulation of translation in an unbiased manner (Ingolia et al., 2012) has opened up new avenues to elucidate gene expression in memory formation (Cho et al., 2015; Eacker et al., 2017). However, independent of type of analysis and the timepoint or -frame of gene expression that was analysed with respect to the generation of fear memories, one factor has been largely neglected: The contribution of the electrical footshock to gene expression observed post-CFC. Only a few published studies investigated the effects of delivering an electrical shock to an animal on gene expression in the brain and all of them focussed on specific genes rather than taking a genome-wide approach (Federighi et al., 2013; Rosen et al., 1998). Experiencing an electrical shock that can elicit the formation of a fear memory, we hypothesise, can also have a significant impact on gene expression in the brain, potentially confounding the discovery of true memory genes.

5.1.4 Aims

The aim of the work presented in this chapter was to dissect the contribution of the footshock only and training conditions, to the changes in mRNA expression and translation in dorsal hippocampus of animals trained with a commonly used CFC protocol. A molecular response to the footshock only can be an underestimated confounding factor, in particular for omics based studies. While improving the general understanding of the molecular happenings in response to an electrical shock and the actual CFC paradigm, we also wanted to define marker genes that change their expression specifically in response to the CFC protocol and not in the shock only control group.

5.2 Materials and methods

5.2.1 Contextual fear conditioning

All behavioural training and part of the tissue dissection was carried out by Dr. Gilliard Lach.

To generate material for ribosome profiling, WT mice were trained using a contextual fear conditioning protocol. All animals were handled for three days prior to behavioural experiments. Animals in the training group were allowed to explore the fear-conditioning context for two minutes and given two consecutive footshocks of 0.5 mA, duration 4 s, with a 30 s interval in between. After the footshocks, the animals were allowed to explore the context for another minute, before being removed to their homecage. Animals in the shock only group were transferred to the fear conditioning apparatus from their homecage and immediately received one 4 s long 0.5 mA footshock and were removed to their homecage immediately after. Control animals (homecage) remained in their homecage until sacrificing. All animals were sacrificed 20 min after administering the stimulus (training/shock only/homecage) and their dorsal hippocampi dissected. Tissue from 5-6 animals was pooled to obtain sufficient material for ribosome profiling. We used 10-week old animals for all experiments.

For the groups tested for long-term memory (n = 12 per experimental group, training/shock only/homecage), 24 h after the training session, mice were tested for contextual fear memory expression by being placed in the conditioning context and % freezing being scored for a 5 minute period, in 5 s intervals, either "freezing" or "not freezing". The value for % freezing represents the number of 5 s intervals where freezing was observed divided by the total number of intervals scored.

5.2.2 Object location task

All behavioural training and part of the tissue dissection was carried out by Dr Gilliard Lach.

WT animals were trained in an adapted version of an object location memory task from the lab. In brief, there were three experimental groups, homecage, sham and object. Homecage animals received handling only and remained in their homecage for the duration of the behavioural trainings. The sham and the object groups received two habituation sessions in the empty object arena on two consecutive days, followed by 20 min in a dark box to consolidate memories. On day 3, the sham group was allowed to explore the empty arena three times for 5 min with a 20 min inter training interval (ITI). The Object group was allowed to do the same, however, not in the empty arena, but the arena with two objects. All animals were culled and dissected 20 min after the training session on day three. Only dorsal hippocampi were analysed.

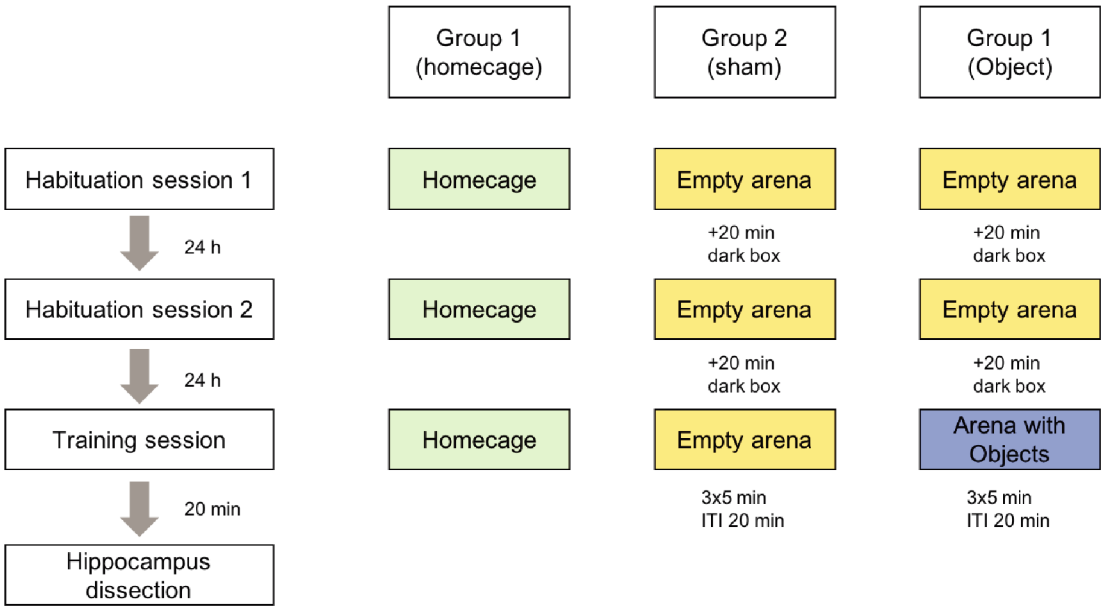

Figure 5.1 Experimental design of the object location task. Animals were trained on three consecutive days after handling, in one of three groups (homecage, sham, Object) as indicated. On day three, animals were sacrificed 20 min after the last session and dorsal hippocampi were dissected and snap-frozen in liquid nitrogen.

5.2.3 Quantitative real-time polymerase chain reaction (qRT-PCR)

Extracted total RNA from the Ribosome Profiling samples and total RNA extracted with the RNeasy Mini Kit (Qiagen, 74104) was used for qRT-PCR. 1 µg of each sample was reverse transcribed into cDNA using SuperScript™ IV

Table 5.1 qPCR Primers, all designed for this project, except GAPDH primers which were previously published by Huang et al. (2011)

Gene Name	Forward Primer (sense)	Reverse Primer (anti-sense)
Egr2	CACCTAGAAACCAGACCTTCAC	GATGCCCGCACTCACAATA
c-fos	ATT GTC GAG GTG GTC TGA ATG	TCG AAA GAC CTC AGG GTA GAA
Arc	GGAGGGAGGTCTTCTACCGTC	CCCCCACACCTACAGAGACA
Ankrd60	GCCTGAAGCGAGGACATTTA	AGGGCTGGATTTCTCCAAAG
Asmt	GAGCGCCTGCTGTTCAT	GTCGCAGATGACCCTGAAG
Col11a1	GGCTGAGAGTGTAACAGAGATG	TAGGAGTCTCAGTCTGGTAAGG
Robo3	CTTAAGGAAGAGGAGGGAAGGA	GTTGGAGGCTACGCACATATAC
Leng8	GGGTTCCAGATACTTGGTAAGG	AGTGCCTTCTGGTTGTTACTC
Klhdc8a	CTACTTCTGTCCTGCCCATATC	GGCCTCTAAGGTTCCAACTATC
Hs3st2	AAATAGCTGGGCGTCTTCTC	CCACTTCTTCGACAGGAACTAC
Camk2d	GTGTGCAACCCTTGCTTTAC	CCCTTTGTGGCTCTCATCTT
Tuba1a	CCTGCTGGGAGCTCTACT	GGGTTCCAGGTCTACGAA
GAPDH	ACCACAGTCCATGCCATCAC	TCCACCACCCTGTTGCTGTA

Table 5.2 qPCR cycling conditions and melting curve

Step	Temperature	Duration	Cycles
UDG activation	50℃	2 min	hold
Dual-Lock™DNA polymerase	95℃	2 min	hold
Denature	95℃	15 s	$\times 40$
Anneal/extend	60℃	1 min	
Step	**Ramp rate**	**Temperature**	**Time**
1	1.6℃/s	95℃	15 s
2	1.6℃/s	60℃	1 min
3	0.15℃/s	95℃	15 s

VILO™ Master Mix (ThermoFisher Scientific). Appropriate dilutions of the cDNA were used in the qPCR reaction, using PowerUp™ SYBR™ Green Master Mix (Thermofisher). Relevant primer sequences can be found in Table 5.1, primers were used at 5 µM and cycling conditions were according to the manufacturers specifications (summarised in Table 5.2). Reactions were run in an AriaMx Real-time PCR System (Agilent).

Raw data was analysed using the AriaMx software. Expression fold change was calculated using the $\Delta\Delta C_t$ method, normalising to loading control (GAPDH expression within the same sample) and homecage.

$$FC = 2^{((C_{t,GIE} - C_{t,LC}) - (C_{t,GIC} - C_{t,LC}))}$$

C_t is the cycle threshold (number of cycles at which the signal exceeds background). $C_{t,GIE}$ is the value for the gene of interest in the experimental condition, $C_{t,GIE}$ the value for the gene of interest in the experimental condition, and $C_{t,LC}$ the value for the loading control.

5.2.4 Other methods

Ribosome profiling (including GO analysis and UTR analysis) and Western blotting methods are described in Chapter 2 "General materials and methods". DAVID analysis and IPA were carried out by Dr Inês S. Amorim, results analysed and summarised by Konstanze Simbriger.

5.3 Results

5.3.1 Ribosome profiling

We generated ribosome profiling libraries from dorsal hippocampi that were dissected 20 min after treatment (homecage/shock only/CFC) and snap-frozen (Figure 5.2). The 20 min time point was chosen, because we were interested in early changes in gene expression elicited by the behavioural paradigm. Tissue was pooled across several animals to obtain sufficient material and two technical sequencing replicates were generated from the pooled tissue for each treatment group (Figure 5.3). After the sequencing, we confirmed that our data was indeed originating from ribosomal footprints, of good quality and that the replicates were reliable. To this end, we analysed the read length distributions, as they are expected to be between 28 and 32 nt for canonical footprints, while the randomly fragmented total RNA samples show bigger fragments and a more random distribution (Figure 5.4 A). Ribosomal footprint reads will preferentially align with the first reading frame (RF) of a gene, since they are expected to originate from translating ribosomes. As shown in Figure 5.4 B, this is indeed the case, while the total RNA fragments align with all RFs equally. Furthermore, when focussing on the regions around the start and stop codons of each gene, we see that footprints preferentially align with the coding sequence and show a strong three-nucleotide periodicity. Beginnings of footprint reads also show a strong peak at -12 nt from the start codon, which implies that the captured ribosomes were initiating translation, as 12 nt is the distance from the side of the ribosome to the A-site of the ribosome (Figure 5.4 C). Furthermore, replicates were highly reproducible between each other, as exemplified by the $r^2 > 0.98$ for all replicate pairs (Figure 5.5).

Using Xtail, we identified 168 differentially translated genes (DTGs) in the shock only condition compared to homecage. 69 of these genes were upregulated and 99 downregulated (Table C.1). For the CFC condition compared to homecage, we identified 84 DTGs, of which 42 were up- and 42 were downregulated (Figure 5.6 A, B; Table C.2). Of these DTGs, some overlapped between the different groups: shock and CFC upregulated shared 4 genes, shock and CFC downregulated shared 8 genes, and one DTG was upregulated in shock and downreglated in CFC (Figure 5.6 B).

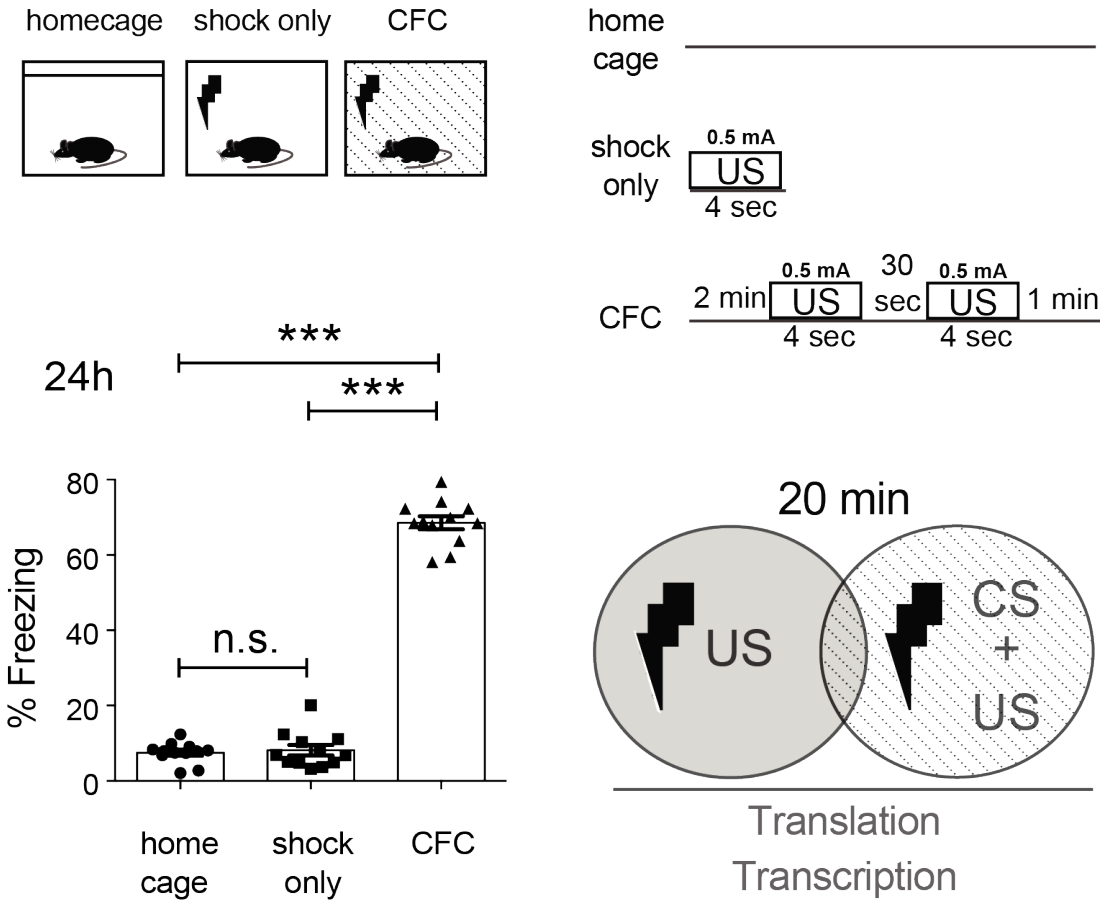

Figure 5.2 Diagram of the experimental design, describing the three experimental groups, homecage, shock only and CFC. Top: Animals in the homecage group remained in their homecage for the full duration of the experiment. Shock only animals received one 4 s footshock of 0.5 mA, immediately after being put into the context and were immediately removed to their homecage after. Animals of the CFC group were allowed to explore the context for two minutes, followed by two 4 s 0.5 mA footshocks with a 30 s interval and remained in the context for another minute before being removed to their homecage. **Bottom left:** Fear-conditioned animals (CFC group) show significant freezing behaviour when re-exposed to the fear-conditioning apparatus (context, CS) 24 h after training, whereas the other two groups show insignificant freezing behaviour in response to the context. Values are represented as mean $\pm$ standard deviation, including the individual data points. **Bottom right:** We were interested in transcriptional and translational changes after shock only (US) and in early fear memory formation (CS + US), so we picked a dissection timepoint of 20 min after the training to collect samples for ribosome profiling.

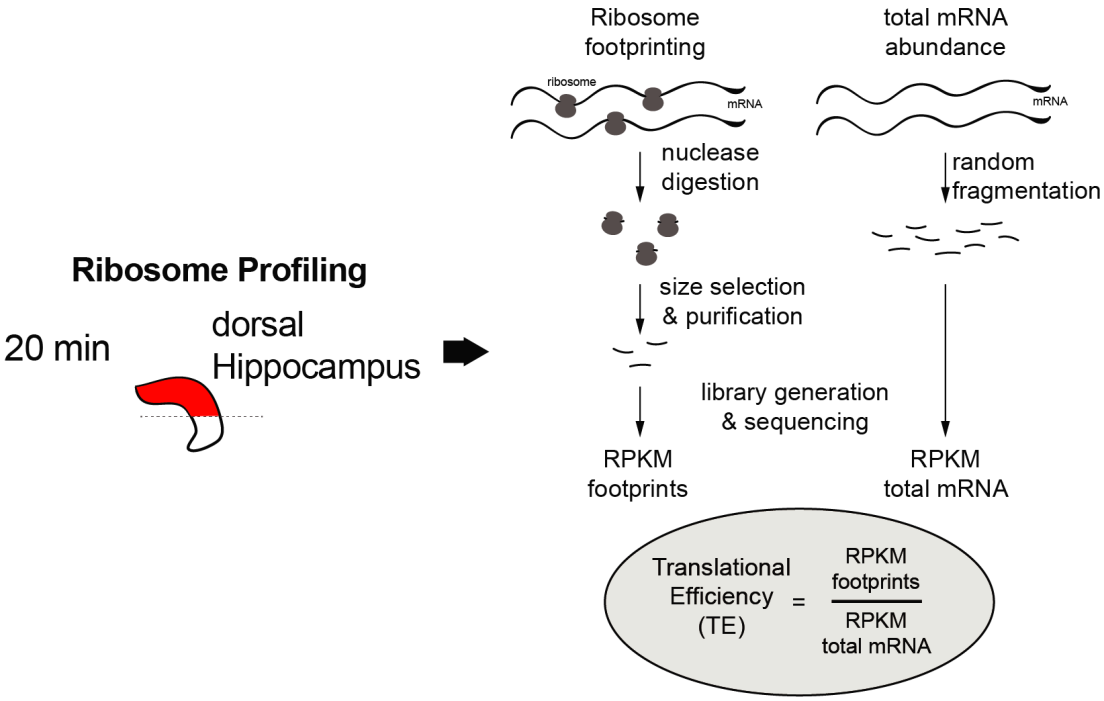

Figure 5.3 Flow diagram of the ribosome profiling strategy. Dorsal hippocampi were dissected 20 min after the experiment and snap-frozen. Polysomes were isolated and part of the lysate digested with RNase I and ribosomal footprints isolated, while from the remainder of the lysate total mRNA was extracted and heat-fragmented to yield similarly sized fragments to the footprints. cDNA sequencing libraries were generated from all fragments (footprints and total RNA) for each sample and sequenced. TE was calculated by dividing the RPKMs of footprints with total RNA.

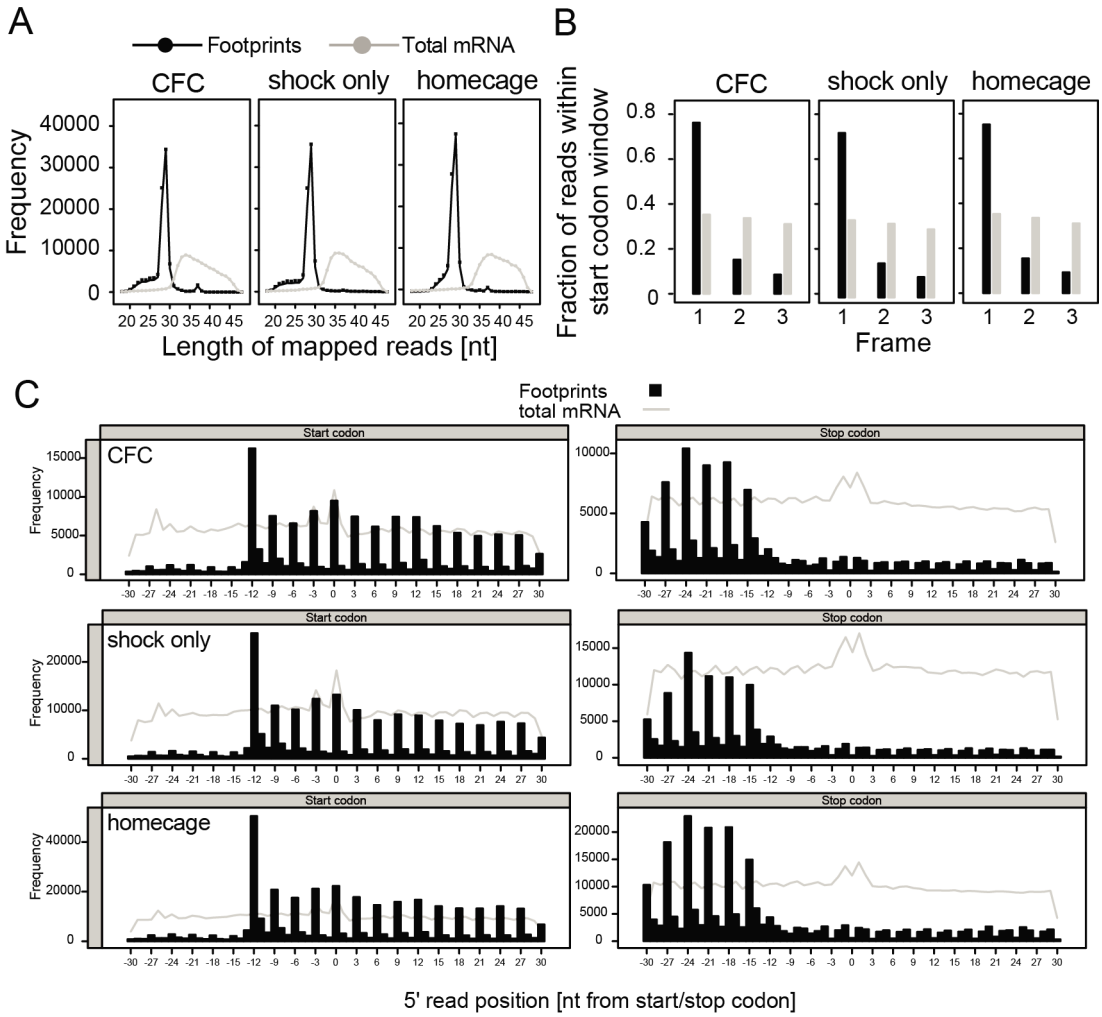

Figure 5.4 Ribosome profiling data is of good quality and reproducibility. A RPF samples show a distinct frequency peak between 28 and 30 nt, whereas total RNA samples show a broader distribution at a slightly larger size. **B** Footprints align preferentially with the first RF of their respective message, while total RNA samples align randomly with all three reading frames. **C** Around the region of the start and stop codons of each gene, footprints exhibit an increased density, compared to the rest of the coding sequence. Furthermore, footprints show a distinct three-nucleotide periodicity, whereas randomly fragmented total RNA distributes equally along the message. Notably, a small peak is visible in the footprint samples 12 nt before the start codon. This is due to the offset of the start of the footprint and the ribosomal P-site.

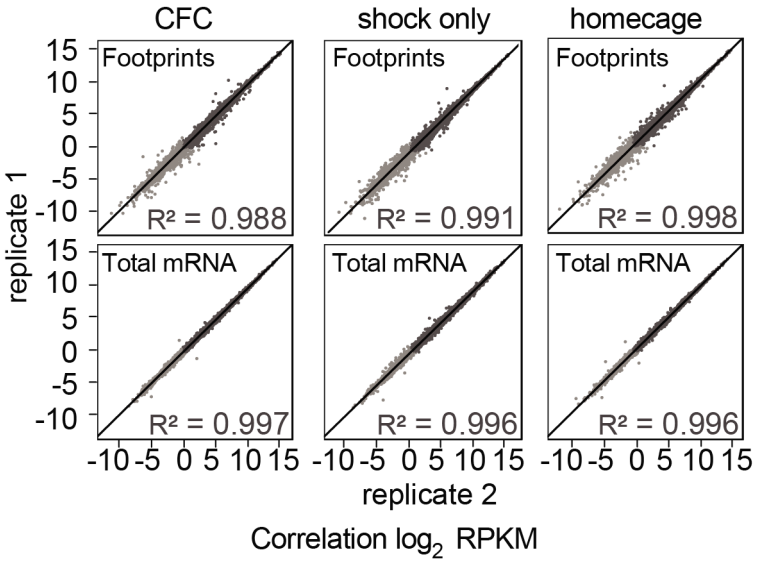

Figure 5.5 Ribosome profiling data shows high reproducibility. Scatterplots of replicate 1 vs replicate 2 of the data, confirming high reproducibility of replicates for both total RNA and footprints within the different conditions. Correlation coefficients for each comparison are noted on the respective plot.

Similarly, we identified changes in transcription through differential expression analysis. A total of 86 genes showed significant changes in transcription between shock only and homecage groups. Of these 86 differentially expressed genes (DEGs), 63 were upregulated and 23 downregulated (Table C.3). In the CFC group, a total of 155 DEGs was identified, of which 99 were upregulated and 56 downregulated compared to homecage (Figure 5.7 A, B; Table C.4). The CFC and shock upregulated gene groups shared 15 genes, and CFC and shock downregulated groups shared 2 genes. Genes that were upregulated in CFC and downregulated in shock were 3 and genes downregulated in CFC, but upregulated in shock 8 (Figure 5.7 B). The genes that were regulated by shock are summarised in Figure 5.8, genes that were common between the shock and CFC conditions in Figure 5.9, and genes that were uniquely regulated in CFC in Figure 5.10.

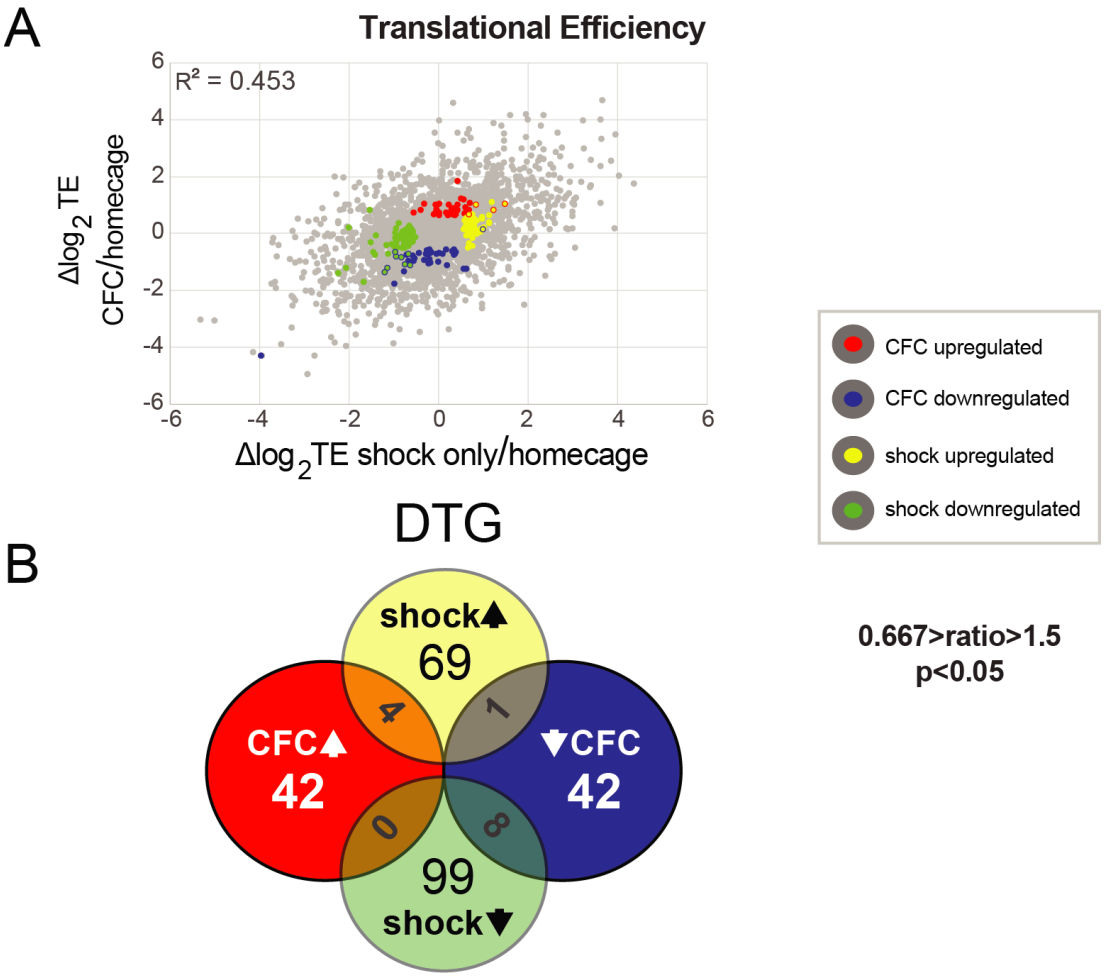

Figure 5.6 Differentially translated genes. A Changes in TE in response to shock or CFC, normalised to homecage. log_2 fold change values are plotted, coloured points represent significantly changed genes in each group as summarised in the legend. **B** The number of DTGs in each group and overlaps are summarised.

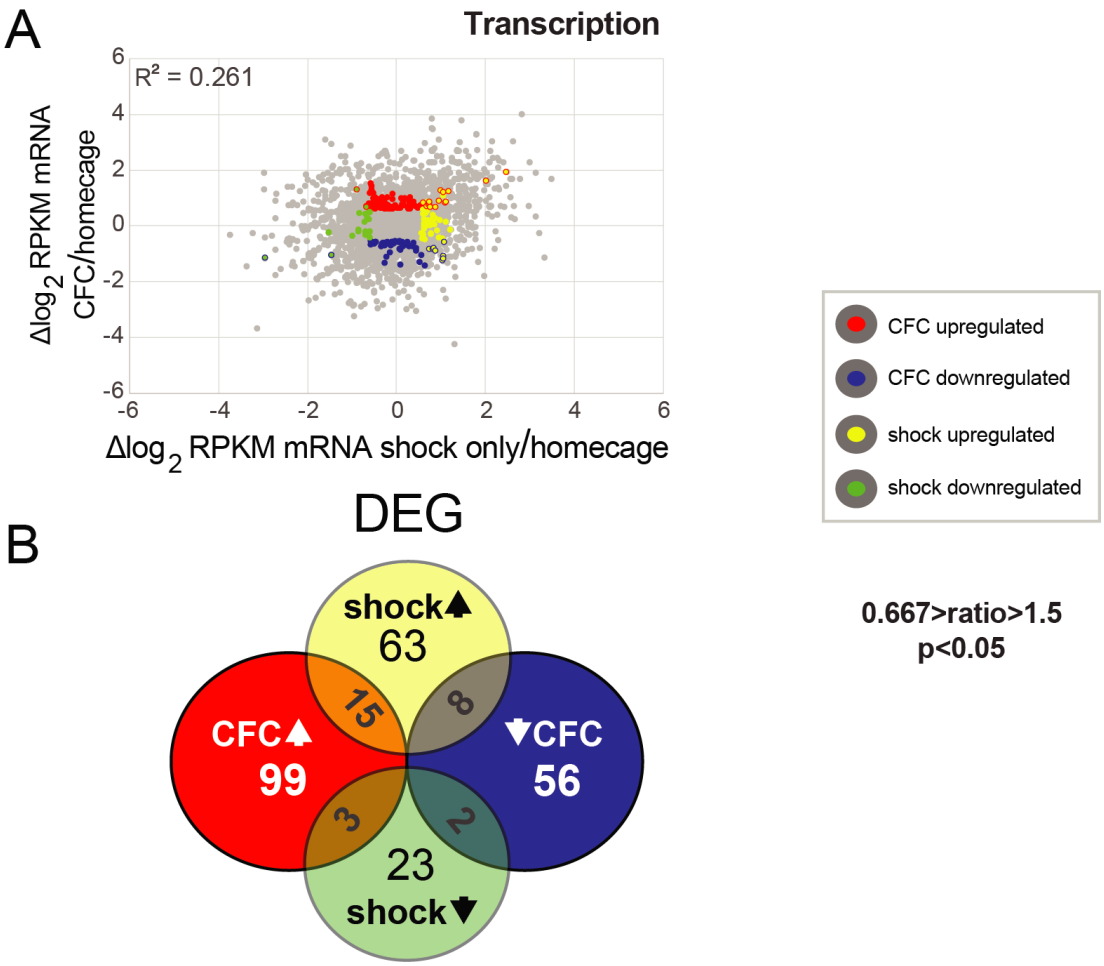

Figure 5.7 Differentially expressed genes. **A** Changes in mRNA abundance in response to shock or CFC, normalised to homecage. log_2 fold change values are plotted, coloured points represent significantly changed genes in each group as summarised in the legend. **B** The number of DEGs in each group and overlaps are summarised.

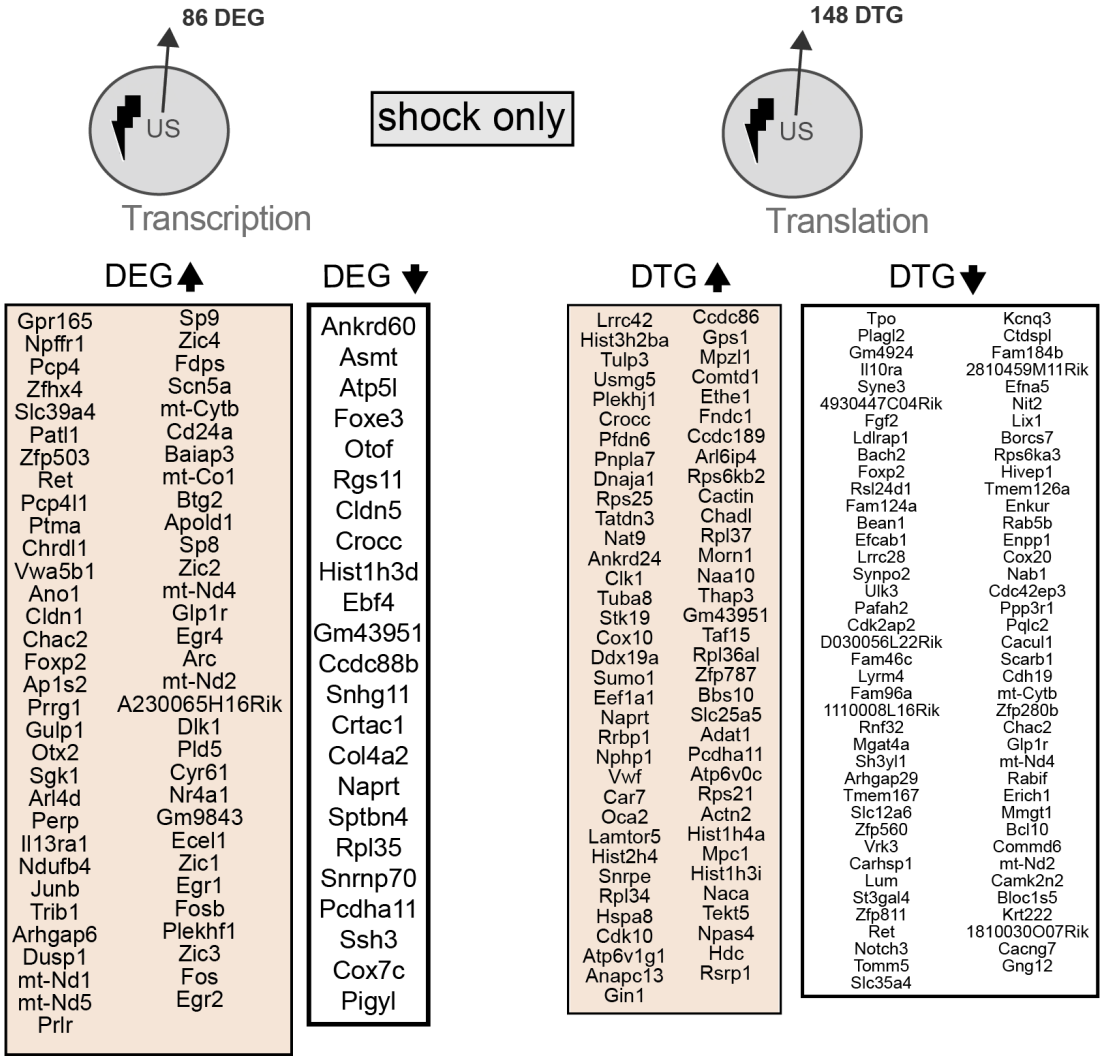

Figure 5.8 DEGs and DTGs that are regulated in response to shock only. Genes that were either up- or downregulated transcriptionally or translationally in response to a single footshock (unconditioned stimulus, US), compared to homecage.

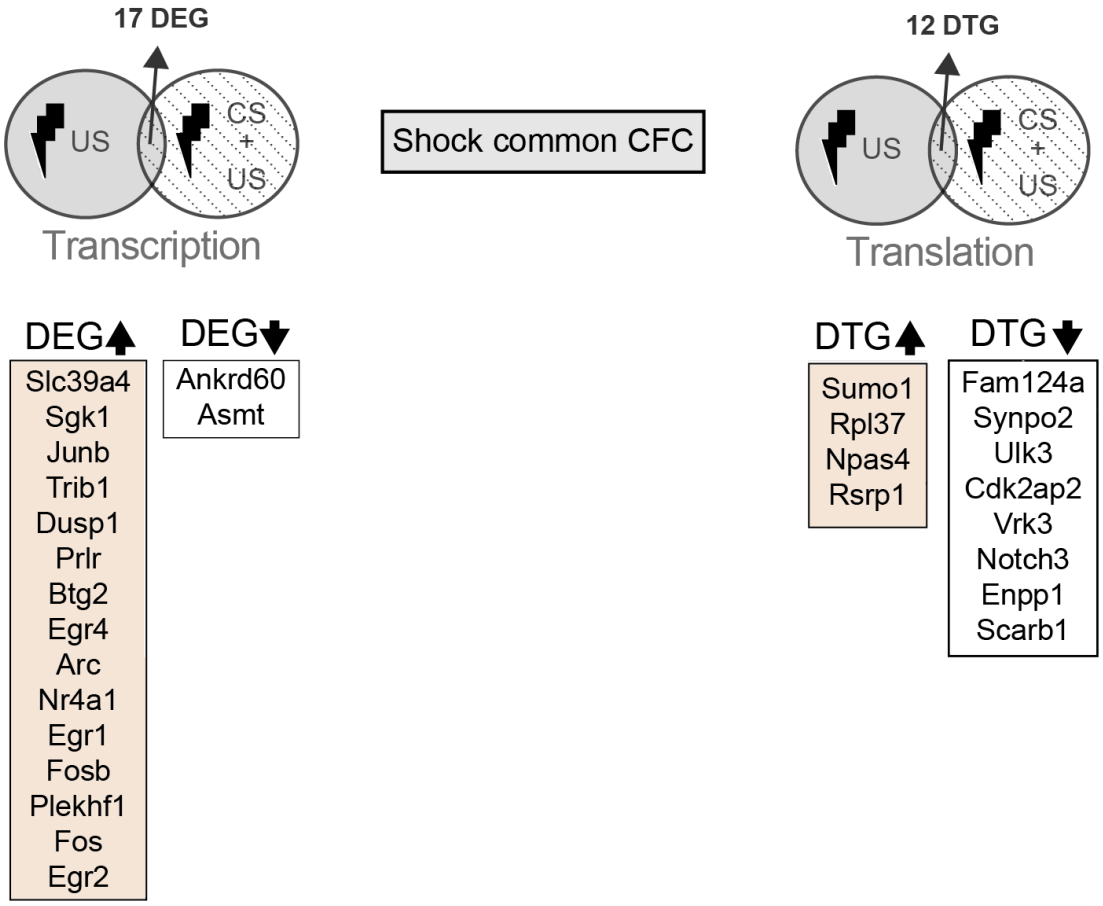

Figure 5.9 DEGs and DTGs that are regulated in both the shock control and the CFC groups. Overlap of the genes that were either up- or downregulated transcriptionally or translationally in response to CFC (CS + US) and shock only (US), compared to the homecage condition

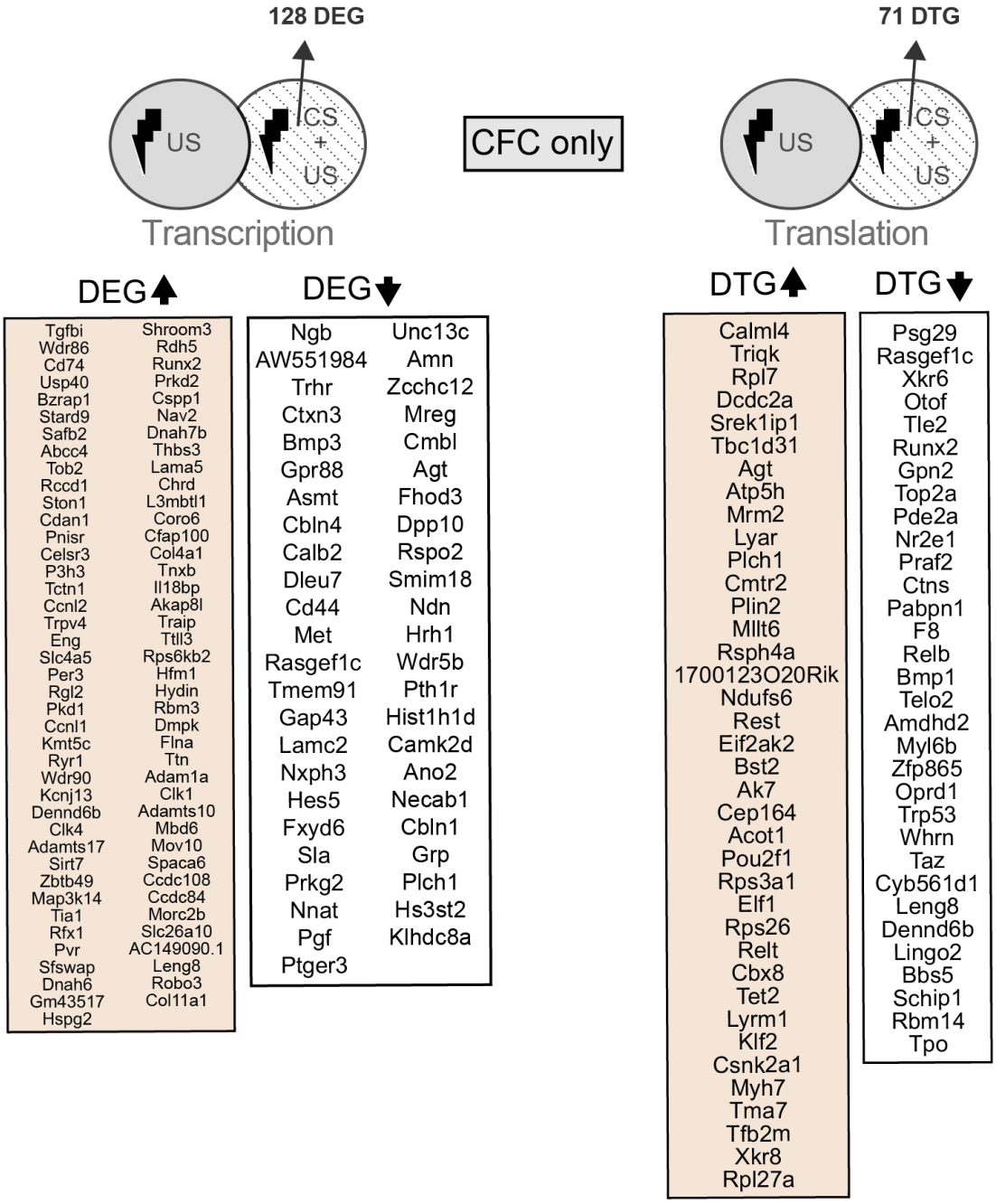

Figure 5.10 DEGs and DTGs that are regulated uniquely in the CFC group. Genes that were either up- or downregulated transcriptionally or translationally in response to CFC (CS + US), compared to homecage and that were not in the shock only (US) groups.

5.3.1.1 GO analysis

To gather a better understanding of the genes being regulated by shock only and CFC, we conducted gene ontology (GO) analysis, using DAVID (Huang et al., 2009a,b) and IPA (Qiagen). To this end, we analysed only two groups of DEGs and DTGs each: genes that were regulated by shock (Figure 5.8) and genes that were uniquely regulated in CFC (CFC genes with the overlap of CFC and shock genes removed)(Figure 5.10). Genes were analysed in different categories, including cellular component (CC), molecular function (MF), biological process (BP), and Kyoto Encyclopedia of Genes and Genomes (KEGG) pathways.

For the DEGs identified in the shock only group, several groups related to energy metabolism at the mitochondrion and terms related to DNA binding and transcription factors were enriched in all four categories (Figure 5.11). This may point towards the need to alter cellular states in response to a fearful stimulus and start a wave of transcription and translation to form a memory.

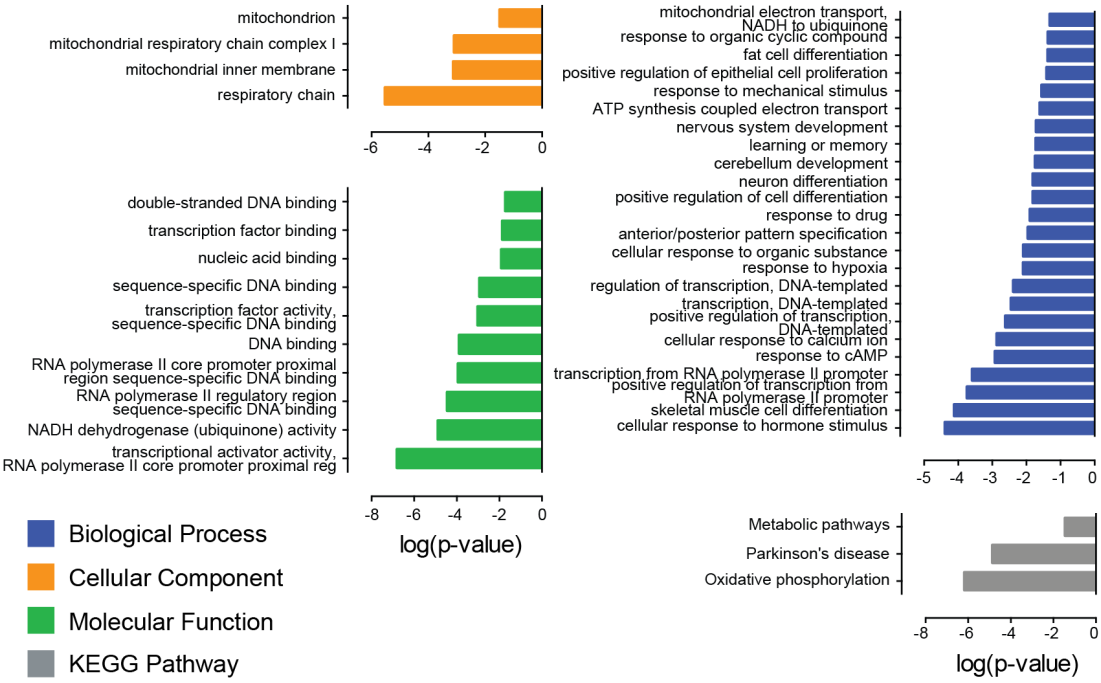

Figure 5.11 DAVID analysis of DEGs in shock only. Terms identified as significantly enriched in the categories biological process, cellular component, molecular function, and KEGG pathway. The name of the terms are shown with their respective $\log_{10}$(p-value) represented as a bar graph.

In the DTGs of the shock only group, we identified several terms in three of the categories, that are related to the ribosome (Ribosome pathways, ribosome and large ribosomal subunit CC, and structural constituent of ribosome MF). Some CC terms were related to the ECM, extracellular exosome and lysosomes. Genes related to the regulation of translation appeared to be involved as well, as translation is the most significant term in BP and the MAPK pathway was identified in KEGG pathways. Lastly, several genes related to the nucleosome and chromosomes were identified, indicating the need of the cell to alter the DNA packaging status to respond to a stimulus, such as an electrical shock (Figure 5.12).

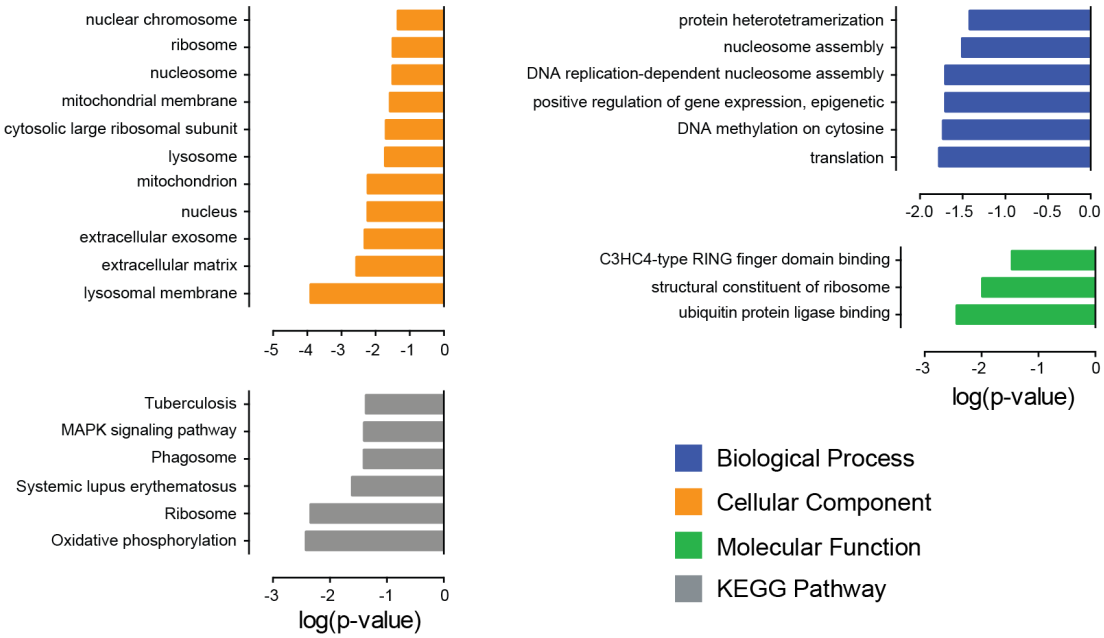

Figure 5.12 DAVID analysis of DTGs in shock only. Terms identified as significantly enriched in the categories biological process, cellular component, molecular function, and KEGG pathway. The name of the terms are shown with their respective $\log_{10}$(p-value) represented as a bar graph.

Using IPA, we identified enriched canonical pathways relating to the mitochondrion and oxidative phosphorylation in shock only DEGs and DTGs (Figure 5.13).

Several terms, in more than one category, relating to the ECM (proteinaceous extracelllular matrix, extracellular matrix, extracellular space, extracellular region. extracellular matrix organisation, and ECM-receptor interaction) were identified in the DEGs unique to the CFC group. The ECM has been shown to play an important role in synaptic plasticity, including fear memory formation (Dityatev,

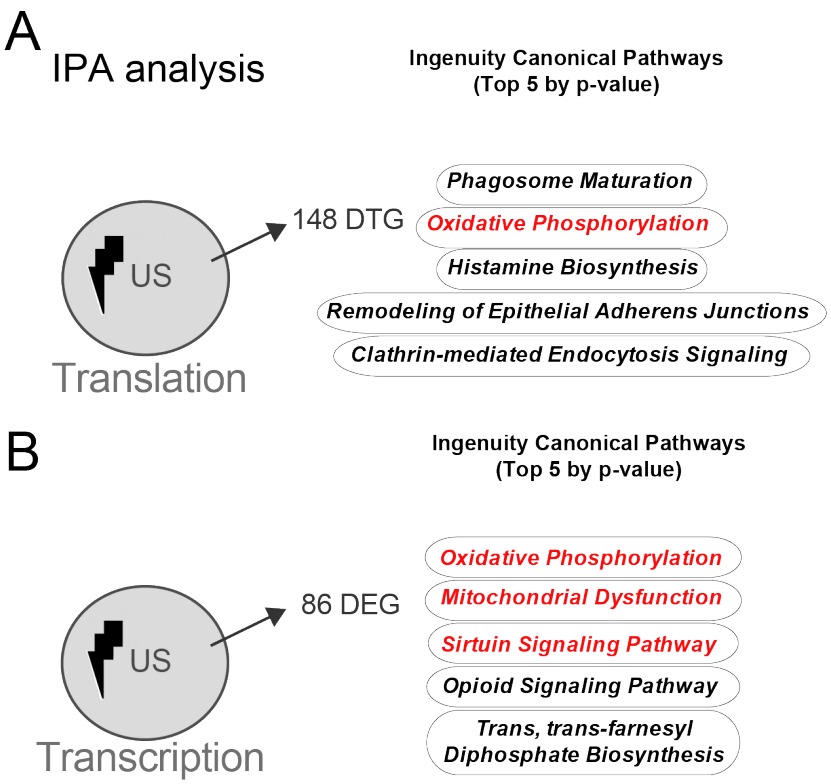

Figure 5.13 IPA analysis of DTGs and DEGs shock only. Top 5 Ingenuity Canonical Pathways (by p-value) identified by IPA in the **A** DTGs and **B** DEGs. The highlighted (red) pathways are related to mitochondrial function.

2014; Hylin et al., 2013). Additionally, several terms relating to mRNA translation regulation were enriched in the DEGs (Figure 5.14).

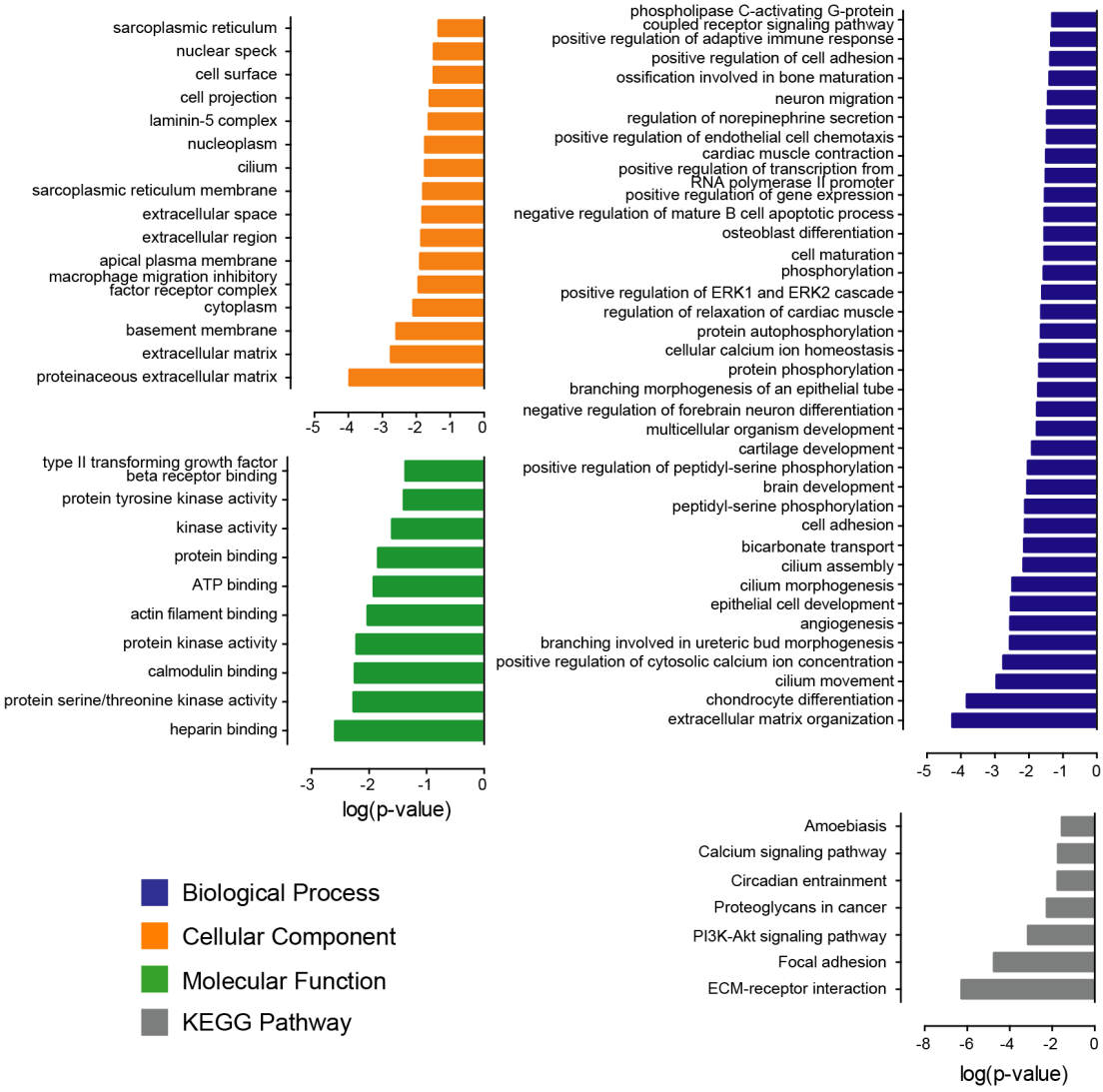

Figure 5.14 DAVID analysis of unique DEGs in CFC. Terms identified as significantly enriched in the categories biological process, cellular component, molecular function, and KEGG pathway. The name of the terms are shown with their respective $\log_{10}$(p-value) represented as a bar graph.

Similarly to the shock only DTGs, the CFC DTGs were enriched in ribosome related terms (ribosome CC, structural constituent of ribosome, Ribosome KEGG, rRNA methylation). Furthermore, they were enriched for terms relating to transcription and translation (including transcription factor complex, nucleus, transcriptional activator activity, DNA binding, transcription, translation, and more; Figure 5.15). This is evidence for the importance of transcription and translation in the process of forming fear-related memories.

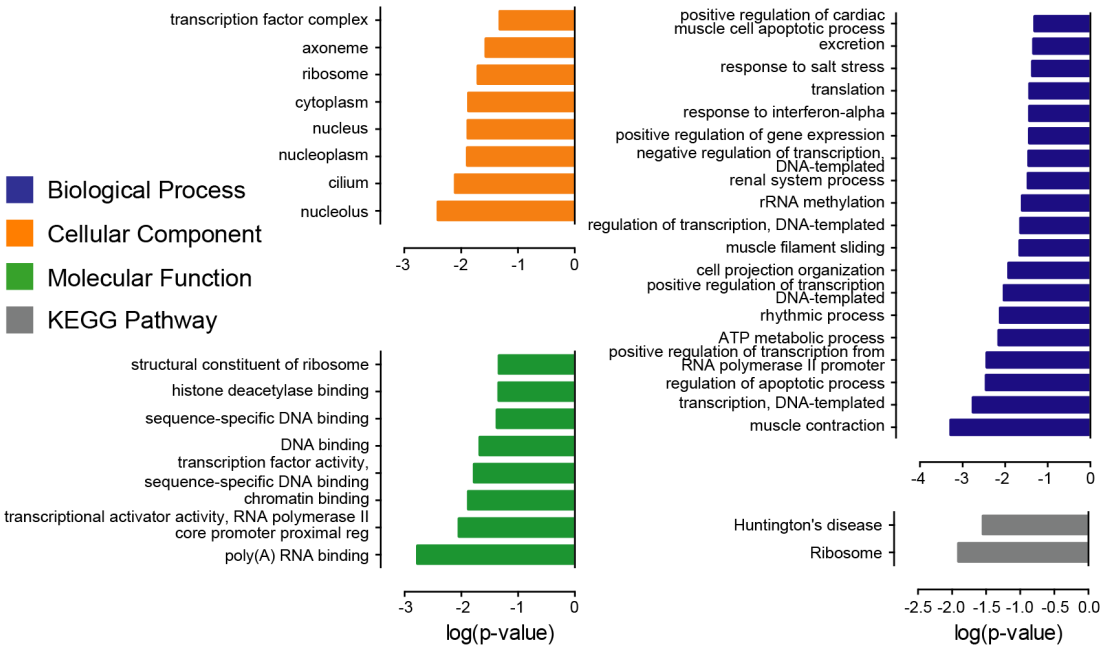

Figure 5.15 DAVID analysis of unique DTGs in CFC. Terms identified as significantly enriched in the categories biological process, cellular component, molecular function, and KEGG pathway. The name of the terms are shown with their respective $\log_{10}$(p-value) represented as a bar graph.

Notable pathways identified with IPA in the DTGs included eIF2 signalling and role of PKR in interferon induction response, as well as axonal guidance signalling in the DEGs (Figure 5.16).

Cho et al. (2015) had previously reported a translational suppression of genes related to the translational machinery in hippocampus and cultured hippocampal neurons, but not in other cell types. Since by now there is more ribosome profiling data (across different tissues) available from publications and our DAVID analysis identified several terms related to ribosomes and translation in our DTGs, we decided to carry out further analysis of our data, with expression of ribosomal genes in mind. Nevertheless, our analysis shows results in disagreement with Cho et al. (2015)'s findings. We clearly detected polyribosomes in both dorsal hippocampal tissue and DIV25 hippocampal neurons, at comparable levels to HEK293 cells (Figure 5.17A), indicating normal levels of proteins of the translational machinery. Using Western blotting in different tissue lysates (hippocampus, kidney, liver muscle, and spleen), we were were able to detect comparable levels of two proteins of the small ribosomal subunit (rpS6 and rpS15) at equal levels in all tested tissues (Figure 5.17 B). Three proteins of the large ribosomal subunit (rpL13, rpL10a, and rpL11) were detectable in hippocampus but expressed at a lower level compared to other

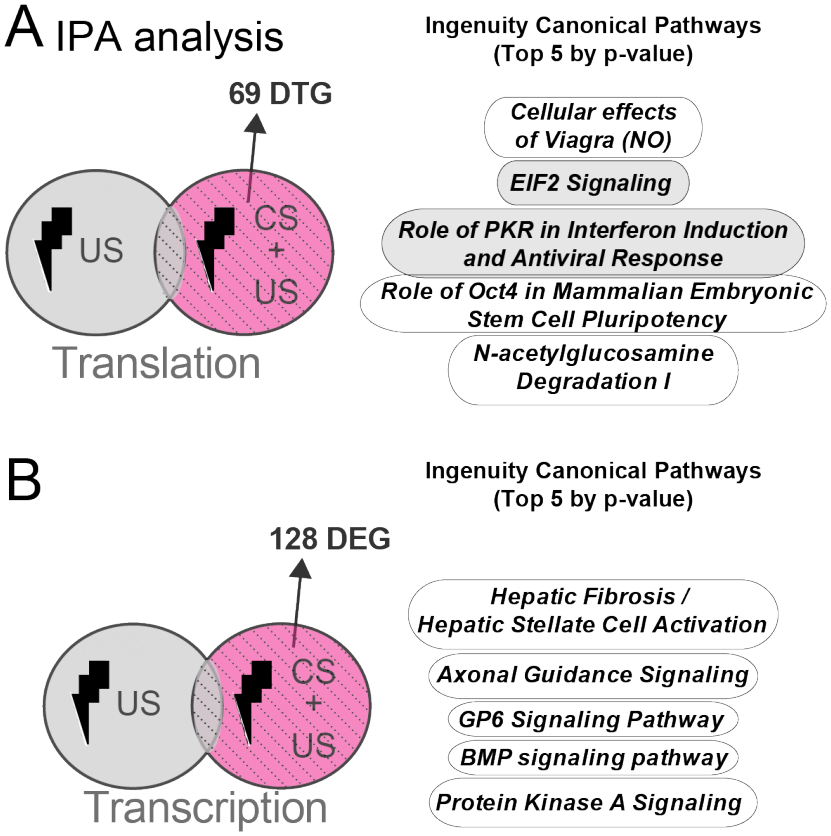

Figure 5.16 IPA analysis of unique DTGs and DEGs CFC. Top 5 Ingenuity Canonical Pathways (by p-value) identified by IPA in the **A** DTGs and **B** DEGs. The shaded pathways are relevant gene expression pathways.

tissues (Figure 5.17 B). When looking at overall TE of the whole translatome compared to the ribosomal and mitochondrial ribosomal translatome in several different tissues and cell types, we saw a general trend for lower TE values in the ribosomal translatome across all datasets (Figure 5.17 C). Collectively, our data does not support a translational repression of genes of the ribosomal machinery, specifically in brain, but does not exclude any specific ways of regulating translation and perhaps making it more efficient in neurons.

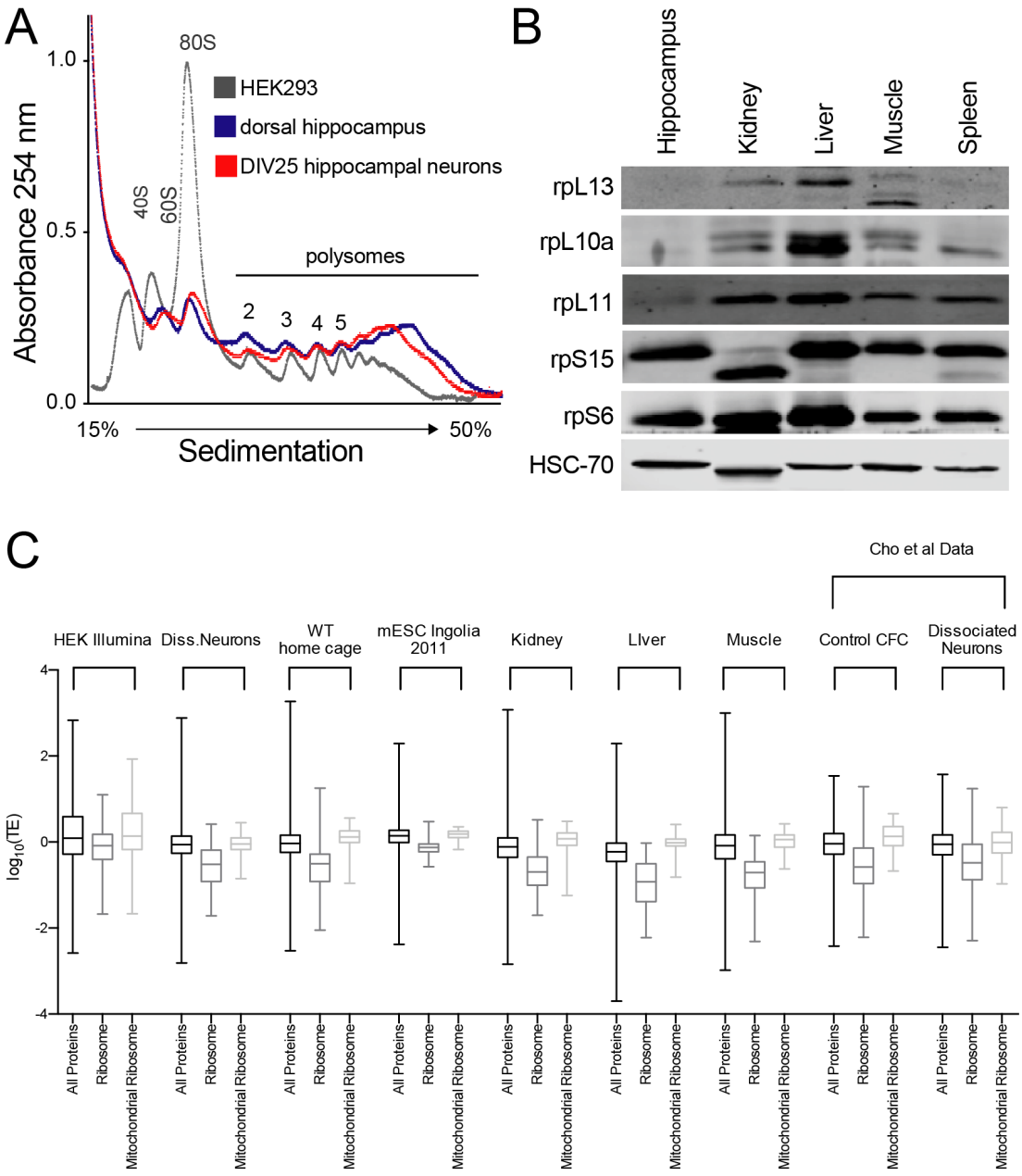

Figure 5.17 Ribosomal genes do not show a particular pattern of expression. A Polysome profiles of HEK293 cells, dorsal hippocampus, and DIV25 primary hippocampal neurons. The HEK293 profile shows a stronger 80S monosome peak, but all three samples show comparable levels of polysome associated mRNAs. **B** Immunoblots against ribosomal proteins in different murine tissues. HSC-70 is shown as a loading control. As evidenced by these blots, not all ribosomal proteins are expressed at equal levels across all tissues (rpL13, rpL10a, and rpL11), however, some of the ribosomal proteins are expressed at comparable levels in all tissues tested (rpS6 and rpS15). **B** Box plots of TEs of mRNAs encoding ribosomal proteins, mitochondrial ribosomal proteins, or all other proteins. Overall, ribosomal protein genes show a trend towards reduced TE in comparison to the two other groups, across different tissues and cell types. HEK Illumina is a test data set from the Truseq Ribosome Profiling Kit, Diss. Neurons Primary dissociated cortical neurons (data from our lab), mESC Ingolia 2011 a published dataset from murine embryonic stem cells (Ingolia et al., 2011), Kidney published data (Castelo-Szekely et al., 2017), Liver published data (Janich et al., 2015), Muscle published data (Drummond et al., 2017), published data from Cho et al. (2015).

5.3.1.2 UTR analysis

Untranslated regions (UTRs) of mRNAs can contain sequence elements, which may regulate the translation of the associated transcript and thereby explain changes in translational efficiency in response to a specific signal. Therefore, we analysed the UTRs of DTGs from the CFC group, along with a control group of unchanged genes, that were randomly selected from our data set, for known UTR motifs using a stand-alone version of Utrscan (Pesole and Liuni, 1999), which scans input sequences for all known UTR motifs. The results are summarised in Figure 5.18, shown are only motifs that were identified in the gene groups more than once. Several trends were observed, as described below, however, none of these trends reached statistical significance. The 5' UTR of genes downregulated by CFC showed an increased abundance of upstream open reading frames (uORFs), compared to control and upregulated genes. Both groups of DTGs also appeared to contain less internal ribosome entry sites (IRES) in their 5' UTR, compared to the control gene group. Within the 3' UTR, UNR binding sites appear more frequently in both up- and downregulated DTGs, compared to the control group, whereas SXL binding sites (SXL BS) and GY-boxes are less abundant compared to the control genes. Cytosolic polyadenylation elements (CPE) appear more abundant in 3' UTRs of upregulated genes compared to downregulated and control DTGs. Alcohol dehydrogenase 3' UTR downregulation control element (ADHDRE), G-quadruplex structure (PG4), and K-box are less abundant in the downregulated group

compared to the other two groups. Brd box and GU-rich destabilization element (GRE) are motifs that are less abundant in the DTG down group and more abundant in the DTG up group compared to control genes. The polyadenylation signal (PAS) was less frequently identified in the CFC upregulated group compared to control and downregulated genes. Very little is known about UTR motifs and their relation to synaptic plasticity and memory, however, we know some motifs respond specifically to defined signals from pathways regulating translation that are essential to memory formation. For example, mTORC1 has been shown to regulate translation of mRNAs containing TOP elements (Thoreen et al., 2012) and translation of uORF-containing mRNAs may be regulated by eIF2α(Costa-Mattioli et al., 2007; Eacker et al., 2017) and impinge on memory translation.

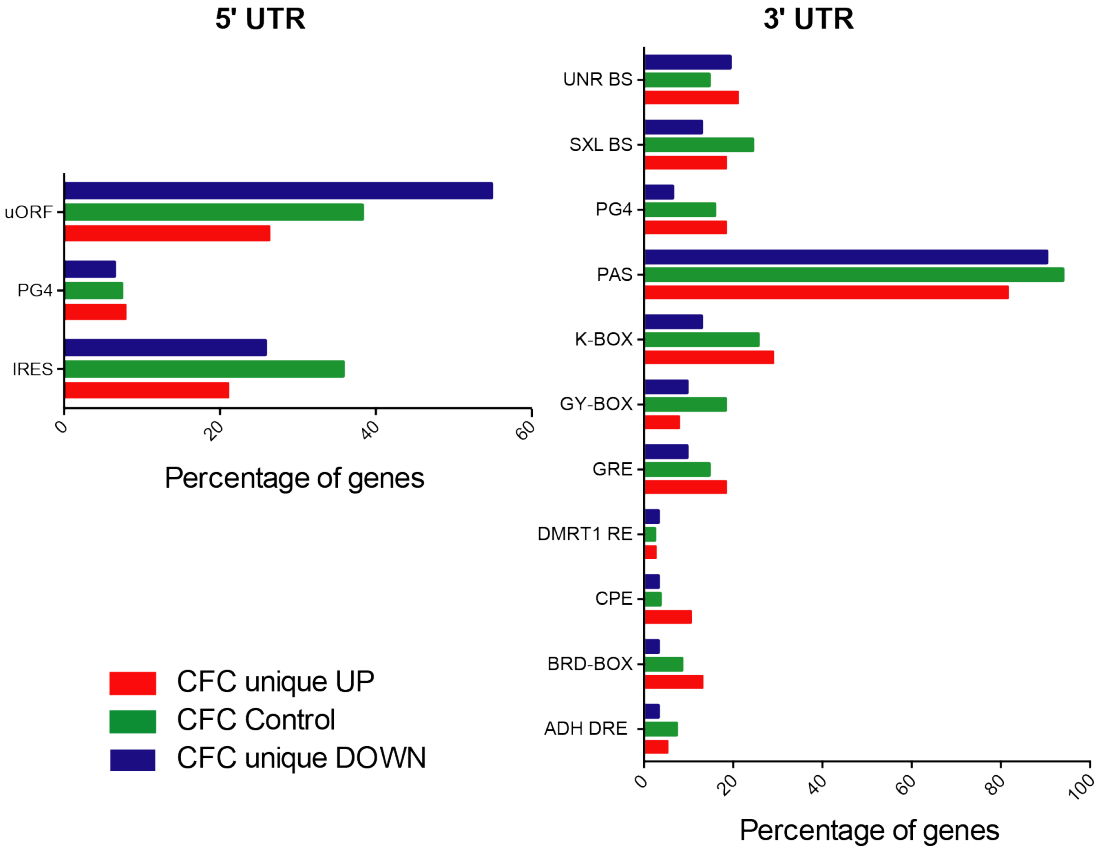

Figure 5.18 UTR motifs identified in DTGs. Known UTR motifs identified in 3' and 5' UTR, respectively, in DTGs specific to CFC. The data is presented as percentage of genes, in each indicated group, that contain the motif at least once in their UTR.

We also extracted and calculated some basic UTR characteristics, such as length, GC content and Gibbs free energy (a value that can be used to describe the complexity of secondary structures that an RNA molecule is most likely

to adopt in order to increase its stability). We did not observe any significant differences in the length of the 3' UTRs, but upregulated DTGs contained longer 5' UTRs than downregulated DTGs (one-way ANOVA). Genes downregulated by CFC had higher GC content in their 3' UTR compared to upregulated genes. The GC content in the 5' UTR was only different, when comparing the control gene group with the upregulated genes. The Gibbs free energy calculated for the UTRs only showed a significant difference in the 5' UTR, when comparing downregulated genes with upregulated genes. Downregulated genes exhibited lower Gibbs free energy, which indicates a higher complexity in the secondary structure.

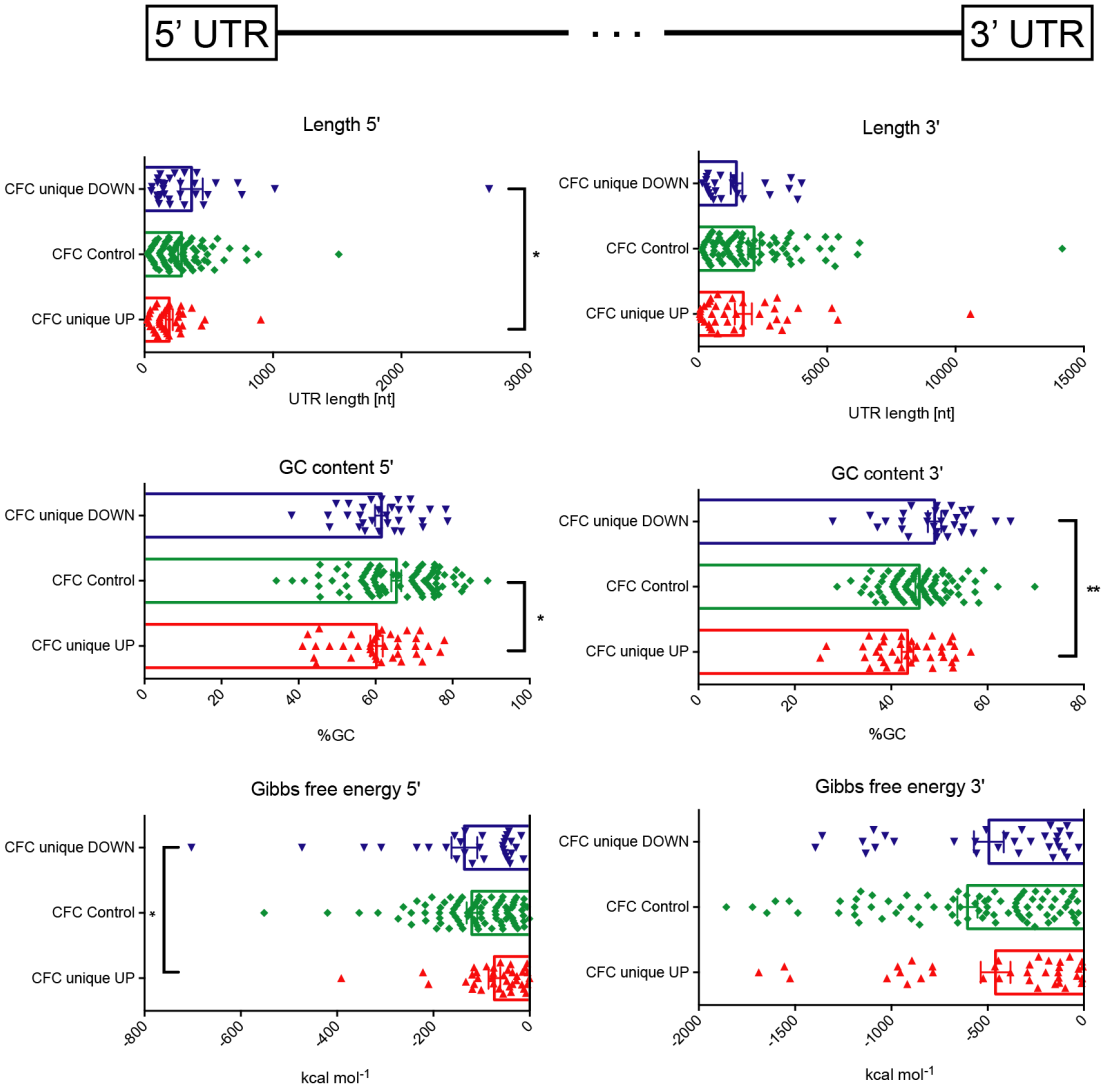

Figure 5.19 Summary of the basic UTR statistics for DTGs in CFC. Summary of length, GC content and Gibbs free energy of UTRs retrieved for DTGs in CFC. Bar graphs for the indicated values representing the means and standard error of the mean, as well as individual data points for each gene. Shown are percentage of GC nucleotides in the UTR, length of UTR, and Gibbs free (folding) energy of UTR sequence. Significance in multiple comparisons one-way ANOVA is indicated on the graphs (* $p \leq 0.05$, ** $p \leq 0.01$.)

5.3.2 qPCR of targets

To validate the specificity of our sequencing data and see if we could use any of our targets as marker genes of memory formation, we picked two to three DEGs from each of the following groups: *CFC/shock only common upregulated* (c-fos, Arc, Egr2), *CFC/shock only common downregulated* (Ankrd60, Asmt), *CFC unique upregulated* (Col11a1, Robo3, Leng8), and *CFC unique downregulated* (Hs3st2, Camk2d, Klhdc8a).

c-fos (Fos proto-oncogene), a transcription factor, is a commonly used marker of recent neuronal activity and important in cancer and cell growth.

Egr2 (early growth response protein 2), a transcription factor, is involved in cell growth and migration.

Arc (activity-regulated cytoskeleton-associated protein) is a master regulator of synaptic plasticity.

Col11a1 (Collagen, type XI, alpha-1) is a collagen coding gene associated with genetic disorders and is differentially expressed in the superficial-deep CA1 hippocampal axis, linked to hippocampal place cells and spatial memory (Cembrowski et al., 2016; Mallory and Giocomo, 2018)

Robo3 (roundabout guidance receptor 3) is a member of the roundabout family and codes for a gene of key function in axonal navigation during neurodevelopment (Friocourt and Chédotal, 2017).

Leng8 (leucocyte receptor cluster gene 8) is highly expressed in brain and predicted to be involved in RNA transport and was previously shown to be upregulated in mouse hippocampus 1 h after CFC (Peleg et al., 2010).

Akrd60 (ankyrin repeat domain 60) is a gene of unknown function.

Asmt (acetylserotonin O-methyltransferase) is an enzyme that catylyzes the final step in melatonin biosynthesis. It has previously been associated with psychiatric disorders.

Hs3st2 (heparan sulfate-glucosamine 3-sulfotransferase 2) is an enzyme that generates distinct heparan sulfate fine structures and is expressed predominantly in the brain and may thus play a role in the nervous system.

Camk2d (Calcium/Calmodulin dependent protein kinase II delta) is a calcium dependent kinase important for several aspects of glutamatergic plasticity, this gene encodes the delta chain of the protein.

Klhdc8a (kelch domain-containing protein 8a) is a a gene commonly found to be upregulated in glioma and commonly expressed in nervous tissue.

c-fos, Egr2, and Arc are in the group of IEGs commonly used to show recent neuronal activity. We ran qPCRs targeting the listed genes and with the exception of Ankrd60 and Asmt confirmed the differential expression of our targets. Upon further investigation into the ribosome profiling raw data, Ankrd60 and Asmt appeared to be false positives identified by the differential expression analysis (Table 5.3) and were excluded from the target validation.

Table 5.3 Raw RPKM values for Asmt and Ankrd60, showing that the differential expression between conditions is inconsistent within the replicates and most likely a false positive.

Gene Symbol	homecage 1	homecage 2	shock only 1	shock only 2	CFC 1	CFC 2
Asmt	0.8201	1.2447	0.2112	0.5534	0.5165	0.4519
Ankrd60	4.405	0.5085	0.5325	0.1077	1.8356	0.3115

Notably, c-fos and Arc, which are commonly used as markers for memory formation, are not specifically associated with the fear memory, but also with the shock only condition, in which no memory forms. Therefore, some of the genes we identified that are uniquely up- or downregulated in the CFC group, e.g. Col11a1, Robo3 or Leng8 may be more suitable markers of memory formation. To test this hypothesis, on a more "softer" type of memory task, we trained WT animals in a modified object location (OL) task, mimicking the controls we used in the CFC protocol. OL memory is also hippocampus and location-dependent, but does not contain a fear component. We trained animals as detailed in Figure 5.1, dissected their dorsal hippocampi 20 min after the training or mock training session and extracted RNA for qPCR. When quantifying expression of the genes identified in the CFC tissue, we saw some similarities in expression. C-fos, Arc and Egr2 followed the same expression pattern in OL as in CFC, as they were upregulated in both sham and training groups. The genes identified as uniquely down- or upregulated in CFC, compared to homecage and shock did not follow the same expression pattern in OL trained animals. Camk2d was downregulated in both sham and training and Hs3st2 showed great variability between replicates that made it difficult to draw any conclusions. Our targets

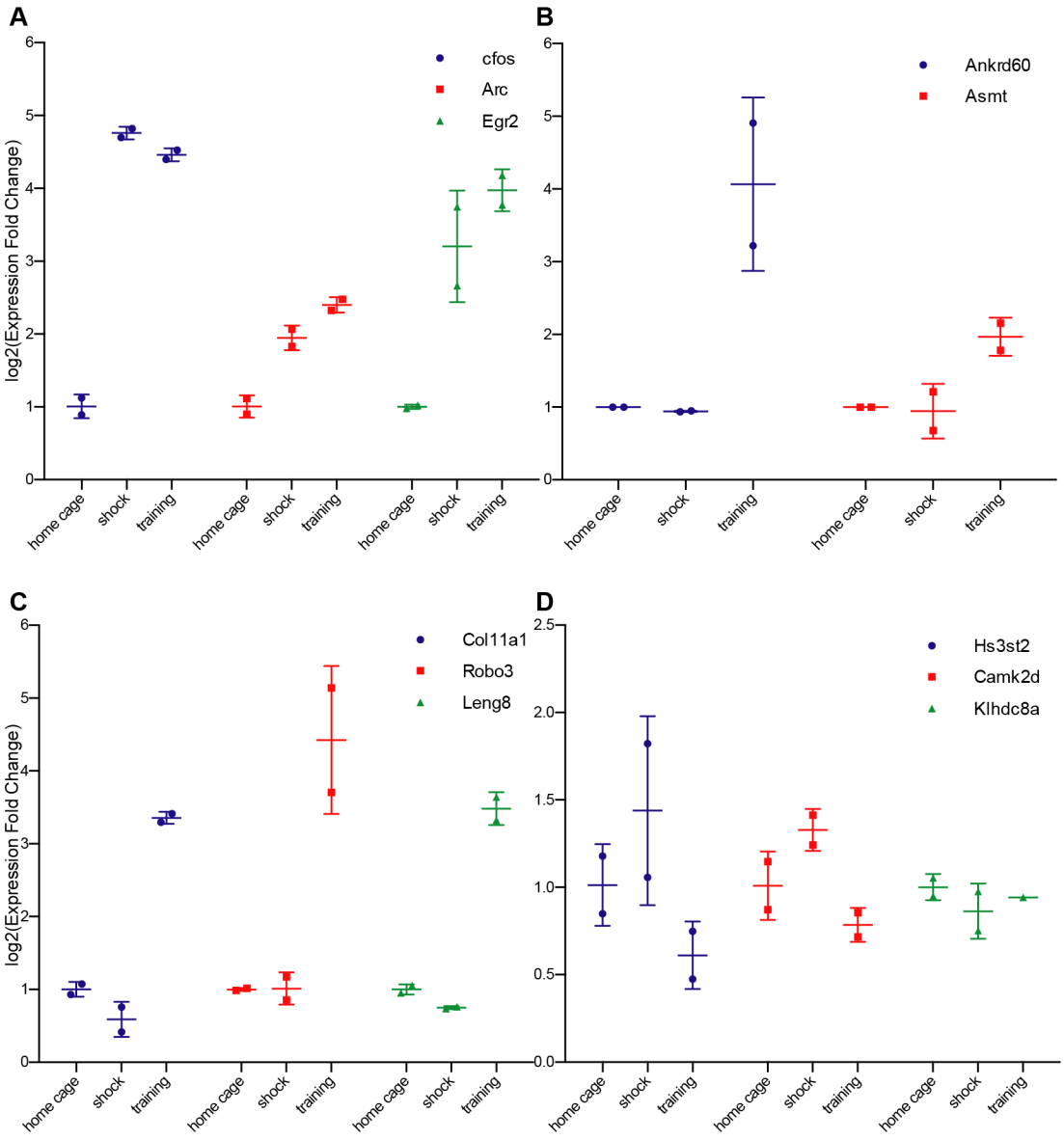

Figure 5.20 Quantification of qPCRs of potential marker genes of memory formation. $\Delta\Delta C_t$ quantification of qPCRs of indicated mRNAs in each sample. **A** mRNAs that were upregulated in both shock only and CFC groups in the total mRNA sequencing data. **B** mRNAs that were downregulated in both shock only and CFC groups in the total sequencing mRNA data. **C** mRNAs that were upregulated in the CFC group, but not in the shock only group, in the total sequencing mRNA data. **D** mRNAs that were downregulated uniquely in the CFC group, but not in the shock only group, in the total sequencing mRNA data. Values are represented as mean $\pm$ standard deviation, including the individual data points (n = 2, except for the training group for Klhdc8a n =1).

from the genes uniquely upregulated in CFC, Col11a1, Robo3, and Leng8, were downregulated in both sham and training groups. Taken together, this implies

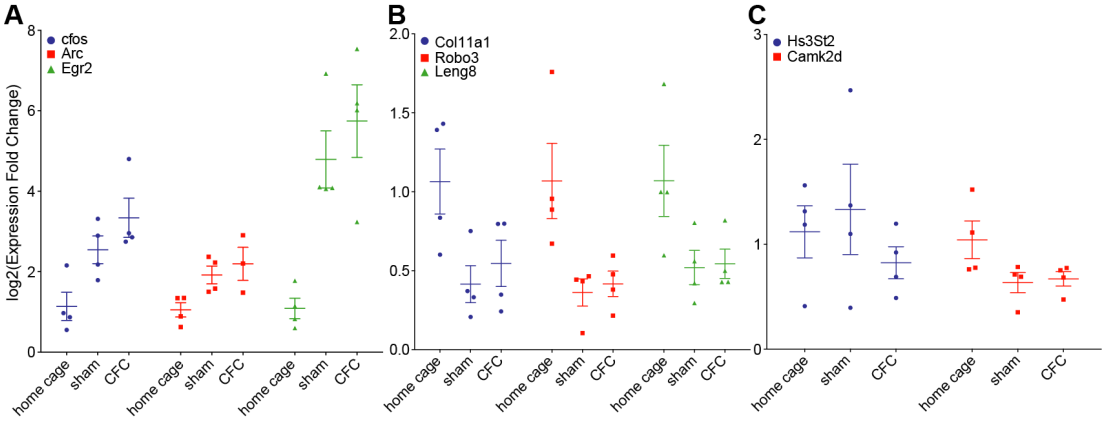

Figure 5.21 Quantification of qPCR in animals trained in the OL task. qPCRs of indicated mRNAs in each sample. **A** mRNAs that were upregulated in both shock only and CFC groups. **B** mRNAs that were upregulated in the CFC group, but not in the shock only group. **C** mRNAs that were downregulated in the CFC group, but not in the shock only group. Values are represented as mean ± standard deviation, including the individual data points.

that our newly identified markers for early memory, are suitable for fear-related memories but not other memory tasks such as OL tasks.

5.4 Discussion

With this project we set out to dissect the contribution of the electrical shock as a potentially confounding factor in experiments studying gene expression in a contextual fear conditioning paradigm. We showed that a single electrical shock, as it is commonly used to fear condition rodents (which is insufficient to produce a context-dependent memory, Figure 5.2), is sufficient to elicit significant gene expression, within both transcription and translation, in the mouse dorsal hippocampus only 20 min after behavioural training. Furthermore, using GO analysis, we showed that differentially expressed and translated genes in the shock only group were involved in several functions/pathways related to gene expression. In the CFC group, DEGs and DTGs produced GO terms related to synaptic plasticity, gene expression, and signalling pathways were identified. We analysed UTRs of DTGs for enrichment in motifs and/or some basic statistics such as length, GC content, and Gibbs free energy, finding no significant differences, but some interesting trends towards differential usage in some of the categories. qPCR of targets identified with ribosome profiling confirmed several candidate genes as potential markers for memory formation (in the fashion of immediate early genes, e.g. cfos, Arc, Egr2), namely Col11a1, Robo3, Leng8, Hs3st2, Camk2d, and Klhdc8a. When tested in a less invasive memory task (object location), however, these marker genes were suboptimal.

We have shown convincingly that the contribution of the electrical shock in fear conditioning paradigms is non-negligible when conducting gene/protein expression studies. A considerable number of genes that changed expression in the dorsal hippocampus of conditioned animals overlapped with genes differentially regulated in the group that received only a foot shock (approx. 18% of DEGs and 15.5% of DTGs of the CFC group). Thus, when studying fear-related gene-expression it is of great importance to carefully design experiments and use appropriate controls.

GO analysis revealed interesting categories for all data sets examined. Shock only genes, both DEGs and DTGs, were enriched for terms relating to the mitochondrion and energy metabolism. This could relate to a heightened state of readiness to synthesise new mRNAs and proteins. As shown by our data, a single footshock elicited considerable changes in both transcription (68 genes) and translation (168 genes) in the dorsal hippocampus within just 20 min. Memory formation in the brain requires both transcription and translation

(Alberini and Kandel, 2015; Costa-Mattioli et al., 2009), which are both energy dependent processes. Furthermore, several GO terms were related to DNA transcription, supporting our hypothesis. Importantly, quite a few IEGs, which we have shown to be regulated by shock, function as transcription factors, which may explain the enrichment in transcription related GO terms.

In the CFC unique group, we found enrichment in different terms relating to the ECM as well as intracellular signalling pathways impinging on translation. Both of these are key to synaptic plasticity and memory formation (Costa-Mattioli et al., 2009; Dityatev, 2014; Hylin et al., 2013). Furthermore, terms related to both transcription and translation were enriched, again highlighting their importance in the formation of new memories.

A published study using ribosome profiling of the brain (Cho et al., 2015) had suggested that translation of ribosomal genes is suppressed in neuronal cells compared to all proteins and mitochondrial ribosomal genes. Cho et al. (2015) did not observe these changes in mouse embryonic stem cells or other tissues (kidney, testis, liver). We analysed several of our own (dissociated WT cortical neurons, and homecage data) and some published ribosomal profiling data sets (murine embryonic stem cells (Ingolia et al., 2011), Kidney (Castelo-Szekely et al., 2017), Liver (Janich et al., 2015), Muscle (Drummond et al., 2017), Cho et al. (2015) published data, and a HEK293 sample data set from Illumina) for TE of ribosomal genes. As shown in Figure 5.17 C, except for HEK293 cells (which are a highly translationally active cell type), all tissues and cell types analysed showed a pattern of lower TE in ribosomal genes compared to all other proteins. However, using polysome profiling of HEK293 cells, dorsal hippocampal tissue, and DIV25 hippocampal neurons, we observed comparable density of polysomes in all cell types/tissues. Western blots of different tissue lysates (hippocampus, kidney, liver, muscle, spleen) for several small and large ribosomal subunit proteins revealed varied expression across all tissues tested, but no particular pattern of suppression in neurons as shown by Cho et al. (2015). The collected data point towards a distinct way of ribosomal protein expression in neuronal cells/tissue, which is not necessarily governed by a general repression of translation of said proteins. The conducted Western blots are more suggestive of a different combination of ribosomal proteins in neuronal cells, compared to other cell types/tissues. Furthermore, there is ample evidence that expression patterns of ribosomal genes may vary greatly between tissues (Guimaraes and Zavolan, 2016; Mills et al., 2018; Smagin

et al., 2018). We therefore conclude that the phenotype described by Cho et al. (2015) is indeed more complex and awaits further elucidation.

UTR motifs and basic features can be key to translation regulation and many of them have been reported to specifically regulate the translation of a subset of mRNAs (Hinnebusch et al., 2016; Mazumder et al., 2003). We analysed 3' and 5' UTRs of all DTGs (up- and downregulated) that were unique to CFC, as well as a control group of unchanged genes for the presence of known UTR motifs using Utrscan (Pesole and Liuni, 1999). We did find some trends towards changes in abundance of motifs in the three groups, however, none of the comparisons reached significance in a two-way ANOVA. The trend towards an increased number of uORFs in transcripts downregulated by CFC resembles the phenotypes observed by Eacker et al. (2017) and may be explained through the role that phospho-eIF2α plays in the regulation of memory-related genes (Costa-Mattioli et al., 2005, 2007; Eacker et al., 2017)

Additionally, we collected some basic quantifiable measures of the UTRs, namely length (in nt), GC content, and Gibbs free energy (folding free energy). In the unique CFC DTGs, 5' UTRs of upregulated genes were significantly shorter than 5' UTRs of downregulated genes. UTR length can be important for translation regulation, as the longer the sequence, the more regulatory elements can be contained and the potential for complex secondary structures increases. Furthermore, long 5' UTRs may require eIF4A helicase to resolve the sequence and allow cap-binding by eIF4E and preinitiation complex recruitment. High GC content and highly negative folding free energy can be used to predict the presence of secondary structures within the analysed sequence. In the 5' UTR, upregulated genes showed less negative folding free energy (compared to downregulated, $p \leq 0.05$), which may point towards lower complexity 5' UTRs in transcripts upregulated by fear conditioning and a potential dependence of downregulated genes on eIF4A1 helicase activity. The 3' UTRs followed a similar trend, where GC content was lower in upregulated genes compared to downregulated genes. Taken together, our UTR analysis revealed no definite translational control mechanism, but, nevertheless points towards some avenues that may prove interesting in further investigation.

When exploring our ribosome profiling data, we found genes that were upregulated and are commonly used to confirm early memory formation, IEGs (e.g. cfos, Arc, Egr2). We find that these IEGs should be used with caution in

combination with memory tasks containing a potential confounding factor such as the foot shock in CFC (compare Figure 5.20). A single footshock, that is insufficient to establish significant long-term fear memories associated to the context it was delivered in (Figure 5.2), is sufficient to induce IEG transcription. Following on from this discovery, we chose several genes (Col11a1, Robo3, Leng8, Hs3st2, Camk2d, Klhdc8a) that showed specific expression patterns in the different behavioural groups in the profiling data and quantified their expression using qPCR (Figure 5.20). Some of the genes we tested as marker genes, may be suitable alternatives to conventional IEGs (Figure 5.20 C), however, in a brief experiment testing the validity of our selected genes, using a different memory task (object location memory), the only genes showing the same trends in expression as in CFC were the canonical IEGs. This points strongly towards a role of the IEGs encoding novelty rather than a specific memory. Thus, examining more genes and characterising them carefully is necessary to eventually establish marker genes that are suitable for different forms of memories.

5.4.1 Conclusions

In this chapter, we showed that omics studies in the brain to better understand genes relevant to memory formation need to be carefully planned and relevant controls need to be carried out. Our basic version of the contextual fear conditioning task showed significant regulation of transcription and translation after both presentation with only the unconditioned stimulus (shock only) as well as after the full training protocol that included exposure to the conditioned stimulus (context, training group). Furthermore, the shock only and training groups showed significant overlaps in the genes that were expressed. This fact highlights the importance of using suitable genes as markers of memory formation. For example, commonly used IEGs, such as c-fos and Arc, were upregulated in both shock and training groups, so they should be used carefully as a marker of true memory formation. The novel marker genes we tested (e.g. Col11a1, Robo3, Leng8), were convincing in the presented CFC task, but did not yield as clear a result in a less invasive task, namely object location memory. More of the genes identified in our study should be tested for suitability as memory genes, that differentiate between the shock and the true memory response.

Chapter 6

Monitoring translation in synaptic fractions using a ribosome profiling strategy

The following chapter has been accepted as a manuscript for publication with the Journal of Neuroscience Methods in October 2019.

Konstanze Simbriger, Inês S. Amorim, Kleanthi Chalkiadaki, Gilliard Lach, Seyed Mehdi Jafarnejad, Arkady Khoutorsky and Christos G. Gkogkas *Monitoring translation in synaptic fractions using a ribosome profiling strategy*

6.1 Abstract

Background

The aim of this study was to develop a method to study genome-wide local translation in biochemically isolated synaptic fractions (synaptoneurosomes). This methodology is of particular interest for neurons, due to the cardinal role of local translational control in neuronal sub-compartments, such as dendrites, for plasticity, learning, memory, and for disorders of the nervous system.

New method

We combined established methods for purifying synaptoneurosomes, with translational profiling (ribosome profiling), a method that employs unbiased next generation sequencing to simultaneously assess transcription and translation in a single sample.

Results

The two existing methods are compatible to use in combination and yield high quality sequencing data, which are specific to synaptic compartments. This new protocol provides an easy to implement workflow, which combines biochemical isolation of synaptoneurosomes of varying levels of purity (crude or Percoll gradient purified) with the use of a commercial kit to generate sequencing libraries.

Comparison with existing method

Compared to previous studies of the synaptic translatome, our method shows less contamination with non-neuronal cell types or non-synaptic compartments, increasing the specificity of the data obtained.

Conclusions

Combining the isolation of functional synaptic units with ribosome profiling offers a powerful tool to study local translation in synaptic compartments both in health and disease.

6.2 Introduction

Neurons are highly specialised cells, which require tight spatial and temporal control of protein synthesis, in order to maintain their functionality and efficiently respond to neuronal activity and external stimuli. Since neuronal compartments, such as dendrites and pre-synaptic terminals, are often situated at great distances from the cell soma, neurons have developed mechanisms to transport mRNAs in a suppressed state to different remote compartments within the cell and allow initiation of protein synthesis in a local and timely manner (Rangaraju et al., 2017). Local translation is important for a variety of cellular mechanisms, including axonal guidance, growth cone development and synaptic plasticity, thus influencing neuronal development and crucial processes such as learning and memory (Holt and Schuman, 2013; Klann and Dever, 2004). In addition, aberrant local translation is a feature of several neuropsychiatric and neurodegenerative disorders (Donlin-Asp et al., 2017; Liu-Yesucevitz et al., 2011). Therefore, it is vital to our understanding of brain function that we clarify the mechanisms that govern local synaptic translation in health and disease.

Due to the technical challenges of studying local translation, there is no definitive answer yet regarding the precise composition of the synaptic translatome (transcripts in a cell or tissue, which may be translated at a given point in time) and how it is regulated (Rangaraju et al., 2017). The translatome differs from the proteome, since it represents the pool of mRNAs that are associated with translating ribosomes. Thus, changes in ribosome occupancy may not precisely reflect changes in the proteome. However, it has been shown on several instances that measuring ribosome occupancy allows for more confident estimations of protein expression than transcriptome analysis (RNA-Seq or microarrays) (Carlyle et al., 2018; Schwanhäusser et al., 2011; Vogel, 2011). To study local translation several approaches have been employed, including microdissection of the neuropil layer within the hippocampal CA1 region from fresh tissue (Tushev et al., 2018), fluorescence activated synaptosome sorting (FASS) combined with RNA-Seq (Hafner et al., 2019), and the use of tripartite microfluidic systems that separate the soma, axon, and pre-synapse of cultured neurons into different compartments (Baleriola et al., 2014). Although useful to get an insight into the local translatome, these methods have several limitations. While microdissected tissues contain significant contaminations from glia and non-neuronal cells, which require extensive bioinformatics analysis to eliminate

(Tushev et al., 2018), culture systems fail to mimic the complexity of in vivo neuronal networks and are limited to the specific brain regions and developmental ages from which stable neuronal cultures can be obtained. Furthermore, recent approaches have employed Translating Ribosome Affinity Purification (TRAP), but despite the fact that they offer cell-type specificity, they require genetic manipulation to introduce an exogenous tag (Green Fluorescent Protein) on ribosomal proteins (Eacker et al., 2017; Ouwenga et al., 2017).

Here, we present the combination of a well-established method for synaptoneurosome (SN) preparation (adapted from Dunkley et al. (2008)) with the ribosome profiling methodology (Ingolia et al., 2012, 2009). SN are biochemically isolated pre- and post-synaptic components that are obtained through gentle homogenisation of nervous tissue under isotonic conditions. These preparations have the advantage that they can be rapidly isolated from any brain region, from animals of any age, and have little contamination from non-synaptic components and non-neuronal cell types. Ribosome profiling is an unbiased RNA sequencing-based strategy to assess the transcriptional and translational, i.e. their association with translating ribosomes, state of cells. Therefore, our method allows the study of the synaptic translatome from whole brain tissue or brain regions of interest in an unbiased way.

6.3 Methods

6.3.1 Animals

C57Bl/6J animals were bred and maintained at facilities at the University of Edinburgh. Animals were weaned at postnatal day 21 and thereafter housed in cages of up to 4 animals, in temperature (20-21℃) and humidity (55%) controlled rooms. Animals were kept on a 12 h light/dark cycle and were provided access to food and water *ad libitum*. All experimental procedures were performed in accordance with UK Home Office regulations.

6.3.2 Preparation of synaptoneurosomes (SN)

Synaptoneurosomes were prepared from the forebrain (whole brain dissection - olfactory bulbs and cerebellum were removed) of 10-week-old C57Bl/6J male mice. Crude SN and Percoll SN were prepared as described in (Dunkley et al., 2008), with minor modifications (Fig 6.1A). Briefly, animals were culled by cervical dislocation followed by decapitation and the brain dissected rapidly. The freshly dissected forebrain was homogenized (on ice) in ice-cold sucrose buffer (320 mM sucrose, 5 mM Tris pH 7.4, 1 mM EDTA) and centrifuged for 10 min, at 1,000 x g, 4℃. The pellet (P1) was resuspended in sucrose buffer and centrifuged as before. The resulting pellet (P1) was kept as the “non-synaptic fraction” and the combined supernatant from both spins (S1) was further centrifuged for 10 min at 21,000 x g, 4℃, to pellet crude SN (P2).

To prepare Percoll SN, the crude pellet (P2) was resuspended in 3% Percoll (GE Healthcare) in sucrose buffer and centrifuged through a discontinuous 10%-24% Percoll gradient, at 30,750 x g for 9 min at 4℃, with minimum acceleration and no deceleration on a JA-25.50 fixed angle rotor in a Beckman Avanti JA-25 centrifuge. The material between layers 24% and 10% was collected, resuspended in Ionic Media (20 mM HEPES pH 7.4, 10 mM Glucose, 1.2 mM Na_2HPO_4, 1 mM $MgCl_2$, 5 mM $NaHCO_3$, 5 mM KCl, 140 mM NaCl), and centrifuged for 15 min at 21,000 x g, 4℃. Cycloheximide (100 µg/ml) was added to all buffers to stall translating ribosomes and stabilise them in their position on the mRNA.

6.3.3 Western Blotting

Protein was extracted from samples by addition of RIPA buffer [50 mM Tris pH 8.0, 150 mM NaCl, 1% NP-40, 0.5% sodium deoxycholate, 0.1% SDS, protease and phosphatase inhibitors (Roche, cOmplete and PhosSTOP mini tablets)] and homogenisation using a motorized pestle (Kimble, 749540 0000). Samples were incubated on ice for 15 min, with occasional vortexing, and centrifuged for 20 min at 16,000 x g at 4℃ to clear the lysate from cellular debris. The protein concentration of each sample was determined by Bradford assay (Bio-Rad, 5000112).

Samples were prepared in SDS sample buffer (50 mM Tris pH 6.8, 100 mM DTT, 2% SDS, 10% Glycerol, 0.1% bromophenol blue), heated for 5 min to 95℃ and resolved on polyacrylamide gels. Proteins were transferred to 0.2 µm nitrocellulose membranes (Bio-Rad, 1620112), blocked in 5% BSA in TBS-T (10 mM Tris pH 7.6, 150 mM NaCl, 0.1% Tween-20) for 1 h at room temperature (RT), incubated with primary antibodies in 1% BSA in TBS-T overnight at 4℃, and with secondary antibodies in 1% BSA in TBS-T for 1 h at RT. Between incubations, membranes were washed extensively in TBS-T. Blots were imaged using an Odyssey Imaging System (Li-COR Biosciences) at a resolution of 169 µm.

Antibodies used for Western blotting are summarized in Tables 6.1 and 6.2

Table 6.1 Details of primary antibodies used.

Target	Species	Supplier	Cat No	Dilution
GAD67	mouse	Millipore	MAB5406	1:1,000
GAPDH	rabbit	Cell Signalling	2118	1:5,000
HDAC3 7G6C5	mouse	GeneTex	GTX83173	1:1,000
Myelin Basic Protein	mouse	abcam	ab62631	1:1,000
PSD95	rabbit	Cell Signalling	3450	1:1,000
Ribosomal Protein L11	rabbit	Cell Signalling	18163	1:1,000
Ribosomal Protein L13a	rabbit	Cell Signalling	2765	1:500
Ribosomal Protein S6	mouse	Santa Cruz	sc-74459	1:5,000
Ribosomal Protein S15	rabbit	abcam	ab157193	1:1,000
SV2A	mouse	DSHB University of Iowa	AB_2315387	1:1,000
Synaptophysin 1	rabbit	Synaptic Systems	101 002	1:1,000

Table 6.2 Details of secondary antibodies used.

Description	Species	Supplier	Cat No	Dilution
IRDye® 680RD Donkey anti-Rabbit IgG (H+L)	Donkey	Li-COR Biosciences	926-68073	1:5,000
IRDye® 800CW Donkey anti-Mouse IgG (H+L)	Donkey	Li-COR Biosciences	926-32212	1:5,000

6.3.4 Ribosome Profiling (RPF)

Ribosome profiling was adapted from (Ingolia et al., 2012, 2009) for use with the TruSeq Ribo Profile (Mammalian) Kit (Illumina, RPMHMR12126) and the NEXTflex™Small RNA Sequencing Kit v3 (Bioo Scientific, NOVA 5132 06). The TruSeq Ribo Profile protocol was followed until the end-repair step, after which the NEXTflex™Small RNA Sequencing Kit v3 was used for generating sequencing libraries. Polysomes were extracted from SN preparations through homogenisation in TruSeq Polysome Buffer (Illumina). A fraction of the lysates was kept as an internal mRNA control (total mRNA), while the remaining fraction was digested with TruSeq Ribo Profile Nuclease (RNase I) (footprints) and purified through a MicroSpin S-400 column (GE Healthcare) to enrich for small RNA fragments. From synaptoneurosomes prepared from one full forebrain (one animal), we extracted between 600 ng and 4 µg of RNA after this step, depending on the sample type (footprints usually show lower yield than total RNA). All samples (footprints and total mRNA) went through a ribosomal RNA depletion protocol using the Ribo-Zero Gold (Human/Mouse/Rat) Kit (Illumina, MRZG12324). The total mRNA was heat-fragmented according to the TruSeq Ribo Profile Kit, whereas the footprint samples were further purified on a 15% TBE-Urea polyacrylamide gel (ThermoFisher Scientific, EC68852BOX) to select for fragments running between 28 and 30 nucleotides. The quality and concentration of samples was assessed by running an Agilent Small RNA chip Bioanalyzer assay (Agilent Technologies, 5067 1548), which allows assessing the size distribution and concentration of RNA samples sized below 200 nt using as little as 50 ng of RNA sample. Libraries were generated using the NEXTflex™Small RNA Sequencing Kit v3, according to the manufacturer's instructions. The NEXTflex™Small RNA Sequencing Kit v3 is particularly suitable for these applications, as library generation is successful even at very low input levels (we have used as little as 3 ng of purified, rRNA depleted footprints as total input). Synaptoneurosomes can also be prepared from specific brain regions, in which case we would recommend pooling tissue from more than one animal to achieve comparable quantities of RNA. Bioinformatics analysis

was performed as previously described (Amorim et al., 2018a). Translational Efficiency (TE) was calculated as the ratio between reads per kilobase per million mapped reads (RPKM) of footprints and RPKM of total mRNA for each gene.

Note:
Since the submission of this manuscript, the two Illumina kits (RPMHMR12126, MRZG12324) have become obsolete. We recommend following the original published protocol (Ingolia et al., 2012), but scaling down volumes for the footprinting step (to 100 µl), replacing the sucrose cushion with MicroSpin S-400 purification (as summarized in the Illumina protocol), and using a commercial kit for the rRNA depletion (e.g. NEBNext® rRNA Depletion Kit, New England Biolabs, E6350).

To confirm validity of our data set, we determined the overlap between the 1000 most abundant transcripts in our SN preparations and a published list of mRNAs identified in SN prepared from adult mouse hippocampi (You et al., 2015).

6.3.5 Gene Ontology Analysis

Gene Ontology (GO) analysis was performed using the online tool DAVID (Database for Annotation, Visualization and Integrated Discovery; version 6.8) (Huang et al., 2009b). Filtered gene lists were submitted to DAVID and GO annotations gathered for Biological Function, and Cellular Component.

6.4 Results

6.4.1 Isolation of synaptically enriched fractions

We prepared SN from whole mouse forebrain using two different methods, which yield synaptically enriched fractions of different purity levels. Crude SN offer a quick and simple way of isolating synaptically enriched fractions from brain tissue. However, even though this method might be suitable for certain purposes, crude SN are contaminated with myelin, non-synaptic mitochondria, and other cellular debris. If a purer sample is required, crude SN can be centrifuged through discontinuous Percoll gradients to remove most contaminants (Fig. 6.1A).

As demonstrated by immunoblotting (Fig. 6.1C), our protocol reliably produced synaptic fractions depleted of nuclear components and enriched in both excitatory and inhibitory synaptic proteins. In the case of the Percoll gradient purified SN, these were also depleted of further contaminating cellular components, such as myelin basic protein (MBP, two isoforms (Libich, 2009)). Furthermore, we probed our samples with antibodies against ribosomal proteins to show that there are adequate levels of ribosomal proteins present in synaptic fractions (Fig. 6.1D).

6.4.2 Ribosome profiling in synaptoneurosomes

Having successfully isolated synaptic fractions from brain tissue, we proceeded with processing them for ribosome profiling (Fig. 6.1B). The crude and Percoll SN were lysed and separated in two fractions, so total mRNA (a proxy for transcription) and footprints (a proxy for translation) could be assessed within each sample. For footprint analysis, the samples were digested with RNase I, to generate footprints of around 28-30 nucleotides (nt) in length. Total mRNA was heat-fragmented to yield sequence fragments similar in size to footprints. Both sets of samples were run through a ribosomal RNA removal kit, to eliminate highly abundant ribosomal RNA contaminants, and sequencing libraries were prepared from footprints and total mRNA fragments.

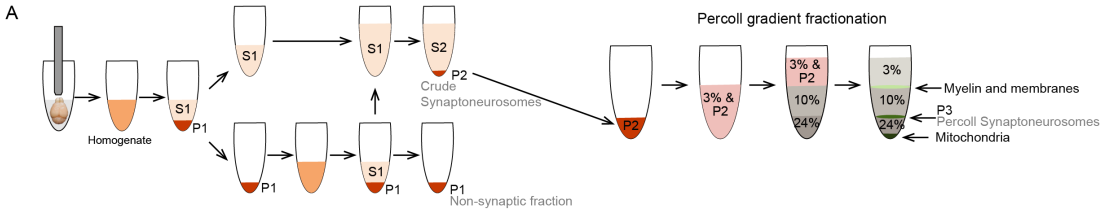
A
Homogenate
S1
P1
S2
P2
Crude
Synaptoneurosomes
Non-synaptic fraction
Percoll gradient fractionation
3% & P2
10%
24%
3%
Myelin and membranes
P3
Percoll Synaptoneurosomes
Mitochondria

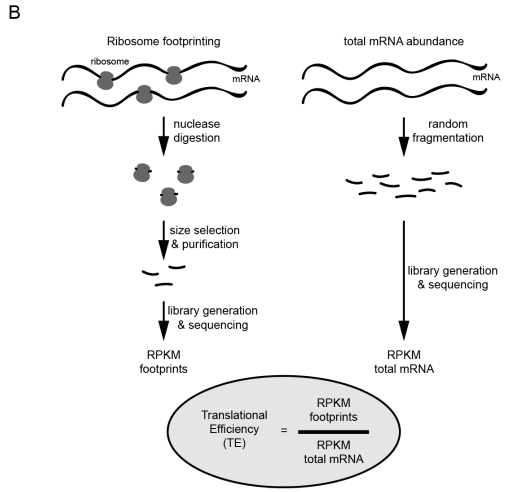
B
Ribosome footprinting
ribosome
mRNA
nuclease
digestion
size selection
& purification
library generation
& sequencing
RPKM
footprints
total mRNA abundance
random
fragmentation
library generation
& sequencing
RPKM
total mRNA
Translational
Efficiency
(TE)
=
RPKM
footprints
RPKM
total mRNA

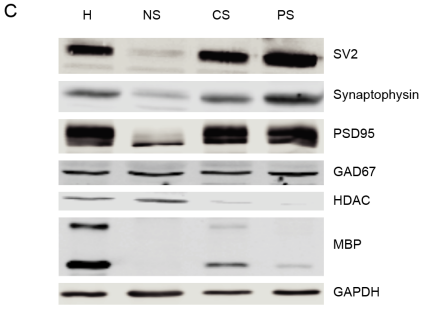
C
H
NS
CS
PS
SV2
Synaptophysin
PSD95
GAD67
HDAC
MBP
GAPDH

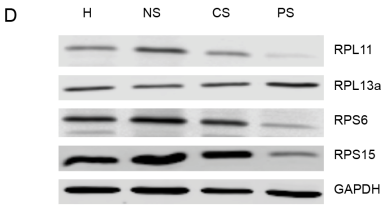
D
H
NS
CS
PS
RPL11
RPL13a
RPS6
RPS15
GAPDH

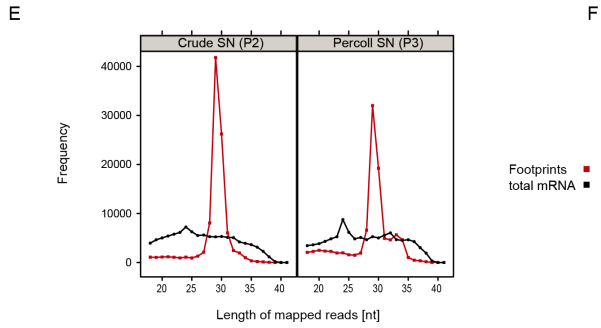
E
Crude SN (P2)
Percoll SN (P3)
Frequency
Length of mapped reads [nt]
Footprints
total mRNA

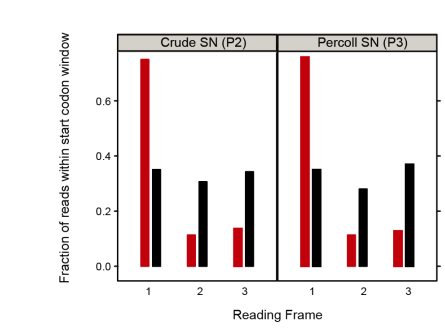
F
Crude SN (P2)
Percoll SN (P3)
Fraction of reads within start codon window
Reading Frame

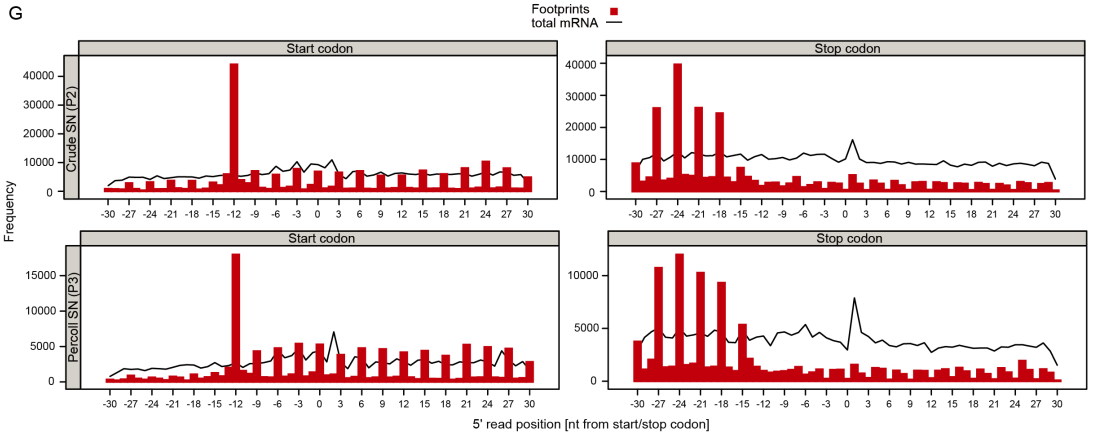
G
Footprints
total mRNA
Start codon
Stop codon
Crude SN (P2)
Percoll SN (P3)
Frequency
5' read position [nt from start/stop codon]

Figure 6.1 Schematic diagram of the preparation of SN (A) and the ribosome profiling workflow (B). A detailed description can be found in section 2 (Methods). (C) Immunoblots of the indicated proteins in the different fractions obtained during the preparation of SN. Note the depletion of nuclear proteins (HDAC) and the enrichment in both excitatory and inhibitory synaptic proteins (synaptic vesicle glycoprotein 2A – SV2, synaptophysin, glutamic acid decarboxylase 67 – GAD67, and postsynaptic density protein 95 – PSD95) in crude and Percoll SN. PSD95 blots show two bands very close in size, representing αand βisoforms of the protein, respectively (Chetkovich et al., 2002). In addition, Percoll SN show a major decrease in myelin components (MBP) of both major isoforms. GAPDH was used as a loading control. H: tissue homogenate, NS: non-synaptic fraction, CS: crude synaptoneurosomes, PS: Percoll synaptoneurosomes. (D) Immunoblots confirming the presence of ribosomal proteins (large ribosomal proteins 11 and 13a, small ribosomal proteins 6 and 15) in the SN fractions. GAPDH was used as a loading control. (E) Size distribution of the aligned sequencing reads from the indicated samples. Total mRNA reads show a random size distribution, whereas ribosomal footprints show a distinct peak between 28 and 30 nt. (F) Reading frame usage in the total mRNA and footprint samples, showing the preferential alignment within the first reading frame in the footprint samples, compared to the total mRNA samples which have been randomly fragmented. (G) The total number of read fragments aligning around the start and stop codons of the coding sequence of all genes. Footprints show a 3 nt periodicity, compared to total mRNA reads.

We succeeded in generating high quality ribosome profiling libraries from both crude and Percoll SN (Fig. 6.1E-G). Quality control graphs confirmed the restricted size distribution of footprints, as well as the random size of total mRNA fragments (Fig. 6.1E). Analysis of the usage of reading frames showed that the majority of footprints aligned with their main reading frame sequence (Fig. 6.1F, Frame 1), as would be expected for actively translating ribosomes. In addition, mapping of the footprints along each transcript showed that the 5'-ends of the RPFs start at 12 to 13 nt upstream of start codons and decrease significantly in frequency at approximately 15 nt upstream of the stop codon, specific to the size and shape of initiating and terminating ribosomes, respectively. The footprints further exhibit a characteristic 3-nt periodicity (Fig. 6.1G), a consequence of translating in 3-nt codons. In contrast, the equal distribution of total mRNA fragments between the 3 main reading frames and their lack of 3-nt nucleotide periodicity highlights the random nature of the heat fragmentation process and the specificity of the footprint data (Fig. 6.1F-G).

6.4.3 Gene Ontology Analysis

Sequencing identified transcripts from over 10,000 protein coding genes. Therefore, to facilitate further analysis and to focus on the most abundant transcripts in synapses, we selected the 1,000 most abundant (top 1,000) genes corresponding to the transcripts in our total mRNA and translational efficiency (TE) datasets with the highest RPKM or TE values, respectively, for both the crude and Percoll protocols.

First, we compared our data to a published dataset exploring the transcriptome of SN generated from mouse hippocampi (You et al., 2015) (Fig. 6.2A-B). Even though some regional heterogeneity would be expected when comparing synaptosomes isolated from hippocampal with those extracted from forebrain tissue, we found a ~30% overlap for the top 1,000 genes (total mRNA) for both the crude and Percoll SN. This shows that our data is comparable to data generated from similar experiments by other labs, and that there is a pool of highly abundant mRNAs enriched in synapses, which may support core synaptic functions across brain regions. Secondly, we performed Gene Ontology (GO) analysis of the top 1,000 genes in our samples to define ontological groups of genes enriched in our SN preparations (Fig. 6.2C-F). Overall, performing GO analysis using DAVID revealed a highly significant enrichment ($p \leq 0.0001$) of Biological Process and Cellular Component GO terms related to synaptic function in our gene lists (Fig. 6.2C-F). Total mRNA samples showed highly significant enrichments ($p \leq 0.0001$) in Cellular Components such as membrane, synapse, post-synaptic density and dendrites, emphasising the synaptic nature of the samples (Fig. 6.2C-D). Interestingly, TE datasets were particularly enriched ($p \leq 0.0001$) in transcripts coding for mitochondrial, extracellular matrix and extracellular exosome proteins (Fig. 6.2E-F). Biological Processes GO terms followed the same trends, with TE data showing enrichment for metabolic and oxidation-reduction processes (Fig. 6.2E-F), whereas the total mRNA data presents an enrichment ($p \leq 0.0001$) in a broader range of important synaptic processes, including nervous system development, ion transport, neuron migration and long-term synaptic potentiation (Fig. 6.2C-D).

Taken together, these results show that our method reliably identifies transcripts localised to the synapse, as well as the subset of these mRNAs that are associated to ribosomes and are likely to be locally translated.

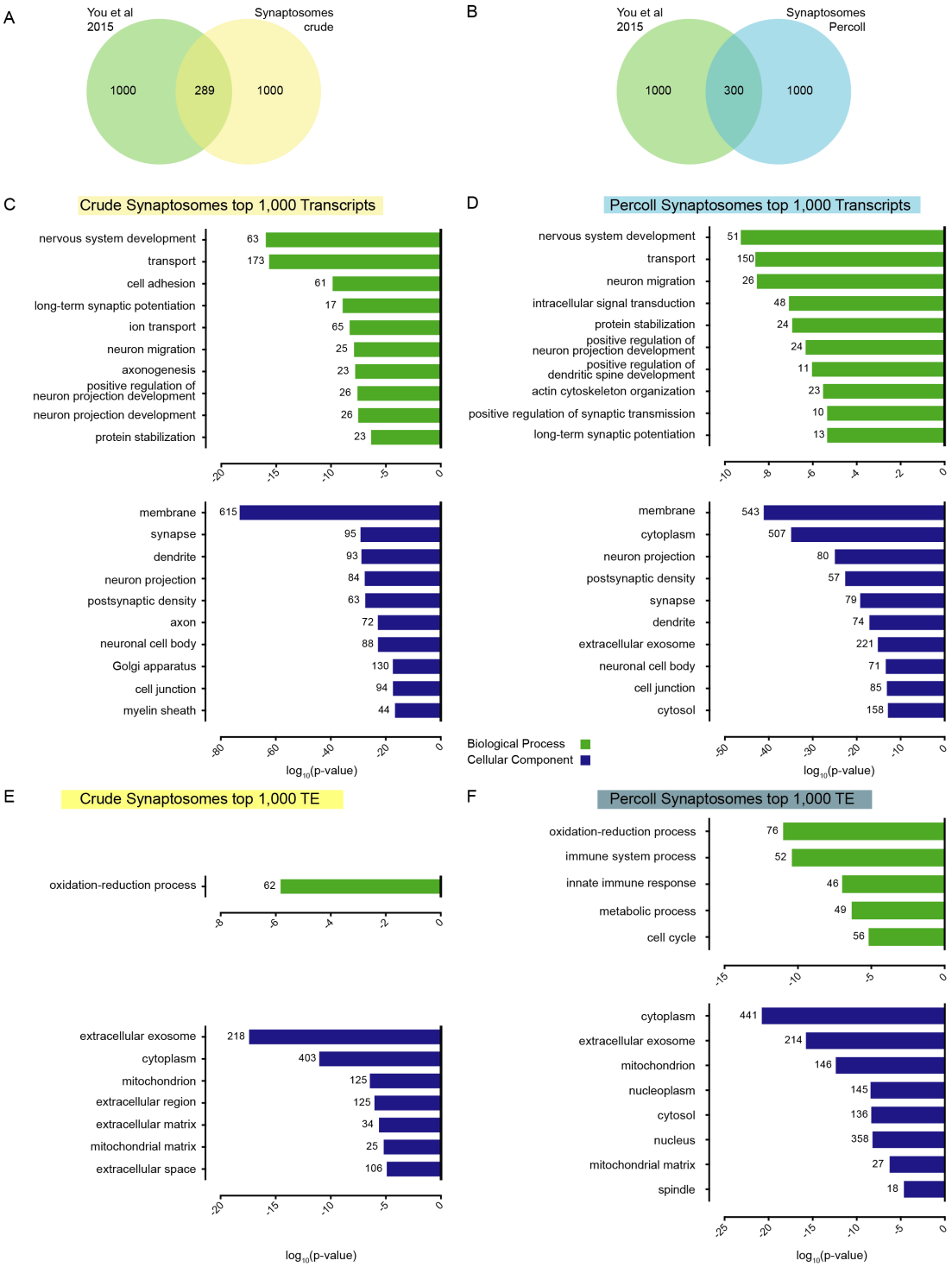

Figure 6.2 (A-B) Comparison of our identified top 1,000 genes with the 1,000 most abundant genes in hippocampal SN from You et al. (2015). The overlap between the published data and our crude and Percoll SN are 289 and 300 genes, respectively. (C-F) Most significant results from the GO analysis of the 1,000 most abundant transcripts identified in the SN fractions (C-D), and the 1,000 genes with the highest TE in the SN fractions (E-F). The numbers accompanying each bar on the graphs indicate the number of genes in the respective group.

6.5 Discussion

Here we present a new methodology based on two previously established protocols, allowing us to study simultaneously the synaptic translatome and transcriptome of neurons. We further demonstrate that our method yields high quality RNA sequencing data displaying an enrichment in genes related to synaptic function.

Studying synaptic translation in an unbiased way poses a great challenge, due to the technical difficulty of isolating pure dendritic or axonal fractions containing mRNA (Rangaraju et al., 2017). Ribosome profiling has been previously used to study translation in the rodent brain (Amorim et al., 2018a; Cho et al., 2015) and provides an unbiased, genome-wide assessment of both the total transcriptome and translatome. Studying the translatome is important because translation contributes significantly to regulating protein levels, especially at synapses (Vogel, 2011). By purifying synaptic compartments from live brain tissue, using a well-established method, we were able to generate ribosome profiling libraries, which allow for gaining a significant insight into the transcriptome and translatome of SN.

By performing GO analysis of the top 1,000 synaptic transcribed and translated mRNAs, we showed an enrichment in synaptically relevant transcripts in both the total mRNAs and the ribosome associated fractions, as well as a considerable overlap with comparable published data (Fig. 6.2A-B). GO analysis of our transcriptome targets (Fig. 6.2C-D) showed significant enrichment in Cellular Component terms relating to the synapse (post synaptic density, dendrite, synapse, axon, etc) and Biological Process terms such as long-term synaptic potentiation and ion transport. Interestingly, GO analysis of the most abundant genes in the ribosome associated fraction (TE dataset) showed an enrichment in energy metabolism- and mitochondria-related terms (Fig. 6.2E-F). This is in agreement with the high abundance of mitochondria at the synapse and the elevated energetic demand required for the maintenance of synaptic functions (Rangaraju et al., 2019). The contrast between total mRNA and TE data highlights the fundamental difference between the transcripts present at synaptic fractions and their level of translation, stressing the importance of assessing both the transcriptome and translatome of a given sample.

The choice between using crude or Percoll SN depends on the requirements of each particular experiment. Both preparations are enriched in synaptic components and contain good amounts of ribosomal proteins (Fig. 6.1C-D) and RNA. Total mRNA and footprint libraries can be prepared from either type of sample, and GO analysis shows similar enrichments in relevant synapse-related terms (Fig. 6.2). Percoll SN have the advantage of being less contaminated with myelin and extra-synaptic mitochondria (Fig. 6.1C, Fig. 6.2C), but require longer preparation times and the use of freshly dissected tissue. Percoll SN yield lower amounts of mRNA and footprints than crude SN, which may require pooling of samples from different animals for small brain regions. Ultimately, the researcher needs to take into consideration the balance between the purity of samples and technical feasibility of the experiment.

Combining SN isolation with translational profiling has the potential of answering important questions within the field of localised neuronal translation in an unbiased fashion. SN can be isolated from whole brain, prepared from specific brain regions or sorted using flow cytometry to yield specific populations (Biesemann et al., 2014; Hafner et al., 2019). In addition, SN are commonly used as functional *in vitro* models of synaptic activity, which can be assessed at baseline or can easily be stimulated or treated with a variety of agents. The combination of this powerful tool with ribosome profiling allows researchers to precisely analyse the local translatome at synapses and to study translational regulation in response to neuronal activity or in models of neurological disorders.

6.6 Conclusion

The combination of the unbiased method of ribosome profiling, to study transcripts that are being actively translated, with well-established protocols of isolating functional synaptic fractions provides a powerful tool to study localised translation at the synapse.

Chapter 7

General Discussion

7.1 Discussion

Overall, the goal of the work described in this thesis was to gain a better understanding of mRNA translation in the brain in both health and disease. To this end, we showed how translation in the brain of a mouse model overexpressing human MMP-9 brainwide compares to translation in the brain of a mouse model of FXS and how the phosphorylation of eIF4E Ser209 regulates translation of a specific subset of mRNAs. We further showed that in a classical Pavlovian fear conditioning paradigm, a session where only an electrical shock is administered to the animal, but no connection to the potentially dangerous novel environment is formed, is sufficient to induce significant gene expression that overlaps considerably with gene expression after fear conditioning training. Lastly, we extended the method of ribosome profiling for use in synaptoneurosomes to study local translation at synaptic terminals.

In Chapter 3, we showed that TgMMP9 animals, which had previously been shown to display key phenotypes of Fmr1KO mice, showed little to no changes in global translation, regulation of signalling pathways impinging on translation, and transcription and translation of specific transcripts. Ribosome profiling of Fmr1KO mice revealed very small numbers of DEGs and DTGs, comparable to TgMMP9 profiling. We conclude that in the forebrain of adult TgMMP9 and Fmr1KO mice translation is not significantly changed. Us not observing bigger changes in translation, especially in the Fmr1KO mice, where upregulated

global translation has been postulated as a key phenotype before, may be due to several factors, including but not limited to the comparably old animals (in relation to other studies), the use of whole forebrain rather than individual brain regions or targeting cell types. Furthermore, protein synthesis may be regulated at a level that is not detectable with ribosome profiling.

In Chapter 4, we applied ribosome profiling to a novel mouse model of depression, harbouring a phospho-dead version of the cap-binding protein eIF4E. Our data showed that phospho-eIF4E regulates the translation of a specific subset of mRNAs involved with the serotonin pathway and inflammation. We further found that 3' UTRs of upregulated genes in *4EKi* contained significantly less GAIT motifs, while 5' UTRs of downregulated genes were significantly shorter. We propose a model in which phospho-eIF4E regulates the translation of inflammatory genes through the GAIT complex and genes regulated by eIF4E contain long and structured 5' UTRs requiring eIF4A1 helicase for translation initiation.

In Chapter 5, we investigated the effects of a single electrical shock on gene expression in the dorsal hippocampus, compared to contextual fear conditioning. The results show a considerable overlap in both transcription and translation of genes that are expressed after shock only and after CFC. The length and complexity of the 5' UTR of genes upregulated by CFC may further present as an important factor for understanding gene expression in memory, but awaits further research.

In Chapter 6, we extended the ribosome profiling strategy of monitoring translation to work in synaptoneurosomes, biochemically isolated synaptic terminals. Local translation in neuronal cells is of key importance for the cell to maintain proper function, but presents a challenge when studying tissue. With our combination of two established methods, we add a new and easy to use protocol to allow monitoring of translation at synapses. Ribosome profiling of synaptoneurosomes offers a great basis for studying synaptic translation in response to diverse stimuli, such as drugs, inhibitors or excitation, in health and models of disease.

We successfully applied ribosome profiling to several neural tissues, which at the time, when this study was devised, had not been published. Ribosome profiling is a great method to gather an omic type overview over ribosomal occupancy of mRNAs. mRNA expression levels, as assessed using microar-

rays or conventional RNA-Seq experiments have been shown to not always accurately resemble protein levels (Schwanhäusser et al., 2011). Ribosome profiling, on the other hand, showed greater overlaps with mass spectrometry data (Carlyle et al., 2018). This supports a role for ribosome profiling as a tool for discovery of differentially translated genes at different conditions, as well as pathways and ontology terms that may be relevant. However, results should be carefully validated for their expression and studied in more detail after profiling experiments, as ribosome profiling offers information on the ribosome occupancy of mRNAs rather than the protein abundance (Ingolia, 2014).

7.2 Conclusion

Taken together, the work presented in this thesis shows that ribosome profiling is an invaluable tool to gain a better understanding of the translational regulation of mRNAs in the brain. Specifically, in the context of neuropsychiatric disorders, such as MDD and ASD, that show dysregulated translation phenotypes it has proven useful in discovering novel patterns in mRNA translation regulation. Furthermore, applied to animals trained in a memory task, it identified key genes involved in early memory formation. We have shown that it can be applied in various ways and is sensitive enough to pick up on even small changes in transcription or translation both at a global and a local scale, therefore supporting its use as a discovery tool.

References

Abdallah, M. W. and Michel, T. (2013). Matrix metalloproteinases in autism spectrum disorders. *J. Mol. Psychiatry*, 1:16.

Abdallah, M. W., Pearce, B. D., Larsen, N., Greaves-Lord, K., Nørgaard-Pedersen, B., Hougaard, D. M., Mortensen, E. L., and Grove, J. (2012). Amniotic Fluid MMP-9 and Neurotrophins in Autism Spectrum Disorders: An Exploratory Study: Amniotic fluid MMP-9 and neurotrophins in ASD. *Autism Research*, 5(6):428–433.

Aguilar-Valles, A., Haji, N., Gregorio, D. D., Matta-Camacho, E., Eslamizade, M. J., Popic, J., Sharma, V., Cao, R., Rummel, C., Tanti, A., Wiebe, S., Nuñez, N., Comai, S., Nadon, R., Luheshi, G., Mechawar, N., Turecki, G., Lacaille, J.-C., Gobbi, G., and Sonenberg, N. (2018). Translational control of depression-like behavior via phosphorylation of eukaryotic translation initiation factor 4e. *Nature Communications*, 9(1):2459.

Aguliar-Valles, A., Kim, J., Jung, S., Woodside, B., and Luheshi, G. N. (2014). Role of brain transmigrating neutrophils in depression-like behavior during systemic infection. *Molecular Psychiatry*, 19(5):633.

Alaiyed, S. and Conant, K. (2019). A Role for Matrix Metalloproteases in Antidepressant Efficacy. *Frontiers in Molecular Neuroscience*, 12.

Alberini, C. M. (2009). Transcription Factors in Long-Term Memory and Synaptic Plasticity. *Physiological Reviews*.

Alberini, C. M. and Kandel, E. R. (2015). The Regulation of Transcription in Memory Consolidation. *Cold Spring Harbor Perspectives in Biology*, 7(1):a021741.

American Psychiatric Association (2000). *Diagnostic and Statistical Manual of Mental Disorders, Fourth Edition: DSM-IV-TR®*. American Psychiatric Association.

Amorim, I. S., Kedia, S., Kouloulia, S., Simbriger, K., Gantois, I., Jafarnejad, S. M., Li, Y., Kampaite, A., Pooters, T., Romanò, N., and Gkogkas, C. G. (2018a). Loss of eIF4e phosphorylation engenders depression-like behaviors via selective mRNA translation. *Journal of Neuroscience*, pages 2673–17.

Amorim, I. S., Lach, G., and Gkogkas, C. G. (2018b). The Role of the Eukaryotic Translation Initiation Factor 4e (eIF4e) in Neuropsychiatric Disorders. *Frontiers in Genetics*, 9.

Atkins, C. M., Selcher, J. C., Petraitis, J. J., Trzaskos, J. M., and Sweatt, J. D. (1998). The MAPK cascade is required for mammalian associative learning. *Nature Neuroscience*, 1(7):602.

Avni, D., Biberman, Y., and Meyuhas, O. (1997). The 5' Terminal Oligopyrimidine Tract Confers Translational Control on Top Mrnas in a Cell Type-and Sequence Context-Dependent Manner. *Nucleic Acids Research*, 25(5):995–1001.

Baleriola, J., Walker, C. A., Jean, Y. Y., Crary, J. F., Troy, C. M., Nagy, P. L., and Hengst, U. (2014). Axonally Synthesized ATF4 Transmits a Neurodegenerative Signal across Brain Regions. *Cell*, 158(5):1159–1172.

Banko, J. L., Hou, L., Poulin, F., Sonenberg, N., and Klann, E. (2006). Regulation of Eukaryotic Initiation Factor 4e by Converging Signaling Pathways during Metabotropic Glutamate Receptor-Dependent Long-Term Depression. *Journal of Neuroscience*, 26(8):2167–2173.

Barnes, P., Kirtley, A., and Thomas, K. L. (2012). Quantitatively and qualitatively different cellular processes are engaged in CA1 during the consolidation and reconsolidation of contextual fear memory. *Hippocampus*, 22(2):149–171.

Baumeister, D., Akhtar, R., Ciufolini, S., Pariante, C. M., and Mondelli, V. (2016). Childhood trauma and adulthood inflammation: a meta-analysis of peripheral C-reactive protein, interleukin-6 and tumour necrosis factor-α. *Molecular Psychiatry*, 21(5):642–649.

Baxter, A. J., Brugha, T. S., Erskine, H. E., Scheurer, R. W., Vos, T., and Scott, J. G. (2014). The epidemiology and global burden of autism spectrum disorders. *Psychological Medicine*, FirstView:1–13.

Bear, M. F., Huber, K. M., and Warren, S. T. (2004). The mGluR theory of fragile X mental retardation. *Trends in Neurosciences*, 27(7):370–377.

Benjamini, Y. and Hochberg, Y. (1995). Controlling the False Discovery Rate: A Practical and Powerful Approach to Multiple Testing. *Journal of the Royal Statistical Society. Series B (Methodological)*, 57(1):289–300.

Bhattacharya, A., Kaphzan, H., Alvarez-Dieppa, A. C., Murphy, J. P., Pierre, P., and Klann, E. (2012). Genetic removal of p70 S6 kinase 1 corrects molecular, synaptic, and behavioral phenotypes in fragile X syndrome mice. *Neuron*, 76(2):325–337.

Bicker, S., Lackinger, M., Weiß, K., and Schratt, G. (2014). MicroRNA-132, -134, and -138: a microRNA troika rules in neuronal dendrites. *Cellular and Molecular Life Sciences*, 71(20):3987–4005.

Biesemann, C., Grønborg, M., Luquet, E., Wichert, S. P., Bernard, V., Bungers, S. R., Cooper, B., Varoqueaux, F., Li, L., Byrne, J. A., Urlaub, H., Jahn, O., Brose, N., and Herzog, E. (2014). Proteomic screening of glutamatergic mouse brain synaptosomes isolated by fluorescence activated sorting. *The EMBO Journal*, 33(2):157–170.

Biever, A., Puighermanal, E., Nishi, A., David, A., Panciatici, C., Longueville, S., Xirodimas, D., Gangarossa, G., Meyuhas, O., Hervé, D., Girault, J.-A., and Valjent, E. (2015). PKA-Dependent Phosphorylation of Ribosomal Protein S6 Does Not Correlate with Translation Efficiency in Striatonigral and Striatopallidal Medium-Sized Spiny Neurons. *Journal of Neuroscience*, 35(10):4113–4130.

Bilousova, T. V., Dansie, L., Ngo, M., Aye, J., Charles, J. R., Ethell, D. W., and Ethell, I. M. (2008). Minocycline promotes dendritic spine maturation and improves behavioural performance in the fragile X mouse model. *Journal of Medical Genetics*, 46(2):94–102.

Blixt, A., Mahlapuu, M., Aitola, M., Pelto-Huikko, M., Enerbäck, S., and Carlsson, P. (2000). A forkhead gene, FoxE3, is essential for lens epithelial proliferation and closure of the lens vesicle. *Genes & Development*, 14(2):245–254.

Bodian, D. (1965). A Suggestive Relationship of Nerve Cell Rna with Specific Synaptic Sites. *Proceedings of the National Academy of Sciences*, 53(2):418–425.

Bourtchouladze, R., Abel, T., Berman, N., Gordon, R., Lapidus, K., and Kandel, E. R. (1998). Different Training Procedures Recruit Either One or Two Critical Periods for Contextual Memory Consolidation, Each of Which Requires Protein Synthesis and PKA. *Learning & Memory*, 5(4):365–374.

Bradshaw, K. D., Emptage, N. J., and Bliss, T. V. P. (2003). A role for dendritic protein synthesis in hippocampal late LTP. *European Journal of Neuroscience*, 18(11):3150–3152.

Bramham, C. R., Jensen, K. B., and Proud, C. G. (2016). Tuning Specific Translation in Cancer Metastasis and Synaptic Memory: Control at the MNK–eIF4e Axis. *Trends in Biochemical Sciences*, 41(10):847–858.

Bramham, C. R., Worley, P. F., Moore, M. J., and Guzowski, J. F. (2008). The Immediate Early Gene Arc/Arg3.1: Regulation, Mechanisms, and Function. *Journal of Neuroscience*, 28(46):11760–11767.

Brownell, I., Dirksen, M., and Jamrich, M. (2000). Forkhead Foxe3 maps to the dysgenetic lens locus and is critical in lens development and differentiation. *genesis*, 27(2):81–93.

Bruchas, M. R., Schindler, A. G., Shankar, H., Messinger, D. I., Miyatake, M., Land, B. B., Lemos, J. C., Hagan, C. E., Neumaier, J. F., Quintana, A., Palmiter, R. D., and Chavkin, C. (2011). Selective p38α MAPK Deletion in Serotonergic Neurons Produces Stress Resilience in Models of Depression and Addiction. *Neuron*, 71(3):498–511.

Budimirovic, D. B. and Kaufmann, W. E. (2011). What Can We Learn about Autism from Studying Fragile X Syndrome? *Developmental Neuroscience*, 33(5):379–394.

Buffington, S. A., Huang, W., and Costa-Mattioli, M. (2014). Translational Control in Synaptic Plasticity and Cognitive Dysfunction. *Annual Review of Neuroscience*, 37(1):17–38.

Cao, R., Gkogkas, C. G., de Zavalia, N., Blum, I. D., Yanagiya, A., Tsukumo, Y., Xu, H., Lee, C., Storch, K.-F., Liu, A. C., Amir, S., and Sonenberg, N. (2015). Light-regulated translational control of circadian behavior by eIF4e phosphorylation. *Nature Neuroscience*, 18(6):855–862.

Carlyle, B. C., Kitchen, R. R., Zhang, J., Wilson, R. S., Lam, T. T., Rozowsky, J. S., Williams, K. R., Sestan, N., Gerstein, M. B., and Nairn, A. C. (2018). Isoform-Level Interpretation of High-Throughput Proteomics Data Enabled by Deep Integration with RNA-seq. *Journal of Proteome Research*, 17(10):3431–3444.

Carracedo, A. and Pandolfi, P. P. (2008). The PTEN–PI3k pathway: of feedbacks and cross-talks. *Oncogene*, 27(41):5527–5541.

Castelo-Szekely, V., Arpat, A. B., Janich, P., and Gatfield, D. (2017). Translational contributions to tissue specificity in rhythmic and constitutive gene expression. *Genome Biology*, 18(1):116.

Cembrowski, M. S., Bachman, J. L., Wang, L., Sugino, K., Shields, B. C., and Spruston, N. (2016). Spatial Gene-Expression Gradients Underlie Prominent Heterogeneity of CA1 Pyramidal Neurons. *Neuron*, 89(2):351–368.

Chaaya, N., Battle, A. R., and Johnson, L. R. (2018). An update on contextual fear memory mechanisms: Transition between Amygdala and Hippocampus. *Neuroscience & Biobehavioral Reviews*, 92:43–54.

Chen, G. and Manji, H. K. (2006). The extracellular signal-regulated kinase pathway: an emerging promising target for mood stabilizers:. *Current Opinion in Psychiatry*, 19(3):313–323.

Chetkovich, D. M., Bunn, R. C., Kuo, S.-H., Kawasaki, Y., Kohwi, M., and Bredt, D. S. (2002). Postsynaptic Targeting of Alternative Postsynaptic Density-95 Isoforms by Distinct Mechanisms. *Journal of Neuroscience*, 22(15):6415–6425.

Cho, J., Yu, N.-K., Choi, J.-H., Sim, S.-E., Kang, S. J., Kwak, C., Lee, S.-W., Kim, J.-i., Choi, D. I., Kim, V. N., and Kaang, B.-K. (2015). Multiple repressive mechanisms in the hippocampus during memory formation. *Science*, 350(6256):82–87.

Cho, J.-H., Rendall, S. D., and Gray, J. M. (2017). Brain-wide maps of Fos expression during fear learning and recall. *Learning & Memory*, 24(4):169–181.

Colina, R., Costa-Mattioli, M., Dowling, R. J. O., Jaramillo, M., Tai, L.-H., Breitbach, C. J., Martineau, Y., Larsson, O., Rong, L., Svitkin, Y. V., Makrigiannis, A. P., Bell, J. C., and Sonenberg, N. (2008). Translational control of the innate immune response through IRF-7. *Nature*, 452(7185):323–328.

Comery, T. A., Harris, J. B., Willems, P. J., Oostra, B. A., Irwin, S. A., Weiler, I. J., and Greenough, W. T. (1997). Abnormal dendritic spines in fragile X knockout mice: Maturation and pruning deficits. *Proceedings of the National Academy of Sciences*, 94(10):5401–5404.

Costa-Mattioli, M., Gobert, D., Harding, H., Herdy, B., Azzi, M., Bruno, M., Bidinosti, M., Mamou, C. B., Marcinkiewicz, E., Yoshida, M., Imataka, H., Cuello, A. C., Seidah, N., Sossin, W., Lacaille, J.-C., Ron, D., Nader, K., and Sonenberg, N. (2005). Translational control of hippocampal synaptic plasticity and memory by the eIF2α kinase GCN2. *Nature*, 436(7054):1166.

Costa-Mattioli, M., Gobert, D., Stern, E., Gamache, K., Colina, R., Cuello, C., Sossin, W., Kaufman, R., Pelletier, J., Rosenblum, K., Krnjević, K., Lacaille, J.-C., Nader, K., and Sonenberg, N. (2007). eIF2α Phosphorylation Bidirectionally Regulates the Switch from Short- to Long-Term Synaptic Plasticity and Memory. *Cell*, 129(1):195–206.

Costa-Mattioli, M. and Monteggia, L. M. (2013). mTOR complexes in neurodevelopmental and neuropsychiatric disorders. *Nature Neuroscience*, 16(11):1537–1543.

Costa-Mattioli, M., Sossin, W. S., Klann, E., and Sonenberg, N. (2009). Translational Control of Long-Lasting Synaptic Plasticity and Memory. *Neuron*, 61(1):10–26.

Cracco, J. B., Serrano, P., Moskowitz, S. I., Bergold, P. J., and Sacktor, T. C. (2005). Protein synthesis-dependent LTP in isolated dendrites of CA1 pyramidal cells. *Hippocampus*, 15(5):551–556.

Curzon, P., Rustay, N. R., and Browman, K. E. (2009). Cued and Contextual Fear Conditioning for Rodents. In Buccafusco, J. J., editor, *Methods of Behavior Analysis in Neuroscience*, Frontiers in Neuroscience. CRC Press/Taylor & Francis, Boca Raton (FL), 2nd edition.

Dagestad, G., Kuipers, S. D., Messaoudi, E., and Bramham, C. R. (2006). Chronic fluoxetine induces region-specific changes in translation factor eIF4e and eEF2 activity in the rat brain. *European Journal of Neuroscience*, 23(10):2814–2818.

Darnell, J. C., Van Driesche, S. J., Zhang, C., Hung, K. Y. S., Mele, A., Fraser, C. E., Stone, E. F., Chen, C., Fak, J. J., Chi, S. W., Licatalosi, D. D., Richter, J. D., and Darnell, R. B. (2011). FMRP Stalls Ribosomal Translocation on mRNAs Linked to Synaptic Function and Autism. *Cell*, 146(2):247–261.

Davis, H. P. and Squire, L. R. (1984). Protein synthesis and memory: a review. *Psychological Bulletin*, 96(3):518–559.

Dityatev, A., editor (2014). *Brain extracellular matrix in health and disease*. Number 214 in Progress in brain research. Elsevier, Amsterdam, 1. ed edition. OCLC: 905416740.

Dityatev, A., Schachner, M., and Sonderegger, P. (2010). The dual role of the extracellular matrix in synaptic plasticity and homeostasis. *Nature Reviews Neuroscience*, 11(11):735–746.

Dobin, A., Davis, C. A., Schlesinger, F., Drenkow, J., Zaleski, C., Jha, S., Batut, P., Chaisson, M., and Gingeras, T. R. (2013). STAR: ultrafast universal RNA-seq aligner. *Bioinformatics (Oxford, England)*, 29(1):15–21.

Donegan, J. J. and Lodge, D. J. (2017). Hippocampal Perineuronal Nets Are Required for the Sustained Antidepressant Effect of Ketamine. *International Journal of Neuropsychopharmacology*, 20(4):354–358.

Donlin-Asp, P. G., Rossoll, W., and Bassell, G. J. (2017). Spatially and temporally regulating translation via mRNA-binding proteins in cellular and neuronal function. *FEBS Letters*, 591(11):1508–1525.

Dowlati, Y., Herrmann, N., Swardfager, W., Liu, H., Sham, L., Reim, E. K., and Lanctôt, K. L. (2010). A Meta-Analysis of Cytokines in Major Depression. *Biological Psychiatry*, 67(5):446–457.

Drummond, M. J., Reidy, P. T., Baird, L. M., Dalley, B. K., and Howard, M. T. (2017). Leucine Differentially Regulates Gene-Specific Translation in Mouse Skeletal Muscle. *The Journal of Nutrition*, 147(9):1616–1623.

Dulawa, S. C. and Hen, R. (2005). Recent advances in animal models of chronic antidepressant effects: The novelty-induced hypophagia test. *Neuroscience & Biobehavioral Reviews*, 29(4):771–783.

Duman, C. H., Schlesinger, L., Kodama, M., Russell, D. S., and Duman, R. S. (2007). A Role for MAP Kinase Signaling in Behavioral Models of Depression and Antidepressant Treatment. *Biological Psychiatry*, 61(5):661–670.

Dunkley, P. R., Jarvie, P. E., and Robinson, P. J. (2008). A rapid Percoll gradient procedure for preparation of synaptosomes. *Nature Protocols*, 3(11):1718–1728.

Dwivedi, Y., Rizavi, H. S., Roberts, R. C., Conley, R. C., Tamminga, C. A., and Pandey, G. N. (2001). Reduced activation and expression of ERK1/2 MAP kinase in the post-mortem brain of depressed suicide subjects. *Journal of Neurochemistry*, 77(3):916–928.

Dziembowska, M., Pretto, D. I., Janusz, A., Kaczmarek, L., Leigh, M. J., Gabriel, N., Durbin-Johnson, B., Hagerman, R. J., and Tassone, F. (2013). High MMP-9 activity levels in fragile X syndrome are lowered by minocycline. *American Journal of Medical Genetics Part A*, 161(8):1897–1903.

Dölen, G., Osterweil, E., Rao, B. S. S., Smith, G. B., Auerbach, B. D., Chattarji, S., and Bear, M. F. (2007). Correction of Fragile X Syndrome in Mice. *Neuron*, 56(6):955–962.

Eacker, S. M., Crawford, K., Brichta, L., Riessland, M., Ingolia, N. T., Greengard, P., Dawson, T. M., and Dawson, V. L. (2017). Experience-dependent translational state defined by cell type-specific ribosome profiling. *bioRxiv*, page 169425.

English, J. D. and Sweatt, J. D. (1997). A Requirement for the Mitogen-activated Protein Kinase Cascade in Hippocampal Long Term Potentiation. *Journal of Biological Chemistry*, 272(31):19103–19106.

Federighi, G., Traina, G., Macchi, M., Ciampini, C., Bernardi, R., Baldi, E., Bucherelli, C., Brunelli, M., and Scuri, R. (2013). Modulation of Gene Expression in Contextual Fear Conditioning in the Rat. *PLOS ONE*, 8(11):e80037.

Feig, S. and Lipton, P. (1993). Pairing the cholinergic agonist carbachol with patterned Schaffer collateral stimulation initiates protein synthesis in hippocampal CA1 pyramidal cell dendrites via a muscarinic, NMDA-dependent mechanism. *Journal of Neuroscience*, 13(3):1010–1021.

Feoktistova, K., Tuvshintogs, E., Do, A., and Fraser, C. S. (2013). Human eIF4e promotes mRNA restructuring by stimulating eIF4a helicase activity. *Proceedings of the National Academy of Sciences*, 110(33):13339–13344.

Flexner, L. B., Flexner, J. B., and Stellar, E. (1965). Memory and cerebral protein synthesis in mice as affected by graded amounts of puromycin. *Experimental Neurology*, 13(3):264–272.

Flynn, A. and Proud, C. G. (1995). Serine 209, Not Serine 53, Is the Major Site of Phosphorylation in Initiation Factor eIF-4e in Serum-treated Chinese Hamster Ovary Cells. *Journal of Biological Chemistry*, 270(37):21684–21688.

Fox, P. L. (2015). Discovery and investigation of the GAIT translational control system. *RNA*, 21(4):615–618.

Fragkouli, A., Papatheodoropoulos, C., Georgopoulos, S., Stamatakis, A., Stylianopoulou, F., Tsilibary, E. C., and Tzinia, A. K. (2012). Enhanced neuronal plasticity and elevated endogenous sAPPα levels in mice overexpressing MMP9. *Journal of Neurochemistry*, 121(2):239–251.

Frey, U., Krug, M., Reymann, K. G., and Matthies, H. (1988). Anisomycin, an inhibitor of protein synthesis, blocks late phases of LTP phenomena in the hippocampal CA1 region in vitro. *Brain Research*, 452(1):57–65.

Friocourt, F. and Chédotal, A. (2017). The Robo3 receptor, a key player in the development, evolution, and function of commissural systems. *Developmental Neurobiology*, 77(7):876–890.

Furic, L., Rong, L., Larsson, O., Koumakpayi, I. H., Yoshida, K., Brueschke, A., Petroulakis, E., Robichaud, N., Pollak, M., Gaboury, L. A., Pandolfi, P. P., Saad, F., and Sonenberg, N. (2010). eIF4e phosphorylation promotes tumorigenesis and is associated with prostate cancer progression. *Proceedings of the National Academy of Sciences*, 107(32):14134–14139.

Gal-Ben-Ari, S., Kenney, J. W., Ounalla-Saad, H., Taha, E., David, O., Levitan, D., Gildish, I., Panja, D., Pai, B., Wibrand, K., Simpson, T. I., Proud, C. G., Bramham, C. R., Armstrong, J. D., and Rosenblum, K. (2012). Consolidation and translation regulation. *Learning & Memory*, 19(9):410–422.

Gallo, F. T., Katche, C., Morici, J. F., Medina, J. H., and Weisstaub, N. V. (2018). Immediate Early Genes, Memory and Psychiatric Disorders: Focus on c-Fos, Egr1 and Arc. *Frontiers in Behavioral Neuroscience*, 12.

Gantois, I., Khoutorsky, A., Popic, J., Aguilar-Valles, A., Freemantle, E., Cao, R., Sharma, V., Pooters, T., Nagpal, A., Skalecka, A., Truong, V. T., Wiebe, S., Groves, I. A., Jafarnejad, S. M., Chapat, C., McCullagh, E. A., Gamache, K., Nader, K., Lacaille, J.-C., Gkogkas, C. G., and Sonenberg, N. (2017). Metformin ameliorates core deficits in a mouse model of fragile X syndrome. *Nature Medicine*, 23(6):674–677.

Gao, J., Wang, W.-Y., Mao, Y.-W., Gräff, J., Guan, J.-S., Pan, L., Mak, G., Kim, D., Su, S. C., and Tsai, L.-H. (2010). A novel pathway regulates memory and plasticity via SIRT1 and miR-134. *Nature*, 466(7310):1105–1109.

García-Fuster, M. J., Díez-Alarcia, R., Ferrer-Alcón, M., La Harpe, R., Meana, J. J., and García-Sevilla, J. A. (2014). FADD adaptor and PEA-15/ERK1/2 partners in major depression and schizophrenia postmortem brains: Basal contents and effects of psychotropic treatments. *Neuroscience*, 277:541–551.

Gkogkas, C., Sonenberg, N., and Costa-Mattioli, M. (2010). Translational Control Mechanisms in Long-lasting Synaptic Plasticity and Memory. *Journal of Biological Chemistry*, 285(42):31913–31917.

Gkogkas, C. G., Khoutorsky, A., Cao, R., Jafarnejad, S. M., Prager-Khoutorsky, M., Giannakas, N., Kaminari, A., Fragkouli, A., Nader, K., Price, T. J., Konicek, B. W., Graff, J. R., Tzinia, A. K., Lacaille, J.-C., and Sonenberg, N. (2014). Pharmacogenetic Inhibition of eIF4e-Dependent Mmp9 mRNA Translation Reverses Fragile X Syndrome-like Phenotypes. *Cell Reports*, 9(5):1742–1755.

Gkogkas, C. G., Khoutorsky, A., Ran, I., Rampakakis, E., Nevarko, T., Weatherill, D. B., Vasuta, C., Yee, S., Truitt, M., Dallaire, P., Major, F., Lasko, P., Ruggero, D., Nader, K., Lacaille, J.-C., and Sonenberg, N. (2013). Autism-related deficits via dysregulated eIF4e-dependent translational control. *Nature*, 493(7432):371–377.

Global Burden of Disease Collaborative Network (2018). Global Burden of Disease Study 2017 (GBD 2017) Results. Institute for Health Metrics and Evaluation (IHME) http://ghdx.healthdata.org/gbd-results-too.

Goldsmith, D. R., Rapaport, M. H., and Miller, B. J. (2016). A meta-analysis of blood cytokine network alterations in psychiatric patients: comparisons between schizophrenia, bipolar disorder and depression. *Molecular Psychiatry*, 21(12):1696–1709.

Gordon, A. and Hannon, G. J. (2010). Fastx-toolkit. FASTQ/A short-reads pre-processing tools. http://hannonlab.cshl.edu/fastx_toolkit/.

Gourley, S. L., Wu, F. J., Kiraly, D. D., Ploski, J. E., Kedves, A. T., Duman, R. S., and Taylor, J. R. (2008). Regionally Specific Regulation of ERK MAP Kinase in a Model of Antidepressant-Sensitive Chronic Depression. *Biological Psychiatry*, 63(4):353–359.

Grecksch, G. and Matthies, H. (1980). Two sensitive periods for the amnesic effect of anisomycin. *Pharmacology Biochemistry and Behavior*, 12(5):663–665.

Griggs, E. M., Young, E. J., Rumbaugh, G., and Miller, C. A. (2013). MicroRNA-182 Regulates Amygdala-Dependent Memory Formation. *Journal of Neuroscience*, 33(4):1734–1740.

Guimaraes, J. C. and Zavolan, M. (2016). Patterns of ribosomal protein expression specify normal and malignant human cells. *Genome Biology*, 17(1):236.

Hafner, A.-S., Donlin-Asp, P. G., Leitch, B., Herzog, E., and Schuman, E. M. (2019). Local protein synthesis is a ubiquitous feature of neuronal pre- and postsynaptic compartments. *Science*, 364(6441):eaau3644.

Hamon, M. and Blier, P. (2013). Monoamine neurocircuitry in depression and strategies for new treatments. *Progress in Neuro-Psychopharmacology and Biological Psychiatry*, 45:54–63.

Hay, N. and Sonenberg, N. (2004). Upstream and downstream of mTOR. *Genes & Development*, 18(16):1926–1945.

Heiman, M., Schaefer, A., Gong, S., Peterson, J. D., Day, M., Ramsey, K. E., Suárez-Fariñas, M., Schwarz, C., Stephan, D. A., Surmeier, D. J., Greengard, P., and Heintz, N. (2008). A Translational Profiling Approach for the Molecular Characterization of CNS Cell Types. *Cell*, 135(4):738–748.

Herdy, B., Jaramillo, M., Svitkin, Y. V., Rosenfeld, A. B., Kobayashi, M., Walsh, D., Alain, T., Sean, P., Robichaud, N., Topisirovic, I., Furic, L., Dowling, R. J. O., Sylvestre, A., Rong, L., Colina, R., Costa-Mattioli, M., Fritz, J. H., Olivier, M., Brown, E., Mohr, I., and Sonenberg, N. (2012). Translational control of the activation of transcription factor NF-κB and production of type I interferon by phosphorylation of the translation factor eIF4e. *Nature Immunology*, 13(6):543–550.

Hinnebusch, A. G., Ivanov, I. P., and Sonenberg, N. (2016). Translational control by 5'-untranslated regions of eukaryotic mRNAs. *Science*, 352(6292):1413–1416.

Hodes, G. E., Pfau, M. L., Leboeuf, M., Golden, S. A., Christoffel, D. J., Bregman, D., Rebusi, N., Heshmati, M., Aleyasin, H., Warren, B. L., Labonté, B., Horn, S., Lapidus, K. A., Stelzhammer, V., Wong, E. H. F., Bahn, S., Krishnan, V., Bolaños-Guzman, C. A., Murrough, J. W., Merad, M., and Russo, S. J. (2014). Individual differences in the peripheral immune system promote resilience versus susceptibility to social stress. *Proceedings of the National Academy of Sciences*, 111(45):16136–16141.

Holt, C. E. and Schuman, E. M. (2013). The Central Dogma Decentralized: New Perspectives on RNA Function and Local Translation in Neurons. *Neuron*, 80(3):648–657.

Hoogendoorn, C. J., Roy, J. F., and Gonzalez, J. S. (2017). Shared Dysregulation of Homeostatic Brain-Body Pathways in Depression and Type 2 Diabetes. *Current Diabetes Reports*, 17(10):90.

Huang, D. W., Sherman, B. T., and Lempicki, R. A. (2009a). Bioinformatics enrichment tools: paths toward the comprehensive functional analysis of large gene lists. *Nucleic Acids Research*, 37(1):1–13.

Huang, D. W., Sherman, B. T., and Lempicki, R. A. (2009b). Systematic and integrative analysis of large gene lists using DAVID bioinformatics resources. *Nature Protocols*, 4(1):44–57.

Huang, H.-P., Chen, P.-H., Yu, C.-Y., Chuang, C.-Y., Stone, L., Hsiao, W.-C., Li, C.-L., Tsai, S.-C., Chen, K.-Y., Chen, H.-F., Ho, H.-N., and Kuo, H.-C. (2011). Epithelial Cell Adhesion Molecule (EpCAM) Complex Proteins Promote Transcription Factor-mediated Pluripotency Reprogramming. *Journal of Biological Chemistry*, 286(38):33520–33532.

Huang, Y.-Y. and Kandel, E. R. (2005). Theta frequency stimulation induces a local form of late phase LTP in the CA1 region of the hippocampus. *Learning & Memory*, 12(6):587–593.

Huber, K. M., Roder, J. C., and Bear, M. F. (2001). Chemical induction of mGluR5-and protein synthesis–dependent long-term depression in hippocampal area CA1. *Journal of Neurophysiology*, 86(1):321–325.

Hubert, L. J. and Levin, J. R. (1976). A general statistical framework for assessing categorical clustering in free recall. *Psychological Bulletin*, 83(6):1072–1080.

Huntley, G. W. (2012). Synaptic circuit remodelling by matrix metalloproteinases in health and disease. *Nature Reviews Neuroscience*, 13(11):743–757.

Hylin, M. J., Orsi, S. A., Moore, A. N., and Dash, P. K. (2013). Disruption of the perineuronal net in the hippocampus or medial prefrontal cortex impairs fear conditioning. *Learning & Memory*, 20(5):267–273.

Ingolia, N. T. (2014). Ribosome profiling: new views of translation, from single codons to genome scale. *Nature Reviews Genetics*, 15(3):205–213.

Ingolia, N. T., Brar, G. A., Rouskin, S., McGeachy, A. M., and Weissman, J. S. (2012). The ribosome profiling strategy for monitoring translation in vivo by deep sequencing of ribosome-protected mRNA fragments. *Nature Protocols*, 7(8):1534–1550.

Ingolia, N. T., Ghaemmaghami, S., Newman, J. R. S., and Weissman, J. S. (2009). Genome-Wide Analysis in Vivo of Translation with Nucleotide Resolution Using Ribosome Profiling. *Science*, 324(5924):218–223.

Ingolia, N. T., Lareau, L. F., and Weissman, J. S. (2011). Ribosome Profiling of Mouse Embryonic Stem Cells Reveals the Complexity and Dynamics of Mammalian Proteomes. *Cell*, 147(4):789–802.

Izquierdo, I., Furini, C. R. G., and Myskiw, J. C. (2016). Fear Memory. *Physiological Reviews*, 96(2):695–750.

Janich, P., Arpat, A. B., Castelo-Szekely, V., Lopes, M., and Gatfield, D. (2015). Ribosome profiling reveals the rhythmic liver translatome and circadian clock regulation by upstream open reading frames. *Genome Research*, 25(12):1848–1859.

Janusz, A., Miłek, J., Perycz, M., Pacini, L., Bagni, C., Kaczmarek, L., and Dziembowska, M. (2013). The Fragile X Mental Retardation Protein Regulates Matrix Metalloproteinase 9 mRNA at Synapses. *The Journal of Neuroscience*, 33(46):18234–18241.

Joshi, B., Cai, A.-L., Keiper, B. D., Minich, W. B., Mendez, R., Beach, C. M., Stepinski, J., Stolarski, R., Darzynkiewicz, E., and Rhoads, R. E. (1995). Phosphorylation of Eukaryotic Protein Synthesis Initiation Factor 4e at Ser-209. *Journal of Biological Chemistry*, 270(24):14597–14603.

Joshi, S. and Platanias, L. C. (2014). Mnk kinase pathway: Cellular functions and biological outcomes. *World Journal of Biological Chemistry*, 5(3):321–333.

Jung, H., Gkogkas, C. G., Sonenberg, N., and Holt, C. E. (2014). Remote Control of Gene Function by Local Translation. *Cell*, 157(1):26–40.

Kandel, E. R. (2001). The Molecular Biology of Memory Storage: A Dialogue Between Genes and Synapses. *Science*, 294(5544):1030–1038.

Kandel, E. R., Dudai, Y., and Mayford, M. R. (2014). The Molecular and Systems Biology of Memory. *Cell*, 157(1):163–186.

Kang, H. and Schuman, E. M. (1996). A Requirement for Local Protein Synthesis in Neurotrophin-Induced Hippocampal Synaptic Plasticity. *Science*, 273(5280):1402–1406.

Kanterewicz, B. I., Urban, N. N., McMahon, D. B. T., Norman, E. D., Giffen, L. J., Favata, M. F., Scherle, P. A., Trzăskos, J. M., Barrionuevo, G., and Klann, E. (2000). The Extracellular Signal-Regulated Kinase Cascade Is Required for NMDA Receptor-Independent LTP in Area CA1 But Not Area CA3 of the Hippocampus. *Journal of Neuroscience*, 20(9):3057–3066.

Kappelmann, N., Lewis, G., Dantzer, R., Jones, P. B., and Khandaker, G. M. (2018). Antidepressant activity of anti-cytokine treatment: a systematic review and meta-analysis of clinical trials of chronic inflammatory conditions. *Molecular Psychiatry*, 23(2):335–343.

Katoh, K. and Standley, D. M. (2013). MAFFT Multiple Sequence Alignment Software Version 7: Improvements in Performance and Usability. *Molecular Biology and Evolution*, 30(4):772–780.

Keeley, M. B., Wood, M. A., Isiegas, C., Stein, J., Hellman, K., Hannenhalli, S., and Abel, T. (2006). Differential transcriptional response to nonassociative and associative components of classical fear conditioning in the amygdala and hippocampus. *Learning & Memory*, 13(2):135–142.

Kelleher, R. J., Govindarajan, A., Jung, H.-Y., Kang, H., and Tonegawa, S. (2004). Translational Control by MAPK Signaling in Long-Term Synaptic Plasticity and Memory. *Cell*, 116(3):467–479.

Kelleher III, R. J. and Bear, M. F. (2008). The Autistic Neuron: Troubled Translation? *Cell*, 135(3):401–406.

Klann, E. and Dever, T. E. (2004). Biochemical mechanisms for translational regulation in synaptic plasticity. *Nature Reviews Neuroscience*, 5(12):931–942.

Knauf, U., Tschopp, C., and Gram, H. (2001). Negative Regulation of Protein Translation by Mitogen-Activated Protein Kinase-Interacting Kinases 1 and 2. *Molecular and Cellular Biology*, 21(16):5500–5511.

Konicek, B. W., Stephens, J. R., McNulty, A. M., Robichaud, N., Peery, R. B., Dumstorf, C. A., Dowless, M. S., Iversen, P. W., Parsons, S., Ellis, K. E., McCann, D. J., Pelletier, J., Furic, L., Yingling, J. M., Stancato, L. F., Sonenberg, N., and Graff, J. R. (2011). Therapeutic Inhibition of MAP Kinase Interacting Kinase Blocks Eukaryotic Initiation Factor 4e Phosphorylation and Suppresses Outgrowth of Experimental Lung Metastases. *Cancer Research*, 71(5):1849–1857.

Konopka, W., Kiryk, A., Novak, M., Herwerth, M., Parkitna, J. R., Wawrzyniak, M., Kowarsch, A., Michaluk, P., Dzwonek, J., Arnsperger, T., Wilczynski, G., Merkenschlager, M., Theis, F. J., Köhr, G., Kaczmarek, L., and Schütz, G. (2010). MicroRNA Loss Enhances Learning and Memory in Mice. *Journal of Neuroscience*, 30(44):14835–14842.

Kreisel, T., Frank, M. G., Licht, T., Reshef, R., Ben-Menachem-Zidon, O., Baratta, M. V., Maier, S. F., and Yirmiya, R. (2014). Dynamic microglial alterations underlie stress-induced depressive-like behavior and suppressed neurogenesis. *Molecular Psychiatry*, 19(6):699–709.

Köhler, O., Benros, M. E., Nordentoft, M., Farkouh, M. E., Iyengar, R. L., Mors, O., and Krogh, J. (2014). Effect of Anti-inflammatory Treatment on Depression, Depressive Symptoms, and Adverse Effects: A Systematic Review and Meta-analysis of Randomized Clinical Trials. *JAMA Psychiatry*, 71(12):1381–1391.

Lachance, P. E. D., Miron, M., Raught, B., Sonenberg, N., and Lasko, P. (2002). Phosphorylation of Eukaryotic Translation Initiation Factor 4e Is Critical for Growth. *Molecular and Cellular Biology*, 22(6):1656–1663.

Langmead, B., Trapnell, C., Pop, M., and Salzberg, S. L. (2009). Ultrafast and memory-efficient alignment of short DNA sequences to the human genome. *Genome Biology*, 10(3):R25.

Laplante, M. and Sabatini, D. M. (2012). mTOR Signaling in Growth Control and Disease. *Cell*, 149(2):274–293.

Libich, G. H. a. D. S. (2009). The Classic Basic Protein of Myelin – Conserved Structural Motifs and the Dynamic Molecular Barcode Involved in Membrane Adhesion and Protein-Protein Interactions. *Current Protein & Peptide Science*.

Liu-Yesucevitz, L., Bassell, G. J., Gitler, A. D., Hart, A. C., Klann, E., Richter, J. D., Warren, S. T., and Wolozin, B. (2011). Local RNA Translation at the Synapse and in Disease. *Journal of Neuroscience*, 31(45):16086–16093.

Love, M. I., Huber, W., and Anders, S. (2014). Moderated estimation of fold change and dispersion for RNA-seq data with DESeq2. *Genome Biology*, 15(12):550.

Lovelace, J. W., Wen, T. H., Reinhard, S., Hsu, M. S., Sidhu, H., Ethell, I. M., Binder, D. K., and Razak, K. A. (2016). Matrix metalloproteinase-9 deletion rescues auditory evoked potential habituation deficit in a mouse model of Fragile X Syndrome. *Neurobiology of Disease*, 89:126–135.

Macdonald, P. (2001). Diversity in translational regulation. *Current Opinion in Cell Biology*, 13(3):326–331.

Mallory, C. S. and Giocomo, L. M. (2018). Heterogeneity in hippocampal place coding. *Current Opinion in Neurobiology*, 49:158–167.

Mayford, M., Baranes, D., Podsypanina, K., and Kandel, E. R. (1996). The 3-untranslated region of CaMKIIα is a cis-acting signal for the localization and translation of mRNA in dendrites. *Proceedings of the National Academy of Sciences*, 93(23):13250–13255.

Mayford, M., Siegelbaum, S. A., and Kandel, E. R. (2012). Synapses and Memory Storage. *Cold Spring Harbor Perspectives in Biology*, 4(6):a005751.

Mayr, C. (2017). Regulation by 3'-Untranslated Regions. *Annual Review of Genetics*, 51(1):171–194.

Mazumder, B., Seshadri, V., and Fox, P. L. (2003). Translational control by the 3'-UTR: the ends specify the means. *Trends in Biochemical Sciences*, 28(2):91–98.

McGaugh, J. L. (2000). Memory–a Century of Consolidation. *Science*, 287(5451):248–251.

McKendrick, L., Morley, S. J., Pain, V. M., Jagus, R., and Joshi, B. (2001). Phosphorylation of eukaryotic initiation factor 4e (eIF4e) at Ser209 is not required for protein synthesis in vitro and in vivo. *European Journal of Biochemistry*, 268(20):5375–5385.

Medina-Martinez, O., Brownell, I., Amaya-Manzanares, F., Hu, Q., Behringer, R. R., and Jamrich, M. (2005). Severe Defects in Proliferation and Differentiation of Lens Cells in Foxe3 Null Mice. *Molecular and Cellular Biology*, 25(20):8854–8863.

Miller, A. H. and Raison, C. L. (2016). The role of inflammation in depression: from evolutionary imperative to modern treatment target. *Nature Reviews Immunology*, 16(1):22–34.

Mills, S. C., Enganti, R., and Arnim, A. G. v. (2018). What makes ribosomes tick? *RNA Biology*, 15(1):44–54.

Monné, L. (2006). Functioning of the Cytoplasm. In *Advances in Enzymology and Related Areas of Molecular Biology*, pages 1–69. John Wiley & Sons, Ltd.

Mukhopadhyay, R., Ray, P. S., Arif, A., Brady, A. K., Kinter, M., and Fox, P. L. (2008). DAPK-ZIPK-L13a Axis Constitutes a Negative-Feedback Module Regulating Inflammatory Gene Expression. *Molecular Cell*, 32(3):371–382.

Nagy, V., Bozdagi, O., Matynia, A., Balcerzyk, M., Okulski, P., Dzwonek, J., Costa, R. M., Silva, A. J., Kaczmarek, L., and Huntley, G. W. (2006). Matrix Metalloproteinase-9 Is Required for Hippocampal Late-Phase Long-Term Potentiation and Memory. *The Journal of Neuroscience*, 26(7):1923–1934.

Nanni, V., Uher, R., and Danese, A. (2012). Childhood Maltreatment Predicts Unfavorable Course of Illness and Treatment Outcome in Depression: A Meta-Analysis. *American Journal of Psychiatry*, 169(2):141–151.

Napoli, I., Mercaldo, V., Boyl, P. P., Eleuteri, B., Zalfa, F., De Rubeis, S., Di Marino, D., Mohr, E., Massimi, M., Falconi, M., Witke, W., Costa-Mattioli, M., Sonenberg, N., Achsel, T., and Bagni, C. (2008). The Fragile X Syndrome Protein Represses Activity-Dependent Translation through CYFIP1, a New 4e-BP. *Cell*, 134(6):1042–1054.

O'Connor, J. C., Lawson, M. A., André, C., Moreau, M., Lestage, J., Castanon, N., Kelley, K. W., and Dantzer, R. (2009). Lipopolysaccharide-induced depressive-like behavior is mediated by indoleamine 2,3-dioxygenase activation in mice. *Molecular Psychiatry*, 14(5):511–522.

Ohira, K., Takeuchi, R., Iwanaga, T., and Miyakawa, T. (2013). Chronic fluoxetine treatment reduces parvalbumin expression and perineuronal netsin gamma-aminobutyric acidergic interneurons of the frontal cortex in adultmice. *Molecular Brain*, 6(1):43.

Osterweil, E. K., Chuang, S.-C., Chubykin, A. A., Sidorov, M., Bianchi, R., Wong, R. K. S., and Bear, M. F. (2013). Lovastatin Corrects Excess Protein Synthesis and Prevents Epileptogenesis in a Mouse Model of Fragile X Syndrome. *Neuron*, 77(2):243–250.

Osterweil, E. K., Krueger, D. D., Reinhold, K., and Bear, M. F. (2010). Hypersensitivity to mGluR5 and ERK1/2 Leads to Excessive Protein Synthesis in the Hippocampus of a Mouse Model of Fragile X Syndrome. *The Journal of Neuroscience*, 30(46):15616–15627.

Ouwenga, R., Lake, A. M., O'Brien, D., Mogha, A., Dani, A., and Dougherty, J. D. (2017). Transcriptomic Analysis of Ribosome-Bound mRNA in Cortical Neurites In Vivo. *Journal of Neuroscience*, 37(36):8688–8705.

Panja, D., Kenney, J. W., D'Andrea, L., Zalfa, F., Vedeler, A., Wibrand, K., Fukunaga, R., Bagni, C., Proud, C. G., and Bramham, C. R. (2014). Two-Stage Translational Control of Dentate Gyrus LTP Consolidation Is Mediated by Sustained BDNF-TrkB Signaling to MNK. *Cell Reports*, 9(4):1430–1445.

Pantazopoulos, H. and Berretta, S. (2016). In Sickness and in Health: Perineuronal Nets and Synaptic Plasticity in Psychiatric Disorders.

Peixoto, R. T., Kunz, P. A., Kwon, H., Mabb, A. M., Sabatini, B. L., Philpot, B. D., and Ehlers, M. D. (2012). Transsynaptic Signaling by Activity-Dependent Cleavage of Neuroligin-1. *Neuron*, 76(2):396–409.

Peleg, S., Sananbenesi, F., Zovoilis, A., Burkhardt, S., Bahari-Javan, S., Agis-Balboa, R. C., Cota, P., Wittnam, J. L., Gogol-Doering, A., Opitz, L., Salinas-Riester, G., Dettenhofer, M., Kang, H., Farinelli, L., Chen, W., and Fischer, A. (2010). Altered Histone Acetylation Is Associated with Age-Dependent Memory Impairment in Mice. *Science*, 328(5979):753–756.

Pesole, G. and Liuni, S. (1999). Internet resources for the functional analysis of 5' and 3' untranslated regions of eukaryotic mRNAs. *Trends in genetics: TIG*, 15(9):378.

Peter, M., Scheuch, H., Burkard, T. R., Tinter, J., Wernle, T., and Rumpel, S. (2012). Induction of immediate early genes in the mouse auditory cortex after auditory cued fear conditioning to complex sounds. *Genes, Brain and Behavior*, 11(3):314–324.

Poo, M.-m., Pignatelli, M., Ryan, T. J., Tonegawa, S., Bonhoeffer, T., Martin, K. C., Rudenko, A., Tsai, L.-H., Tsien, R. W., Fishell, G., Mullins, C., Gonçalves, J. T., Shtrahman, M., Johnston, S. T., Gage, F. H., Dan, Y., Long, J., Buzsáki, G., and Stevens, C. (2016). What is memory? The present state of the engram. *BMC Biology*, 14(1):40.

Poplawski, S. G., Peixoto, L., Porcari, G. S., Wimmer, M. E., McNally, A. G., Mizuno, K., Giese, K. P., Chatterjee, S., Koberstein, J. N., Risso, D., Speed, T. P., and Abel, T. (2016). Contextual fear conditioning induces differential alternative splicing. *Neurobiology of Learning and Memory*, 134:221–235.

Pothuizen, H. H. J., Zhang, W.-N., Jongen-Rêlo, A. L., Feldon, J., and Yee, B. K. (2004). Dissociation of function between the dorsal and the ventral hippocampus in spatial learning abilities of the rat: a within-subject, within-task comparison of reference and working spatial memory. *European Journal of Neuroscience*, 19(3):705–712.

Pyronnet, S., Imataka, H., Gingras, A.-C., Fukunaga, R., Hunter, T., and Sonenberg, N. (1999). Human eukaryotic translation initiation factor 4g (eIF4g) recruits Mnk1 to phosphorylate eIF4e. *The EMBO Journal*, 18(1):270–279.

Quackenbush, J. (2002). Microarray data normalization and transformation. *Nature Genetics*, 32(4s):496–501.

Quevedo, J., Vianna, M. R. M., Roesler, R., de Paris, F., Izquierdo, I., and Rose, S. P. R. (1999). Two Time Windows of Anisomycin-Induced Amnesia for Inhibitory Avoidance Training in Rats: Protection from Amnesia by Pretraining but not Pre-exposure to the Task Apparatus. *Learning & Memory*, 6(6):600–607.

Rangaraju, V., Dieck, S. t., and Schuman, E. M. (2017). Local translation in neuronal compartments: how local is local? *EMBO reports*, page e201744045.

Rangaraju, V., Lauterbach, M., and Schuman, E. M. (2019). Spatially Stable Mitochondrial Compartments Fuel Local Translation during Plasticity. *Cell*, 0(0).

Rao, A. and Steward, O. (1991). Evidence that protein constituents of postsynaptic membrane specializations are locally synthesized: analysis of proteins synthesized within synaptosomes. *Journal of Neuroscience*, 11(9):2881–2895.

Rao, J. S., Ertley, R. N., Lee, H.-J., DeMar Jr, J. C., Arnold, J. T., Rapoport, S. I., and Bazinet, R. P. (2007). n-3 Polyunsaturated fatty acid deprivation in rats decreases frontal cortex BDNF *via* a p38 MAPK-dependent mechanism. *Molecular Psychiatry*, 12(1):36–46.

Rao-Ruiz, P., Couey, J. J., Marcelo, I. M., Bouwkamp, C. G., Slump, D. E., Matos, M. R., Loo, R. J. v. d., Martins, G. J., Hout, M. v. d., IJcken, W.

F. v., Costa, R. M., Oever, M. C. v. d., and Kushner, S. A. (2019). Engram-specific transcriptome profiling of contextual memory consolidation. *Nature Communications*, 10(1):2232.

Richter, J. D. and Klann, E. (2009). Making synaptic plasticity and memory last: mechanisms of translational regulation. *Genes & Development*, 23(1):1–11.

Robichaud, N., del Rincon, S. V., Huor, B., Alain, T., Petruccelli, L. A., Hearnden, J., Goncalves, C., Grotegut, S., Spruck, C. H., Furic, L., Larsson, O., Muller, W. J., Miller, W. H., and Sonenberg, N. (2015). Phosphorylation of eIF4e promotes EMT and metastasis via translational control of SNAIL and MMP-3. *Oncogene*, 34(16):2032–2042.

Roesler, R. (2017). Molecular mechanisms controlling protein synthesis in memory reconsolidation. *Neurobiology of Learning and Memory*, 142:30–40.

Romagnani, S. (2000). T-cell subsets (Th1 versus Th2). *Annals of Allergy, Asthma & Immunology*, 85(1):9–21.

Rosen, J. B., Fanselow, M. S., Young, S. L., Sitcoske, M., and Maren, S. (1998). Immediate-early gene expression in the amygdala following footshock stress and contextual fear conditioning. *Brain Research*, 796(1):132–142.

Rudelli, R. D., Brown, W. T., Wisniewski, K., Jenkins, E. C., Laure-Kamionowska, M., Connell, F., and Wisniewski, H. M. (1985). Adult fragile X syndrome. Clinico-neuropathologic findings. *Acta Neuropathologica*, 67(3-4):289–295.

Rush, A. J., Trivedi, M. H., Wisniewski, S. R., Nierenberg, A. A., Stewart, J. W., Warden, D., Niederehe, G., Thase, M. E., Lavori, P. W., Lebowitz, B. D., McGrath, P. J., Rosenbaum, J. F., and Sackeim, H. A. (2006). Acute and Longer-Term Outcomes in Depressed Outpatients Requiring One or Several Treatment Steps: A STAR*D Report. *Am J Psychiatry*, page 13.

Saab, B. J. and Mansuy, I. M. (2014). Neuroepigenetics of memory formation and impairment: The role of microRNAs. *Neuropharmacology*, 80:61–69.

Santini, E., Huynh, T. N., and Klann, E. (2014). Mechanisms of Translation Control Underlying Long-Lasting Synaptic Plasticity and the Consolidation of Long-Term Memory. In *Progress in Molecular Biology and Translational Science*, volume 122, pages 131–167. Elsevier.

Santini, E., Huynh, T. N., MacAskill, A. F., Carter, A. G., Pierre, P., Ruggero, D., Kaphzan, H., and Klann, E. (2013). Exaggerated translation causes synaptic and behavioural aberrations associated with autism. *Nature*, 493(7432):411–415.

Saxton, R. A. and Sabatini, D. M. (2017). mTOR Signaling in Growth, Metabolism, and Disease. *Cell*, 168(6):960–976.

Schafe, G. E., Atkins, C. M., Swank, M. W., Bauer, E. P., Sweatt, J. D., and LeDoux, J. E. (2000). Activation of ERK/MAP Kinase in the Amygdala Is Required for Memory Consolidation of Pavlovian Fear Conditioning. *Journal of Neuroscience*, 20(21):8177–8187.

Schepetilnikov, M., Dimitrova, M., Mancera-Martínez, E., Geldreich, A., Keller, M., and Ryabova, L. A. (2013). TOR and S6k1 promote translation reinitiation of uORF-containing mRNAs via phosphorylation of eIF3h. *The EMBO Journal*, 32(8):1087–1102.

Schmidt, E. K., Clavarino, G., Ceppi, M., and Pierre, P. (2009). SUnSET, a nonradioactive method to monitor protein synthesis. *Nature Methods*, 6(4):275–277.

Schwanhäusser, B., Busse, D., Li, N., Dittmar, G., Schuchhardt, J., Wolf, J., Chen, W., and Selbach, M. (2011). Global quantification of mammalian gene expression control. *Nature*, 473(7347):337–342.

Sharma, A., Hoeffer, C. A., Takayasu, Y., Miyawaki, T., McBride, S. M., Klann, E., and Zukin, R. S. (2010). Dysregulation of mTOR Signaling in Fragile X Syndrome. *The Journal of Neuroscience*, 30(2):694–702.

Sharma, S. D., Metz, J. B., Li, H., Hobson, B. D., Hornstein, N., Sulzer, D., Tang, G., and Sims, P. A. (2019). Widespread Alterations in Translation Elongation in the Brain of Juvenile Fmr1 Knockout Mice. *Cell Reports*, 26(12):3313–3322.e5.

Sidhu, H., Dansie, L. E., Hickmott, P. W., Ethell, D. W., and Ethell, I. M. (2014). Genetic Removal of Matrix Metalloproteinase 9 Rescues the Symptoms of Fragile X Syndrome in a Mouse Model. *The Journal of Neuroscience*, 34(30):9867–9879.

Smagin, D. A., Kovalenko, I. L., Galyamina, A. G., Orlov, Y. L., Babenko, V. N., and Kudryavtseva, N. N. (2018). Heterogeneity of Brain Ribosomal Genes Expression Following Positive Fighting Experience in Male Mice as Revealed by RNA-Seq. *Molecular Neurobiology*, 55(1):390–401.

Smith, R. W. P., Blee, T. K. P., and Gray, N. K. (2014). Poly(A)-binding proteins are required for diverse biological processes in metazoans. *Biochemical Society Transactions*, 42(4):1229–1237.

Sonenberg, N. and Hinnebusch, A. G. (2009). Regulation of Translation Initiation in Eukaryotes: Mechanisms and Biological Targets. *Cell*, 136(4):731–745.

Stanton, P. K. and Sarvey, J. M. (1984). OF PROTEIN SYNTHESIS. *The Journal of Neuroscience*, 4(12):9.

Steward, O. and Levy, W. B. (1982). Preferential localization of polyribosomes under the base of dendritic spines in granule cells of the dentate gyrus. *Journal of Neuroscience*, 2(3):284–291.

Sutton, M. A. and Schuman, E. M. (2006). Dendritic Protein Synthesis, Synaptic Plasticity, and Memory. *Cell*, 127(1):49–58.

Szepesi, Z., Bijata, M., Ruszczycki, B., Kaczmarek, L., and Wlodarczyk, J. (2013). Matrix Metalloproteinases Regulate the Formation of Dendritic Spine Head Protrusions during Chemically Induced Long-Term Potentiation. *PLoS ONE*, 8(5):e63314.

The Dutch-Belgian Fragile X Consortium (1994). Fmr1 knockout mice: A model to study fragile X mental retardation. *Cell*, 78(1):23–33.

Thomas, G. M. and Huganir, R. L. (2004). MAPK cascade signalling and synaptic plasticity. *Nature Reviews Neuroscience*, 5(3):173.

Thomas, M. G., Pascual, M. L., Maschi, D., Luchelli, L., and Boccaccio, G. L. (2014). Synaptic control of local translation: the plot thickens with new characters. *Cellular and Molecular Life Sciences*, 71(12):2219–2239.

Thomson, S. R., Seo, S. S., Barnes, S. A., Louros, S. R., Muscas, M., Dando, O., Kirby, C., Wyllie, D. J. A., Hardingham, G. E., Kind, P. C., and Osterweil, E. K. (2017). Cell-Type-Specific Translation Profiling Reveals a Novel Strategy for Treating Fragile X Syndrome. *Neuron*, 95(3):550–563.e5.

Thoreen, C. C., Chantranupong, L., Keys, H. R., Wang, T., Gray, N. S., and Sabatini, D. M. (2012). A unifying model for mTORC1-mediated regulation of mRNA translation. *Nature*, 485(7396):109–113.

Tischmeyer, W. and Grimm, R. (1999). Activation of immediate early genes and memory formation. *Cellular and Molecular Life Sciences (CMLS)*, 55(4):564–574.

Torre, E. R. and Steward, O. (1992). Demonstration of local protein synthesis within dendrites using a new cell culture system that permits the isolation of living axons and dendrites from their cell bodies. *Journal of Neuroscience*, 12(3):762–772.

Tushev, G., Glock, C., Heumüller, M., Biever, A., Jovanovic, M., and Schuman, E. M. (2018). Alternative 3' UTRs Modify the Localization, Regulatory Potential, Stability, and Plasticity of mRNAs in Neuronal Compartments. *Neuron*, 98(3):495–511.e6.

Ueda, T., Watanabe-Fukunaga, R., Fukuyama, H., Nagata, S., and Fukunaga, R. (2004). Mnk2 and Mnk1 Are Essential for Constitutive and Inducible Phosphorylation of Eukaryotic Initiation Factor 4e but Not for Cell Growth or Development. *Molecular and Cellular Biology*, 24(15):6539–6549.

Vickers, C. A., Dickson, K. S., and Wyllie, D. J. A. (2005). Induction and maintenance of late-phase long-term potentiation in isolated dendrites of rat hippocampal CA1 pyramidal neurones. *The Journal of Physiology*, 568(3):803–813.

Vogel, C. (2011). Translation's coming of age. *Molecular Systems Biology*, 7(1):498.

Waskiewicz, A. J., Flynn, A., Proud, C. G., and Cooper, J. A. (1997). Mitogen-activated protein kinases activate the serine/threonine kinases Mnk1 and Mnk2. *The EMBO Journal*, 16(8):1909–1920.

Weiler, I. J. and Greenough, W. T. (1991). Potassium ion stimulation triggers protein translation in synaptoneurosomal polyribosomes. *Molecular and Cellular Neuroscience*, 2(4):305–314.

Wen, T. H., Afroz, S., Reinhard, S. M., Palacios, A. R., Tapia, K., Binder, D. K., Razak, K. A., and Ethell, I. M. (2018). Genetic Reduction of Matrix Metalloproteinase-9 Promotes Formation of Perineuronal Nets Around Parvalbumin-Expressing Interneurons and Normalizes Auditory Cortex Responses in Developing Fmr1 Knock-Out Mice. *Cerebral Cortex*, pages 1–14.

Wiera, G., Wozniak, G., Bajor, M., Kaczmarek, L., and Mozrzymas, J. W. (2013). Maintenance of long-term potentiation in hippocampal mossy fiber—CA3 pathway requires fine-tuned MMP-9 proteolytic activity. *Hippocampus*, 23(6):529–543.

Więdłocha, M., Marcinowicz, P., Krupa, R., Janoska-Jaździk, M., Janus, M., Dębowska, W., Mosiołek, A., Waszkiewicz, N., and Szulc, A. (2018). Effect of antidepressant treatment on peripheral inflammation markers – A meta-analysis. *Progress in Neuro-Psychopharmacology and Biological Psychiatry*, 80:217–226.

World Health Organization (2017a). Depression and Other Common Mental Disorders: Global Health Estimates. https://apps.who.int/iris/bitstream/handle/10665/254610/WHO-MSD-MER-2017.2-eng.pdf;jsessionid=A6D9B00742210D07EB1695E7B83325AF?sequence=1.

World Health Organization (2017b). WHO/Europe | Mental health - Depression in Europe: facts and figures. http://www.euro.who.int/en/health-topics/noncommunicable-diseases/mental-health/news/news/2012/10/depression-in-europe/depression-in-europe-facts-and-figures.

Xiao, Z., Zou, Q., Liu, Y., and Yang, X. (2016). Genome-wide assessment of differential translations with ribosome profiling data. *Nature Communications*, 7:11194.

Yarmolinsky, M. B. and Haba, G. L. D. L. (1959). Inhibition by Puromycin of Amino Acid Incorporation into Protein. *Proceedings of the National Academy of Sciences*, 45(12):1721–1729.

Yong, V. W. (2005). Metalloproteinases: Mediators of Pathology and Regeneration in the CNS. *Nature Reviews Neuroscience*, 6(12):931–944.

You, X., Vlatkovic, I., Babic, A., Will, T., Epstein, I., Tushev, G., Akbalik, G., Wang, M., Glock, C., Quedenau, C., Wang, X., Hou, J., Liu, H., Sun, W., Sambandan, S., Chen, T., Schuman, E. M., and Chen, W. (2015). Neural circular RNAs are derived from synaptic genes and regulated by development and plasticity. *Nature Neuroscience*, 18(4):603–610.

Zhu, J. J., Qin, Y., Zhao, M., Van Aelst, L., and Malinow, R. (2002). Ras and Rap Control AMPA Receptor Trafficking during Synaptic Plasticity. *Cell*, 110(4):443–455.

Zoghbi, H. Y. and Bear, M. F. (2012). Synaptic Dysfunction in Neurodevelopmental Disorders Associated with Autism and Intellectual Disabilities. *Cold Spring Harbor Perspectives in Biology*, 4(3):a009886.

Zuker, M. (2003). Mfold web server for nucleic acid folding and hybridization prediction. *Nucleic Acids Research*, 31(13):3406–3415.

Appendix A

Table A.1 DEGs and associated statistics for TgMMP9

Ensembl gene ID	Gene symbol	avg TgMMP9WT	avg TgMMP9OE	Ratio	$\log_2$ ratio	z-score	p-value	FDR
ENSMUSG00000038700	Hoxb5	0.19104383	0.0650875	0.34069406	-1.5534513	-2.3529429	0.01862549	0.02793824
ENSMUSG00000044518	Foxe3	10.8264372	3.81924517	0.35277027	-1.5031991	-6.7423114	1.56E-11	2.10E-10
ENSMUSG00000039728	Slc6a5	18.0335427	6.75019502	0.37431331	-1.4176818	-7.3535941	1.93E-13	5.21E-12
ENSMUSG00000032572	Col6a4	11.5371158	4.95603468	0.42957311	-1.2190244	-6.2766181	3.46E-10	3.11E-09
ENSMUSG00000018830	Myh11	54.2150514	32.1046339	0.59217197	-0.7559119	-4.9477507	7.51E-07	5.07E-06
ENSMUSG00000055333	Fat2	1.81667981	1.09516246	0.60283736	-0.7301593	-2.0713326	0.03832772	0.05174243
ENSMUSG00000027517	Ankrd60	6.75130015	4.16731821	0.61726158	-0.6960461	-3.7602775	0.00016972	0.00035251
ENSMUSG00000001930	Vwf	21.506693	14.041232	0.65287732	-0.6151162	-4.3344897	1.46E-05	5.64E-05
ENSMUSG00000000263	Glra1	15.2639653	9.98721738	0.65430032	-0.6119751	-3.9429449	8.05E-05	0.00019756
ENSMUSG00000035783	Acta2	3.90818207	2.58257516	0.6608124	-0.5976873	-2.933944	0.00334685	0.00602432
ENSMUSG00000032807	Alox12b	23.5542926	15.6416244	0.66406683	-0.5905997	-4.092013	4.28E-05	0.00011546
ENSMUSG00000095041	AC149090.1	12.5554664	19.3783814	1.54342187	0.62613245	4.28470211	1.83E-05	6.18E-05
ENSMUSG00000022831	Hcls1	16.9220369	26.3360933	1.55631933	0.63813811	4.85777572	1.19E-06	6.41E-06
ENSMUSG00000048096	Lmod1	2.81237164	4.44606163	1.58089407	0.6607407	2.47008817	0.01350798	0.02145384
ENSMUSG00000074384	AI429214	1.81677347	2.90256265	1.59764698	0.67594866	2.79705886	0.00515701	0.00870246
ENSMUSG00000054519	Zfp867	30.293658	48.4840852	1.60046981	0.67849547	4.17565259	2.97E-05	8.91E-05
ENSMUSG00000020914	Top2a	3.42683429	5.50255755	1.60572619	0.6832259	3.78440912	0.00015407	0.00034667
ENSMUSG00000028438	Kif24	7.49589942	12.2868328	1.63914056	0.71293957	4.69491406	2.67E-06	1.20E-05
ENSMUSG00000017737	Mmp9	0.67848622	1.22493522	1.8053944	0.85231404	2.21143422	0.02700578	0.03837664
ENSMUSG00000040148	Hmx3	1.71153712	3.33650787	1.94942186	0.96304633	3.6650732	0.00024727	0.00047687

Table A.2 DTGs and associated statistics for TgMMP9

Ensembl gene ID	Gene symbol	$\log_2$ FC TE	p-value	TE ratio	FDR
ENSMUSG00000060288	Ppih	-4.564431125	0.01996982	0.20693609	0.0798793
ENSMUSG00000028188	Spata1	-3.164204193	0.03264199	0.28091842	0.09545801
ENSMUSG00000055523	Gucy2g	-2.421900655	0.0302616	0.33517666	0.09545801
ENSMUSG00000038843	Gcnt1	-1.136568901	0.00651624	0.4720283	0.05616479
ENSMUSG00000074384	AI429214	-1.030955796	0.00048576	0.50016423	0.02013618
ENSMUSG00000023336	Wfdc1	-0.85686031	0.00670953	0.54081543	0.05616479
ENSMUSG00000101972	Hist1h3i	-0.824865678	0.00640628	0.54947697	0.05616479
ENSMUSG00000032478	Nme6	-0.791423349	0.01810786	0.56685843	0.07860338
ENSMUSG00000020914	Top2a	-0.790425982	0.00826101	0.53850065	0.05664695
ENSMUSG00000039552	Rsph4a	-0.741482927	0.00145117	0.58819714	0.02968006
ENSMUSG00000029659	Medag	-0.734425238	0.03575759	0.58965649	0.09545801
ENSMUSG00000027115	Kif18a	-0.713407083	0.03412168	0.64982452	0.09545801
ENSMUSG00000048865	Arhgap30	-0.701483911	0.02516476	0.6213438	0.0902481
ENSMUSG00000046561	Arsj	-0.69596296	0.04735762	0.61438456	0.10332572
ENSMUSG00000029499	Pxmp2	-0.659632377	0.01150387	0.62073319	0.05828869
ENSMUSG00000078853	Igtp	-0.652149826	0.0110897	0.6425648	0.05828869
ENSMUSG00000052384	Nrros	-0.6218521	0.03597676	0.64118497	0.09545801
ENSMUSG00000025504	Eps8l2	-0.620737077	0.01273213	0.64598794	0.05828869
ENSMUSG00000055027	Smyd1	-0.615771187	0.02632236	0.64175703	0.0902481
ENSMUSG00000095041	AC149090.1	-0.614801712	0.0467194	0.60508015	0.10332572
ENSMUSG00000030725	Lipt2	-0.610834812	0.03508937	0.64906739	0.09545801
ENSMUSG00000031382	Asb11	-0.537798974	0.01883206	0.66102068	0.07860338
ENSMUSG00000034164	Emid1	0.5461177	0.04176425	1.51226637	0.10019018
ENSMUSG00000064080	Fbln2	0.561293077	0.03443414	1.52561169	0.09545801
ENSMUSG00000006471	Ndor1	0.564903842	0.04486058	1.58868591	0.10253848
ENSMUSG00000066721	Zfp575	0.588438673	0.02628385	1.57209698	0.0902481
ENSMUSG00000091712	Sec14l5	0.628242419	0.00216417	1.55403737	0.02968006
ENSMUSG00000073565	Prr16	0.633430105	0.03151809	1.60069609	0.09545801
ENSMUSG00000091604	Gm17349	0.640367408	0.03679111	1.50903877	0.09545801
ENSMUSG00000069270	Hist1h2ac	0.655952145	0.04278956	1.52908879	0.10019018
ENSMUSG00000020090	Npffr1	0.660521397	0.04268853	1.58303726	0.10019018
ENSMUSG00000074918	Inafm2	0.668372339	0.00062926	1.55602186	0.02013618
ENSMUSG00000033788	Dysf	0.673860636	0.01275065	1.53204451	0.05828869
ENSMUSG00000049571	Cfap46	0.68569214	0.02325861	1.72292619	0.08931305
ENSMUSG00000040616	Tmem51	0.727488976	0.00793152	1.66377792	0.05664695
ENSMUSG00000030795	Fus	0.759998768	0.00060642	1.70827484	0.02013618
ENSMUSG00000003418	St8sia6	0.779374788	0.00189188	1.76358674	0.02968006
ENSMUSG00000024451	Arap3	0.789752652	0.01008332	1.6798259	0.05828869
ENSMUSG00000032807	Alox12b	0.804363309	0.00657328	1.76823008	0.05616479
ENSMUSG00000090958	Lrrc32	0.836408166	0.01040115	1.72431509	0.05828869
ENSMUSG00000050382	Kif7	0.956948028	0.01238913	1.97915808	0.05828869
ENSMUSG00000035299	Mid1	1.067274176	0.00197746	1.97501717	0.02968006
ENSMUSG00000048174	Tmem81	1.313918659	0.0070206	2.36476446	0.05616479
ENSMUSG00000093806	Asmt	1.534341534	0.0414665	3.26053649	0.10019018

Table A.3 DEGs and associated statistics for Fmr1KO

Ensembl gene ID	Gene symbol	avg Fmr1WT	avg Fmr1KO	Ratio	$\log_2$ ratio	z-score	p-value	FDR
ENSMUSG00000000838	Fmr1	771.6247368	175.183979	0.22703261	-2.1390286	-9.3397201	9.66E-21	3.67E-19
ENSMUSG00000044518	Foxe3	8.564011577	2.315084857	0.27032715	-1.8872217	-8.0587519	7.71E-16	1.46E-14
ENSMUSG00000035383	Pmch	0.308564612	0.148521547	0.48133046	-1.0549004	-2.1219173	0.03384468	0.05144391
ENSMUSG00000093806	Asmt	20.3600044	11.31369201	0.5556822	-0.8476681	-5.2075379	1.91E-07	1.82E-06
ENSMUSG00000091898	Tnnc1	4.20625246	2.372933029	0.56414422	-0.8258641	-3.3966682	0.00068212	0.00152473
ENSMUSG00000020673	Tpo	5.051014739	2.920863736	0.57827266	-0.7901782	-3.5891208	0.0003318	0.00078801
ENSMUSG00000036198	Arhgap36	2.779074749	1.617817819	0.58214261	-0.7805555	-3.2291731	0.00124149	0.00248297
ENSMUSG00000070564	Ntn5	6.424132937	3.788060789	0.58966102	-0.7620423	-4.5496383	5.37E-06	2.27E-05
ENSMUSG00000056999	Ide	12.04163186	7.216150352	0.59926681	-0.7387296	-4.9048946	9.35E-07	5.79E-06
ENSMUSG00000063681	Crb1	1.25256424	0.750702398	0.59933245	-0.7385716	-2.0704787	0.03840754	0.0561341
ENSMUSG00000002324	Rec8	16.43806247	9.929431204	0.60405119	-0.7272573	-4.6729044	2.97E-06	1.41E-05
ENSMUSG00000038805	Six3	11.19120771	6.845145465	0.61165387	-0.7092126	-4.1337786	3.57E-05	0.0001356
ENSMUSG00000072812	Ahnak2	2.207451869	1.358138766	0.61525181	-0.7007511	-3.0308548	0.00243863	0.00441275
ENSMUSG00000057751	Megf6	2.344761338	1.443185919	0.61549374	-0.7001839	-2.7970609	0.00515698	0.00852023
ENSMUSG00000048772	Tmem53	1.085038961	0.668746933	0.61633449	-0.6982146	-2.1784826	0.02937013	0.0465027
ENSMUSG00000041679	Lrrc29	16.09215714	9.949927507	0.61830912	-0.6935998	-4.0912617	4.29E-05	0.00014821
ENSMUSG00000038550	Ciart	1.569368812	0.982263863	0.6258974	-0.6760019	-2.0177003	0.04362249	0.05931238
ENSMUSG00000020891	Alox8	1.558073232	0.985933521	0.63279023	-0.6602008	-1.9646793	0.04945137	0.06479834
ENSMUSG00000090667	Gm765	17.97394627	11.3865189	0.63350133	-0.6585804	-4.0013584	6.30E-05	0.0001841
ENSMUSG00000022602	Arc	26.94283863	17.11100881	0.6350856	-0.654977	-5.4683157	4.54E-08	5.75E-07
ENSMUSG00000044912	Syt16	11.92611235	7.644160525	0.64095996	-0.6416939	-4.0202863	5.81E-05	0.00018407
ENSMUSG00000054667	Irs4	4.72591783	3.029196552	0.64097529	-0.6416594	-2.8952281	0.00378883	0.00654434
ENSMUSG00000050074	Spink8	9.206852567	5.943052753	0.6455032	-0.6315039	-3.5978433	0.00032087	0.00078801
ENSMUSG00000032511	Scn5a	48.41511417	31.61858019	0.65307251	-0.6146849	-4.8788922	1.07E-06	5.79E-06
ENSMUSG00000036357	Gpr101	9.52534019	6.235435855	0.65461556	-0.6112802	-3.3419324	0.00083197	0.00175639
ENSMUSG00000038775	Vill	9.978626361	6.591400038	0.66055184	-0.5982563	-3.8345168	0.00012581	0.00034149
ENSMUSG00000011171	Vipr2	1.276675227	2.213608861	1.73388565	0.79400876	3.06557067	0.00217255	0.00412785
ENSMUSG00000026579	F5	1.777194489	4.083202393	2.29755517	1.20009951	5.09753253	3.44E-07	2.62E-06
ENSMUSG00000001827	Folr1	0.034934261	0.087895439	2.51602398	1.33114567	2.01692003	0.04370386	0.05931238

Table A.4 DTGs and associated statistics for Fmr1KO

Ensembl gene ID	Gene symbol	log_2 FC TE	p-value	TE ratio	FDR
ENSMUSG00000000838	Fmr1	-1.1964779	2.35E-14	0.43205818	3.58E-12
ENSMUSG00000069917	Hba-a2	-0.9572793	0.01430241	0.51572763	0.10148363
ENSMUSG00000033307	Mif	-0.8539936	0.00298833	0.5424435	0.06055493
ENSMUSG00000041736	Tspo	-0.7727913	0.02123128	0.55153324	0.12206254
ENSMUSG00000022969	Il10rb	-0.78332	0.01338087	0.56690428	0.10148363
ENSMUSG00000025794	Rpl14	-0.8547736	0.00029657	0.57345138	0.01126957
ENSMUSG00000060708	Bloc1s4	-0.6577806	0.01370417	0.59513522	0.10148363
ENSMUSG00000007877	Tcap	-0.7143553	0.02060953	0.60253582	0.12206254
ENSMUSG00000040681	Hmgn1	-0.772124	0.02910577	0.60443114	0.14746922
ENSMUSG00000029994	Anxa4	-0.7200395	0.00651209	0.61355937	0.08495948
ENSMUSG00000030042	Pole4	-0.6503158	0.00726627	0.61697337	0.08495948
ENSMUSG00000063897	CAAA01118383.1	-0.6161239	0.00724439	0.63642828	0.08495948
ENSMUSG00000007833	Aldh16a1	-0.6299192	0.00889073	0.64042334	0.09397368
ENSMUSG00000032959	Pebp1	-0.6062976	7.79E-05	0.6469305	0.00394545
ENSMUSG00000030681	Mvp	-0.5811201	0.01602555	0.64717607	0.10149518
ENSMUSG00000056895	Hist3h2ba	-0.5280245	0.01532034	0.65228155	0.10148363
ENSMUSG00000024048	Myl12a	-0.5843734	0.00414018	0.65378825	0.06293079
ENSMUSG00000025492	Ifitm3	-0.5870171	0.03199838	0.66188033	0.15689527
ENSMUSG00000022559	Fbxl6	-0.6580876	0.0031786	0.6651256	0.06055493
ENSMUSG00000025290	Rps24	0.55333758	0.00348541	1.50168551	0.06055493
ENSMUSG00000089665	Fcor	0.6103239	0.01175737	1.53610428	0.0992845
ENSMUSG00000027230	Creb3l1	0.61816384	0.04940182	1.54479656	0.21454507
ENSMUSG00000060568	Fam78b	0.63791306	0.00927372	1.59386307	0.09397368
ENSMUSG00000079018	Ly6c1	0.62166696	0.03753684	1.59618506	0.17829998
ENSMUSG00000001930	Vwf	0.72776962	0.00280435	1.60781727	0.06055493
ENSMUSG00000034595	Ppp1r18	0.72843563	0.01078101	1.64211941	0.0963949
ENSMUSG00000064363	mt-Nd4	0.85185638	0.046435	1.83583386	0.21388243
ENSMUSG00000044461	Shisa2	0.977416	0.02339739	1.83974133	0.12263461
ENSMUSG00000037725	Ckap2	0.89312292	0.0232463	1.84015102	0.12263461
ENSMUSG00000002603	Tgfb1	0.93726161	0.00358549	1.85361069	0.06055493
ENSMUSG00000063681	Crb1	0.86351473	0.04909519	1.85813354	0.21454507
ENSMUSG00000074802	Gas2l3	0.90634822	0.01046225	1.89052542	0.0963949
ENSMUSG00000003166	Dgcr2	1.22745157	0.01535608	2.23028448	0.10148363
ENSMUSG00000056656	Apol8	1.84358127	0.02168216	2.64474164	0.12206254
ENSMUSG00000044518	Foxe3	3.98721971	1.01E-05	13.0199853	0.00076718

Appendix B

Table B.1 DTGs and associated TE values and fold changes for *4EKi*

Ensembl Gene ID	Gene symbol	log2 FC TE	TE ratio
ENSMUSG00000021342	Prl	-7.10410239	0.00726862
ENSMUSG00000020713	Gh	-7.06399226	0.00747354
ENSMUSG00000027483	Bpifa1	-2.51783099	0.17460527
ENSMUSG00000006574	Slc4a1	-2.06452484	0.23906505
ENSMUSG00000024871	Doc2g	-1.95741528	0.25748936
ENSMUSG00000022483	Col2a1	-1.7107256	0.30550638
ENSMUSG00000032496	Ltf	-1.67950063	0.31219068
ENSMUSG00000020125	Elane	-1.61310061	0.32689504
ENSMUSG00000029306	Ibsp	-1.42309735	0.37291084
ENSMUSG00000032484	Ngp	-1.41774774	0.37429619
ENSMUSG00000002249	Tead3	-1.40985878	0.37634852
ENSMUSG00000002249	Tead3	-1.40964812	0.37640348
ENSMUSG00000021803	Cdhr1	-1.26807454	0.41521356
ENSMUSG00000027073	Prg2	-1.24868388	0.42083194
ENSMUSG00000056071	S100a9	-1.21232962	0.43157116
ENSMUSG00000001435	Col18a1	-1.17150985	0.44395647
ENSMUSG00000034664	Itga2b	-1.15254287	0.44983167
ENSMUSG00000001348	Acp5	-1.13719817	0.45464167
ENSMUSG00000026822	Lcn2	-1.09574874	0.46789323
ENSMUSG00000020660	Pomc	-1.09025107	0.46967963
ENSMUSG00000025420	Katnal2	-1.06384532	0.47835536
ENSMUSG00000066842	Hmcn1	-1.0137687	0.49525083
ENSMUSG00000018830	Myh11	-0.97005063	0.51048815
ENSMUSG00000031962	Cdh15	-0.96281133	0.51305617
ENSMUSG00000001473	Tubb6	-0.93314287	0.5237162
ENSMUSG00000024421	Lama3	-0.93111283	0.52445365
ENSMUSG00000027966	Col11a1	-0.92809725	0.52555103
ENSMUSG00000048562	Sp8	-0.92468834	0.52679431
ENSMUSG00000069516	Lyz2	-0.92418963	0.52697644
ENSMUSG00000025504	Eps8l2	-0.92177546	0.52785901
ENSMUSG00000026579	F5	-0.91206064	0.5314255
ENSMUSG00000033257	Ttll4	-0.8842624	0.54176444
ENSMUSG00000028339	Col15a1	-0.87920122	0.54366836
ENSMUSG00000068394	Cep152	-0.87919479	0.54367078
ENSMUSG00000028268	Gbp3	-0.87026398	0.54704674
ENSMUSG00000026043	Col3a1	-0.85972281	0.55105843
ENSMUSG00000064080	Fbln2	-0.8474209	0.55577741
ENSMUSG00000024164	C3	-0.83816551	0.55935438

Ensembl Gene ID	Gene symbol	log2 FC TE	TE ratio
ENSMUSG00000038058	Nod1	-0.83227552	0.56164268
ENSMUSG00000021069	Pygl	-0.82500919	0.56447861
ENSMUSG00000015950	Ncf1	-0.82326552	0.56516126
ENSMUSG00000042997	Nhlrc3	-0.81775675	0.56732339
ENSMUSG00000035021	Baz1a	-0.81651575	0.56781161
ENSMUSG00000014773	Dll1	-0.81558598	0.56817766
ENSMUSG00000042540	Acot5	-0.81545012	0.56823117
ENSMUSG00000001506	Col1a1	-0.80965454	0.57051846
ENSMUSG00000028364	Tnc	-0.80953613	0.57056528
ENSMUSG00000002055	Spag5	-0.79804384	0.57512847
ENSMUSG00000074818	Pdzd7	-0.79527639	0.57623277
ENSMUSG00000035576	L3mbtl1	-0.79369605	0.57686433
ENSMUSG00000017737	Mmp9	-0.79170596	0.57766062
ENSMUSG00000020527	Myo19	-0.79163751	0.57768802
ENSMUSG00000041741	Pde3a	-0.79062226	0.5780947
ENSMUSG00000055541	Lair1	-0.78925777	0.57864171
ENSMUSG00000054404	Slfn5	-0.78811307	0.57910101
ENSMUSG00000009350	Mpo	-0.78571753	0.58006339
ENSMUSG00000031328	Flna	-0.77956445	0.58254264
ENSMUSG00000052957	Gas1	-0.77102746	0.58599999
ENSMUSG00000030247	Kcnj8	-0.76946893	0.58663338
ENSMUSG00000004127	Trmt10a	-0.76945073	0.58664078
ENSMUSG00000000555	Itga5	-0.76720044	0.58755653
ENSMUSG00000031004	Mki67	-0.76719123	0.58756028
ENSMUSG00000023066	Rttn	-0.76680459	0.58771776
ENSMUSG00000100254	Trpc2	-0.76602789	0.58803426
ENSMUSG00000005225	Plekha8	-0.76554279	0.58823201
ENSMUSG00000024330	Col11a2	-0.76501505	0.58844723
ENSMUSG00000049538	Adamts16	-0.76430383	0.58873739
ENSMUSG00000037795	N4bp2	-0.76110741	0.59004324
ENSMUSG00000054889	Dsp	-0.75548044	0.59234909
ENSMUSG00000030536	Iqgap1	-0.75176464	0.59387671
ENSMUSG00000071984	Fndc1	-0.74525502	0.59656241
ENSMUSG00000057969	Sema3b	-0.742488	0.59770769
ENSMUSG00000018143	Mafk	-0.73967504	0.59887423
ENSMUSG00000025077	Dclre1a	-0.73781862	0.59964534
ENSMUSG00000032175	Tyk2	-0.73513652	0.60076117
ENSMUSG00000068114	Ccdc134	-0.73506893	0.60078932
ENSMUSG00000021260	Hhipl1	-0.73405451	0.60121191
ENSMUSG00000030528	Blm	-0.7339676	0.60124813
ENSMUSG00000045903	Npas4	-0.73288448	0.60169969
ENSMUSG00000014039	Prdm15	-0.73144103	0.60230201
ENSMUSG00000030417	Pdcd5	-0.73014683	0.60284256
ENSMUSG00000021754	Map3k1	-0.72626263	0.60446779
ENSMUSG00000004609	Cd33	-0.72497629	0.60500699
ENSMUSG00000030055	Rab43	-0.72102877	0.60666468
ENSMUSG00000026104	Stat1	-0.7181271	0.60788609
ENSMUSG00000090946	Ccdc71l	-0.71542143	0.6090272
ENSMUSG00000038506	Dcun1d2	-0.70959958	0.61148983
ENSMUSG00000025993	Slc40a1	-0.70583889	0.61308589
ENSMUSG00000037552	Plekhg2	-0.70582644	0.61309118
ENSMUSG00000021408	Ripk1	-0.70388333	0.61391749
ENSMUSG00000012640	Zfp715	-0.70154118	0.61491496
ENSMUSG00000026017	**Carf**	-0.70117736	0.61507005
ENSMUSG00000036555	Iqce	-0.70010042	0.61552936

Ensembl Gene ID	Gene symbol	log2 FC TE	TE ratio
ENSMUSG00000002814	Top3a	-0.69885213	0.61606218
ENSMUSG00000039936	Pik3cd	-0.69771252	0.61654901
ENSMUSG00000024186	Rgs11	-0.6957545	0.61738635
ENSMUSG00000027931	Npr1	-0.6943739	0.61797745
ENSMUSG00000039787	Cercam	-0.69357056	0.61832166
ENSMUSG00000044906	4930503L19Rik	-0.69195396	0.6190149
ENSMUSG00000049287	Iba57	-0.68917926	0.62020658
ENSMUSG00000037846	Rtkn2	-0.68810679	0.6206678
ENSMUSG00000051599	Pcdhb2	-0.68779671	0.62080122
ENSMUSG00000024135	Srbd1	-0.68678366	0.62123729
ENSMUSG00000048424	Ranbp3l	-0.68498494	0.62201232
ENSMUSG00000037709	Fam13a	-0.68440186	0.62226376
ENSMUSG00000032202	Rab27a	-0.68134788	0.6235824
ENSMUSG00000004891	Nes	-0.67815137	0.62496557
ENSMUSG00000026349	Ccnt2	-0.67728119	0.62534265
ENSMUSG00000002325	Irf9	-0.67604466	0.62587885
ENSMUSG00000029661	Col1a2	-0.6744137	0.62658681
ENSMUSG00000028776	Tinagl1	-0.66985346	0.62857053
ENSMUSG00000033453	Adamts15	-0.66981824	0.62858588
ENSMUSG00000024098	Twsg1	-0.66962745	0.62866901
ENSMUSG00000026784	Pdss1	-0.66946849	0.62873828
ENSMUSG00000030223	Ptpro	-0.66714525	0.62975158
ENSMUSG00000033669	Zfp7	-0.66219606	0.63191567
ENSMUSG00000025815	Dhtkd1	-0.66168708	0.63213865
ENSMUSG00000015879	Fam184b	-0.66091683	0.63247623
ENSMUSG00000005682	Pan2	-0.65815712	0.63368724
ENSMUSG00000037016	Frem2	-0.65802298	0.63374617
ENSMUSG00000031628	Casp3	-0.65709807	0.63415259
ENSMUSG00000027750	Postn	-0.6496409	0.63743896
ENSMUSG00000033276	Stk36	-0.64924412	0.63761429
ENSMUSG00000022325	Pop1	-0.64910456	0.63767598
ENSMUSG00000046618	Olfml2a	-0.64731702	0.63846657
ENSMUSG00000032332	Col12a1	-0.64137758	0.64110049
ENSMUSG00000035493	Tgfbi	-0.64064597	0.64142568
ENSMUSG00000061898	Rbak	-0.63840788	0.64242152
ENSMUSG00000040711	Sh3pxd2b	-0.63774656	0.64271606
ENSMUSG00000028414	Fktn	-0.6371243	0.64299334
ENSMUSG00000032511	Scn5a	-0.63691239	0.64308779
ENSMUSG00000036036	Zfp57	-0.63428689	0.64425919
ENSMUSG00000031508	Ankrd10	-0.6336724	0.64453366
ENSMUSG00000036036	Zfp57	-0.633531	0.64459683
ENSMUSG00000035914	Cd276	-0.6281648	0.64699891
ENSMUSG00000024610	Cd74	-0.62810237	0.64702691
ENSMUSG00000021224	Numb	-0.62464761	0.64857818
ENSMUSG00000035258	Abi3bp	-0.62421031	0.6487748
ENSMUSG00000061517	Sox21	-0.6231718	0.64924198
ENSMUSG00000040690	Col16a1	-0.62262804	0.64948673
ENSMUSG00000068959	Zfp619	-0.62219948	0.64967969
ENSMUSG00000020482	Ccdc117	-0.61949102	0.65090052
ENSMUSG00000057722	Lepr	-0.61935099	0.6509637
ENSMUSG00000057706	Mex3b	-0.6175724	0.65176672
ENSMUSG00000037474	Dtl	-0.6170708	0.65199337
ENSMUSG00000058402	Zfp420	-0.61552079	0.65269424
ENSMUSG00000020272	Stk10	-0.61524027	0.65282116
ENSMUSG00000042138	Msantd2	-0.61380747	0.65346983

Ensembl Gene ID	Gene symbol	log2 FC TE	TE ratio
ENSMUSG00000041911	Dlx1	-0.61013506	0.65513537
ENSMUSG00000032006	Pdgfd	-0.61001017	0.65519208
ENSMUSG00000020649	Rrm2	-0.6096446	0.65535813
ENSMUSG00000030786	Itgam	-0.60952838	0.65541092
ENSMUSG00000021203	Otub2	-0.60939973	0.65546937
ENSMUSG00000073700	Klhl21	-0.60903866	0.65563344
ENSMUSG00000046351	Zfp322a	-0.60844892	0.6559015
ENSMUSG00000030322	Mbd4	-0.60775225	0.65621831
ENSMUSG00000054737	Zfp182	-0.60701094	0.65655558
ENSMUSG00000079038	D130040H23Rik	-0.60599597	0.65701765
ENSMUSG00000067942	Zfp160	-0.60108158	0.65925953
ENSMUSG00000028927	Padi2	-0.60001129	0.65974879
ENSMUSG00000029253	Cenpc1	-0.59923284	0.66010488
ENSMUSG00000023088	Abcc1	-0.59912025	0.66015639
ENSMUSG00000056870	Gulp1	-0.59757938	0.66086185
ENSMUSG00000027361	Gabpb1	-0.59625424	0.66146914
ENSMUSG00000034160	Ogt	-0.59573765	0.66170604
ENSMUSG00000015522	Arnt	-0.5957246	0.66171202
ENSMUSG00000021203	Otub2	-0.59518304	0.66196046
ENSMUSG00000052446	Zfp961	-0.59422627	0.66239961
ENSMUSG00000015659	Serac1	-0.5933912	0.66278314
ENSMUSG00000026176	Ctdsp1	-0.59331431	0.66281846
ENSMUSG00000069135	Fgfr1op	-0.59250049	0.66319246
ENSMUSG00000030671	Pde3b	-0.59140999	0.66369394
ENSMUSG00000044548	Dact1	-0.59139418	0.66370121
ENSMUSG00000024236	Svil	-0.59003328	0.66432758
ENSMUSG00000055065	Ddx17	-0.5875076	0.66549162
ENSMUSG00000071291	Zfp58	-0.58696841	0.66574038
ENSMUSG00000034845	Plvap	-0.58676637	0.66583362
ENSMUSG00000022089	Bin3	-0.586497	0.66595795
ENSMUSG00000029701	Rbm28	-0.58644758	0.66598077
ENSMUSG00000009621	Vav2	-0.586264	0.66606552
ENSMUSG00000024968	Rcor2	-0.58449614	0.66688221
ENSMUSG00000031644	Nek1	-0.5843274	0.66696021
ENSMUSG00000016933	Plcg1	-0.58374724	0.66722847
ENSMUSG00000026193	Fn1	-0.583559	0.66731554
ENSMUSG00000035545	Leng8	-0.58331331	0.66742919
ENSMUSG00000041261	Car8	-0.58298056	0.66758315
ENSMUSG00000041353	Tmem29	-0.58274288	0.66769314
ENSMUSG00000028476	Reck	-0.58086998	0.6685605
ENSMUSG00000025529	Zfp711	-0.58038289	0.66878626
ENSMUSG00000019846	Lama4	-0.58036571	0.66879422
ENSMUSG00000062116	Zfp954	-0.58033306	0.66880936
ENSMUSG00000058638	Zfp110	-0.57972065	0.66909332
ENSMUSG00000032528	Vipr1	-0.57841219	0.66970043
ENSMUSG00000041238	Rbbp8	-0.57810062	0.66984508
ENSMUSG00000060301	2610008E11Rik	-0.57775806	0.67000415
ENSMUSG00000005397	Nid1	-0.57659997	0.6705422
ENSMUSG00000031174	Rpgr	-0.57581064	0.67090917
ENSMUSG00000041731	Pgm5	-0.57518964	0.67119802
ENSMUSG00000031583	Wrn	-0.57421156	0.67165321
ENSMUSG00000032743	D430042O09Rik	-0.57349256	0.67198803
ENSMUSG00000029009	Mthfr	-0.57228049	0.67255283
ENSMUSG00000040033	Stat2	-0.57225969	0.67256253
ENSMUSG00000033416	Gucd1	-0.57157704	0.67288085

Ensembl Gene ID	Gene symbol	log2 FC TE	TE ratio
ENSMUSG00000044617	Zbtb39	-0.57117177	0.67306989
ENSMUSG00000001123	Lgals9	-0.57030238	0.67347562
ENSMUSG00000044982	Sft2d3	-0.56982515	0.67369843
ENSMUSG00000048939	Atp13a5	-0.56916525	0.67400666
ENSMUSG00000001521	Tulp3	-0.56635224	0.67532214
ENSMUSG00000060063	Alox5ap	-0.56442844	0.67622326
ENSMUSG00000079215	Zfp664	-0.56380758	0.67651434
ENSMUSG00000048445	Ccdc57	-0.56373029	0.67655058
ENSMUSG00000027792	Bche	-0.56363843	0.67659366
ENSMUSG00000026880	Stom	-0.5631007	0.67684589
ENSMUSG00000032267	Usp28	-0.56173513	0.67748686
ENSMUSG00000058145	Adamts17	-0.56111292	0.67777911
ENSMUSG00000031986	Sprtn	-0.56061086	0.67801502
ENSMUSG00000015522	Arnt	-0.55964451	0.67846932
ENSMUSG00000032303	Chrna3	-0.55940801	0.67858055
ENSMUSG00000003752	Itpkc	-0.55880748	0.67886307
ENSMUSG00000020788	Atp2a3	-0.55794628	0.67926844
ENSMUSG00000063564	Col23a1	-0.55464896	0.6808227
ENSMUSG00000039632	Ccdc151	-0.55401985	0.68111965
ENSMUSG00000074483	Bglap	-0.55372882	0.68125706
ENSMUSG00000016487	Ppfibp1	-0.55340971	0.68140776
ENSMUSG00000016487	Ppfibp1	-0.55323124	0.68149207
ENSMUSG00000020019	Ntn4	-0.5527281	0.68172977
ENSMUSG00000027676	Ccdc39	-0.55138312	0.68236563
ENSMUSG00000021706	Zfyve16	-0.55113225	0.68248429
ENSMUSG00000027111	Itga6	-0.54978956	0.68311977
ENSMUSG00000017969	Ptgis	-0.54868434	0.68364329
ENSMUSG00000050600	Zfp831	-0.54803861	0.68394935
ENSMUSG00000003865	Gys1	-0.54736621	0.68426819
ENSMUSG00000052551	Adarb2	-0.54733221	0.68428432
ENSMUSG00000016087	Fli1	-0.54722961	0.68433298
ENSMUSG00000034009	Rxfp1	-0.54562512	0.68509449
ENSMUSG00000028597	Gpx7	-0.54463408	0.68556527
ENSMUSG00000002617	Zfp40	-0.54456536	0.68559792
ENSMUSG00000026648	Dclre1c	-0.5438777	0.68592479
ENSMUSG00000022335	Zfat	-0.54241104	0.68662246
ENSMUSG00000038705	Gmeb2	-0.54112217	0.68723615
ENSMUSG00000002835	Chaf1a	-0.54069037	0.68744187
ENSMUSG00000027253	Lrp4	-0.54009826	0.68772407
ENSMUSG00000045934	Mtmr11	-0.54008098	0.6877323
ENSMUSG00000030607	Acan	-0.53994341	0.68779789
ENSMUSG00000021806	Nid2	-0.53914331	0.68817944
ENSMUSG00000031285	Dcx	-0.53773044	0.68885372
ENSMUSG00000031239	Itm2a	-0.53731055	0.68905424
ENSMUSG00000056673	Kdm5d	-0.53588977	0.68973316
ENSMUSG00000001098	Kctd10	-0.53561527	0.68986441
ENSMUSG00000031502	Col4a1	-0.53480497	0.69025198
ENSMUSG00000020128	Vps54	-0.53467956	0.69031199
ENSMUSG00000017550	Atad5	-0.53414093	0.69056976
ENSMUSG00000020263	Appl2	-0.53412163	0.690579
ENSMUSG00000026655	Fam107b	-0.53343704	0.69090677
ENSMUSG00000050973	Gdpgp1	-0.53272638	0.69124719
ENSMUSG00000033083	Tbc1d4	-0.53255473	0.69132944
ENSMUSG00000020674	Pxdn	-0.53054707	0.69229217
ENSMUSG00000049232	Tigd2	-0.53033997	0.69239155

Ensembl Gene ID	Gene symbol	log2 FC TE	TE ratio
ENSMUSG00000028078	Dclk2	-0.52953225	0.69277931
ENSMUSG00000041180	Hectd2	-0.52845712	0.69329578
ENSMUSG00000042476	Abcb4	-0.52816274	0.69343726
ENSMUSG00000029283	Cdc7	-0.52751748	0.69374748
ENSMUSG00000030243	Recql	-0.5274531	0.69377843
ENSMUSG00000042793	Lgr6	-0.52653488	0.69422014
ENSMUSG00000025982	Sf3b1	-0.52610865	0.69442527
ENSMUSG00000002870	Mcm2	-0.52599337	0.69448076
ENSMUSG00000006958	Chrd	-0.52592688	0.69451277
ENSMUSG00000024451	Arap3	-0.52544186	0.69474629
ENSMUSG00000040624	Plekhg1	-0.52470056	0.69510337
ENSMUSG00000004105	Angptl2	-0.52400812	0.69543707
ENSMUSG00000036103	Colec12	-0.52356389	0.69565124
ENSMUSG00000020218	Wif1	-0.52312535	0.69586273
ENSMUSG00000030093	Wnt7a	-0.52216788	0.69632471
ENSMUSG00000033740	St18	-0.5216239	0.69658731
ENSMUSG00000050846	Zfp623	-0.52160489	0.69659649
ENSMUSG00000028073	Pear1	-0.5204282	0.69716488
ENSMUSG00000044033	Ccdc141	-0.51914131	0.69778703
ENSMUSG00000020140	Lgr5	-0.51872441	0.6979887
ENSMUSG00000027778	Ift80	-0.51690027	0.6988718
ENSMUSG00000027677	Ttc14	-0.51568967	0.69945848
ENSMUSG00000025821	Zfp282	-0.5151204	0.69973453
ENSMUSG00000019986	Ahi1	-0.51509557	0.69974658
ENSMUSG00000038323	1700066M21Rik	-0.51482623	0.69987723
ENSMUSG00000001119	Col6a1	-0.51339458	0.70057209
ENSMUSG00000028391	Wdr31	-0.51314551	0.70069305
ENSMUSG00000037108	Zcwpw1	-0.5126305	0.70094322
ENSMUSG00000029122	Evc	-0.51123562	0.70162127
ENSMUSG00000040373	Cacng5	-0.5108293	0.7018189
ENSMUSG00000037400	Atp11b	-0.51022562	0.70211263
ENSMUSG00000067586	S1pr3	-0.51017253	0.70213847
ENSMUSG00000050315	Synpo2	-0.51013442	0.70215701
ENSMUSG00000047213	Ythdf3	-0.5095822	0.70242583
ENSMUSG00000023990	Tfeb	-0.50858292	0.70291253
ENSMUSG00000038718	Pbx3	-0.50832978	0.70303588
ENSMUSG00000001998	Ap4e1	-0.50760622	0.70338856
ENSMUSG00000029290	Zfp326	-0.5067913	0.70378599
ENSMUSG00000064210	Ano6	-0.50580786	0.7042659
ENSMUSG00000025280	Polr3a	-0.50561778	0.7043587
ENSMUSG00000024542	Cep192	-0.50541092	0.7044597
ENSMUSG00000013629	Cad	-0.50454888	0.70488075
ENSMUSG00000036611	Eepd1	-0.50428159	0.70501136
ENSMUSG00000057367	Birc2	-0.50427966	0.7050123
ENSMUSG00000074282	Zfp94	-0.50340969	0.70543757
ENSMUSG00000045817	Zfp36l2	-0.50311105	0.70558361
ENSMUSG00000049878	Rlf	-0.5029468	0.70566394
ENSMUSG00000025323	Sp4	-0.50257883	0.70584395
ENSMUSG00000074282	Zfp94	-0.50244175	0.70591102
ENSMUSG00000026395	Ptprc	-0.50228837	0.70598607
ENSMUSG00000026097	Ormdl1	-0.50206971	0.70609308
ENSMUSG00000063550	Nup98	-0.50023146	0.70699334
ENSMUSG00000046572	Zfp518b	-0.49925894	0.70747009
ENSMUSG00000051910	Sox6	-0.49881248	0.70768906
ENSMUSG00000027878	Notch2	-0.49881195	0.70768932

Ensembl Gene ID	Gene symbol	log2 FC TE	TE ratio
ENSMUSG00000046982	Tshz1	-0.49827699	0.70795178
ENSMUSG00000046311	Zfp62	-0.49761011	0.70827911
ENSMUSG00000024451	Arap3	-0.49754526	0.70831095
ENSMUSG00000091387	Gcnt4	-0.4970758	0.70854147
ENSMUSG00000004626	Stxbp2	-0.49660876	0.70877088
ENSMUSG00000047793	Sned1	-0.49643116	0.70885814
ENSMUSG00000045689	Pcdhb4	-0.49479423	0.70966289
ENSMUSG00000030725	Lipt2	-0.49456569	0.70977531
ENSMUSG00000031337	Mtm1	-0.49407157	0.71001846
ENSMUSG00000052406	Rexo4	-0.49361439	0.71024349
ENSMUSG00000030249	Abcc9	-0.49350551	0.71029709
ENSMUSG00000027947	Il6ra	-0.49263626	0.71072519
ENSMUSG00000035351	Nup37	-0.49255705	0.71076422
ENSMUSG00000047036	Zfp445	-0.49232669	0.71087771
ENSMUSG00000039789	Zfp597	-0.49231302	0.71088445
ENSMUSG00000020473	Aebp1	-0.49208398	0.71099732
ENSMUSG00000041215	Yeats2	-0.49180278	0.71113591
ENSMUSG00000028369	Svep1	-0.49134284	0.71136266
ENSMUSG00000044646	Zbtb7c	-0.49129653	0.7113855
ENSMUSG00000022443	Myh9	-0.49062322	0.71171758
ENSMUSG00000028228	Cpne3	-0.4895052	0.71226934
ENSMUSG00000028496	Mllt3	-0.4894328	0.71230509
ENSMUSG00000032508	Myd88	-0.48937549	0.71233339
ENSMUSG00000020695	Mrc2	-0.48848264	0.71277437
ENSMUSG00000037010	Apln	-0.48795888	0.71303318
ENSMUSG00000025198	Erlin1	-0.48774616	0.71313832
ENSMUSG00000046311	Zfp62	-0.4875746	0.71322313
ENSMUSG00000029913	Prdm5	-0.48752397	0.71324816
ENSMUSG00000021666	Gfm2	-0.4874471	0.71328617
ENSMUSG00000047773	Ankfn1	-0.48730441	0.71335672
ENSMUSG00000030339	Ltbr	-0.4872984	0.71335969
ENSMUSG00000024789	Jak2	-0.48727762	0.71336997
ENSMUSG00000033486	Catsper2	-0.48702001	0.71349736
ENSMUSG00000018932	Map2k3	-0.48691532	0.71354914
ENSMUSG00000038836	Agbl3	-0.48633418	0.71383662
ENSMUSG00000038025	Phf2	-0.48608382	0.71396051
ENSMUSG00000071042	Rasgrp3	-0.4858701	0.71406628
ENSMUSG00000028995	Fam126a	-0.48560841	0.71419582
ENSMUSG00000039062	Anpep	-0.48554855	0.71422545
ENSMUSG00000020914	Top2a	-0.48515081	0.71442238
ENSMUSG00000048039	Isg20l2	-0.485056	0.71446934
ENSMUSG00000002265	Peg3	-0.48452521	0.71473225
ENSMUSG00000008090	Fgfrl1	-0.48449396	0.71474773
ENSMUSG00000054237	Fra10ac1	-0.48442125	0.71478375
ENSMUSG00000045466	Zfp956	-0.48441829	0.71478522
ENSMUSG00000054387	Mdm4	-0.48428105	0.71485322
ENSMUSG00000034800	Zfp661	-0.48371596	0.71513327
ENSMUSG00000039286	Fndc3b	-0.48320374	0.71538723
ENSMUSG00000025537	Phkg1	-0.48282326	0.71557592
ENSMUSG00000020412	Ascc2	-0.48266246	0.71565568
ENSMUSG00000043257	Pigv	-0.48215042	0.71590973
ENSMUSG00000025220	Mgea5	-0.48210274	0.71593339
ENSMUSG00000038990	Cables2	-0.48017024	0.71689303
ENSMUSG00000040693	Slco4c1	-0.48014898	0.71690359
ENSMUSG00000026188	Tmem169	-0.48008459	0.71693559

Ensembl Gene ID	Gene symbol	log2 FC TE	TE ratio
ENSMUSG00000060510	Zfp266	-0.47985905	0.71704767
ENSMUSG00000028389	Zfp37	-0.4798425	0.7170559
ENSMUSG00000036446	Lum	-0.47837492	0.7177857
ENSMUSG00000102049	Zbed6	-0.47814657	0.71789932
ENSMUSG00000042496	Prdm10	-0.47771038	0.7181164
ENSMUSG00000048546	Tob2	-0.47577707	0.71907937
ENSMUSG00000056174	Col8a2	-0.47576895	0.71908342
ENSMUSG00000027678	Ncoa3	-0.4756526	0.71914141
ENSMUSG00000031434	Morc4	-0.4749211	0.71950614
ENSMUSG00000037286	Stag1	-0.47450375	0.71971431
ENSMUSG00000044783	Hjurp	-0.47431285	0.71980955
ENSMUSG00000086596	Susd5	-0.47426176	0.71983504
ENSMUSG00000005410	Mcm5	-0.47406871	0.71993137
ENSMUSG00000025812	Pard3	-0.47352872	0.72020089
ENSMUSG00000025608	Podxl	-0.47331945	0.72030536
ENSMUSG00000021256	Vash1	-0.47319434	0.72036783
ENSMUSG00000004661	Arid3b	-0.47249064	0.72071929
ENSMUSG00000055737	Ghr	-0.47234302	0.72079304
ENSMUSG00000032554	Trf	-0.47206206	0.72093342
ENSMUSG00000038357	Camp	-0.47193627	0.72099628
ENSMUSG00000016552	Foxred2	-0.47193099	0.72099892
ENSMUSG00000028273	Pdlim5	-0.47078267	0.72157304
ENSMUSG00000034987	Hrh2	-0.4706898	0.72161948
ENSMUSG00000029206	Nsun7	-0.47028753	0.72182073
ENSMUSG00000020700	Map3k3	-0.46992501	0.72200213
ENSMUSG00000019874	Fabp7	-0.46887665	0.72252697
ENSMUSG00000042548	Asxl1	-0.46849074	0.72272027
ENSMUSG00000016918	Sulf1	-0.46820795	0.72286195
ENSMUSG00000046020	Pofut1	-0.46774069	0.72309611
ENSMUSG00000025648	Pfkfb4	-0.46753152	0.72320095
ENSMUSG00000039831	Arhgap29	-0.46722509	0.72335458
ENSMUSG00000027889	Ampd2	-0.46668066	0.7236276
ENSMUSG00000048058	Ldlrad3	-0.46650833	0.72371404
ENSMUSG00000019794	Katna1	-0.46632979	0.72380361
ENSMUSG00000021311	Mtr	-0.46614533	0.72389616
ENSMUSG00000055240	Zfp101	-0.46588678	0.72402591
ENSMUSG00000023972	Ptk7	-0.46583638	0.7240512
ENSMUSG00000022604	Cep97	-0.46542518	0.7242576
ENSMUSG00000031283	Chrdl1	-0.46535257	0.72429405
ENSMUSG00000025199	Chuk	-0.46498824	0.72447698
ENSMUSG00000022677	Fopnl	-0.46482696	0.72455798
ENSMUSG00000038342	Mlxip	-0.46473677	0.72460327
ENSMUSG00000037174	Elf2	-0.46453381	0.72470522
ENSMUSG00000020363	Gfpt2	-0.46436272	0.72479117
ENSMUSG00000005553	Atp4a	-0.46436113	0.72479197
ENSMUSG00000028864	Hgf	-0.46411475	0.72491576
ENSMUSG00000059005	Hnrnpa3	-0.46392363	0.7250118
ENSMUSG00000025239	Limd1	-0.46312546	0.72541302
ENSMUSG00000001918	Slc1a5	-0.46262291	0.72566575
ENSMUSG00000020362	Cnot6	-0.46245059	0.72575243
ENSMUSG00000028164	Manba	-0.46224416	0.72585628
ENSMUSG00000023886	Smoc2	-0.46181584	0.72607182
ENSMUSG00000059273	Zc3h4	-0.46162602	0.72616736
ENSMUSG00000030592	Ryr1	-0.46149396	0.72623383
ENSMUSG00000031885	Cbfb	-0.46082666	0.72656982

Ensembl Gene ID	Gene symbol	log2 FC TE	TE ratio
ENSMUSG00000027164	Traf6	-0.46058437	0.72669185
ENSMUSG00000033382	Trappc8	-0.46020822	0.72688134
ENSMUSG00000017491	Rarb	-0.46005754	0.72695726
ENSMUSG00000029249	Rest	-0.45994847	0.72701222
ENSMUSG00000024219	Anks1	-0.45978228	0.72709598
ENSMUSG00000076435	Acsf2	-0.45966003	0.72715759
ENSMUSG00000039254	Pomt1	-0.45920485	0.72738705
ENSMUSG00000055480	Zfp458	-0.45890271	0.7275394
ENSMUSG00000022610	Mapk12	-0.4583515	0.72781743
ENSMUSG00000078202	Nrarp	-0.45833126	0.72782764
ENSMUSG00000036246	Gmip	-0.45827932	0.72785384
ENSMUSG00000029131	Dnajb6	-0.4579587	0.72801562
ENSMUSG00000042104	Uggt2	-0.45769001	0.72815122
ENSMUSG00000000976	Heatr6	-0.45755124	0.72822126
ENSMUSG00000027829	Ccnl1	-0.45747432	0.72826009
ENSMUSG00000032409	Atr	-0.45678065	0.72861033
ENSMUSG00000041702	Btbd7	-0.45644354	0.7287806
ENSMUSG00000048832	Vps37c	-0.45635484	0.72882541
ENSMUSG00000034799	Unc13a	-0.45613958	0.72893416
ENSMUSG00000030393	Zik1	-0.45578805	0.7291118
ENSMUSG00000030002	Dusp11	-0.45504203	0.72948892
ENSMUSG00000056014	A430033K04Rik	-0.45462625	0.72969918
ENSMUSG00000039804	Ncoa5	-0.45448732	0.72976946
ENSMUSG00000030231	Plekha5	-0.45368389	0.73017598
ENSMUSG00000024908	Ppp6r3	-0.45301838	0.73051288
ENSMUSG00000003382	Etv3	-0.45288859	0.73057861
ENSMUSG00000020100	Slc29a3	-0.45288692	0.73057945
ENSMUSG00000002428	Hltf	-0.45278994	0.73062857
ENSMUSG00000032582	Rbm6	-0.45271828	0.73066486
ENSMUSG00000042408	Zmym6	-0.45169951	0.731181
ENSMUSG00000024534	Sncaip	-0.45138287	0.7313415
ENSMUSG00000025188	Hps1	-0.45127786	0.73139473
ENSMUSG00000026814	Eng	-0.45089325	0.73158974
ENSMUSG00000032607	Amt	-0.45075231	0.73166122
ENSMUSG00000037313	Tacc3	-0.45061565	0.73173053
ENSMUSG00000053907	Mat2a	-0.45053483	0.73177152
ENSMUSG00000074220	Zfp382	-0.45045534	0.73181184
ENSMUSG00000042207	Kdm5b	-0.44985542	0.73211621
ENSMUSG00000053965	Pde5a	-0.44972374	0.73218304
ENSMUSG00000029401	Rilpl2	-0.4491898	0.73245407
ENSMUSG00000054051	Ercc6	-0.44917848	0.73245982
ENSMUSG00000037752	Xkr8	-0.4490704	0.73251469
ENSMUSG00000018819	Lsp1	-0.44877612	0.73266413
ENSMUSG00000066571	4931406P16Rik	-0.4487143	0.73269552
ENSMUSG00000035649	Zcchc7	-0.44865301	0.73272665
ENSMUSG00000024169	Ift140	-0.44845476	0.73282734
ENSMUSG00000063810	Alms1	-0.448234	0.73293949
ENSMUSG00000063796	Slc22a8	-0.44809554	0.73300983
ENSMUSG00000028465	Tln1	-0.44780528	0.73315733
ENSMUSG00000021390	Ogn	-0.44780374	0.73315811
ENSMUSG00000026220	Slc16a14	-0.44743468	0.73334568
ENSMUSG00000026240	Cops7b	-0.44743322	0.73334642
ENSMUSG00000021240	Abcd4	-0.44739346	0.73336663
ENSMUSG00000035293	G2e3	-0.44730892	0.73340961
ENSMUSG00000032911	Cspg4	-0.44707893	0.73352654

Ensembl Gene ID	Gene symbol	log2 FC TE	TE ratio
ENSMUSG00000071256	Zfp213	-0.44684322	0.7336464
ENSMUSG00000026404	Ddx59	-0.44668654	0.73372608
ENSMUSG00000028019	Pdgfc	-0.44658395	0.73377825
ENSMUSG00000030098	Grip2	-0.44621827	0.73396427
ENSMUSG00000036334	Igsf10	-0.44605384	0.73404792
ENSMUSG00000009741	Ubp1	-0.44594114	0.73410527
ENSMUSG00000001062	Vps9d1	-0.44593189	0.73410997
ENSMUSG00000028456	Unc13b	-0.44574592	0.73420461
ENSMUSG00000046637	Ttc34	-0.44522673	0.73446888
ENSMUSG00000026305	Lrrfip1	-0.44516183	0.73450192
ENSMUSG00000023015	Racgap1	-0.44513881	0.73451364
ENSMUSG00000032126	Hmbs	-0.4446051	0.73478542
ENSMUSG00000026657	Frmd4a	-0.44432755	0.73492679
ENSMUSG00000038080	Kdm1b	-0.44356257	0.73531658
ENSMUSG00000022822	Abcc5	-0.44337543	0.73541197
ENSMUSG00000048347	Pcdhb18	-0.44302751	0.73558934
ENSMUSG00000040187	Arntl2	-0.44224645	0.73598769
ENSMUSG00000022960	Donson	-0.44171463	0.73625905
ENSMUSG00000024620	Pdgfrb	-0.44167703	0.73627824
ENSMUSG00000035161	Ints6	-0.44163587	0.73629925
ENSMUSG00000071267	Zfp942	-0.44155042	0.73634286
ENSMUSG00000024033	Rsph1	-0.44139927	0.73642001
ENSMUSG00000020781	Tsen54	-0.44139242	0.7364235
ENSMUSG00000031706	Rfx1	-0.44130208	0.73646962
ENSMUSG00000015839	Nfe2l2	-0.44070314	0.73677543
ENSMUSG00000028521	Slc35d1	-0.43972917	0.737273
ENSMUSG00000020717	Pecam1	-0.43928912	0.73749792
ENSMUSG00000025723	Nmb	-0.43891014	0.73769168
ENSMUSG00000049791	Fzd4	-0.43881615	0.73773974
ENSMUSG00000020709	Adap2	-0.43860773	0.73784632
ENSMUSG00000029587	Zfp12	-0.43827745	0.73801526
ENSMUSG00000053950	Adnp2	-0.43827571	0.73801615
ENSMUSG00000039087	Rreb1	-0.4379202	0.73819804
ENSMUSG00000022948	Setd4	-0.43763294	0.73834503
ENSMUSG00000031825	Crispld2	-0.43743116	0.73844831
ENSMUSG00000117748	Chtf8	-0.4372543	0.73853884
ENSMUSG00000004655	Aqp1	-0.43714804	0.73859324
ENSMUSG00000023952	Gtpbp2	-0.43705713	0.73863978
ENSMUSG00000048503	Tmem136	-0.43688417	0.73872834
ENSMUSG00000022718	Dgcr8	-0.43679251	0.73877527
ENSMUSG00000032580	Rbm5	-0.43676248	0.73879066
ENSMUSG00000035595	1600002K03Rik	-0.43653218	0.7389086
ENSMUSG00000038593	Tctn1	-0.43644449	0.73895351
ENSMUSG00000022865	Cxadr	-0.43630466	0.73902514
ENSMUSG00000020312	Shc2	-0.43596666	0.7391983
ENSMUSG00000028082	Sh3d19	-0.43560126	0.73938554
ENSMUSG00000053347	Zfp943	-0.43518935	0.73959668
ENSMUSG00000020423	Btg2	-0.43497032	0.73970897
ENSMUSG00000019856	Fam184a	-0.43426651	0.74006992
ENSMUSG00000003824	Syce2	-0.43394722	0.74023373
ENSMUSG00000024610	Cd74	-0.43364487	0.74038888
ENSMUSG00000031520	Vegfc	-0.43359478	0.74041458
ENSMUSG00000075229	Ccdc58	-0.43339589	0.74051667
ENSMUSG00000057551	Zfp317	-0.43336463	0.74053271
ENSMUSG00000031134	Rbmx	-0.4328118	0.74081653

Ensembl Gene ID	Gene symbol	log2 FC TE	TE ratio
ENSMUSG00000030826	Bcat2	-0.43239511	0.74103053
ENSMUSG00000001305	Rrp15	-0.43178664	0.74134313
ENSMUSG00000038697	Taf5l	-0.43145569	0.74151322
ENSMUSG00000030042	Pole4	-0.43112028	0.74168563
ENSMUSG00000091712	Sec14l5	-0.43104159	0.74172608
ENSMUSG00000054893	Zfp667	-0.43082852	0.74183564
ENSMUSG00000030929	Eri2	-0.43078687	0.74185705
ENSMUSG00000004099	Dnmt1	-0.4303884	0.74206198
ENSMUSG00000028212	Ccne2	-0.43030017	0.74210737
ENSMUSG00000022529	Zfp263	-0.43009722	0.74221177
ENSMUSG00000004677	Myo9b	-0.42964178	0.74244611
ENSMUSG00000029174	Tbc1d1	-0.42952163	0.74250795
ENSMUSG00000004665	Cnn2	-0.42894782	0.74280333
ENSMUSG00000033991	Ttc37	-0.4288311	0.74286342
ENSMUSG00000031378	Abcd1	-0.42830614	0.74313378
ENSMUSG00000060862	Zbtb40	-0.42756282	0.74351677
ENSMUSG00000008200	Fnbp4	-0.42745378	0.74357296
ENSMUSG00000016520	Lnx2	-0.42709376	0.74375854
ENSMUSG00000025403	Shmt2	-0.42694082	0.7438374
ENSMUSG00000023951	Vegfa	-0.42693229	0.74384179
ENSMUSG00000064023	Klk8	-0.42679662	0.74391175
ENSMUSG00000029635	Cdk8	-0.42676496	0.74392807
ENSMUSG00000032803	Cdv3	-0.42665024	0.74398723
ENSMUSG00000045912	C2cd4c	-0.42634348	0.74414544
ENSMUSG00000030522	Mtmr10	-0.42582598	0.74441241
ENSMUSG00000026516	Nvl	-0.42560804	0.74452488
ENSMUSG00000042099	Kank3	-0.42552874	0.7445658
ENSMUSG00000034485	Uaca	-0.42530354	0.74468203
ENSMUSG00000060716	Plekhh1	-0.42489614	0.74489236
ENSMUSG00000070564	Ntn5	-0.42474726	0.74496923
ENSMUSG00000028653	Trit1	-0.42436228	0.74516805
ENSMUSG00000031928	Mre11a	-0.42430847	0.74519584
ENSMUSG00000049728	Zfp668	-0.42400947	0.7453503
ENSMUSG00000060568	Fam78b	-0.42399367	0.74535846
ENSMUSG00000029127	Zbtb49	-0.42344012	0.74564451
ENSMUSG00000039577	Nphp4	-0.42329163	0.74572125
ENSMUSG00000019813	Cep57l1	-0.42328825	0.745723
ENSMUSG00000034218	Atm	-0.42242967	0.74616693
ENSMUSG00000020752	Recql5	-0.42238651	0.74618925
ENSMUSG00000000881	Dlg3	-0.42232312	0.74622204
ENSMUSG00000031665	Sall1	-0.42160341	0.7465944
ENSMUSG00000030727	Rabep2	-0.42120532	0.74680044
ENSMUSG00000024201	Kdm4b	-0.42101863	0.74689708
ENSMUSG00000043572	Pars2	-0.42098378	0.74691513
ENSMUSG00000030616	Sytl2	-0.42077079	0.74702541
ENSMUSG00000067594	Krt77	-0.42064869	0.74708863
ENSMUSG00000050234	Gja4	-0.42046534	0.74718358
ENSMUSG00000029427	Zcchc8	-0.42045315	0.7471899
ENSMUSG00000032374	Plod2	-0.42011045	0.74736741
ENSMUSG00000058486	Wdr91	-0.41982157	0.74751707
ENSMUSG00000027217	Tspan18	-0.41971423	0.74757269
ENSMUSG00000004151	Etv1	-0.41970157	0.74757925
ENSMUSG00000020063	Sirt1	-0.41951241	0.74767728
ENSMUSG00000054383	Pnma1	-0.41944118	0.74771419
ENSMUSG00000026389	Steap3	-0.41924397	0.74781641

Ensembl Gene ID	Gene symbol	log2 FC TE	TE ratio
ENSMUSG00000068115	Ninl	-0.41911659	0.74788244
ENSMUSG00000051439	Cd14	-0.41856798	0.74816689
ENSMUSG00000022297	Fzd6	-0.41855529	0.74817347
ENSMUSG00000034617	Mtrr	-0.41778773	0.74857163
ENSMUSG00000024477	Pggt1b	-0.41744264	0.7487507
ENSMUSG00000032350	Gclc	-0.4173505	0.74879852
ENSMUSG00000031503	Col4a2	-0.4172642	0.74884332
ENSMUSG00000051427	Ccdc157	-0.41725388	0.74884867
ENSMUSG00000034903	Cobll1	-0.41705964	0.74894951
ENSMUSG00000035671	Zswim4	-0.41693745	0.74901294
ENSMUSG00000035151	Elmod2	-0.41690405	0.74903028
ENSMUSG00000019961	Tmpo	-0.41674685	0.7491119
ENSMUSG00000054770	Kctd18	-0.41647559	0.74925277
ENSMUSG00000032834	Pwp2	-0.41631652	0.74933538
ENSMUSG00000038010	Ccdc138	-0.41618802	0.74940213
ENSMUSG00000030757	Zkscan2	-0.4158249	0.74959077
ENSMUSG00000034738	Nostrin	-0.41576072	0.74962412
ENSMUSG00000024659	Anxa1	-0.41546327	0.74977869
ENSMUSG00000039738	Slx4	-0.41542059	0.74980087
ENSMUSG00000018412	Kansl1	-0.41540046	0.74981134
ENSMUSG00000026354	Lct	-0.41535895	0.74983291
ENSMUSG00000032750	Gab3	0.591126413	1.50642246
ENSMUSG00000023067	Cdkn1a	0.591983622	1.5073178
ENSMUSG00000101972	Hist1h3i	0.599934705	1.51564797
ENSMUSG00000039754	Alkbh4	0.606198985	1.52224332
ENSMUSG00000000693	Loxl3	0.615827294	1.5324365
ENSMUSG00000003545	Fosb	0.616586792	1.53324345
ENSMUSG00000037722	Gnpnat1	0.617368319	1.53407426
ENSMUSG00000052430	Bmpr1b	0.617821526	1.53455625
ENSMUSG00000026831	1700007K13Rik	0.625993062	1.54327275
ENSMUSG00000029878	Dbpht2	0.626392946	1.54370057
ENSMUSG00000046330	Rpl37a	0.628931076	1.54641879
ENSMUSG00000037805	Rpl10a	0.629131902	1.54663407
ENSMUSG00000040258	Nxph4	0.632254652	1.54998543
ENSMUSG00000049112	Oxtr	0.633192687	1.55099355
ENSMUSG00000026189	Pecr	0.635430009	1.55340069
ENSMUSG00000034401	Spata6	0.637216969	1.55532596
ENSMUSG00000105827	Hist2h2bb	0.642198334	1.5607055
ENSMUSG00000074218	Cox7a1	0.642734861	1.56128603
ENSMUSG00000077450	Rab11b	0.64686015	1.56575681
ENSMUSG00000020562	Efcab10	0.659365671	1.57938804
ENSMUSG00000043822	Adamtsl5	0.663525036	1.58394807
ENSMUSG00000068874	Selenbp1	0.664614389	1.58514453
ENSMUSG00000026495	Efcab2	0.666610385	1.58733913
ENSMUSG00000027401	Tgm3	0.669489387	1.59050994
ENSMUSG00000033318	Gstt2	0.670645157	1.59178464
ENSMUSG00000040219	Ttc12	0.681262718	1.60354264
ENSMUSG00000045471	Hcrt	0.70125423	1.6259177
ENSMUSG00000017404	Rpl19	0.701995909	1.62675378
ENSMUSG00000029084	Cd38	0.707178741	1.63260835
ENSMUSG00000031548	Sfrp1	0.711367757	1.63735569
ENSMUSG00000046834	Krt1	0.737289632	1.66704105
ENSMUSG00000047344	Lancl3	0.763175262	1.69722197
ENSMUSG00000043687	1190005I06Rik	0.783220776	1.7209686

Ensembl Gene ID	Gene symbol	log2 FC TE	TE ratio
ENSMUSG00000022820	Ndufb4	0.799833661	1.74090039
ENSMUSG00000109523	Gdf1	0.812670876	1.75646019
ENSMUSG00000020930	Ccdc103	0.840118796	1.79019755
ENSMUSG00000055799	Tcf7l1	0.840235323	1.79034215
ENSMUSG00000044287	Nrn1l	0.854734296	1.80842566
ENSMUSG00000003436	Dll3	0.878756324	1.83878949
ENSMUSG00000071553	Cpa2	0.881453289	1.84223012
ENSMUSG00000000263	Glra1	0.8942031	1.85858298
ENSMUSG00000062997	Rpl35	0.899020045	1.86479888
ENSMUSG00000047109	Cldn14	1.147332996	2.21504037
ENSMUSG00000062825	Actg1	1.157169955	2.23019515
ENSMUSG00000001504	Irx2	1.173836838	2.2561091
ENSMUSG00000006764	Tph2	1.667413227	3.17644541
ENSMUSG00000090862	Rps13	2.410211774	5.31552347
ENSMUSG00000039728	Slc6a5	3.321074023	9.99408178
ENSMUSG00000020838	Slc6a4	3.467887672	11.0646635

Appendix C

Table C.1 DTGs and associated statistics for shock

Ensembl gene ID	Gene symbol	$\log_2$ FC TE	p-value	TE ratio	FDR
ENSMUSG00000020673	Tpo	-3.617752	0.00065065		0.01736025
ENSMUSG00000051413	Plagl2	-2.18277	0.04154927	0.23021329	0.16465107
ENSMUSG00000073427	Gm4924	-2.0032794	0.01555409	0.25439324	0.10538542
ENSMUSG00000032089	Il10ra	-1.9468426	0.00685571	0.35674873	0.06637575
ENSMUSG00000054150	Syne3	-1.5833004	0.01570886	0.50039441	0.10538542
ENSMUSG00000021098	4930447C04Rik	-1.5441764	0.03879356	0.34545096	0.15814409
ENSMUSG00000037225	Fgf2	-1.5371617	0.04671031	0.35332057	0.177666
ENSMUSG00000037295	Ldlrap1	-1.5355105	0.01567658	0.43004305	0.10538542
ENSMUSG00000040270	Bach2	-1.4551975	0.01072688	0.39800847	0.08621983
ENSMUSG00000029563	Foxp2	-1.3571073	0.00355983	0.41147195	0.04832865
ENSMUSG00000032215	Rsl24d1	-1.2009474	0.02046833	0.56626841	0.11897913
ENSMUSG00000035184	Fam124a	-1.1717076	0.00081294	0.48754796	0.01923966
ENSMUSG00000031872	Bean1	-1.1381437	0.034472	0.46725977	0.15147108
ENSMUSG00000068617	Efcab1	-1.0623766	0.00874065	0.53236214	0.0752226
ENSMUSG00000030556	Lrrc28	-1.0515188	5.66E-06	0.50472929	0.00089131
ENSMUSG00000050315	Synpo2	-1.0500884	0.02076282	0.54320911	0.11897913
ENSMUSG00000032308	Ulk3	-1.019798	0.00780614	0.5089679	0.07096997
ENSMUSG00000037366	Pafah2	-0.9740293	0.04866577	0.52044997	0.17949452
ENSMUSG00000024856	Cdk2ap2	-0.9732957	0.00141833	0.55700624	0.02767031
ENSMUSG00000047044	D030056L22Rik	-0.9651352	0.02604158	0.51917536	0.13446927
ENSMUSG00000044468	Fam46c	-0.9578993	0.01412092	0.52531396	0.09942998
ENSMUSG00000046573	Lyrm4	-0.9565538	4.57E-06	0.52091653	0.00089131
ENSMUSG00000032381	Fam96a	-0.9440983	0.02943274	0.54034969	0.14405562
ENSMUSG00000021023	1110008L16Rik	-0.9372473	0.00225441	0.5551357	0.03624074
ENSMUSG00000029130	Rnf32	-0.9299234	0.0175606	0.53237818	0.1108269
ENSMUSG00000026110	Mgat4a	-0.9295378	6.28E-06	0.53844986	0.00089131
ENSMUSG00000020669	Sh3yl1	-0.9274534	0.03712627	0.52955239	0.15505678
ENSMUSG00000039831	Arhgap29	-0.9116953	0.00433148	0.54179241	0.05197781
ENSMUSG00000012422	Tmem167	-0.8988259	0.00134269	0.5522463	0.02723739
ENSMUSG00000027130	Slc12a6	-0.8709196	0.01811383	0.55358495	0.1121355
ENSMUSG00000045519	Zfp560	-0.8261663	0.01101141	0.57482165	0.08686779
ENSMUSG00000002205	Vrk3	-0.8251077	0.00431486	0.61470328	0.05197781
ENSMUSG00000008393	Carhsp1	-0.8205531	0.01495188	0.57806313	0.10441806
ENSMUSG00000036446	Lum	-0.8039762	0.01792261	0.57222883	0.1121355
ENSMUSG00000032038	St3gal4	-0.7908166	0.02461796	0.5903489	0.13158856
ENSMUSG00000055202	Zfp811	-0.7900755	0.03332178	0.58950033	0.14942186
ENSMUSG00000030110	Ret	-0.786577	0.01510014	0.64026865	0.10459611
ENSMUSG00000038146	Notch3	-0.7861747	0.03297079	0.63249489	0.14863022

Ensembl gene ID	Gene symbol	log_2 FC TE	p-value	TE ratio	FDR
ENSMUSG00000078713	Tomm5	-0.7831322	0.01068922	0.58783659	0.08621983
ENSMUSG00000033272	Slc35a4	-0.779016	0.02833641	0.59036152	0.14082934
ENSMUSG00000056258	Kcnq3	-0.7525845	2.21E-06	0.6055939	0.0006288
ENSMUSG00000047409	Ctdspl	-0.7482537	0.03608503	0.60893095	0.15372224
ENSMUSG00000015879	Fam184b	-0.7429586	0.02752422	0.60881486	0.13958712
ENSMUSG00000026227	2810459M11Rik	-0.7248579	0.03194453	0.60872213	0.14568411
ENSMUSG00000048915	Efna5	-0.7244378	0.03527671	0.623164	0.15147108
ENSMUSG00000022751	Nit2	-0.7211196	0.03091227	0.66587881	0.14405562
ENSMUSG00000047786	Lix1	-0.717511	0.00010908	0.6179273	0.00619581
ENSMUSG00000062376	Borcs7	-0.7057825	0.02023442	0.63943267	0.11897913
ENSMUSG00000031309	Rps6ka3	-0.7047946	0.00065203	0.63620767	0.01736025
ENSMUSG00000021366	Hivep1	-0.6971192	0.00953257	0.63459564	0.07885195
ENSMUSG00000030615	Tmem126a	-0.6930184	0.00513542	0.62708765	0.05833832
ENSMUSG00000026679	Enkur	-0.692925	0.04983858	0.63872508	0.18297718
ENSMUSG00000000711	Rab5b	-0.6894744	0.01293343	0.62918602	0.09418191
ENSMUSG00000037370	Enpp1	-0.687979	0.03220555	0.66120765	0.14595282
ENSMUSG00000026500	Cox20	-0.6841982	0.01617464	0.6313655	0.10600607
ENSMUSG00000002881	Nab1	-0.6772515	0.01977901	0.63273532	0.11897913
ENSMUSG00000036533	Cdc42ep3	-0.6664647	0.0171872	0.63949095	0.10927984
ENSMUSG00000033953	Ppp3r1	-0.6663489	1.75E-06	0.64156938	0.0006288
ENSMUSG00000028744	Pqlc2	-0.6586411	0.0486229	0.64429428	0.17949452
ENSMUSG00000033417	Cacul1	-0.6549375	0.00387554	0.67566281	0.0485582
ENSMUSG00000037936	Scarb1	-0.6523707	0.01529475	0.67503822	0.10508976
ENSMUSG00000047216	Cdh19	-0.651156	0.01849876	0.65033179	0.1133881
ENSMUSG00000064370	mt-Cytb	-0.6506543	0.00024832	0.64415663	0.00881531
ENSMUSG00000049764	Zfp280b	-0.6439039	0.04197443	0.65153427	0.1654864
ENSMUSG00000020309	Chac2	-0.6431582	0.03512668	0.67655243	0.15147108
ENSMUSG00000024027	Glp1r	-0.6406111	0.03450499	0.67087733	0.15147108
ENSMUSG00000064363	mt-Nd4	-0.640591	0.01261877	0.66377707	0.09268266
ENSMUSG00000042229	Rabif	-0.6393728	0.00081143	0.6548105	0.01923966
ENSMUSG00000051978	Erich1	-0.6376937	0.03047831	0.68942734	0.14405562
ENSMUSG00000061273	Mmgt1	-0.6346574	0.00167798	0.65686717	0.02978415
ENSMUSG00000028191	Bcl10	-0.6341577	0.03662462	0.65610899	0.15447612
ENSMUSG00000075486	Commd6	-0.6283082	0.00085725	0.65838497	0.01934394
ENSMUSG00000064345	mt-Nd2	-0.6272921	0.01927426	0.65141666	0.11729761
ENSMUSG00000051146	Camk2n2	-0.6246307	0.0003923	0.67004349	0.01336952
ENSMUSG00000038982	Bloc1s5	-0.6064126	0.02245804	0.66637914	0.12424839
ENSMUSG00000035849	Krt222	-0.6062158	0.00188432	0.66837378	0.03160118
ENSMUSG00000044148	1810030O07Rik	-0.6056433	0.00561813	0.66971098	0.0606913
ENSMUSG00000069806	Cacng7	-0.5938456	0.00086276	0.68394624	0.01934394
ENSMUSG00000036402	Gng12	-0.5922243	0.00641968	0.68384703	0.06522401
ENSMUSG00000028617	Lrrc42	0.59400178	0.01661087	1.6125374	0.10721565
ENSMUSG00000056895	Hist3h2ba	0.59904272	0.03373205	1.50274978	0.14968596
ENSMUSG00000001521	Tulp3	0.60111854	0.02836709	1.54893123	0.14082934
ENSMUSG00000071528	Usmg5	0.6040308	0.00147445	1.55125001	0.02791617
ENSMUSG00000035278	Plekhj1	0.61226875	0.00532611	1.56625885	0.05893305
ENSMUSG00000040860	Crocc	0.61277429	0.00830756	1.56648316	0.07372963
ENSMUSG00000024309	Pfdn6	0.61467579	0.00020373	1.55418422	0.00774337
ENSMUSG00000036833	Pnpla7	0.61596305	0.02527497	1.55027573	0.13292764
ENSMUSG00000028410	Dnaja1	0.61812326	0.00644679	1.56273056	0.06522401
ENSMUSG00000009927	Rps25	0.62171048	0.02843034	1.66582619	0.14082934
ENSMUSG00000026632	Tatdn3	0.62609318	0.04707898	1.57934177	0.17782411
ENSMUSG00000015542	Nat9	0.64299618	0.0386536	1.62718834	0.15814409
ENSMUSG00000054708	Ankrd24	0.64578255	0.03082994	1.63475686	0.14405562

Ensembl gene ID	Gene symbol	log_2 FC TE	p-value	TE ratio	FDR
ENSMUSG00000026034	Clk1	0.64603577	0.00257503	1.59072662	0.040557
ENSMUSG00000030137	Tuba8	0.64973291	0.03197527	1.6165548	0.14568411
ENSMUSG00000061207	Stk19	0.65069631	0.04214853	1.58106834	0.1654864
ENSMUSG00000042148	Cox10	0.65343713	0.02433272	1.61012014	0.13142668
ENSMUSG00000015023	Ddx19a	0.65938616	0.01659467	1.61611722	0.10721565
ENSMUSG00000026021	Sumo1	0.66396365	0.00142898	1.6082923	0.02767031
ENSMUSG00000037742	Eef1a1	0.67030322	8.05E-06	1.64397569	0.00096025
ENSMUSG00000022574	Naprt	0.67101792	0.04849349	1.62385835	0.17949452
ENSMUSG00000027422	Rrbp1	0.67292529	0.00056371	1.63300154	0.01600932
ENSMUSG00000027378	Nphp1	0.67426133	0.01212445	1.62609737	0.09171589
ENSMUSG00000001930	Vwf	0.67437614	0.0121642	1.62248573	0.09171589
ENSMUSG00000031883	Car7	0.67896616	0.03949733	1.62916744	0.15988383
ENSMUSG00000030450	Oca2	0.68477204	0.03872318	1.62504646	0.15814409
ENSMUSG00000087260	Lamtor5	0.71284256	0.02550933	1.69012805	0.13333712
ENSMUSG00000091405	Hist2h4	0.71329506	0.00078653	1.65093969	0.01923966
ENSMUSG00000090553	Snrpe	0.71456416	0.01993048	1.6927484	0.11897913
ENSMUSG00000062006	Rpl34	0.71468971	0.03027346	1.65156051	0.14405562
ENSMUSG00000015656	Hspa8	0.71760177	9.02E-06	1.72015384	0.00096025
ENSMUSG00000033862	Cdk10	0.73276132	0.02437255	1.67867211	0.13142668
ENSMUSG00000039105	Atp6v1g1	0.73601757	0.00650709	1.70252039	0.06522401
ENSMUSG00000035048	Anapc13	0.73749573	0.00402396	1.67803599	0.0496871
ENSMUSG00000026333	Gin1	0.73939504	0.01686042	1.69255101	0.10800813
ENSMUSG00000024732	Ccdc86	0.74152618	0.02074998	1.72500977	0.11897913
ENSMUSG00000025156	Gps1	0.74424141	0.03371138	1.76047601	0.14968596
ENSMUSG00000026566	Mpzl1	0.75609883	0.01232495	1.71004219	0.09211279
ENSMUSG00000021773	Comtd1	0.75611936	0.01395874	1.7081012	0.09910704
ENSMUSG00000064254	Ethe1	0.75761018	0.00938197	1.71461531	0.07836704
ENSMUSG00000071984	Fndc1	0.75963205	0.01023388	1.75081755	0.0838391
ENSMUSG00000057176	Ccdc189	0.77358362	0.04811423	1.72884506	0.17949452
ENSMUSG00000029404	Arl6ip4	0.77713972	0.003043	1.7465363	0.04394292
ENSMUSG00000024830	Rps6kb2	0.77990173	0.02006149	1.755864	0.11897913
ENSMUSG00000034889	Cactin	0.7902478	0.00916223	1.77930511	0.07806217
ENSMUSG00000063765	Chadl	0.80174978	0.0280156	1.73999549	0.14082934
ENSMUSG00000041841	Rpl37	0.80821511	0.03094152	1.80440507	0.14405562
ENSMUSG00000029049	Morn1	0.8205632	0.02511993	1.74786868	0.13292764
ENSMUSG00000031388	Naa10	0.83266197	0.00576628	1.81591707	0.0606913
ENSMUSG00000039759	Thap3	0.83680758	0.03006537	1.93170173	0.14405562
ENSMUSG00000107877	Gm43951	0.84120086	0.02571148	1.83771004	0.13357426
ENSMUSG00000020680	Taf15	0.85210051	0.00014912	1.83228886	0.00705854
ENSMUSG00000049751	Rpl36al	0.85416641	0.00761031	1.78998134	0.07047809
ENSMUSG00000046792	Zfp787	0.86653495	0.02433498	1.8547978	0.13142668
ENSMUSG00000035759	Bbs10	0.87001482	0.03537881	1.8626403	0.15147108
ENSMUSG00000016319	Slc25a5	0.91541154	4.63E-05	1.89544729	0.0031243
ENSMUSG00000031949	Adat1	0.92967721	0.02363369	1.92440378	0.12990906
ENSMUSG00000007440	Pcdha11	0.95759275	0.01323107	2.02601869	0.0955328
ENSMUSG00000024121	Atp6v0c	0.95821031	0.02114505	2.00106683	0.11897913
ENSMUSG00000039001	Rps21	0.96468231	0.00288818	1.99863995	0.04317071
ENSMUSG00000052374	Actn2	0.96516404	0.0073888	2.01726633	0.06917867
ENSMUSG00000060093	Hist1h4a	0.97581113	0.01387034	2.00438613	0.09910704
ENSMUSG00000023861	Mpc1	0.99888386	0.03649927	2.40328144	0.15447612
ENSMUSG00000101972	Hist1h3i	1.08260144	0.02098792	2.09073064	0.11897913
ENSMUSG00000061315	Naca	1.08458243	0.00054746	2.24893793	0.01600932
ENSMUSG00000039179	Tekt5	1.15989278	0.0067127	2.26667393	0.06578942
ENSMUSG00000045903	Npas4	1.18281207	0.00012239	2.39749099	0.0065172
ENSMUSG00000027360	Hdc	1.18411849	0.02033109	2.37196702	0.11897913

Ensembl gene ID	Gene symbol	log_2 FC TE	p-value	TE ratio	FDR
ENSMUSG00000037266	Rsrp1	1.47878496	2.05E-29	2.8414	1.75E-26

Table C.2 DTGs and associated statistics for CFC

Ensembl gene ID	Gene symbol	$\log_2$ FC TE	p-value	TE ratio	FDR
ENSMUSG00000023159	Psg29	-6.2262903	0.04314977		0.33053106
ENSMUSG00000020673	Tpo	-2.6698702	0.01313988		0.21023809
ENSMUSG00000020374	Rasgef1c	-1.7937871	0.00905926	0.40784678	0.19042474
ENSMUSG00000035067	Xkr6	-1.3580433	0.02787854	0.38663624	0.29544429
ENSMUSG00000035184	Fam124a	-1.2739209	0.00041743	0.4467533	0.06010944
ENSMUSG00000050315	Synpo2	-1.2616656	0.01040711	0.43876942	0.20388084
ENSMUSG00000062372	Otof	-1.2193356	0.03943895	0.40237731	0.32785138
ENSMUSG00000038146	Notch3	-1.1634471	0.00271277	0.46281779	0.14935555
ENSMUSG00000037936	Scarb1	-1.1575633	3.68E-05	0.46434005	0.01588077
ENSMUSG00000034771	Tle2	-1.1510067	0.00262339	0.45235485	0.14935555
ENSMUSG00000039153	Runx2	-1.0440489	0.00524099	0.49687474	0.14935555
ENSMUSG00000028848	Gpn2	-1.0434147	0.03984305	0.49159172	0.32785138
ENSMUSG00000020914	Top2a	-1.0221269	0.03894606	0.49434631	0.32785138
ENSMUSG00000110195	Pde2a	-1.0037565	0.00205896	0.49190571	0.1368415
ENSMUSG00000019803	Nr2e1	-0.9768454	0.00018071	0.50653333	0.03903355
ENSMUSG00000031149	Praf2	-0.944592	0.00412237	0.51355986	0.14935555
ENSMUSG00000005949	Ctns	-0.930225	0.00465958	0.56472696	0.14935555
ENSMUSG00000032308	Ulk3	-0.9028882	0.01308814	0.55116493	0.21023809
ENSMUSG00000002205	Vrk3	-0.8579277	0.00386162	0.58821709	0.14935555
ENSMUSG00000022194	Pabpn1	-0.8557817	0.02731306	0.51191315	0.29544429
ENSMUSG00000102206	Pcdha11	-0.8391648	0.04183974	0.55947664	0.33053106
ENSMUSG00000031196	F8	-0.8155063	0.04413383	0.57029624	0.33053106
ENSMUSG00000002983	Relb	-0.8078747	0.02232338	0.56403873	0.29427512
ENSMUSG00000022098	Bmp1	-0.7980051	0.00107759	0.57293311	0.11265356
ENSMUSG00000024170	Telo2	-0.7795944	0.00130882	0.57642471	0.1130817
ENSMUSG00000037370	Enpp1	-0.7789996	0.04248057	0.57454432	0.33053106
ENSMUSG00000036820	Amdhd2	-0.7787194	0.0310293	0.61384833	0.30203566
ENSMUSG00000039824	Myl6b	-0.7719903	0.04121707	0.59402877	0.33053106
ENSMUSG00000074405	Zfp865	-0.7499963	0.00535882	0.58866357	0.14935555
ENSMUSG00000050511	Oprd1	-0.7410161	0.0412376	0.59603504	0.33053106
ENSMUSG00000059552	Trp53	-0.7198707	0.00534075	0.60401998	0.14935555
ENSMUSG00000027777	Schip1	-0.719105	0.00727704	0.61849568	0.17464894
ENSMUSG00000039137	Whrn	-0.7141203	0.02230195	0.61139491	0.29427512
ENSMUSG00000009995	Taz	-0.7014611	0.0156908	0.6104483	0.23762621
ENSMUSG00000024856	Cdk2ap2	-0.6930992	0.02247935	0.66090056	0.29427512
ENSMUSG00000048796	Cyb561d1	-0.687836	0.03000744	0.60811184	0.2980049
ENSMUSG00000035545	Leng8	-0.6342135	0.00400717	0.62913505	0.14935555
ENSMUSG00000006456	Rbm14	-0.6059123	0.03434738	0.65280526	0.30315041
ENSMUSG00000015377	Dennd6b	-0.6039434	0.01194161	0.65619413	0.20836388
ENSMUSG00000045083	Lingo2	-0.5953069	0.01595176	0.65517079	0.23762621
ENSMUSG00000063145	Bbs5	-0.5935867	0.00874055	0.65937951	0.19042474
ENSMUSG00000032246	Calml4	0.5929731	0.0069313	1.50306992	0.17110413
ENSMUSG00000055963	Triqk	0.61054622	0.03970877	1.55178144	0.32785138
ENSMUSG00000043716	Rpl7	0.62930297	0.03302978	1.52133698	0.30203566
ENSMUSG00000035910	Dcdc2a	0.62962378	0.03448669	1.54437091	0.30315041
ENSMUSG00000021716	Srek1ip1	0.6312135	0.00535796	1.53310213	0.14935555
ENSMUSG00000026021	Sumo1	0.63370225	0.00408794	1.54638425	0.14935555
ENSMUSG00000022364	Tbc1d31	0.6355712	0.04950783	1.53370948	0.3368092
ENSMUSG00000031980	Agt	0.63675046	0.01080903	1.53348732	0.20388084
ENSMUSG00000034566	Atp5h	0.64287186	0.00321552	1.5300344	0.14935555
ENSMUSG00000029557	Mrm2	0.6571988	0.02797575	1.5811072	0.29544429
ENSMUSG00000067367	Lyar	0.67302048	0.02764616	1.58514745	0.29544429

Ensembl gene ID	Gene symbol	log_2 FC TE	p-value	TE ratio	FDR
ENSMUSG00000036834	Plch1	0.7014496	0.02600837	1.63446514	0.29544429
ENSMUSG00000046441	Cmtr2	0.70587952	0.04250671	1.63250538	0.33053106
ENSMUSG00000028494	Plin2	0.71050511	0.02859666	1.62390433	0.29544429
ENSMUSG00000038437	Mllt6	0.71231791	0.01104539	1.61622355	0.20388084
ENSMUSG00000039552	Rsph4a	0.72334493	0.04437686	1.60766841	0.33053106
ENSMUSG00000040822	1700123O20Rik	0.72812658	0.00421813	1.67119838	0.14935555
ENSMUSG00000021606	Ndufs6	0.72875632	0.00012245	1.64828477	0.03526589
ENSMUSG00000029249	Rest	0.73490282	0.02872317	1.63479067	0.29544429
ENSMUSG00000024079	Eif2ak2	0.74339196	0.02724764	1.69286567	0.29544429
ENSMUSG00000045903	Npas4	0.75355707	0.0272996	1.72899875	0.29544429
ENSMUSG00000046718	Bst2	0.76201549	0.02736035	1.7200181	0.29544429
ENSMUSG00000041323	Ak7	0.76313833	0.02939023	1.67239125	0.29544429
ENSMUSG00000043987	Cep164	0.77092752	0.03156144	1.70253154	0.30203566
ENSMUSG00000072949	Acot1	0.77889823	0.04790181	1.70107602	0.33568312
ENSMUSG00000026565	Pou2f1	0.79618469	0.04352108	1.72557913	0.33053106
ENSMUSG00000028081	Rps3a1	0.79847509	0.00445295	1.71919227	0.14935555
ENSMUSG00000036461	Elf1	0.84122584	0.0214233	1.77804324	0.29427512
ENSMUSG00000025362	Rps26	0.94136474	0.02514138	1.84422001	0.29544429
ENSMUSG00000008318	Relt	0.94902077	0.00589639	1.87695806	0.1543782
ENSMUSG00000025578	Cbx8	0.95431714	0.0019705	1.83535854	0.1368415
ENSMUSG00000041841	Rpl37	0.95676672	0.0121249	1.94834551	0.20836388
ENSMUSG00000040943	Tet2	0.96500141	0.00814702	1.95563148	0.19024383
ENSMUSG00000030922	Lyrm1	0.97865686	0.03277972	1.95528415	0.30203566
ENSMUSG00000055148	Klf2	1.00454628	0.04649168	1.98488657	0.33474011
ENSMUSG00000074698	Csnk2a1	1.00473079	0.03748036	1.95833871	0.32220766
ENSMUSG00000053093	Myh7	1.00948232	0.04856527	2.07118274	0.33568312
ENSMUSG00000037266	Rsrp1	1.02765508	9.16E-13	2.00781266	7.91E-10
ENSMUSG00000091537	Tma7	1.1904695	0.00117347	2.13697084	0.11265356
ENSMUSG00000026492	Tfb2m	1.2103635	0.04529655	2.33758378	0.33346643
ENSMUSG00000037752	Xkr8	1.89714576	0.00376591	3.27816031	0.14935555
ENSMUSG00000046364	Rpl27a	2.06672019	0.04554287	4.14587128	0.33346643

Table C.3 DEGs and associated statistics for shock

Ensembl gene ID	Gene symbol	avg homecage	avg shock only	Ratio	$\log_2$ ratio	z-score	p-value	FDR
ENSMUSG00000027517	Ankrd60	1.49664375	0.23947912	0.16001077	-2.6437591	-6.6500193	2.93E-11	5.20E-09
ENSMUSG00000093806	Asmt	1.01033582	0.34187436	0.33837696	-1.5632968	-3.5462711	0.00039072	0.00554828
ENSMUSG00000038717	Atp5l	35.914678	16.7166203	0.46545371	-1.1032904	-3.7032747	0.00021283	0.0037716
ENSMUSG00000044518	Foxe3	1.57081092	0.76040049	0.48408149	-1.0466782	-2.677272	0.00742243	0.03647709
ENSMUSG00000062372	Otof	13.4813528	6.98955113	0.51846066	-0.9476936	-3.5318664	0.00041264	0.00563409
ENSMUSG00000024186	Rgs11	1.85091642	1.01738083	0.5496633	-0.8633799	-2.4327989	0.01498262	0.05540449
ENSMUSG00000041378	Cldn5	157.420008	88.4131595	0.56163864	-0.8322859	-3.9549622	7.65E-05	0.00198987
ENSMUSG00000040860	Crocc	140.464883	79.8051198	0.56814998	-0.8156563	-4.6152754	3.93E-06	0.00019909
ENSMUSG00000099583	Hist1h3d	9.41283483	5.37115031	0.57061984	-0.8093982	-3.379154	0.00072709	0.00860393
ENSMUSG00000053552	Ebf4	7.71236419	4.73569083	0.6140388	-0.7035983	-3.5704569	0.00035636	0.00527114
ENSMUSG00000107877	Gm43951	2.22414848	1.38001061	0.62046694	-0.6885737	-2.2153922	0.02673316	0.07300209
ENSMUSG00000047810	Ccdc88b	5.5421786	3.49105462	0.62990655	-0.6667903	-2.7517177	0.00592836	0.03394465
ENSMUSG00000044349	Snhg11	34.7975302	21.9778378	0.63159189	-0.6629354	-3.1926644	0.00140967	0.01283158
ENSMUSG00000042401	Crtac1	5.50453985	3.47871741	0.63197243	-0.6620665	-2.7316082	0.0063026	0.03442192
ENSMUSG00000031503	Col4a2	77.5216481	49.1363982	0.63384099	-0.6578071	-2.686943	0.00721093	0.03647709
ENSMUSG00000022574	Naprt	0.49609978	0.315522	0.63600511	-0.6528897	-2.0343219	0.04191915	0.08946265
ENSMUSG00000011751	Sptbn4	236.632157	153.250671	0.64763248	-0.6267527	-3.3901441	0.00069856	0.00855133
ENSMUSG00000062997	Rpl35	9.75040704	6.38761913	0.65511307	-0.6101842	-2.6059276	0.00916258	0.03966728
ENSMUSG00000063511	Snrnp70	74.0454876	48.5708198	0.65595921	-0.608322	-2.5962689	0.00942423	0.04030844
ENSMUSG00000007440	Pcdha11	11.3017135	7.49656222	0.66331201	-0.5922405	-2.9100551	0.00361365	0.02467012
ENSMUSG00000034616	Ssh3	25.672315	17.0374487	0.66365066	-0.5915041	-2.8733269	0.00406174	0.02670216
ENSMUSG00000017778	Cox7c	6.6405394	4.41164852	0.66435093	-0.5899826	-2.6843384	0.00726735	0.03647709
ENSMUSG00000010607	Pigyl	5.31010356	3.53717668	0.66612198	-0.5861417	-2.408392	0.01602297	0.05851277
ENSMUSG00000031210	Gpr165	3.86833173	5.80739291	1.50126549	0.58617913	2.26958834	0.02323257	0.06820706
ENSMUSG00000020090	Npffr1	50.7177363	77.0022768	1.51825145	0.60241075	2.84631891	0.00442279	0.02803732
ENSMUSG00000090223	Pcp4	28.5947111	43.4659842	1.52007076	0.60413848	3.28420996	0.00102269	0.01037297
ENSMUSG00000025255	Zfhx4	13.4985978	20.6591504	1.53046641	0.61397138	2.27688288	0.02279322	0.06820706
ENSMUSG00000063354	Slc39a4	5.19827302	7.95892669	1.53107131	0.61454148	1.97824307	0.04790129	0.09582224
ENSMUSG00000046139	Patl1	10.6760897	16.3736851	1.53367811	0.61699572	2.02178171	0.04319891	0.09128341
ENSMUSG00000039081	Zfp503	39.8036376	61.3027805	1.5401301	0.62305223	2.99983662	0.00270124	0.02130982

Ensembl gene ID	Gene symbol	avg homecage	avg shock only	Ratio	$\log_2$ ratio	z-score	p-value	FDR
ENSMUSG00000030110	Ret	10.0424186	15.477451	1.54120752	0.62406113	2.84634365	0.00442244	0.02803732
ENSMUSG00000038370	Pcp4l1	16.1424197	25.0259313	1.55032094	0.63256691	2.93273266	0.00335993	0.02338775
ENSMUSG00000026238	Ptma	131.424943	204.861134	1.55876905	0.64040719	3.10831002	0.00188161	0.01629195
ENSMUSG00000031283	Chrdl1	62.6560143	97.9777014	1.56373977	0.64500045	2.94022581	0.00327973	0.02338775
ENSMUSG00000028753	Vwa5b1	95.1576922	149.459452	1.57065024	0.65136195	3.21263398	0.00131524	0.01261917
ENSMUSG00000031075	Ano1	0.90791943	1.42638571	1.57104876	0.65172796	2.13008639	0.03316448	0.08057244
ENSMUSG00000022512	Cldn1	3.77150996	5.95309032	1.57843686	0.65849655	2.55915974	0.01049255	0.04331228
ENSMUSG00000020309	Chac2	4.54258845	7.1705697	1.57852066	0.65857314	2.46168447	0.01382863	0.05167539
ENSMUSG00000029563	Foxp2	11.5087406	18.1771823	1.5794241	0.65939861	2.96315489	0.00304503	0.02299972
ENSMUSG00000031367	Ap1s2	67.7122346	108.191195	1.59780867	0.67609466	3.77254488	0.00016159	0.0035853
ENSMUSG00000047996	Prrg1	13.7924964	22.0641881	1.59972404	0.67782305	3.21745231	0.00129335	0.01261917
ENSMUSG00000056870	Gulp1	1.68901227	2.71182677	1.60556961	0.68308522	2.10727743	0.03509354	0.0828723
ENSMUSG00000021848	Otx2	107.840678	174.228004	1.6156056	0.69207506	3.59738956	0.00032143	0.00496115
ENSMUSG00000019970	Sgk1	23.5282022	38.3367071	1.62939381	0.70433533	3.17558968	0.00149532	0.01327099
ENSMUSG00000034936	Arl4d	0.6553064	1.07337946	1.63798103	0.71191865	2.28696831	0.02219767	0.06820706
ENSMUSG00000019851	Perp	5.80677399	9.55023934	1.64467213	0.71780001	3.3052493	0.00094892	0.01032045
ENSMUSG00000017057	Il13ra1	14.9703798	24.7081547	1.65046946	0.72287644	3.19382125	0.00140403	0.01283158
ENSMUSG00000022820	Ndufb4	0.93243649	1.55272882	1.66523817	0.73572853	2.35946553	0.01830128	0.06269025
ENSMUSG00000052837	Junb	433.155423	729.167595	1.68338559	0.75136567	4.6598278	3.16E-06	0.00018725
ENSMUSG00000032501	Trib1	1.05467075	1.78016992	1.68789162	0.75522227	1.97400144	0.04838158	0.09595229
ENSMUSG00000031355	Arhgap6	2.14815384	3.62658903	1.68823525	0.75551595	2.21672528	0.02664187	0.07300209
ENSMUSG00000024190	Dusp1	37.4516559	63.8238561	1.70416647	0.76906627	3.70013324	0.00021549	0.0037716
ENSMUSG00000064341	mt-Nd1	926.522007	1582.75367	1.70827423	0.77253959	3.87515744	0.00010656	0.00252182
ENSMUSG00000064367	mt-Nd5	1.33521829	2.28201621	1.70909598	0.77323342	2.66510411	0.00769645	0.03647709
ENSMUSG00000005268	Prlr	25.9219824	44.4368308	1.7142528	0.77757988	3.72619466	0.00019439	0.0037716
ENSMUSG00000068859	Sp9	0.61767726	1.0767462	1.74321812	0.8017531	2.39187097	0.01676273	0.06010879
ENSMUSG00000036972	Zic4	0.73692849	1.29039831	1.75104956	0.80821992	2.10703174	0.03511483	0.0828723
ENSMUSG00000059743	Fdps	7.19574324	12.7739814	1.77521362	0.82799264	3.01295989	0.00258713	0.02087344
ENSMUSG00000032511	Scn5a	28.6335433	51.3545769	1.79351107	0.84278665	3.65660931	0.00025557	0.00412403
ENSMUSG00000064370	mt-Cytb	190.09145	343.133366	1.80509627	0.85207578	4.11139443	3.93E-05	0.00116344
ENSMUSG00000047139	Cd24a	2.21339159	4.01386059	1.8134435	0.8587318	2.61505909	0.0089212	0.0390991
ENSMUSG00000047507	Baiap3	3.0149701	5.48296946	1.8185817	0.86281374	2.82587288	0.0047152	0.02892511
ENSMUSG00000064351	mt-Co1	933.694228	1705.43175	1.82654203	0.86911495	4.35467132	1.33E-05	0.00052566

Ensembl gene ID	Gene symbol	avg homecage	avg shock only	Ratio	log_2 ratio	z-score	p-value	FDR
ENSMUSG00000020423	Btg2	2.49491306	4.63852832	1.85919438	0.89467761	2.97164056	0.00296213	0.02285994
ENSMUSG00000090698	Apold1	0.7744406	1.44187805	1.86183168	0.89672265	2.35816368	0.01836559	0.06269025
ENSMUSG00000048562	Sp8	12.1227452	22.9191345	1.89058947	0.91883613	3.40551695	0.00066039	0.00837279
ENSMUSG00000061524	Zic2	69.4077063	133.923502	1.9295192	0.9482414	4.27400596	1.92E-05	0.00068157
ENSMUSG00000064363	mt-Nd4	345.862782	679.629295	1.96502582	0.97454827	5.15130002	2.59E-07	2.11E-05
ENSMUSG00000024027	Glp1r	0.29817512	0.5896959	1.97768313	0.98381129	2.51299719	0.01197103	0.04721906
ENSMUSG00000071341	Egr4	1.15099253	2.28099184	1.98176077	0.98678282	4.16063072	3.17E-05	0.00102424
ENSMUSG00000022602	Arc	1.46946269	2.94568817	2.00460222	1.00331598	3.35110615	0.00080489	0.00921734
ENSMUSG00000064345	mt-Nd2	53.6028366	108.157711	2.01776097	1.01275528	4.42941377	9.45E-06	0.0004193
ENSMUSG00000087075	A230065H16Rik	0.48402078	0.97849119	2.02158919	1.01548985	2.73421869	0.00625285	0.03442192
ENSMUSG00000040856	Dlk1	0.55688563	1.15966616	2.08241349	1.05825656	3.29379739	0.00098844	0.01032045
ENSMUSG00000055214	Pld5	0.30508892	0.63644532	2.08609776	1.06080677	3.02148839	0.00251535	0.02076629
ENSMUSG00000028195	Cyr61	0.24070864	0.50268973	2.08837424	1.06238027	2.31162891	0.02079814	0.06592268
ENSMUSG00000023034	Nr4a1	0.98093302	2.05548297	2.09543663	1.06725089	2.63437526	0.00842923	0.0374047
ENSMUSG00000050299	Gm9843	2.45299085	5.16400362	2.10518666	1.07394816	3.47731728	0.00050646	0.00665899
ENSMUSG00000026247	Ecel1	0.17973225	0.37985026	2.11342299	1.07958155	2.21677903	0.0266382	0.07300209
ENSMUSG00000032368	Zic1	2.366102	5.06985595	2.14270388	1.09943249	3.69130226	0.00022311	0.0037716
ENSMUSG00000038418	Egr1	4.25003835	9.22772069	2.17120881	1.11849848	3.94901453	7.85E-05	0.00198987
ENSMUSG00000003545	Fosb	2.69346479	5.92444158	2.19956155	1.13721597	3.73832794	0.00018525	0.0037716
ENSMUSG00000074170	Plekhf1	0.10278278	0.23664957	2.3024243	1.20315373	1.9812484	0.04756342	0.09582224
ENSMUSG00000067860	Zic3	6.64228216	15.6636712	2.35817613	1.23767147	5.12523192	2.97E-07	2.11E-05
ENSMUSG00000021250	Fos	0.305344	1.2605271	4.12821962	2.04551973	5.43010252	5.63E-08	6.66E-06
ENSMUSG00000037868	Egr2	5.53068308	31.0999154	5.62315991	2.49138108	7.89339885	2.94E-15	1.04E-12

Table C.4 DEGs and associated statistics for CFC

Ensembl gene ID	Gene symbol	avg homecage	avg training	Ratio	$\log_2$ ratio	z-score	p-value	FDR
ENSMUSG00000021032	Ngb	0.782748286	0.2778284	0.35493965	-1.49435436	-3.6721712	0.0002405	0.00328109
ENSMUSG00000038112	AW551984	1.51547842	0.562119738	0.370919	-1.43082393	-3.8920235	9.94E-05	0.00180834
ENSMUSG00000038760	Trhr	6.065528811	2.32303721	0.38299005	-1.38462117	-5.8064514	6.38E-09	1.22E-06
ENSMUSG00000069372	Ctxn3	0.4359629	0.173890339	0.39886499	-1.32602759	-3.0263385	0.00247535	0.01331808
ENSMUSG00000040856	Dlk1	0.556885635	0.229380666	0.41189905	-1.27963728	-2.6457173	0.00815179	0.02994215
ENSMUSG00000026247	Ecel1	0.179732245	0.076368514	0.42490158	-1.2347994	-2.0712851	0.03833216	0.08464096
ENSMUSG00000087075	A230065H16Rik	0.484020785	0.208731023	0.43124393	-1.21342396	-2.7008845	0.00691554	0.02723438
ENSMUSG00000029335	Bmp3	30.02193101	13.62200447	0.45373512	-1.14007776	-3.8523902	0.00011697	0.00186178
ENSMUSG00000068696	Gpr88	1.575073617	0.742490135	0.47140027	-1.0849755	-3.2873842	0.00101123	0.0085842
ENSMUSG00000093806	Asmt	1.01033582	0.483121465	0.47817909	-1.06437704	-3.6244902	0.00028953	0.00371459
ENSMUSG00000067578	Cbln4	6.241854498	3.145795655	0.50398414	-0.98854977	-2.2988515	0.02151337	0.05912308
ENSMUSG00000027517	Ankrd60	1.496643745	0.756167574	0.5052422	-0.98495296	-2.5089918	0.01210763	0.04021839
ENSMUSG00000003657	Calb2	7.033694085	3.667154674	0.52136966	-0.93962147	-2.8967169	0.0037709	0.01714861
ENSMUSG00000048562	Sp8	12.12274523	6.498355198	0.5360465	-0.89956993	-3.5398091	0.00040042	0.00439677
ENSMUSG00000048281	Dleu7	26.72191967	14.35215272	0.53709288	-0.89675651	-3.7007024	0.000215	0.0030419
ENSMUSG00000031355	Arhgap6	2.148153838	1.163179371	0.54147862	-0.88502373	-2.5992361	0.00934315	0.03244621
ENSMUSG00000005087	Cd44	2.690689824	1.457604734	0.54172158	-0.88437654	-2.0964508	0.03604222	0.08299575
ENSMUSG00000032511	Scn5a	28.63354328	15.73813322	0.54963974	-0.86344178	-3.8773367	0.00010561	0.00183371
ENSMUSG00000047507	Baiap3	3.014970103	1.677551537	0.55640735	-0.84578661	-2.8024646	0.00507138	0.02176704
ENSMUSG00000038115	Ano2	2.68012537	1.493625335	0.55729682	-0.84348218	-2.0039095	0.04507976	0.09139334
ENSMUSG00000009376	Met	1.800710349	1.046629089	0.58123123	-0.78281588	-2.1991073	0.02787029	0.07050631
ENSMUSG00000020374	Rasgef1c	8.765642666	5.153544904	0.58792551	-0.76629473	-2.4604226	0.01387735	0.04492497
ENSMUSG00000061702	Tmem91	16.70702554	9.880666258	0.59140786	-0.75777467	-3.2036022	0.0013572	0.01016568
ENSMUSG00000040536	Necab1	39.16523212	23.18330115	0.59193575	-0.7564875	-3.6067425	0.00031007	0.0038208
ENSMUSG00000031654	Cbln1	9.548563555	5.691781742	0.59608775	-0.74640338	-3.0174229	0.00254934	0.01352566
ENSMUSG00000047261	Gap43	996.4855721	597.3235347	0.59943019	-0.73833635	-4.4542706	8.42E-06	0.00035729
ENSMUSG00000026479	Lamc2	9.399754729	5.664252607	0.60259579	-0.73073751	-2.9571769	0.0031047	0.0156052
ENSMUSG00000046719	Nxph3	56.61535104	34.49324016	0.60925596	-0.71487963	-3.05944	0.00221751	0.01228032
ENSMUSG00000048001	Hes5	7.638948519	4.680107328	0.61266381	-0.70683245	-2.0534201	0.04003185	0.08496606
ENSMUSG00000066705	Fxyd6	12.1071616	7.488715098	0.61853598	-0.69307057	-2.6647639	0.00770424	0.02967152
ENSMUSG00000022372	Sla	46.34881766	28.87760682	0.62304948	-0.68258135	-3.129197	0.00175285	0.01121833

Ensembl gene ID	Gene symbol	avg homecage	avg training	Ratio	log_2 ratio	z-score	p-value	FDR
ENSMUSG00000029334	Prkg2	26.194891	16.34498599	0.6239761	-0.68043732	-2.2911547	0.02195447	0.05947948
ENSMUSG00000024517	Grp	76.0322018	47.48392643	0.62452389	-0.67917133	-3.2653568	0.00109326	0.00870757
ENSMUSG00000067786	Nnat	483.1917315	302.1689785	0.62536041	-0.67724021	-4.0370359	5.41E-05	0.00114878
ENSMUSG00000004791	Pgf	36.85877997	23.26440822	0.63117684	-0.66388383	-2.9359814	0.00332494	0.0158766
ENSMUSG00000040016	Ptger3	58.4357897	36.91841246	0.63177742	-0.66251172	-3.0723659	0.00212369	0.01210822
ENSMUSG00000062151	Unc13c	59.50314642	37.67928717	0.63323184	-0.65919429	-3.1532234	0.00161478	0.01120828
ENSMUSG00000036834	Plch1	30.73841034	19.5483629	0.63595881	-0.65299476	-2.9530075	0.00314694	0.01561211
ENSMUSG00000021278	Amn	7.266728708	4.636661094	0.63806718	-0.64821977	-2.6520611	0.00800021	0.02994215
ENSMUSG00000036699	Zcchc12	246.2857432	157.3149449	0.6387497	-0.64667738	-3.1969217	0.00138903	0.010204
ENSMUSG00000039395	Mreg	5.313859787	3.400234908	0.63988043	-0.64412574	-2.1540539	0.03123595	0.07648803
ENSMUSG00000022235	Cmbl	54.26609654	34.96480159	0.64432129	-0.63414782	-2.6564886	0.00789591	0.02986374
ENSMUSG00000031980	Agt	8.10551771	5.223145891	0.64439387	-0.63398533	-2.1155135	0.0343862	0.08209706
ENSMUSG00000034295	Fhod3	253.1996424	163.6056899	0.64615293	-0.63005244	-3.1161826	0.00183209	0.01128803
ENSMUSG00000036815	Dpp10	208.1715667	135.1692886	0.64931677	-0.62300563	-3.1265462	0.00176873	0.01121833
ENSMUSG00000032368	Zic1	2.366102003	1.539599737	0.65069035	-0.61995694	-2.0362206	0.04172821	0.08710478
ENSMUSG00000051920	Rspo2	35.55954745	23.15114562	0.65105288	-0.61915338	-2.8565028	0.00428336	0.01880741
ENSMUSG00000094500	Smim18	95.7121494	62.33547908	0.65128074	-0.61864854	-3.0943722	0.0019723	0.01159105
ENSMUSG00000033585	Ndn	559.1080731	364.6194424	0.65214484	-0.61673569	-3.1806806	0.0014693	0.0103939
ENSMUSG00000053004	Hrh1	0.783079977	0.511759475	0.65352134	-0.61369375	-2.0580172	0.03958848	0.08496606
ENSMUSG00000034379	Wdr5b	2.330847796	1.526146323	0.65476018	-0.61096151	-2.0094596	0.04448841	0.09088007
ENSMUSG00000032492	Pth1r	46.22961104	30.42080972	0.65803733	-0.60375867	-2.940739	0.0032743	0.0158766
ENSMUSG00000052565	Hist1h1d	188.4895938	124.4199607	0.66008928	-0.59926692	-3.2708502	0.00107225	0.00870757
ENSMUSG00000053819	Camk2d	55.84294016	36.8657198	0.66016796	-0.59909498	-2.7641295	0.00570749	0.02319426
ENSMUSG00000046321	Hs3st2	3.906219464	2.587358663	0.662369	-0.59429295	-2.3799927	0.01731298	0.0511927
ENSMUSG00000042115	Klhdc8a	107.9327593	71.76999127	0.66495095	-0.58868016	-2.6259735	0.00864015	0.0304395
ENSMUSG00000035493	Tgfbi	2.07022	3.109148301	1.50184439	0.586735343	2.08085552	0.03744713	0.08464096
ENSMUSG00000055235	Wdr86	20.97252523	31.4980741	1.50187322	0.586763038	2.09580292	0.03609968	0.08299575
ENSMUSG00000024610	Cd74	5.598566216	8.408566823	1.50191433	0.586802522	2.06448486	0.03897177	0.08496606
ENSMUSG00000005501	Usp40	18.05667729	27.12209918	1.50205371	0.586936405	2.67081757	0.00756668	0.02949459
ENSMUSG00000034156	Bzrap1	50.00183934	75.13361302	1.50261698	0.587477314	2.6369664	0.00836511	0.03014597
ENSMUSG00000033705	Stard9	344.9074859	519.5766564	1.50642325	0.591127173	3.04018193	0.00236435	0.01290261
ENSMUSG00000042625	Safb2	74.19308585	111.8979224	1.50819879	0.592826599	2.78425959	0.00536501	0.02251503

Ensembl gene ID	Gene symbol	avg homecage	avg training	Ratio	log_2 ratio	z-score	p-value	FDR
ENSMUSG00000032849	Abcc4	2.192947045	3.311987092	1.5102905	0.594826076	2.45189326	0.01421068	0.04523733
ENSMUSG00000048546	Tob2	43.02829964	65.3923302	1.51975167	0.603835603	3.1059172	0.0018969	0.01150183
ENSMUSG00000038930	Rccd1	57.23699816	87.00496357	1.52008258	0.604149697	3.14465917	0.0016628	0.01120828
ENSMUSG00000033855	Ston1	9.084255774	13.81863327	1.52116295	0.605174701	2.02144668	0.04323355	0.0897566
ENSMUSG00000027284	Cdan1	13.91739029	21.21223501	1.52415321	0.608007927	2.79551355	0.00518173	0.02199358
ENSMUSG00000028248	Pnisr	32.74671103	49.98341302	1.52636437	0.610099402	3.07867731	0.00207922	0.01203426
ENSMUSG00000023473	Celsr3	4.382292431	6.703422861	1.52966124	0.613212185	2.66201618	0.00776741	0.02967152
ENSMUSG00000023191	P3h3	89.31349665	136.7613112	1.53125022	0.614710049	3.81554095	0.00013588	0.00207632
ENSMUSG00000038593	Tctn1	20.10023149	30.80662269	1.53265014	0.616028413	2.777291	0.00548141	0.02251503
ENSMUSG00000029068	Ccnl2	233.7536395	358.7315405	1.53465649	0.617915768	3.01308153	0.00258609	0.01353271
ENSMUSG00000014158	Trpv4	2.839459103	4.364402447	1.53705417	0.620168008	2.38969869	0.0168622	0.05071937
ENSMUSG00000026814	Eng	5.121634811	7.876642627	1.53791571	0.620976433	2.92252938	0.00347201	0.01617448
ENSMUSG00000005268	Prlr	25.9219824	40.09086562	1.54659721	0.629097515	2.93894521	0.00329331	0.0158766
ENSMUSG00000068323	Slc4a5	6.404611309	9.913435165	1.54785899	0.630274044	2.88306654	0.00393824	0.01769892
ENSMUSG00000028957	Per3	356.3002217	552.2048168	1.54983012	0.632110091	3.12279758	0.00179141	0.01121833
ENSMUSG00000041354	Rgl2	63.65744837	98.74046463	1.55112194	0.633312104	3.8647742	0.00011119	0.00184675
ENSMUSG00000020423	Btg2	2.494913057	3.874747914	1.5530593	0.635112913	2.75311375	0.00590314	0.02373683
ENSMUSG00000031503	Col4a2	77.52164815	120.5752024	1.5553746	0.637262083	3.62254258	0.00029172	0.00371459
ENSMUSG00000032855	Pkd1	104.3803804	162.5085925	1.5568883	0.638665437	3.45004394	0.0005605	0.00563445
ENSMUSG00000027829	Ccnl1	7.765478458	12.09409082	1.55741734	0.639155597	2.9181684	0.00352094	0.01620481
ENSMUSG00000059851	Kmt5c	42.06143198	65.89005511	1.56651954	0.647562766	3.33074651	0.00086613	0.00777276
ENSMUSG00000030592	Ryr1	29.37778526	46.02489065	1.56665624	0.647688656	3.05935074	0.00221817	0.01228032
ENSMUSG00000073434	Wdr90	0.320712893	0.502773856	1.56767584	0.648627277	2.00261926	0.04521817	0.09139334
ENSMUSG00000079436	Kcnj13	220.6601059	346.7991576	1.57164412	0.652274572	3.36592194	0.00076288	0.00710784
ENSMUSG00000015377	Dennd6b	2.953217669	4.651453708	1.57504601	0.655393974	2.62418673	0.00868562	0.0304395
ENSMUSG00000019970	Sgk1	23.52820225	37.09899905	1.57678851	0.656989172	2.98123593	0.00287088	0.01462232
ENSMUSG00000020385	Clk4	37.30154619	58.92253056	1.57962703	0.659583958	3.53821296	0.00040285	0.00439677
ENSMUSG00000058145	Adamts17	0.946481949	1.495967242	1.58055549	0.660431688	2.07764831	0.03774176	0.08464096
ENSMUSG00000025138	Sirt7	192.3437087	304.0127772	1.58057042	0.660445317	4.37179603	1.23E-05	0.00042243
ENSMUSG00000029127	Zbtb49	3.189796531	5.047956262	1.58253237	0.662235009	2.04023279	0.04132715	0.08674159
ENSMUSG00000044349	Snhg11	34.7975302	55.13057276	1.5843243	0.663867677	2.85188193	0.00434612	0.01886613
ENSMUSG00000020941	Map3k14	1.063161512	1.691831194	1.59132096	0.670224845	2.29224649	0.02189142	0.05947948
ENSMUSG00000071337	Tia1	5.924202657	9.439536297	1.59338511	0.672094997	2.62738942	0.00860428	0.0304395

Ensembl gene ID	Gene symbol	avg homecage	avg training	Ratio	log_2 ratio	z-score	p-value	FDR
ENSMUSG00000031706	Rfx1	2.610973525	4.169732725	1.59700307	0.675367083	2.40434228	0.0162016	0.04951208
ENSMUSG00000040511	Pvr	6.136652881	9.839262899	1.60335986	0.681098261	2.78016443	0.00543314	0.02251503
ENSMUSG00000029439	Sfswap	16.14710775	25.95365791	1.60732549	0.684662112	2.27492541	0.0229104	0.06120122
ENSMUSG00000052861	Dnah6	82.00214196	132.6706861	1.61789294	0.69411614	4.2345912	2.29E-05	0.00062476
ENSMUSG00000089922	Gm43517	15.29341008	25.09015242	1.64058587	0.714211105	2.87539167	0.00403527	0.01792409
ENSMUSG00000028763	Hspg2	47.85038465	78.54017725	1.64136982	0.714900332	3.23073155	0.00123474	0.00962592
ENSMUSG00000029381	Shroom3	6.704322964	11.02616394	1.64463496	0.717767403	3.14073587	0.00168524	0.01120828
ENSMUSG00000025350	Rdh5	1.405905331	2.318345548	1.64900545	0.721596164	3.31579799	0.00091382	0.00793361
ENSMUSG00000039153	Runx2	3.217503399	5.328332892	1.65604577	0.727742546	2.11639685	0.03431107	0.08209706
ENSMUSG00000041187	Prkd2	0.771817271	1.282715732	1.66194225	0.732870252	2.07321074	0.03815267	0.08464096
ENSMUSG00000056763	Cspp1	0.835204598	1.393748636	1.66875115	0.738768834	2.09396304	0.03626327	0.08299575
ENSMUSG00000052512	Nav2	3.128992055	5.234252925	1.67282397	0.742285643	2.30772726	0.02101431	0.058768
ENSMUSG00000041144	Dnah7b	0.529893159	0.887943771	1.6757034	0.744766818	1.97289674	0.04850733	0.09650937
ENSMUSG00000028047	Thbs3	1.218580994	2.045807234	1.67884387	0.747468069	2.01452816	0.04395411	0.0907593
ENSMUSG00000052837	Junb	433.1554228	728.3868341	1.68158309	0.749820066	4.46226829	8.11E-06	0.00035729
ENSMUSG00000032501	Trib1	1.054670754	1.776956102	1.68484439	0.752615351	2.33205939	0.01969757	0.05573682
ENSMUSG00000015647	Lama5	4.584559458	7.729075581	1.68589276	0.753512766	2.23683947	0.02529683	0.06529318
ENSMUSG00000006958	Chrd	17.1193027	28.95180051	1.69117873	0.758029133	3.49596207	0.00047236	0.00501222
ENSMUSG00000035576	L3mbtl1	0.759669994	1.296734792	1.70697119	0.771438707	2.19140395	0.02842257	0.07096355
ENSMUSG00000020836	Coro6	8.821442132	15.05876431	1.70706378	0.771516958	4.10268149	4.08E-05	0.00104003
ENSMUSG00000048794	Cfap100	0.774602743	1.325411891	1.71108598	0.774912252	2.20204864	0.02766187	0.07044557
ENSMUSG00000031502	Col4a1	9.856235399	16.88684995	1.71331642	0.776791617	3.45834051	0.00054351	0.00561141
ENSMUSG00000033327	Tnxb	6.808812797	11.69274881	1.71729627	0.780138956	3.21105382	0.00132249	0.01010384
ENSMUSG00000070427	Il18bp	3.595135513	6.190396587	1.72188129	0.783985686	2.48629116	0.01290823	0.04250814
ENSMUSG00000063354	Slc39a4	5.198273025	8.955794973	1.72284044	0.784789091	2.30386317	0.02123033	0.058768
ENSMUSG00000002625	Akap8l	456.6289068	787.3255365	1.72421309	0.78593808	4.06197402	4.87E-05	0.00114878
ENSMUSG00000032586	Traip	3.707352128	6.405615817	1.72781424	0.788948124	2.59058242	0.00958137	0.03297372
ENSMUSG00000038418	Egr1	4.250038353	7.343624599	1.72789608	0.789016451	3.1813051	0.00146613	0.0103939
ENSMUSG00000030276	Ttll3	50.28969808	87.1205777	1.73237424	0.792750629	2.14767344	0.03173971	0.07722655
ENSMUSG00000024830	Rps6kb2	0.478200941	0.835814956	1.7478321	0.805566605	2.40082794	0.01635803	0.04959338
ENSMUSG00000043410	Hfm1	6.62164512	11.6139518	1.75393752	0.810597353	3.09912075	0.00194096	0.0115851
ENSMUSG00000003545	Fosb	2.693464791	4.740574694	1.76002846	0.81559876	3.40166652	0.00066976	0.00656024
ENSMUSG00000024190	Dusp1	37.45165594	66.55210757	1.77701375	0.829454844	4.35560209	1.33E-05	0.00042243

Ensembl gene ID	Gene symbol	avg homecage	avg training	Ratio	$\log_2$ ratio	z-score	p-value	FDR
ENSMUSG00000059854	Hydin	4.128448162	7.369529548	1.78506045	0.835972934	3.36793339	0.00075734	0.00710784
ENSMUSG00000031167	Rbm3	13.97432283	25.08422097	1.79502229	0.844001759	2.92418674	0.00345357	0.01617448
ENSMUSG00000071341	Egr4	1.150992528	2.096561504	1.82152486	0.865146685	2.36901302	0.01783563	0.05200923
ENSMUSG00000030409	Dmpk	18.84626508	35.73936186	1.89636311	0.923235234	3.32792811	0.00087494	0.00777276
ENSMUSG00000031328	Flna	101.9779363	194.001863	1.90239056	0.927813458	4.85814703	1.18E-06	7.54E-05
ENSMUSG00000051747	Ttn	1.453788245	2.770222406	1.90551988	0.930184662	2.00978658	0.04445378	0.09088007
ENSMUSG00000072647	Adam1a	3.912717894	7.506229101	1.91841817	0.939917228	4.00776188	6.13E-05	0.00123239
ENSMUSG00000026034	Clk1	221.0027775	428.2025458	1.93754373	0.954228872	5.32925211	9.86E-08	9.42E-06
ENSMUSG00000024299	Adamts10	17.76723154	34.426315	1.93762967	0.954292862	4.3047306	1.67E-05	0.00049128
ENSMUSG00000025409	Mbd6	1.123160897	2.1992787	1.95811545	0.969465825	2.64194039	0.00824326	0.02998975
ENSMUSG00000002227	Mov10	1.368932741	2.687016226	1.96285482	0.972953468	2.70261398	0.00687966	0.02723438
ENSMUSG00000080316	Spaca6	5.542247347	10.89687214	1.96614685	0.975371076	3.97378457	7.07E-05	0.00135113
ENSMUSG00000047021	Ccdc108	3.241822942	6.384717175	1.96948362	0.977817416	3.57600209	0.00034889	0.00403865
ENSMUSG00000043923	Ccdc84	1.92089804	3.792230858	1.97419685	0.981265849	4.04159736	5.31E-05	0.00114878
ENSMUSG00000048602	Morc2b	2.298919927	4.953067749	2.15451947	1.107366138	3.26512821	0.00109415	0.00870757
ENSMUSG00000040441	Slc26a10	0.173006127	0.377855091	2.18405612	1.12700993	2.05569115	0.0398123	0.08496606
ENSMUSG00000095041	AC149090.1	8.26293972	18.43677813	2.23126136	1.157859515	4.67891717	2.88E-06	0.00015738
ENSMUSG00000023034	Nr4a1	0.980933015	2.217213156	2.26031046	1.176520946	3.13787397	0.00170178	0.01120828
ENSMUSG00000074170	Plekhf1	0.102782781	0.238562906	2.32103962	1.214771147	2.5289895	0.01143914	0.03867038
ENSMUSG00000022602	Arc	1.469462691	3.431101616	2.33493619	1.223383124	3.78189407	0.00015564	0.0022867
ENSMUSG00000035545	Leng8	35.53806298	86.13086657	2.42362299	1.277165298	5.37757817	7.55E-08	9.42E-06
ENSMUSG00000024186	Rgs11	1.850916416	4.491798237	2.42679691	1.279053379	3.58178978	0.00034125	0.00403865
ENSMUSG00000032128	Robo3	3.103241502	8.210104303	2.64565433	1.403624575	4.37247379	1.23E-05	0.00042243
ENSMUSG00000027966	Col11a1	3.931506307	11.01462582	2.80162995	1.486266412	5.11806076	3.09E-07	2.36E-05
ENSMUSG00000021250	Fos	0.305344003	0.906103504	2.9674842	1.569240349	3.00446411	0.00266049	0.01373389
ENSMUSG00000037868	Egr2	5.530683077	20.64306149	3.73246147	1.900127367	6.56237518	5.30E-11	2.02E-08